TECHNISCHE UNIVERSITÄT MÜNCHEN

Lehrstuhl für Bioverfahrenstechnik

Asymmetric reductions using novel ene-reductases from cyanobacteria

Yilei Fu

Vollständiger Abdruck der von der Fakultät für Maschinenwesen der Technischen Universität München zur Erlangung des akademischen Grades eines

Doktors der Naturwissenschaften

genehmigten Dissertation.

Vorsitzender:		Univ.-Prof. Dr.-Ing. Andreas Kremling
Prüfer der Dissertation:	1.	Univ.-Prof. Dr.-Ing. Dirk Weuster-Botz
	2.	Univ.-Prof. Dr. rer. nat. Wilfried Schwab

Die Dissertation wurde am 11.09.2013 bei der Technischen Universität München eingereicht und durch die Fakultät für Maschinenwesen am 13.11.2013 angenommen.

Acknowledgements

This doctoral thesis was realized at the Institute of Biochemical Engineering at the Technische Universität München under the supervision of Prof. Dr.-Ing. D. Weuster-Botz. It is a pleasure to thank the many people who made this thesis possible.

Foremost, I would like to express my sincere gratitude to my advisor Prof. Dr.-Ing. D. Weuster-Botz for giving me the opportunity to complete my doctoral thesis at his Institute and for his excellent guidance and great support during the last years. Especially his wide knowledge and his structured way of thinking have been of great value for this thesis.

I would like to thank Prof. Dr. rer. nat. W. Schwab for accepting to be co-examinar and Prof. Dr.-Ing. A. Kremling for taking over the position of the chairman of the jury.

I owe a great debt of gratitude to Dr. rer. nat. Kathrin Castiglione for generously sharing her time and expertise, for her invaluable support and encouragement throughout the research work. I deeply appreciate the insightful discussions and valuable contributions to this project. Thank you also for providing the genomic DNA of the cyanobacterial strains and the FDH mutants.

I would like to thank Prof. Dr. rer. nat. F. Kühn (Molecular Catalysis, Chemistry Department, Technische Universität München) for the opportunity to perform chemical synthesis and GC-MS analysis in his laboratory. I am very grateful to Bo Zhang and Julia Witt for their excellent help in the synthesis and NMR analysis and to Thomas Schröferl for his help in the GC-MS analysis.

I would like to thank the TUM Graduate School for financially supporting my attendance at the international conference Biotrans2013 in Manchester, UK.

I wish to gratefully acknowledge my students for their great experimental assistance, especially Simeon Leupold, Andrea Weber, Ingmar Polte, Michael Muthsam, Sebastian Gumplinger and Nicola Hupp.

My deep gratitude goes to all my colleagues and former colleagues for the practical help in the laboratory and the fruitful discussions and for creating such a pleasant working atmosphere. I should especially mention Markus Amann, Dr. Bernd Anselment, Dr. Danielle Dennewald, Dr. Clara Delhomme, Georg Faust, Dr. Dirk Hebel, Dr. Torben Höfel, Nils Janzen, Harald Krispin, Ilka Sührer, Ellen Truxius, Michael Weiner, as well as Matthias von Roman and Christian Roth from the Bioseparation Engineering and Dr. Dominik Maslak from the TUM Research Center for Industrial Biotechnology. I would like to thank Boqiao Sun for sharing the “Asia” office and his support in the liter-scale cultivation and statistical optimization. Thank you, Anna Groher and Christina Kantzow for being such supportive friends and the great time we spend together. Special thanks to Dr. Kathrin Castiglione and Michael Weiner for proofreading my thesis.

Finally, I owe my deepest gratitude to my parents, my brother and my friends who are always there for me and support me in many ways.

Content

1 Introduction

The chirality of molecules is a critical issue for the fine-chemical and pharmaceutical industry, as well as the flavor and fragrance industry. Though enantiomers have similar physical properties and chemical reactivities towards achiral compounds, their reactivity towards other chiral molecules can result in different responses. For example, carvone, a terpenoid naturally found in essential oils, forms two enantiomers: Whereas (R)-carvone smells like spearmint, (S)-carvone smells like caraway (Figure 1.1). Hereby, interactions with chiral olfactory receptors define the responses of these chiral molecules (Herz 2009). In case of pharmaceutical application of chiral compounds, the stereochemical configuration of a compound can have dramatic consequences as illustrated by the Contergan scandal in the 1950s (Ridings 2013). Today, there is a strong regulation and high demand for the production of enantiopure substances. This is highlighted by the fact that over 50 % of current drug candidates are developed as single enantiomers (Adams et al. 2009).

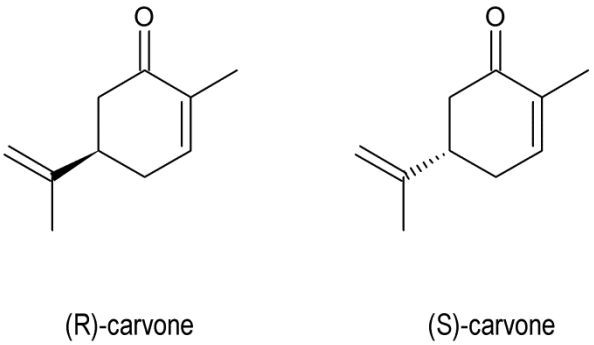

Figure 1.1 Structure of (R)-carvone and (S)-carvone.

Beside the need for chirality and functionality of molecules, the need for sustainability of processes is another important aspect. The awareness of environmental risks arising from classical chemical productions demands the development of environmental-friendly “green chemistry”. These are the main driving forces for the implementation of biotechnology and

biocatalysis (Wenda et al. 2011). The use of whole cells or enzymes as biocatalysts has the potential to fulfill both aspects. One major advantage of enzymes is their high specificity and selectivity (Hollmann et al. 2011). Their acceptance as “green catalysts” derives from their potential application in non-toxic and mild reaction conditions, low waste production and avoidance of metal ions and organic solvents (Wenda et al. 2011).

Though there has been a great progress in the development of biocatalysis in the last decades, the potential has not yet been fully realized. Better and commercially available enzymes are required to provide adequate toolboxes for organic chemists. This would allow the inclusion of these enzymes in the planning of synthetic strategies and further application in processes on the industrial scale (Meyer et al. 2013). Furthermore, biocatalytic processes using whole cells or isolated enzymes have to be developed and optimized to further improve productivity and process economics (Pollard and Woodley 2007).

2 Motivation and objectives

Asymmetric reduction of C=C bonds represents one of the most widely employed strategies for the production of chiral molecules, because it leads to the creation of up to two stereogenic centers (Stuermer et al. 2007). Whereas *cis*-hydrogenation has reached an industrial standard using transition metal-based homogeneous catalysts (Knowles 2002; Noyori 2002), *trans*-hydrogenation is still at a development stage (Winkler et al. 2012). In this field, biocatalysis can offer great opportunities to overcome the limitations of chemical synthesis, as well as provide economical and ecological benefits (Hollmann et al. 2011; Meyer et al. 2013).

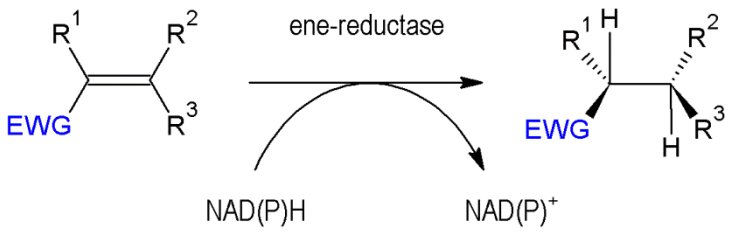

Figure 2.1 Asymmetric reduction of alkenes activated by an electron-withdrawing group (EWG) by ene-reductases.

Ene-reductases (ERs) from the Old yellow enzyme (OYE) family [EC 1.6.99.1] are capable of C=C bond reduction in a *trans*-specific fashion (Figure 2.1). The name “old yellow enzyme” derived from the fact that these NAD(P)H-dependent enzymes contain flavin mononucleotide (FMN), which is essential for the catalysis. Since the discovery in baker´s yeast in 1933 (Warburg and Christian 1933), numerous ERs were found in yeast, fungi, bacteria and plants (Hall et al. 2007; Strassner et al. 1999). However, the industrial application of ene-reductases is still in infancy. The major hindrances comprise the insufficient enzyme stability under operational conditions (Yanto et al. 2010), the strong preference for NADPH, the requirement of cofactor recycling (Durchschein et al. 2012a;

Paul et al. 2012), as well as the lack of established robust whole-cell biotransformations (Winkler et al. 2012).

Cyanobacteria represent a remarkable group of photosynthetic prokaryotes with significant roles in aquatic and terrestrial ecosystems (Rippka et al. 1979). A wide range of bioactive compounds, which can be used as therapeutics, insecticides, and anti-fouling agents, are known to be derived from cyanobacteria (Ducat et al. 2011). Thus, cyanobacteria represent a valuable source for novel enzymes, capable of catalyzing challenging reactions (Hölsch et al. 2008; Hölsch and Weuster-Botz 2010). Whole-cell biotransformations of enones were reported using the freshwater cyanobacterium *Synecococcus* sp. PCC 7942 yielding excellent stereoselectivities (Hirata et al. 2009; Shimoda et al. 2004). However, the efficiency of biotransformations using cyanobacteria was limited by the formation of by-products and long reaction times (Shimoda et al. 2004).

Consequently, the first part of this doctoral thesis aimed at the identification and characterization of novel ene-reductases from *Synechococcus* sp. PCC 7942 and other cyanobacterial strains to find efficient and stable enzymes useful for industrial biocatalysis. The second part concentrated on the development of whole-cell biotransformations involving ene-reductases with respect to further process scale-up.

The following issues were focused in this work:

- Identification of putative ene-reductases in *Synechococcus* sp. PCC 7942 and other cyanobacterial strains
- Recombinant production of putative cyanobacterial ene-reductases in *Escherichia coli* by overexpression of the respective genes and purification of the enzymes
- Comparative characterization of these ene-reductases with regard to the substrate spectrum, cofactor specificity, stereoselectivity and stability
- Evaluation of the whole-cell biotransformation with recombinant *Escherichia coli* overexpressing selected ene-reductases and oxidoreductases for cofactor regeneration
- Development of whole-cell biocatalysts for alkene reduction
- Characterization of the whole-cell biotransformation in different reaction systems
- Optimization of the whole-cell biotransformation process
- Scale-up of the biotransformation process to the liter scale

3 Theoretical Background

3.1 Enzymes in asymmetric synthesis

3.1.1 Advantages and disadvantages of biocatalysts

Compared to traditional chemical methods, with their disadvantages such as high environmental burden due to waste production, usage of heavy metal ions and organic solvents and energy intensive reaction conditions (high temperature and pressure) (Wenda et al. 2011), the use of enzymes as biocatalysts is associated with many advantages for the production of valuable compounds, which are summarized in the following:

- Enzymes are efficient catalysts with 10^8 – 10^{10}-fold higher reaction rates compared to corresponding noncatalyzed reactions, which is also above the rates achieved by chemical catalysts (Wolfenden and Snider 2001).
- Enzymatic reactions are usually performed under mild conditions (pH range of 5 – 8 and temperature range of 20 – 40 °C). In addition, enzymes are completely biodegradable (Faber 2011). These characteristics emphasize their environmental benefits in industrial processes.
- Enzymes can be found for almost every type of organic reactions, pointing out their potential of replacing almost every traditional chemical process. Furthermore, also nonnatural substrates can be accepted by enzymes (Faber 2011).
- Enzymes are active under similar reaction conditions. This enables the application of reaction cascades by multiple enzymes in a single reaction system, simplifying the reaction process (Lopez-Gallego and Schmidt-Dannert 2010).
- The most important benefit of enzymes compared to chemical catalysts is their high specificity and selectivity (Hollmann et al. 2011). Unlike classical chemical syntheses, protection of other functional groups can be circumvented and product

impurities due to side reactions are avoided (Gröger and Asano 2012; Pollard and Woodley 2007). This simplifies downstream processes and lowers economical and ecological expenses.

There are also some drawbacks of enzymes as biocatalysts, which are described in the following:

- Because enzymes are provided in one enantiomeric form, the availability of the desired product is generally limited to one enantiomer. The access to the opposite stereoselectivity is always associated with searching for new enzymes (Faber 2011).
- The stability of enzymes is a critical issue in terms of their application in industrial-scale processes. Operational windows of parameters, such as pH, temperature or salt concentration, are sometimes narrow to avoid inactivation of enzymes (Iyer and Ananthanarayan 2008). Additionally, inhibition of enzymes by high substrate and product concentration can complicate the reaction process (Faber 2011).
- With exception of hydrolases (EC 3), members of all other enzyme classes require cofactors for their catalytic activity. Cofactors can serve as redox equivalent (e.g. flavins, NAD(P)H) or chemical energy (e.g. ATP) and are mostly unstable and expensive substances. Due to their modification during catalytic processes, regeneration strategies are essential to ensure an economically acceptable process (Gröger and Asano 2012).

However, many strategies were developed to eliminate these drawbacks. Enzymes with improved properties regarding catalytic efficiency or stability can be obtained by searching nature´s diversity as well as applying various strategies in the field of protein engineering (Behrens et al. 2011). The cofactor challenge is considered to be solved by applying substrate-coupled or enzyme-coupled cofactor regeneration (Wichmann and Vasic-Racki 2005). In addition, various process strategies, involving the form of applied biocatalyst, reaction systems or process types, can be supportive of circumventing disadvantages of the biocatalyst, addressing inhibition or stability issues of enzymes (Milner and Maguire 2012; Yazbeck et al. 2004).

3.1.2 Discovery of enzymes for efficient bioprocesses

Nature's diversity represents the main source for enzymes. Screening wild-type microorganisms for the desired enzyme activity has been proven to be a good method for exploring novel enzymes. However, the cultivability of microorganisms restricts the range of exploring, because less than 1 % of all microbial species can be cultivated under laboratory conditions. Screening and sequencing of metagenomes, which comprise genomic information of all microorganisms in a given habitat, circumvent this limitation(Aehle and Eck 2012). Since isolated metagenomic DNA is deposited in gene libraries and usually expressed heterologously in *Escherichia coli* for subsequent screening of enzyme activities, high-throughput technologies and efficient screening strategies are essential (Uchiyama and Miyazaki 2009). Whereas the sequence homology-based screening strategy focuses on identifying enzymes with similar functionalities, activity-based screening is preferred for discovery enzymes with new functionalities. Thereby, the results strongly depend on the performance in protein expression (Aehle and Eck 2012; Behrens et al. 2011).

Alternatively, discovery of enzymes by database mining relies on bioinformatic tools in combination with databases, for example UniProt database or GenBank of the National center for biotechnology information (NCBI). The knowledge derived from nucleotide and protein sequences are exploited to find enzyme variants with improved properties. Thereby, conserved amino acid motifs that are characteristic for a target protein family, are compared to identify enzymes catalyzing similar reactions. Subsequent cloning, protein expression and characterization are necessary in this process (Aehle and Eck 2012).

However, native enzymes often do not meet the requirements for a large-scale biocatalytic process with respect to activity, stereoselectivity or process-related properties as stability at certain temperature or pH, in organic solvents or in presence of high substrate or salt concentration (Singh et al. 2013). Instead of adaption of reaction conditions to the enzyme, the trend is to adjust enzyme properties such as substrate scope, stereoselectivity, thermal or solvent stability to the requirement of a given process (Hollmann et al. 2011). Developments in protein engineering techniques in combination with direct evolution strategies notably improved the targeted design of enzyme properties as well as the duration of enzyme optimization (Bornscheuer et al. 2012).

3.1.3 Enzyme classification

Generally, enzymes are classified into six categories according to their catalyzed reactions (International union of biochemistry and molecular biology 1992). An overview of enzyme the classification is given in the following table.

Table 3.1 Classification of enzymes (International union of biochemistry and molecular biology 1992)

EC number	Enzyme class	Reaction type
1	oxidoreductases	transfer of electrons (hydride ions or H atoms); e.g. reduction of C=O and C=C or oxidation of C-H, C=C, C-N and C-O
2	transferases	transfer of functional groups such as amino, acyl, phosphoryl, methyl, nitro, glycosyl groups
3	hydrolases	hydrolysis of e.g. esters, amides, lactones and nitriles, as well as reverse reactions
4	lyases	addition of groups to double bonds or formation of double bonds by removal of groups
5	isomerases	transformation of isomers such as racemizations or epimizations
6	ligases	formation or cleavage of C-C, C-O, C-S or C-N bonds coupled to ATP cleavage

On large, industrial scale, biocatalytic applications are currently dominated by hydrolases (EC 3) in kinetic resolution or desymmetrization reactions to produce enantiopure alcohols, amines and other functionalities (Hollmann et al. 2011). Hydrolases are commercially available in an attractive price range. Their application is simplified due to the fact that no additional cofactor or cofactor regeneration are required. Prominent examples are lipases or esterases (Gröger and Asano 2012).

The second enzyme class with high usefulness in organic chemistry is the group of oxidoreductases (EC 1). Their contribution is mostly focused on ketoreductases (KREDs) (Hollmann et al. 2011). The major driving force of catalytic reduction by KREDs is their high enantioselectivity in the reduction of prochiral ketones, thereby outcompeting chemical catalysts in that point (Huisman et al. 2010). One drawback of the industrial application of oxidoreductases is their demand for nicotinamide cofactors, though the cofactor challenge is almost resolved using affordable regeneration methods (Wichmann and Vasic-Racki 2005).

In contrast to hydrolases and ketoreductases with their established processes in industrial biocatalysis, e.g. ene-reductases (alkene reduction) or monooxygenases (Baeyer-Villiger oxidation) belong to the emerging biocatalytic reactions (Pollard and Woodley 2007).

3.1.4 Methods for cofactor regeneration

With regard to cofactors essential for several enzymatic reactions, it has to be distinguished between tightly bound, self-regenerating cofactors, e.g. biotin or flavins, and "free cofactors", such as pyridine nucleotides and nucleoside triphosphates (NTPs). These "free cofactors" act as transport agents during the catalytic reaction and the modification cannot be regenerated by the catalyst itself. Because cofactors are too expensive to be used in stoichiometric amounts, strategies were developed for *in situ* regeneration (Zhao and van der Donk 2003).

Hereby, several requirements have to be fulfilled for an efficient and economically viable cofactor regeneration method (Zhao and van der Donk 2003):

- Reagents (enzymes, chemical compounds) and equipment have to be easily available, inexpensive and stable during the catalytic reaction.
- The compatibility with the biochemical system is a critical issue. Neither reagents nor by-product of the cofactor regeneration method should interfere with the catalytic reaction or product isolation.
- The regeneration method should be kinetically and thermodynamically in favor of the desired product.
- Most importantly, the total turnover number (TTN) should be as high as possible, but at least ca. $10^3 – 10^5$ for an economically viable process. The TTN is defined as the molar amount of product formed per molar amount of consumed cofactor for one catalytic reaction. Therefore, this parameter includes the catalysts turnover number and possible cofactor loss during the regeneration.

Among all cofactor types, pyridine nucleotides ($NAD(P)^+$/NAD(P)H) are considered as most important cofactors for the industrial biocatalysis, because of their involvement in economically important applications, e.g. with oxidoreductases. Generally, the oxidized forms of pyridine nucleotides ($NAD(P)^+$) are less expensive and more stable than the reduced forms (NAD(P)H). In addition, cofactor costs are 4- to 18-fold lower using NAD(H) compared to NADP(H) (commercial suppliers) and NADH exhibited up to sevenfold higher stability (half-life) compared to NADPH depending on the pH and ionic strength of the reaction system (Wu et al., 1986). Both high costs and low stability of these cofactors (Table 3.2) promote the development of regeneration methods. Chemical (including

photochemical and electrochemical) methods as well as whole-cell and enzymatic methods can be applied for cofactor regeneration (Chenault and Whitesides 1987).

Table 3.2 Stability and cost of cofactors (Wichmann and Vasic-Racki 2005; Wu et al. 1986). n.a. = not available.

Cofactor	**Price, € mol^{-1}**	**Half-life, min (pH 6.0/ ionic strength 50 mM)**	**Half-life, min (pH 5.2/ ionic strength 40 mM)**
NAD^+	2655	n.a.	n.a.
NADH	8868	400	77
$NADP^+$	11417	n.a.	n.a.
NADPH	167846	56	21

Cofactor regeneration by growing cells utilizes the microbial metabolism for NAD(P)H recycling. Carbohydrates (e.g. glucose) are used as sources for reduction equivalents, allowing a NADH regeneration of ~720 U g_{DCW}^{-1}, if glucose and ammonium are used as carbon- and nitrogen sources. But, if the desired enzyme activities exceed ~100 U g_{DCW}^{-1}, the natural cofactor regeneration system may become limiting (Duetz et al. 2001). Consequently, the integration of additional enzymatic cofactor regeneration is required in this case, as well as for resting cells.

If whole-cell systems are not feasible, enzymatic methods are preferred over chemical strategies due to the better biocompatibility and higher selectivity and achievable TTNs. Thereby, it can be differentiated between the substrate-coupled and enzyme-coupled cofactor regeneration (Zhao and van der Donk 2003).

In case of *substrate-coupled cofactor regeneration*, the same enzyme is used for the desired catalytic reaction modifying one substrate and cofactor recycling using another cosubstrate (Figure 3.1). A prominent example is the use of alcohol dehydrogenases (ADHs) for ketone reduction in combination with the oxidation of NADH by the reduction of isopropanol as cheap cosubstrate. In order to overcome thermodynamic limitations, high concentrations of the cosubstrate (alcohol) are required and, additionally, the volatile byproduct acetone can be removed via a stripping process (Goldberg et al. 2006; van der Donk and Zhao 2003). Given the product inhibition caused by high alcohol concentrations, solvent-stable ADHs are generally preferred (Stampfer et al. 2002).

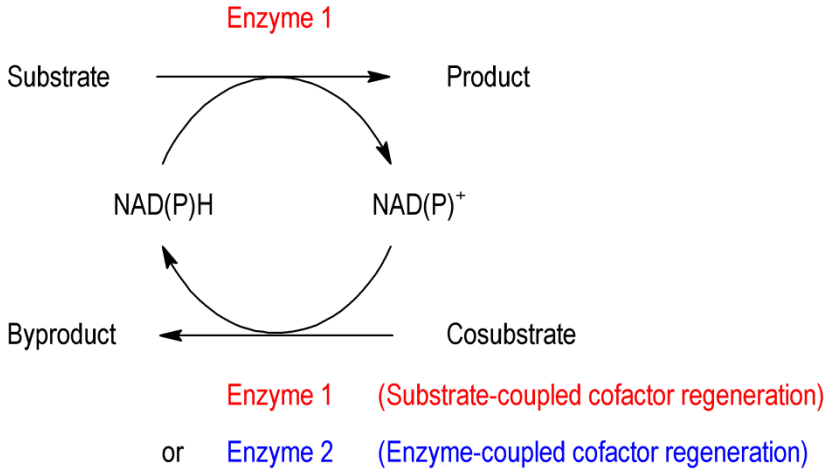

Figure 3.1 Enzymatic methods for cofactor regeneration. For substrate-coupled cofactor regeneration the same enzyme is used. For enzyme-coupled cofactor regeneration, an additional enzyme, e.g. formate dehydrogenase or glucose dehydrogenase, is applied.

The majority of enzymatic, cofactor-requiring processes make use of a second enzyme for cofactor regeneration, which is denoted as the *enzyme-coupled cofactor regeneration* (Figure 3.1). The separation of the desired reaction from the cofactor recycling allows a more flexible reaction system. In addition, thermodynamically favorable conditions can be achieved for both reactions.

Prominent enzyme-coupled cofactor regeneration strategies comprise the use of formate dehydrogenase (EC 1.2.1.2, FDH), glucose dehydrogenase (EC 1.1.1.47, GDH) and glucose-6-phosphate dehydrogenase (EC 1.1.1.49, G6PDH).

FDHs catalyze the oxidation of formate to carbon dioxide, thereby reducing $NAD(P)^+$ to NAD(P)H (Figure 3.2A). The formate/FDH system is often considered as the most suitable enzyme since it fulfills conditions necessary for industrial standards (Tishkov and Popov 2006; Wichmann and Vasic-Racki 2005). The strong driving force caused by the formation of carbon dioxide leads to an almost irreversible reaction. Both the cheap cosubstrate formate and carbon dioxide have no negative effects on the catalyst, reaction or subsequent purification and can be easily removed from the reaction system. Major drawbacks are the strong preference of FDHs for NAD^+, limiting this regeneration method to NADH-dependent enzymes, as well as the relative low specific activity (~10 U mg^{-1}). Nevertheless, using protein engineering techniques, efficient FDH mutants have been generated with both high specific activity towards $NADP^+$ (~10 U mg^{-1}) and high stability (Hoelsch et al. 2012; Tishkov and Popov 2006).

When using GDH for cofactor regeneration, glucose is oxidized to gluconolactone, which spontaneously hydrolyses to gluconic acid. In case of G6PDH, glucose-6-phosphate is oxidized, which makes this enzyme suitable for whole-cell applications, because of the phosphorylation of glucose by the uptake through the cell membrane (Figure 3.2B, 3.2C) (Faber 2011; Kratzer et al. 2008). Though both enzymes exhibit high activities for both NAD^+ and $NADP^+$ (~700 U mg^{-1}), both systems are accompanied by high enzyme cost, possibly difficult product isolation and the requirement of pH regulation (Hilt et al. 1991; Lee and Levy 1992).

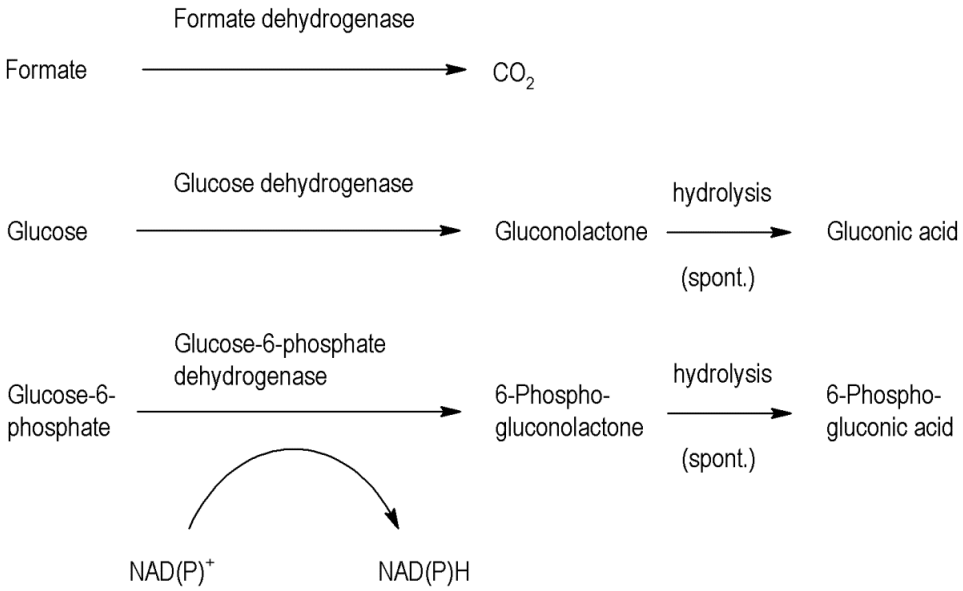

Figure 3.2 Reactions catalyzed by formate dehydrogenase, glucose- and glucose-6-phosphate dehydrogenase for enzyme-coupled cofactor regeneration.

3.2 Fundamentals of biocatalytic processes

3.2.1 Characterization of enzymes

Enzyme characterization comprises the study of the enzyme activity towards a variety of substrates, the stability of enzymes at different reaction conditions, and more thoroughly the enzyme mechanism with the determination of its specific kinetic parameters.

The most fundamental model for enzyme kinetics was described by Michaelis and Menten (1913) which characterized the simplest irreversible catalysis of one substrate by one enzyme to form one product. A scheme of this reaction is given in Figure 3.3.

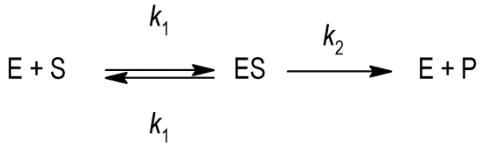

Figure 3.3 Scheme of an irreversible one-substrate-one product reaction. The substrate (S) binds to the enzyme (E) and forms the enzyme-substrate complex (ES). This complex can dissociate into the free enzyme and the substrate, or otherwise release the free enzyme and the formed product (P). The rate constants are described by the constants k_i.

Several assumptions have to be made for a valid Michaelis-Menten model (Equation 3.1):

- The enzyme-substrate complex (ES) is formed by one enzyme (E) and one substrate molecule (S).
- A pseudo-steady state is assumed, where the formation and decay of the enzyme-substrate complex is kept in balance and its concentration can be considered as constant ($\frac{d[ES]}{dt} = 0$).
- The overall reaction is irreversible and a possible reverse reaction of the last step is negligible. This is valid, if initial reaction rates are determined ($[P] \cong 0$).
- The dissociation of the product from the enzyme-substrate complex is considered as the rate-limiting step.

$$v = v_{max} \frac{[S]}{K_M + [S]} \qquad \text{Eq. 3.1}$$

v	reaction rate, mol s^{-1}
v_{max}	maximal reaction rate, mol s^{-1}
$[S]$	substrate concentration, mol L^{-1}
K_M	half-saturation constant, mol L^{-1}

The half-saturation constant K_M is related to the dissociation constant and indicates the affinity of the substrate (Equation 3.2). As the formation of the product represents the rate-limiting step, the catalytic rate is defined by k_{cat} (Equation 3.3), which represents the turnover rate of the enzyme. The catalytic efficiency of an enzyme is given by a combination of both constants ($\frac{k_{cat}}{K_M}$).

$$K_M = \frac{k_{-1} + k_2}{k_1} \qquad \text{Eq. 3.2.}$$

k	kinetic constants, s^{-1}

$$v_{max} = k_2 \cdot [E]_0 = k_{cat} \cdot [E]_0 \qquad \text{Eq. 3.3}$$

v_{max}	maximal reaction rate, mol s^{-1}
k_{cat}	turnover number, s^{-1}
$[E]_0$	enzyme amount at time t = 0, mol

The majority of enzymatic reactions require a more complex model than the Michaelis-Menten model, because two or more substrates are involved in the catalytic process. This also includes the characterization of oxidoreductases with the requirement for a nicotinamide cofactor in addition to the main substrate, representing a two-substrate-two-product reaction. Mechanisms for multi substrate reactions differ according to the order of substrate binding and product desorption. If all substrates must bind before the product dissociation, it is denoted as *sequential* mechanism, which can be divided into *random* or *ordered* according to the substrate binding. If one product is released before all substrates are bound, the reaction follows a *ping-pong* mechanism (Bisswanger 2008).

In case of the *ordered bi-bi* mechanism, the substrate A has to bind to the enzyme before the substrate B can bind. After substrate conversion, the product P has to be released first, before the product Q can be released (Figure 3.4). This mechanism can be applied to several

formate dehydrogenases (Tishkov and Popov 2004). The catalytic reaction of formate dehydrogenases was described in Section 3.1.4.

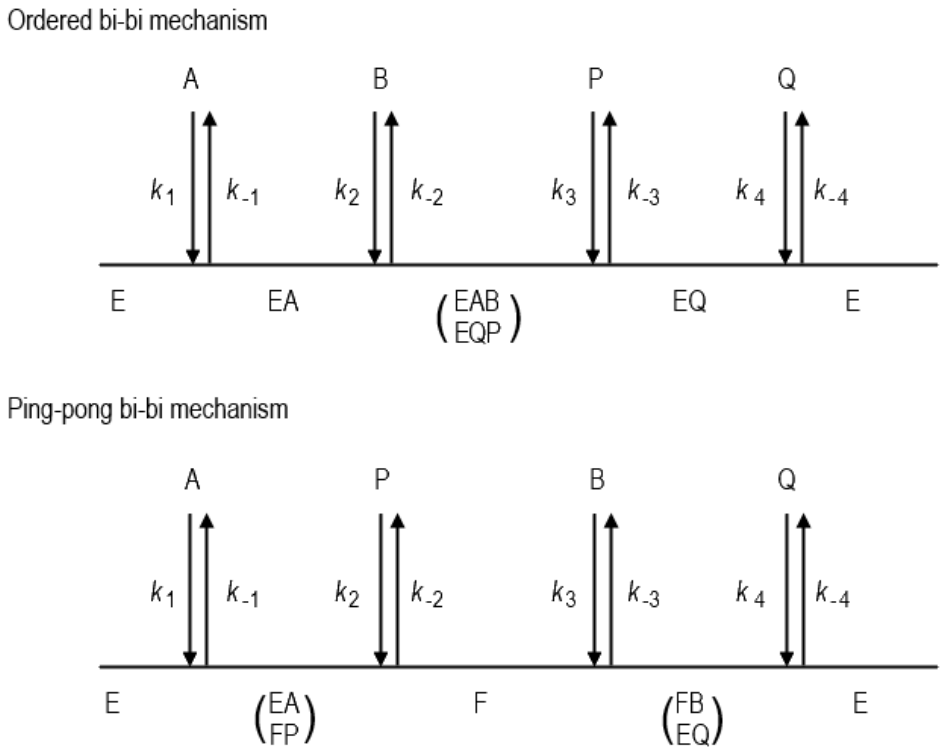

Figure 3.4 Schemes of the ordered bi-bi mechanism and the ping-pong bi-bi mechanisms according to Bisswanger (2008). Substrates and products are termed as A, B and P, Q, respectively. Different enzyme states are named as E, F. EA, EQ, etc. represents the transitory states.

In this project the enzymes of interest are ene-reductases from the old yellow enzyme family, which is presented further in Section 3.4. Ene-reductases catalyze the asymmetric reduction of alkenes. The reaction is also nicotinamide-dependent and proceeds in two steps via a *ping-pong bi-bi* mechanism. In the first step, the substrate A is converted into product P, which is subsequently released. By e.g. incorporating a reactive group derived from the substrate A, the enzyme retains an intermediary form, which interacts with a second substrate B. A second product Q can be formed e.g. by transferring the reactive group. A scheme of the *ping-pong bi-bi* mechanism is depicted in Figure 3.4.

3.2.2 Characterization of biocatalytic processes

In the following, several key parameters for the characterization of biocatalytic process are introduced.

The conversion describes the consumption of a given quantity of substrate dependent on the time of the reaction (Equation 3.4). In contrast, the yield refers to the time-dependent formation of the desired product during the reaction (Equation 3.5). In case of the production of chiral compounds, only the desired enantiomer is considered in this calculation. If only one product without any byproducts is obtained in the catalytic reaction, then the conversion equals the yield.

In addition, it has to be differentiated between the yield of the chemical reaction and the yield of the whole process. The latter variant includes the recovery of the product in the purification process subsequent to the chemical reaction, i.e. the percentage of purified product.

$$X(t) = \frac{n_{S,0} - n_S}{n_{S,0}} \cdot 100\ \% \qquad \text{Eq. 3.4}$$

X	conversion, %
$n_{S,0}$	initial substrate quantity, mol
n_S	substrate quantity at time t, mol

$$Y(t) = \frac{n_P - n_{P,0}}{n_{S,0}} \cdot \frac{|\nu_S|}{|\nu_P|} \cdot 100\ \% \qquad \text{Eq. 3.5}$$

Y	yield, %
$n_{P,0}$	initial product quantity, mol
n_P	product quantity at time t, mol
ν_S	stoichiometric factor of the substrate, -
ν_P	stoichiometric factor of the product, -

The efficiency and productivity of the process can be further described by the space-time yield, which is defined as the product concentration obtained in a given reaction time (Equation 3.6).

$$STY = \frac{n_P}{t \cdot V_R}$$ Eq. 3.6

STY	space-time yield, mol L^{-1} h^{-1}
n_P	product quantity at time t, mol
t	reaction time, h
V_R	reaction volume, L

In case of the production of enantiomers or diastereomers, the enantiomeric excess (ee) or diasteromeric excess (de) provide information about the impurity of the desired product caused by the other enantiomer or diastereomers (Equation 3.7). If only one enantiomer or diastereomer is formed, the enantiomeric or diasteromeric excess will reach 100 %. In case of a racemate (equal quantity of both enantiomers), the enantiomeric excess is 0 %.

$$ee \; or \; de = \frac{|n_R - n_S|}{n_R + n_S} \cdot 100\ \%$$ Eq. 3.7

ee	enantiomeric excess, %
de	diastereomeric excess, %
n_R	quantity of R-enantiomer or diastereomer, mol
n_S	quantity of S-enantiomer or diastereomer, mol

3.2.3 Objectives for efficient biocatalytic processes

In general, high conversion and stereoselectivity are desirable for an efficient biocatalytic process. A complete conversion of substrate, absence of byproducts and high enantiomeric excess of the product are associated with a simplification in downstream processing and thus lower production costs. This is especially relevant for substrate, byproduct and product with similar physical properties, which would complicate the separation process (Gröger and Asano 2012). Industrial-scale biotransformations also require high volumetric productivities, as well as significant substrate concentrations of at least 5 – 10 % (w/w) (Huisman et al. 2010). Biocatalytic processes can be notably improved by the combination of biocatalyst engineering (e.g. engineering of the enzyme or whole cell biocatalyst) and process intensification (e.g. immobilization, substrate supply and product removal techniques). Table 3.3 gives an overview of basic criteria for efficient biocatalytic processes. Other factors as value generation in the reaction, production costs for the biocatalysts or infrastructural conditions can also influence the process economy (Hollmann et al. 2011).

Table 3.3 Basic requirements for economically feasible and efficient biotransformations (Huisman et al. 2010; Pollard and Woodley 2007)

Parameter	Value
substrate concentration	> 100 g L^{-1}
Conversion	> 95 % within 24 h
(optical) purity of product	> 99.5 % ee; minimum 98 % ee
substrate-to-enzyme ratio	> 50 kg kg^{-1}
substrate-to-cell ratio	>15 kg kg^{-1}
cofactor concentration	< 0.5 g L^{-1} (< 0.5 mM)

3.2.4 Bioprocesses with isolated enzymes vs. whole-cells

Both purified enzymes and whole microbial cells as well as all states in between (e.g. crude enzyme preparations) can be applied for biocatalytic processes. The choice of the physical form of the biocatalyst depends on the catalytic reaction, process scale and demand on product purities.

Biocatalysis using isolated enzymes is mostly preferred for high-value products with particular demand on the product purity. Major drawbacks comprise high production costs of enzymes caused by protein purification as well as enzyme inhibition and the need for additional cofactor regeneration systems. Further, possible inactivation of enzymes during the process has to be considered. In many cases, retaining and recycling of biocatalysts are necessary, e.g. using immobilization techniques or enzyme membrane reactors (Gröger and Asano 2012; Singh et al. 2013; Zajkoska et al. 2013).

Though there has been a great improvement regarding efficiency and cost in protein purification techniques, the production cost for crude enzyme preparations is still up to 70-fold higher compared to whole-cell biocatalysts, with cost increasing with higher purification grade (Tufvesson et al. 2010). In the field of whole-cell biotransformation, following issues have to be addressed:

1. Selection of host strains

The choice of the host strain can notably influence enzyme activity, productivity and byproduct formation. Enzyme repertoire, protein expression, substrate and product transport, energy metabolism and cofactor regeneration define the activity of the whole-cell biocatalyst (Zhou et al. 2010). For example, *Escherichia coli* is preferred as host strain for ketone reduction, because of the lower amount and activity of endogenous ADHs acting as

competing enzymes in comparison to yeast (Hildebrandt et al. 2002). At last, the tolerance of the host strain towards solvents or toxic compounds determines the stability of the biocatalyst during the process (Kuhn et al. 2012).

2. Growing cells vs. resting cells

Whole-cell biotransformation can be either performed with a growing culture or with resting cells, which can affect the handling, productivity of the process and byproduct formation (Faber 2011). The carbon utilization for reduced nicotinamide cofactor regeneration is more efficient when decoupling growth and biotransformation. Using growing cells, a part from carbon and energy is required for biomass production, furnishing high amount of biomass as byproduct. In contrary, the consumption is limited to maintenance in resting cells, resulting in a full exploiting of their metabolism, which leads to higher product yield and specific activity. In addition, resting cells can be recycled and reused (Julsing et al. 2012).

3. Wild-type cells vs. recombinant cells

Whereas whole-cell biotransformation was dominated by the use of wild-type microorganisms in the past, which often decreased yield and stereoselectivity due to competing enzymes, recombinant strains are preferred nowadays. If possible, desired enzymes (as well as enzymes for cofactor regeneration) are overexpressed in the host cell and undesired competing enzymes are knocked out completely. Clearly, high productivities and stereoselectivities can be achieved using such recombinant cells. These genetically engineered microorganisms are often denoted as “designer cells” (Faber 2011; Gröger and Asano 2012).

Table 3.4 shows some benefits and drawbacks for biocatalysis with isolated enzymes, wild-type and recombinant whole-cell biocatalysts.

Table 3.4 Comparison of bioprocesses using isolated enzymes and whole-cell biotransformation with wild-type or engineered microorganisms (adapted from Faber (2011); Peters (1998)).

Criteria	Isolated enzymes	Wild-type cells	Designer cells
availability and costs	constrained availability and high upstream costs caused by protein purification	good availability and low cost regarding biomass production	good availability and low cost regarding biomass production
selectivity of the reaction	high stereoselectivities and product purities	low stereoselectivity and product impurities due to side reactions in host cells	side reactions can be minimized by sufficient rate of the desired reaction or knock-outs
cofactor regeneration	additional recycling of cofactors necessary	regeneration of cofactors occurs within cells	cofactor regeneration can be supported by an additional enzyme (e.g. formate dehydrogenase)
substrate and product transport	no limitations; high concentration tolerance results in higher productivity	reaction rate can be limited by the transport through cell membrane and low concentration tolerance	reaction rate can be limited by the transport through cell membrane and low concentration tolerance
downstream processing	simple	complicated	complicated
space-time yield	moderate to high	low to high	moderate to high
compatibility with organic solvents	reduced activities and stabilities due to denaturation	low tolerance, cytotoxic effects, cofactor leakage	low tolerance, cytotoxic effects, cofactor leakage

3.2.5 *Escherichia coli* as whole-cell biocatalyst

Characteristics of cell growth

The microbial growth cycle can be differentiated into several distinct phases under batch conditions. In the initial lag phase, cells adapt to the new environment by e.g. inducing new enzymes for catabolizing new substrates. In the exponential growth phase (also referred to as the logarithmic phase), cell division leads to an exponentially increase of the cell number at maximum specific growth rate (μ_{max}). The end of this phase arises with the onset of the depletion of essential nutrients or accumulation of toxic metabolites. The subsequent short phase of declining growth is followed by the stationary phase, in which the specific growth

rate is zero. Finally, the cell number declines during the death phase (Blanch and Clark 1997). The growth cycle is illustrated in Figure 3.5.

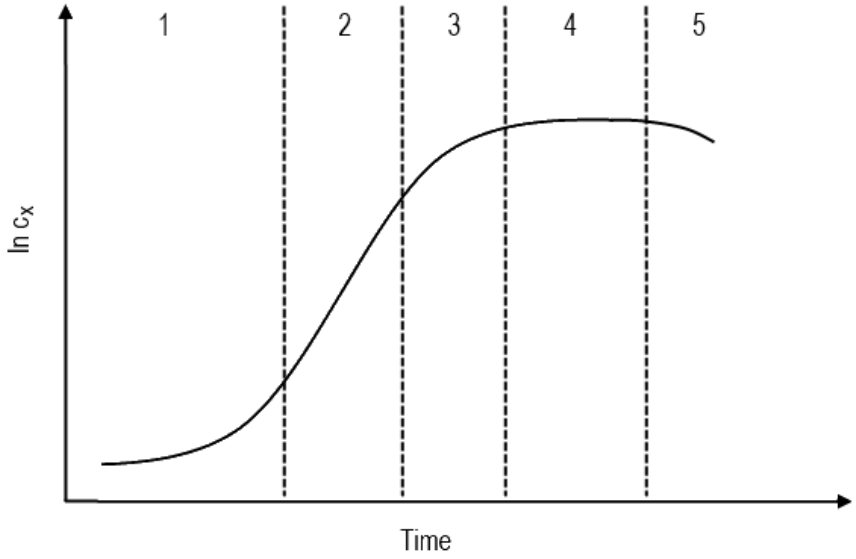

Figure 3.5 Stages of bacterial growth cycle: (1) lag-phase, (2) exponential growth phase, (3) substrate-limiting phase, (4) stationary phase, (5) death phase.

Microbial growth is characterized using the specific growth rate μ, defined as the increase of biomass concentration relative to the actual biomass concentration (Equation 3.8).

$$\mu \equiv \frac{1}{c_X} \cdot \frac{dc_X}{dt} \qquad \text{Eq. 3.8}$$

μ	specific growth rate, h^{-1}
c_X	biomass concentration, $g_{CDW}\ L^{-1}$
t	time, h

During the exponential growth and substrate-limiting phase, the growth rate can be described by the model developed by Monod (1942) (Equation 3.9), presumed that only one substrate is growth limiting and all other cultivation parameters, such as pH, oxygen supply and temperature are constant.

$$\mu = \mu_{max} \cdot \frac{c_S}{K_S + c_S} \qquad \text{Eq. 3.9}$$

μ_{max}	specific growth rate under non-limiting conditions, h^{-1}
c_S	concentration of the limiting substrate, mol L^{-1}
K_S	half-saturation constant, mol L^{-1}

In general, bioprocesses such as cell growth are performed in bioreactors in a batch, fed-batch or continuous mode. For a simplified view of the bioreactor and the contained cells, an ideal stirred tank bioreactor (isotherm, isobar and homogenous) and a non-segregated and unstructured model of the cells are presumed. In that case, the dynamics of a compound is described by coupling mass balances with formal kinetics of uptake and production of substances (Blanch and Clark 1997).

Whereas a batch process is a closed systems without in- or outlet stream, cultivations in a fed-batch mode are operated with one or more nutrients supplied to the system during the process. For fed-batch cultivations, the change in biomass concentration is described by the Equation 3.10.

$$\frac{dc_X}{dt} = \frac{\dot{V}(t)}{V(t)} \cdot c_X + \mu \cdot c_X \qquad \text{Eq. 3.10}$$

c_X	biomass concentration, g_{DCW} L^{-1}
μ	specific growth rate, h^{-1}
V	reaction volume, L
$\dot{V}$	feeding rate L h^{-1}
t	time, h

Fed-batch cultivations have the purpose of controlling substrate concentration in the reaction medium by an appropriate feeding rate. Commonly, low concentrations may prevent excessive byproduct (e.g. acetate) accumulation or inhibition of protein expression. To obtain high cell density, an exponential feeding strategy ensures exponential growth with a self-controlled specific growth rate (μ_{set}) below the maximum specific growth rate of the organism (Jenzsch et al. 2006). Assuming that the substrate consumption for cell maintenance can be neglected, the exponential feed is described by the Equation 3.11.

$$\dot{V}(t) = \frac{\mu_{set} \cdot V(t_{0,feed}) \cdot c_X(t_{0,feed})}{Y_{X,S} \cdot c_{S,feed}} \cdot \exp\left(\mu_{set} \cdot (t - t_{0,feed})\right) \qquad \text{Eq. 3.11}$$

c_X	biomass concentration, g_{DCW} L^{-1}
$c_{S,\,feed}$	concentration of the limiting substrate in the feed, g L^{-1}
μ_{set}	fixed specific growth rate, h^{-1}
V	reaction volume, L
$\dot{V}$	feeding rate, L h^{-1}
$t_{0,\,feed}$	reaction time at begin of the feeding, h
t	time, h
$Y_{X,S}$	biomass to substrate yield, g_{CDW} g_S^{-1}

Transport across the cell membrane

In whole-cell biotransformation, the transport of substrate across the cell membrane to the catalyzing enzyme is often the rate-limiting step of the reaction (Chen 2007). The transport rate and mechanism depends on the molecule type.

The simplest transport mechanism is the simple diffusion, which always occurs in the direction of the chemical gradient. In general, high diffusion rates are obtained by small, unpolar molecules, such as O_2 and CO_2, followed by small, uncharged polar compounds, e.g. water or ethanol. The diffusion of large, uncharged polar molecules (e.g. glucose) is notably decreased and for charged molecules, independent of their size, almost not possible. The transport of polar or charged molecules, which can hardly enter the cell via diffusion, is supported by two classes of membrane proteins. Whereas channel proteins form pores for substances with defined size and charge to pass through, carrier proteins bind to specific solutes and transport by conformation changes. A transport mechanism occurring in the direction of the chemical gradient represents “passive transport”. In contrast, energy is required for the “active transport” against the direction of the chemical gradient (Alberts et al. 2002) (Figure 3.6).

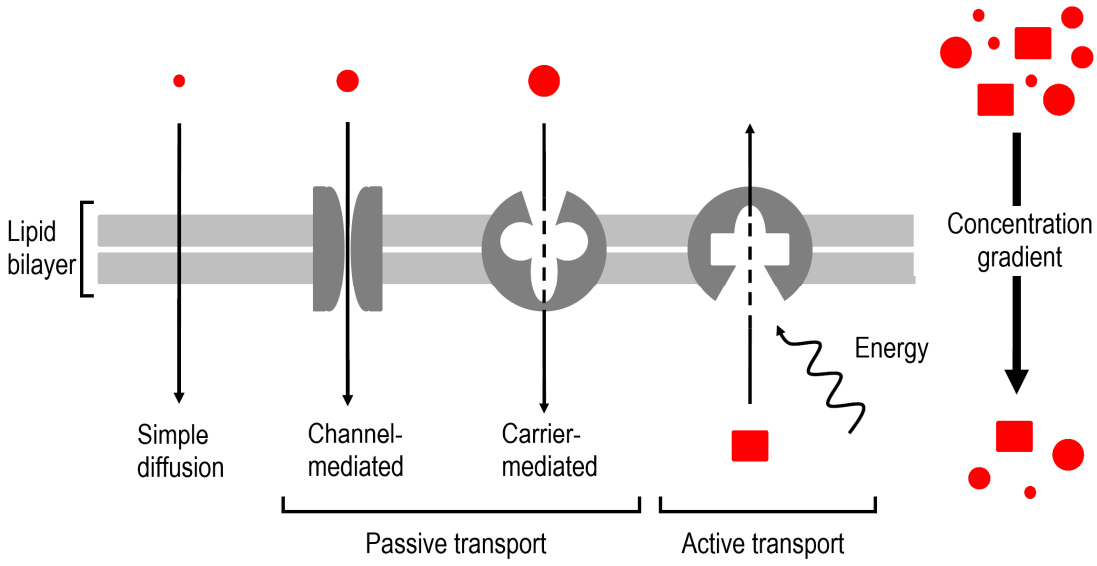

Figure 3.6 Scheme of different transport mechanisms through the cell membrane according to Alberts et al. (2002)

In industrial biocatalysis, especially in the asymmetric reduction of ketones or enones, both substrate and product are often hydrophobic compounds, which cross the cell membrane by simple diffusion. The mass transfer though the cell membrane depends on the membrane

permeability and the concentration gradient (Equation 3.12). The membrane permeability (P_i) comprises the solubility of the compound in the membrane (indicated by the partition coefficient between the liquid and the membrane), as well as the thickness and the diffusion coefficient of the membrane. The mass transfer is illustrated in Figure 3.7.

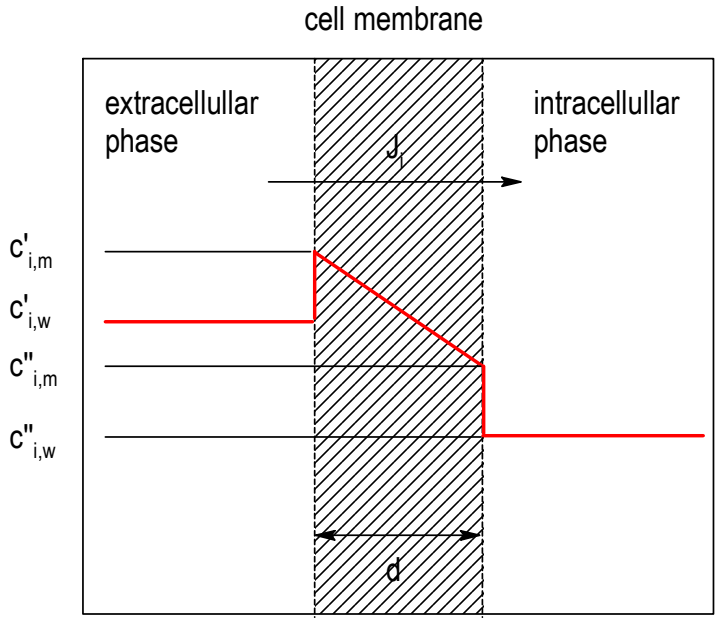

Figure 3.7 Scheme of the diffusion of a lipophilic substance i from the extracellular phase across the cell membrane with a thickness of d into the cell. The course of the concentration in the surrounding liquid ($c_{i,w}$) and in the cell membrane ($c_{i,m}$) are displayed. J_i represents the mass transfer flux density. To simplify, the cell membrane is illustrated as one layer.

$$J_i = P_i \cdot \left(c'_{i,w} - c''_{i,w}\right) = \frac{K_i \cdot D_{i,m}}{d} \cdot \left(c'_{i,w} - c''_{i,w}\right) \qquad \text{Eq. 3.12}$$

J_i	mass transfer flux density, mol s^{-1} m^{-2}
P_i	membrane permeability of i, m s^{-1}
$c_{i,w}$	concentration of i in the surrounding liquid, mol m^{-3}
K_i	partition coefficient of i between the liquid and the membrane, -
$D_{i,m}$	diffusion coefficient of i in the membrane, m^2 s^{-1}
d	thickness of the membrane, m

Interaction of liphophilic molecules with the cell membrane

Though the various types of molecules can be easily transported across the cell membrane without influencing its composition and functionality, some molecules can harm the membrane integrity and cell viability. The toxic effect originates from the accumulation of liphophilic compounds (organic solvents or hydrocarbons) in the membrane bilayer, which depends on the aqueous concentration and the membrane/buffer partition coefficient of the molecules (Sikkema et al. 1994a). As a result of accumulation, the cell membrane loses its integrity and functionality (Sikkema et al. 1994b). This effect is similar for a variety of microorganisms (Heipieper et al. 1994).

Hydrophobicity, expressed by the decadic logarithm of the partition coefficient between octanol and water ($\log P_{o/w}$), indicates the tendency of a compound to dissolve in the cell membrane (Equation 3.13). Generally, partition coefficients are approx. eight times lower in membranes than in octanol (Heipieper et al. 1994). Molecules with similar structure and properties as the phospholipid in the cell membrane, e.g. amphiphatic molecules or compounds with a $\log P_{o/w}$ in the range of 1 – 5, dissolve relatively well in the membranes. In addition, the solubility is also affected by the composition of the cell membrane (Heipieper et al. 1994).

$$P_{o/w} = \frac{c_{i,octanol}}{c_{i,water}} \qquad \text{Eq. 3.13}$$

P	partition coefficient between octanol and water, -
c_i	concentration of the substrate i in the respective phase , mol L^{-1}

3.2.6 Principles of *in situ* substrate supply and product removal

There are several issues to be considered in the process design of biocatalytic reactions either with isolated enzymes or whole cells.

The substrate and product of interest, e.g. prochiral ketone or enone for oxidoreductases as biocatalyst, are often organic compounds with low solubility in aqueous systems. For example, (R)-carvone has a solubility of ~8.8 mmol L^{-1} and forms a second phase, if supplied above the saturation level (Fichan et al. 1999). The solubility can be increased by the addition of solubilizers (e.g. short chain alcohols, dimethyl sulfoxide), which in return can impair the biocatalytic reaction. Depending on the biocatalyst, the substrate

concentration in the aqueous phase can be either rate-limiting for the reaction (depending on the K_M value of the biocatalyst) or even toxic for the biocatalyst.

Some substrates and products are instable in aqueous environment, which is caused either by decomposition, hydrolysis or isomerisation. An example is the industrially valuable chiral product (R)-levodione, which racemises with a rate of −3 % ee per hour in aqueous environment (Fryszkowska et al. 2009). (R)-Levodione is used as a precursor for the production of carotinoids, e.g. zeaxanthin and crytoxanthin (Leuenberger et al. 1976).

For biocatalytic processes, substrate and product inhibition of the enzyme has to be taken in account. Thereby, the reaction rate can be significantly reduced by higher substrate or product concentration. Product inhibition can occur in a competitive, uncompetitive and non-competitive fashion. In contrast substrate inhibition is a special form of uncompetitive inhibition (Bisswanger 2008).

In addition, the stability of all enzymes participating in the reaction can be impaired by the substrate or product. Especially in case of applying enzyme-coupled cofactor regeneration, stability and enzyme properties of the cofactor-regeneration enzymes can be critical for the productivity of the reaction. For example, the half-life of formate dehydrogenase mutants is reduced from > 200 h to ≤ 0.2 h by increasing the concentration of α-haloketones (Hoelsch et al. 2012).

In case of whole-cell biotransformation, the loss of membrane integrity by accumulation of lipophilic product and substrates and subsequent cofactor leakage has to be considered (Bräutigam et al. 2009).

All in all, the substrate and product concentration in the aqueous phase can severely influence the reaction rate and the stability of the biocatalyst. Sometimes, the biocatalyst has to be protected from high substrate and product concentrations. As biocatalytic reactions in aqueous monophasic systems are accompanied by the described problems, several forms of biphasic process setups have been developed to solve these problems by enabling *in situ* substrate feeding and product removal (SFPR). Thereby, the substrate and product concentration in the aqueous phase, in which the biocatalytic reaction occurs, is kept at a minimal level by using a second water-immiscible liquid or solid phase for substrate supply and *in situ* product extraction. In liquid-liquid reaction systems, organic solvents and non-conventional solvents, such as ionic liquids or supercritical fluids, can be applied as a second phase (Matsuda 2013; Weuster-Botz 2007). Bioprocesses with a solid-liquid reaction

system generally use polymeric adsorbent resins as a second phase (Vicenzi et al. 1997). Both technologies of *in situ* substrate feeding and product removal were applied in this project and will be described in detail in the next sections.

3.2.7 Biphasic reaction systems with ionic liquids

In a liquid-liquid biphasic reaction system, the biocatalyst is suspended in the aqueous buffer phase and the second water-immiscible phase serves as substrate reservoir and *in situ* product extractant. This is illustrated for a biotransformation involving ene-reductases in Figure 3.8. Thereby, a large distribution coefficient of substrate and product is desired, allowing large quantities of substrate in the second phase while keeping the concentration low in the aqueous phase (Equation 3.14, 3.15). In case of toxic, low soluble or instable substrate or product, conversion and yield can be increased using a biphasic mode. Furthermore, the product isolation is facilitated due to the *in situ* extraction of a large amount of product, reducing the cost for downstream processing (Bräutigam et al. 2009; Pfruender et al. 2004).

$$D_{1/2} = \frac{c_{i,phase\ 1}}{c_{i,phase\ 2}} \qquad \text{Eq. 3.14}$$

D	distribution coefficient, -
c_i	concentration of the substrate i in the respective phase, mol L^{-1}

$$D_{IL/buffer} = \frac{c_{i,ionic\ liquid}}{c_{i,buffer}} \qquad \text{Eq. 3.15}$$

D	distribution coefficient, -
c_i	concentration of the substrate i in the respective phase, mol L^{-1}

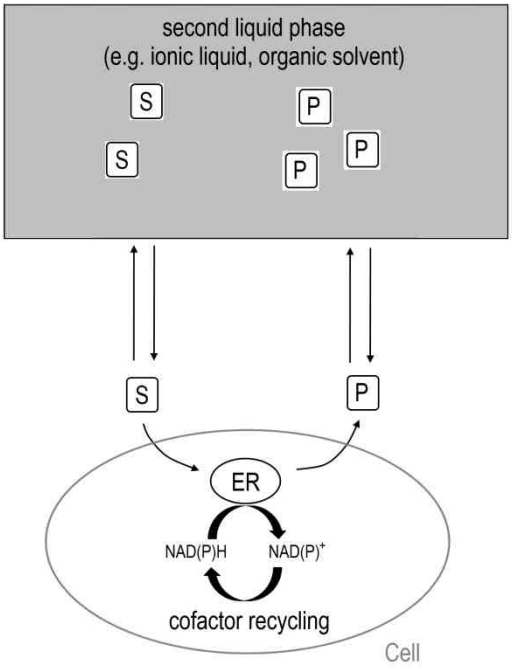

Figure 3.8 Biphasic biotransformation with a second liquid phase (e.g. ionic liquid or organic solvent) for *in situ* substrate feeding product removal. Enzymes (ene-reductases, ERs) can be protected within the cell in case of whole-cell biotransformation. Possible side reactions are not depicted.

However, the biocompatibility of the second water-immiscible phase has to be guaranteed. The negative effect on biocatalytic activity and stability of enzymes and whole-cells can be divided into molecular toxicity and phase toxicity. Molecular toxicity derives from the molecules dissolved in the aqueous phase (Bar 1988; Vermue and Tramper 1995), which can disintegrate the cell membrane in case of whole-cell biocatalysis or result in enzyme denaturation by displacement of the hydration shell of the protein in case of enzymatic reactions (Vermue and Tramper 1995). In contrast, phase toxicity occurs at the interface between the aqueous and the water-immiscible phase. In case of whole-cell biotransformation, the disruption of the cell membrane is considered as the key toxic effect (Vermuë et al. 1993). Using isolated enzymes, the denaturation depends on the total interfacial area which enzymes are exposed to (Vermue and Tramper 1995). Several studies have proven the better biocompatibility of water-immiscible ionic liquid compared to organic solvents (Bräutigam et al. 2009; Weuster-Botz 2007). Thus, the biphasic reaction system using ionic liquids is discussed in the following.

Characteristics of ionic liquids

Ionic liquids (ILs) are defined as salts, generally composed of an organic cation and an inorganic polyatomic anion, with a melting point below 100 °C. The key features of ILs comprise the non-volatile, non-flammable character, high chemical and thermal stability, low viscosity and low vapor pressure, which are derived from the large and asymmetric structure of the composing anion and cation (Dennewald and Weuster-Botz 2012). These ionic solvents show a broad temperature range of ~300 K between the melting point and boiling point. Ionic liquids can even be liquid at room temperature, which are then denoted as "room temperature ionic liquids" (RTILs) (Seddon et al. 2000). In contrast to organic solvents, which are often volatile, flammable and toxic, ILs represent a more secure and environmental friendly alternative. In addition, the physical properties, such as hydrophobicity, viscosity, acidicity/basicity and water miscibility can be adjusted by modifying the structure of the composing anion and cation, which leads to the name "designer solvents" (Seddon 1997). Consequently, suitable and biocompatible ILs can be designed for an efficient biocatalytic process (Dennewald and Weuster-Botz 2012; Gamenara et al. 2012; Zhao 2012). Successful examples were reported for whole-cell biotransformations with a second water-immiscible IL-phase on a preparative scale (Bräutigam et al. 2009; Dennewald et al. 2011).

Several criteria have to be fulfilled for an application of ILs biocatalysis. The biocompability of the solvent represents one critical point for biocatalytic processes. The IL used as solvent or second water-immiscible phase should not harm the biocatalyst or inhibit the reaction. As a general rule for IL selection: The longer the alkyl substituent of the cation, the lower is the tolerance of the organisms toward the solvent (Matsumoto et al. 2004; Pernak et al. 2003). Cations with longer alkyl chains are more lipophilic than those with shorter alkyl chains, and thus show higher solubility in the lipid bilayer of the cell membrane, leading to accumulation and subsequent membrane disintegration and cell toxicity. Depending on the length of the alkyl substituent of the cation, disintegration of the membrane was observed to present as small holes up to total disruption (Evans 2006; Evans 2008). In contrast, the cation head group and the anion have only little effect on the toxicity (Pernak et al. 2003). Regarding the anion, hydrolysis in water was reported for $[BF_4]$, resulting in the formation of acidic compounds and subsequent cell toxicity (Ganske and Bornscheuer 2006). If an appropriate water-immiscible IL is chosen, the biocompatibility

with whole cells can be notably higher compared to organic solvents, because the disintegration of cell membranes is minimized using ILs (Weuster-Botz 2007).

Consistent purities, good availability and high chemical and thermal stability during and subsequent to the biocatalytic process are desirable properties for the IL of choice (Dennewald and Weuster-Botz 2012). In general, ILs show high chemical and thermal stabilities with scarce degradation up to ~200 °C (Kosmulski et al. 2004). Constant stability and quality are also criteria for the recyclability of ILs, lowering the waste production and process cost. The recyclability for ILs has been proven by Dennewald et al. (2011) in 25 subsequent batch biotransformations.

For whole-cell biotransformations, biphasic reaction setups with a second water-immiscible phase are generally preferred. In contrast to monophasic reaction system, where IL can be employed as solvent or cosolvent, the second IL phase in biphasic setup can serve as substrate reservoir and for product removal, limiting the concentration in the aqueous buffer phase at a non-toxic level for the biocatalyst (Dennewald and Weuster-Botz 2012). Thereby, ionic liquids with log$D \geq 2$ in the ionic liquid /buffer system are recommended (Pfruender et al. 2006). In addition, product purification is facilitated in biphasic systems, because the two phases can be separated through gravitational forces and the product can be recovered by distillation, pervaporation or extraction (Dennewald and Weuster-Botz 2012). The structures of cations and anions of the ionic liquids used in this project are presented in Figure 3.9.

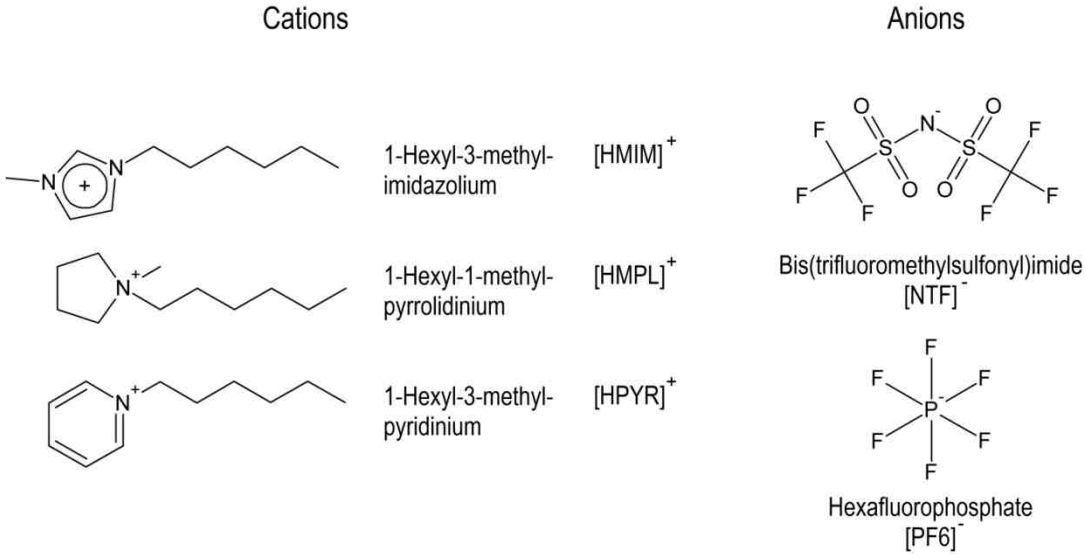

Figure 3.9 Structures of cations and anions of the ionic liquids used in this project.

Characterization of liquid-liquid dispersions

Biphasic reaction systems with a second water-immiscible ionic liquid phase can be beneficial for whole-cell biotransformations. Such systems can be described by the characteristics of liquid-liquid dispersions.

Dispersion is defined as a mixture of at least two immiscible liquids, which form two separate phases without agitation. Induced by the hydrodynamic forces caused by mixing, the liquid of the smaller volume usually forms the dispersed phase with the other liquid as the continuous phase around it. It has to be noted, that the viscosity or other physical properties of the liquids also determine which one would form the dispersed phase (Leng and Calabrese 2004).

The mass transfer between the dispersed phase and the continuous phase mainly depends on the interfacial area, which in turn depends on the drop size of the dispersed phase. Smaller drop size would naturally result in larger interfacial area and thus better mass transfer. The drop size distribution is derived from the equilibrium of the phase disruption and the coalescence of the drops, and thus can be controlled by the stirrer type and speed.

The two-film theory is generally applied for describing the mass transfer between two liquid phases (Lewis 1954; Lewis and Whitman 1924). This model is illustrated in Figure 3.10. Thereby, boundary layers on each side of the interface are represented as fluid films with a thickness δ. The mass transfer from one phase to another occurs via molecular diffusion with the diffusion through both fluid films as the rate limiting step. The concentrations of the substance in the two phases are determined by the distribution coefficient, and a thermodynamic equilibrium is assumed in this model. If one phase is favored due to the larger diffusion coefficient of the compound and appropriate corresponding distribution coefficient, the two-film model can be reduced to an one-film model (Leng and Calabrese 2004).

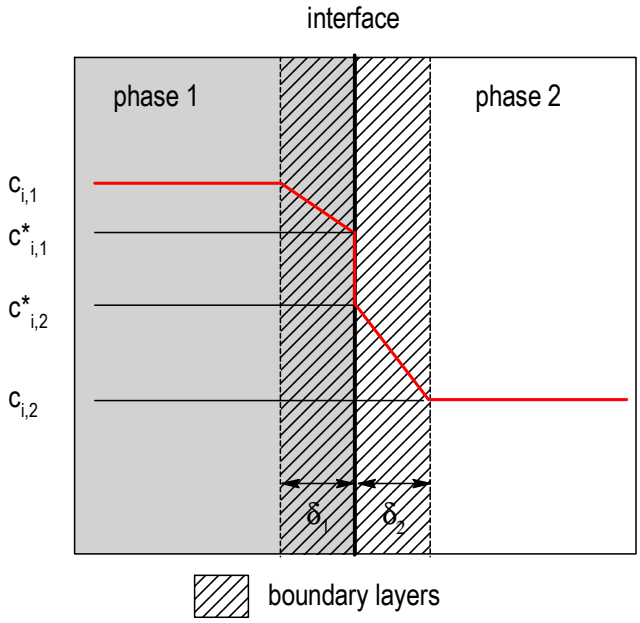

Figure 3.10 Illustration of the two-film model for describing mass transfer in liquid-liquid dispersions. The course of concentration of the compound i in the bulk phase 1 ($c_{i,1}$), at the interface of phase 1 ($c^*_{i,1}$), at the interface of phase 2 ($c^*_{i,2}$) and in the bulk phase 2 ($c_{i,2}$) are shown. The thickness of the boundary layer is defined as δ.

3.2.8 Solid-liquid reaction systems with adsorbent resins

A further development using polymeric adsorbents as “solid extractant” circumvents the problem of molecular and phase toxicity, which often occurs in case of biphasic liquid-liquid reaction systems. Thereby, substrate supply and product removal occurs *in situ* via adsorption onto the high surface area of a solid organic phase, provided by polymeric adsorbent resins. The main driving force is the hydrophobic interaction between the nonpolar substrate and product with the nonpolar resin surface. This technology is denoted as resin-based *in situ* substrate feeding and product removal (resin-based SFPR). As resins are completely insoluble in the aqueous phase, inhibition of biocatalysts by molecular toxicity can be prevented. Also damages induced by phase toxicity can be eliminated, because > 99.9 % of the interfacial area is within the pores of the polymeric resin, reducing the interface with actual contact to enzymes or whole cells (Vicenzi et al. 1997). This technology is presented in Figure 3.11 and discussed in the following.

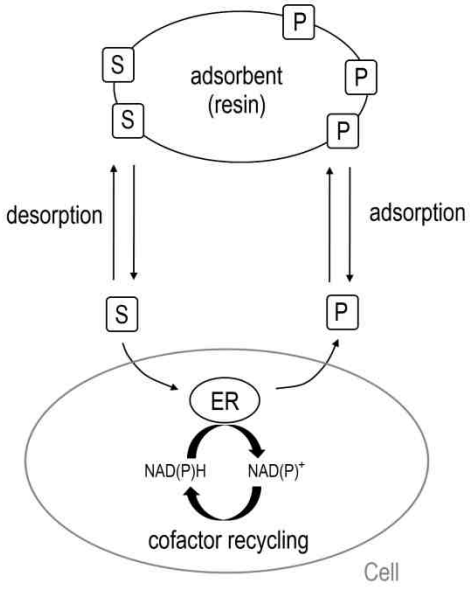

Figure 3.11 *In situ* substrate feeding and product removal using adsorbent resins. Enzymes (ene-reductases, ERs) can be protected within the cell in case of whole-cell biotransformation. Possible side reactions are not depicted.

Characteristics of resins

Resins are porous, synthetic beads with a high polymeric surface area. A variety of polymer types and different sizes of particles and pores are available for different kind of applications. If the appropriate adsorbent resin is used, desired components or contaminants can be separated from a reaction mixture (Katoh and Yoshida 2011). The structure of the adsorbent resin (Amberlite^{TM} XAD4) which was used in this project is exemplarily given in Figure 3.12.

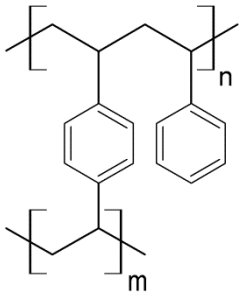

Figure 3.12 The structure of the adsorbent resin Amberlite^{TM} XAD4.

For biocatalytic applications, there are several desired criteria for the selection of resins: (i) a large surface area per unit volume for high adsorbent capacity, (ii) high degree of selective binding but minimized non-specific binding, (ii) high mechanical and chemical stability during the reaction and subsequent product isolation, (iii) low cost, (iiii) biocompatibility and (iv) recyclability (Lye and Woodley 1999). In special, a high affinity for the product is desired, but the affinity for the substrate should not be too high, because this would limit the substrate availability for the biocatalyst and make a complete conversion difficult (Vicenzi et al. 1997).

Generally, high biocompatibility is guaranteed due to the negligible molecular and phase toxicity effects. Nevertheless, it has been proposed that the mechanical shear forces induced by agitated resin beads reduced cell viability in whole-cell biotransformation using growing cells. The resin beads itself show high mechanical and chemical stabilities and were not impaired by higher shear forces (Vicenzi et al. 1997). In addition, product isolation is facilitated, because resins can be easily removed from the reaction medium by filtration. Whereas the resin beads are collected for recycling, enzymes and cells can pass through. After desorption of the desired product by e.g. solvent extraction, resins can be recycled and reused for multiple cycles after a wash step for replacement of the organic molecules by water (Hilker et al. 2005; Vicenzi et al. 1997). The scalability of biotransformations using the resin-based *in situ* SFPR strategy was also proven by Hilker et al. (2005).

Characterization of solid-liquid reaction systems

In general, adsorption can be described as a process, where a substance (solute) in a fluid accumulates on the surface of a suitable solid phase (adsorbent) due to van der Waals, electrostatic or other interactions (Katoh and Yoshida 2011). The adsorption mechanism can be described in three consecutive steps: (i) mass transfer of the solute from the bulk liquid phase to the adsorbent particle surface; (ii) diffusion within the internal structure of the particle to the adsorption site and (iii) the rapid uptake of the solute (Scordino et al. 2003). Both the equilibrium in adsorption, which indicates the affinity between the solute and adsorbent, and the rate of adsorption as a function of time defines the adsorption process.

The monolayer adsorption at equilibrium (balanced rate of adsorption and desorption) is described by the Langmuir isotherm, presuming that the solutes are reversibly adsorbed at homogenous, energetically identical adsorption sites (Equation 3.16). However, at solid-liquid interfaces, the adsorption proceeds beyond a monolayer, therefore the Freundlich

isotherm represents the superior model in that case. This empirical model describes non-ideal adsorption at heterogenous surfaces and is generally applied in practice (Equation 3.17). The capacity of the polymeric adsorbent for a particular solute is indicated by the adsorption isotherm, in particular by the Freundlich constant K_F (Katoh and Yoshida 2011; Scordino et al. 2003).

$$q_s = \frac{K_L C_s}{1 + a_L C_s} \qquad \text{Eq. 3.16}$$

q_s	solute concentration per unit of weight of adsorbent, mg g^{-1}
C_s	solute concentration in the fluid phase, mg L^{-1}
K_L	Langmuir constant, L g^{-1}
a_L	adsorption constant, which indicates the ratio between adsorption and desorption rate constants, L mg^{-1}

$$q_s = K_F \cdot C_s^{b_F} \qquad \text{Eq. 3.17}$$

q_S	solute concentration per unit of weight of adsorbent, mg g^{-1}
C_S	solute concentration in the fluid phase, mg L^{-1}
K_F	Freundlich constant (empirical), L g^{-1}
b_F	empirical adsorption constant, -

The rate of an adsorption process depends on the rate-limiting step, which can change from the mass transfer across the fluid film around the adsorbent to the diffusion within the pores during the adsorption process. In general, the rate of adsorption is proportional to the solute concentration and the number of unoccupied adsorption sites (Katoh and Yoshida 2011).

3.3 Asymmetric reduction of alkenes: chemical methods vs. biocatalysis

The asymmetric hydrogenation of C=C bonds is one of the most widely employed reactions for the production of chiral molecules in chemical industry, because up to two stereogenic centers can be generated in one reaction (Stuermer et al. 2007). As a consequence, asymmetric hydrogenation is one of the emerging chemical fields with high impact on pharmaceutical and chemical industries (Pollard and Woodley 2007).

Homogeneous metal catalysts and organocatalysts

Typically, homogeneous metal catalysts are applied for selective transformations (Bonrath et al. 2012). Especially the field of *cis*-hydrogenation has reached industrial standard using phosphorus containing metal catalysts originating from the work of Knowles and Noyori (Knowles 2002; Noyori 2002). Thereby, optically active BINAP (2,2´bis(diphenylphosphanyl)-1,1´-binaphthyl) in complex with Rh or Ru are predominantly applied as catalysts. BINAP-Rh complexes are industrially used in asymmetric isomerization for the synthesis of (-)-menthol (Knowles 2002). BINAP-Ru complexes are preferred for the asymmetric hydrogenation of various functionalized olefins, e.g. unsaturated carboxylic acids. Prominent examples are the production of naproxen or citronellol (Noyori 2002).

Though phosphorous metal complexes have achieved great success in the asymmetric reduction of unsaturated compounds, major drawbacks comprise (i) the air sensitivity of catalysts, (ii) complicated catalyst synthesis, (iii) removal of metal impurities and above all (iv) the low catalytic efficiency with olefins with aprotic oxygen functionalities as ketones, esters or imines (Dobbs et al. 2000; He and Fan 2010; Ohta et al. 1995; Yang et al. 2004). Approaches using metal-free organocatalysts still have to deal with the reduced atom economy of the process, since molar amounts of the catalyst are required (List and Yang 2006; Ouellet et al. 2005). Enzymes as biocatalysts offer great opportunities in the field of asymmetric hydrogenation to overcome limitations of chemical synthesis, thereby providing economic and ecological benefits.

Biocatalysts

Enzymes that catalyze the reduction of C=C bonds are denoted as “ene-reductases” or “enoate reductases”, often regardless of the respective enzyme class (Durchschein et al. 2012a; Rohdich et al. 2001; Winkler et al. 2012). In general, these enzymes originate from four enzyme classes, which are depicted in Figure 3.13.

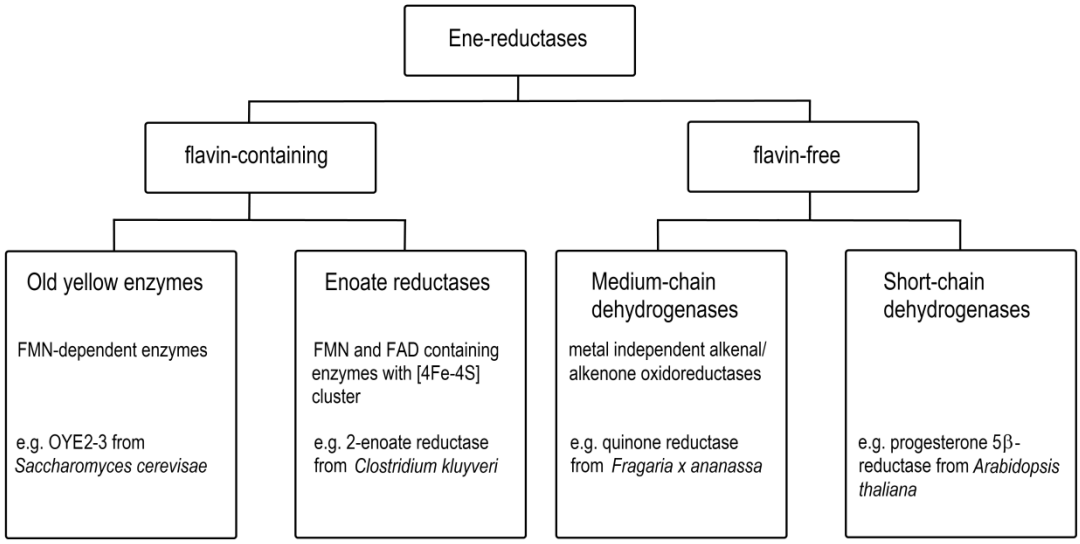

Figure 3.13 Classification of ene-reductases capable of reducing C=C bonds.

Enoate reductases [EC 1.3.1.31] (or 2-enoate reductases), introduced by Simon et al. in 1975, are capable of catalyzing the reduction of weakly-activated 2-enoates, as well as α,β-unsaturated aldehydes, ketones and β,β-disubstituted aromatic nitroalkenes. These enzymes are NADH-dependent and contain flavin mononucleotide (FMN), flavin adenine dinucleotide (FAD), and a [4Fe-4S] cluster to enable the transfer of electrons. Consequently, the presence of oxygen strongly deactivated these enzymes which were generally isolated from anaerobic *Clostridium* species (Fryszkowska et al. 2008; Rohdich et al. 2001; Simon 1992). Strictly anaerobic conditions are required for enzyme purification and catalysis, thus restricting the industrial application of 2-enoate reductases (Stuermer et al. 2007).

Ene-reductase activities were found in enzymes from the medium chain and short chain dehydrogenase/reductase (MDR and SDR) superfamilies. These ene-reductases do not possess flavin as prosthetic group, but require NAD(P)H - preferably NADPH - for catalysis. In special, the leukotriene B_4 dehydrogenase (LTD) subfamily from the zinc-independent MDR superfamily harbor enzymes capable of C=C bond reduction. Examples are NtDBR from *Nicotiana tabacum* or quinonereductase (FaEO) from *Fragaria x ananassa*

(strawberry) (Clish et al. 2000; Durchschein et al. 2012a; Mansell et al. 2013). One example for an ene-reductase from the SDR superfamily is progesterone 5β-reductase (At5β-StR) from *Arabidopsis thaliana* (Durchschein et al. 2012a). These enzymes preferably reduce open chain enals, nitroalkenes, α,β-unsaturated γ-butyrolactones, but often exhibit narrow substrate spectra and low enzyme activities (Durchschein et al. 2012a; Mansell et al. 2013). As the potential of flavin-free ene-reductases has been discovered only recently, little is known about the catalytic efficiency and industrial applicability of these biocatalysts.

The most prominent group of ene-reductases belongs to the old yellow enzyme (OYE) family [EC 1.6.99.1], which was first described in 1933 (Warburg and Christian 1933). These NAD(P)H and FMN-dependent enzymes are capable of reducing a remarkably broad spectrum of activated alkenes in a *trans*-specific fashion, ranging from α,β-unsaturated aldehydes, ketones, imides to nitriles, carboxylic acids and nitroalkenes (Toogood et al. 2010; Winkler et al. 2012). Consequently, these enzymes are considered as promising biocatalysts for the asymmetric reduction of alkenes (Simon and Karl 2010; Wenda et al. 2011). Ene-reductases from the OYE-family represent the focus of this work and will be further referred to as ERs.

3.4 Ene-reductases from the old yellow enzyme family

Ene-reductases from the old yellow enzyme family have received much attention in the last years due to their broad substrate acceptance and high stereoselectivity in the *trans*-specific reduction of activated alkenes, and therefore, have high potential as biocatalysts for industrial applications (Simon and Karl 2010; Winkler et al. 2012).

Since the discovery of OYE1 from baker´s yeast (*Saccharomyces pastorianus*) in 1933, which was the first identified flavoprotein (Warburg and Christian 1933), many ERs have been found widely distributed in bacteria, fungi and plants (Stuermer et al. 2007; Toogood et al. 2010). Given the diversity of OYE members, their physiological roles are found in various pathways, e.g. in the biosynthesis of fatty acids and secondary metabolites, such as morphine (Barna et al. 2002; French and Bruce 1994) or jasmonic acid (Schaller et al. 2000). Some ERs are involved in oxidative stress responses (Brige et al. 2006; Ehira et al. 2010; Fitzpatrick et al. 2003), others catalyze reactions in the detoxification of xenobiotics, such

as nitro esters or nitro aromatics (Blehert et al. 1999; Snape et al. 1997; Williams et al. 2004).

3.4.1 Structure and classification

Despite the diversity of members from the OYE family, residues involved in catalysis, FMN and substrate binding are highly conserved in ERs. All OYEs show an eight stranded (α/β)-barrel (TIM barrel)-fold, surrounded by additional secondary structure elements (α-helices and β-strands). This central β-barrel is covered at the N-terminal portion by a β-hairpin lid. The key element of ERs is the non-covalently bound FMN cofactor, which is positioned at the C-terminal edge of the β-barrel with its si-face accessible to substrates and solvent. The substrate and cofactor binding site is defined by the loops connecting the central β-strands with the adjacent α-helices (Breithaupt et al. 2009; Fox and Karplus 1994; Kitzing et al. 2005).

Based on amino acid sequence alignments, ERs can be divided in two subclasses (Toogood et al. 2010). Both subclasses reveal individual conserved patterns, which also allow the differentiation into monomeric and oligomeric enzymes (Oberdorfer et al. 2011). Members of the ‘‘classical’’ subclass, such as PETNR from *Enterobacter cloacae st.* PB2, are presumed to be monomeric enzymes (Fryszkowska et al. 2009). In contrast, ERs active as dimers, e.g. Yqjm from *Bacillus subtilis*, belong to the ‘‘thermophilic-like’’ subclass (Fitzpatrick et al. 2004).

3.4.2 Reaction types and catalytic mechanism

ERs from the OYE-family are known for their catalytic promiscuity, predominantly derived from the versatility of the flavin cofactor (Hult and Berglund 2007; O'Brien and Herschlag 1999). In the following, the main reactions catalyzed by these enzymes are described.

Reduction of activated alkenes as the main catalytic reaction

The most prominent and industrial relevant reaction catalyzed by ERs is the reduction of electronically activated C=C bonds, e.g. enones or enals. Because this reaction resembles a Michael-type addition, the presence of an electron-withdrawing group of the substrate is

essential for catalysis (Stuermer et al. 2007). In addition, also acetylenic triple bonds are converted into corresponding (E)-alkenes (Müller et al. 2007).

Asymmetric reduction of alkenes catalyzed by ERs proceeds in two steps via a ping pong bi-bi mechanism with both reductive and oxidative substrates binding within the same active site (French and Bruce 1994). The reductive half reaction involves a hydride transfer from NAD(P)H to the N5 atom of the FMN cofactor. In the oxidative part of the reaction, the same hydride of the reduced FMN is stereoselectively transferred onto Cβ of the substrate, while a solvent derived proton is added via a Tyr residue to Cα from the opposite side. As a result, the overall addition of [2H] proceeds in a *trans*-fashion with absolute stereoselectivity (Fox and Karplus 1994; Kohli and Massey 1998; Messiha et al. 2005). The catalytic mechanism is depicted in Figure 3.14. In general, the (R)-enantiomeric product is formed (Hall et al. 2008a; Mueller et al. 2010b). However, a flipped-binding mode for some substrates exists, which can result in low enantioselectivities or even in the formation of the opposite enantiomer (Barna et al. 2001). Thereby, positions of substituents of the molecule can determine the stereochemical outcome (Hall et al. 2008b).

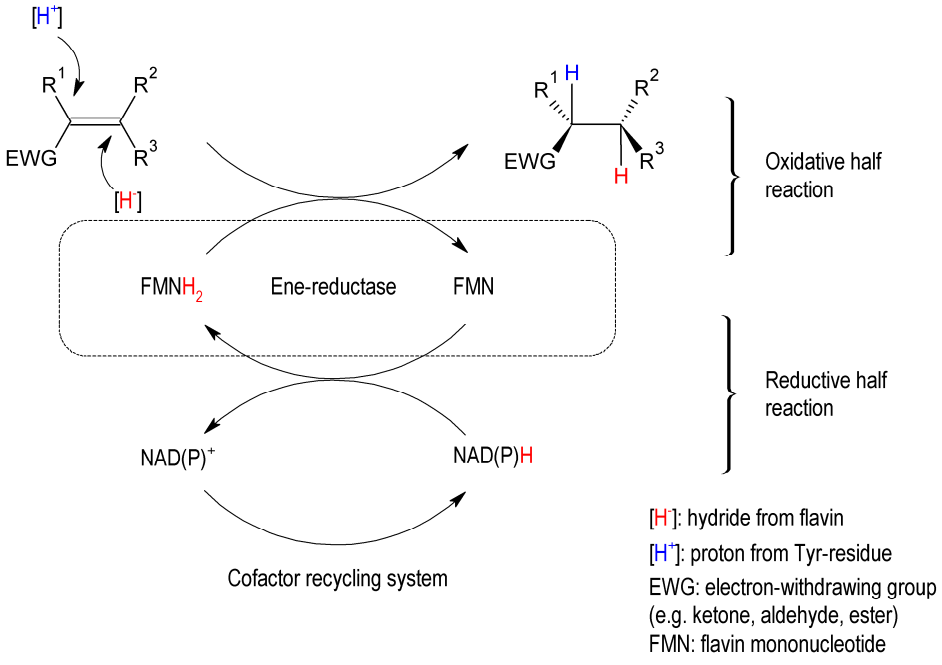

Figure 3.14 Reaction mechanism of the asymmetric reduction of activated alkenes by ene-reductases (modified from Winkler et al. (2012)). Cofactor recycling can be enabled by e.g. enzyme-based methods using formate dehydrogenase or glucose dehydrogenase.

Both NADH and NADPH are accepted as hydrogen donors, but NADPH is in most cases clearly preferred and considered to be the physiological substrate (Kohli and Massey 1998). The ratio of activities with NADPH compared to NADH as cofactor is in a range of 0.02 – 17 (Chaparro-Riggers et al. 2007; Fryszkowska et al. 2009; Mueller et al. 2010a; Williams et al. 2004).

With respect to the oxidative half reaction, the physiological oxidant is unknown for most ERs due to the diversity of OYE members. Molecular oxygen can serve as oxidant, but observed rates are marginal compared to substrates as such as enones (Fox and Karplus 1994). Though molecular oxygen can compete with the desired reaction, reducing enzyme activities up to 48 % (Fryszkowska et al. 2009), most ERs are studied under aerobic conditions due to the difficulties of anaerobic bioreactions in large-scale processes (Fryszkowska et al. 2012).

Side reactions of ene-reductases

Beside the predominant reaction, catalysis of disproportionation (or dismutation) by ERs was observed as well (Vaz et al. 1995). This reaction is considered as a side reaction with low reaction rates derived from the catalytic promiscuity of OYEs (O'Brien and Herschlag 1999). Thereby, the hydride transfer proceeds via flavin from one substrate (e.g. 2-cyclohexen-1-one as H-donor) onto Cβ of a second substrate (e.g. another 2-cyclohexen-1-one as H-acceptor), which is reduced subsequently. A driving force of ca. -30 kcal M^{-1} is provided by the spontaneous tautomerization of the resulting conjugated dienone into a phenol. The overall reduction is nicotinamide-independent (Stueckler et al. 2010; Vaz et al. 1995). In order to create a directed redox process, a combination of a substrate, which is only reduced and a cosubstrate, which is only oxidized, can be applied. For example an α-substituted enone which can be quickly reduced by ERs can be used as H-acceptor, whereas a β-substituted enone with low reactivity can serve as H-donor. This reaction is depicted in Figure 3.15A.

Recently, some ERs were found to be able to catalyze redox-neutral isomerization reactions as another side activity. Thereby, a γ-butyrolactone bearing an *exo*-methylene unit was transformed to the thermodynamically more favoured endo-isomer. The saturated lactone was formed as minor product by the reduction of C=C bond. Reduced flavin and nicotinamide cofactors (preferably NADH) are required for this reaction. A mechanism, where the isomerization proceeds through FMN-mediated hydride addition onto exo-Cβ

followed by hydride abstraction from endo-Cβ´ was proposed by Durchschein et al. (2012b) and is shown in Figure 3.15B.

Additionally, in case of the degration of β-β-disubstituted nitroalkenes, ERs were to found to form carbonyl compounds. Two types of pathways were proposed strongly depending on the nature of enzymes and substrate substitutions (Durchschein et al. 2011). In the Nef-pathway, the formed nitroalkane is reduced in multiple steps (via a nitroso-intermediate and spontaneous tautomerization to an oxime) to an imine, which hydrolyzes in aqueous solution yielding a carbonyl compound and ammonia (Durchschein et al. 2010). Alternatively, XenA from *Pseudomonas putida* was found to preferably reduce the nitro-moiety instead of the C=C bond furnishing the corresponding nitroso-alkene which results in oxazete formation due to spontaneous electrocyclization. At elevated temperatures, the corresponding ketone is formed while HCN is released (Durchschein et al. 2011). Both reactions are shown in Figure 3.15C. Furthermore, ERs are also known to catalyze the dearomatisation of nitroaromatic compounds (e.g. the conversion of 2,4,6-trinitrotoluene (TNT) to a Meisenheimer-monohydride complex) and the reduction of nitrate esters and nitroamines, thereby liberating nitrite ions (Khan et al. 2002; Williams et al. 2004).

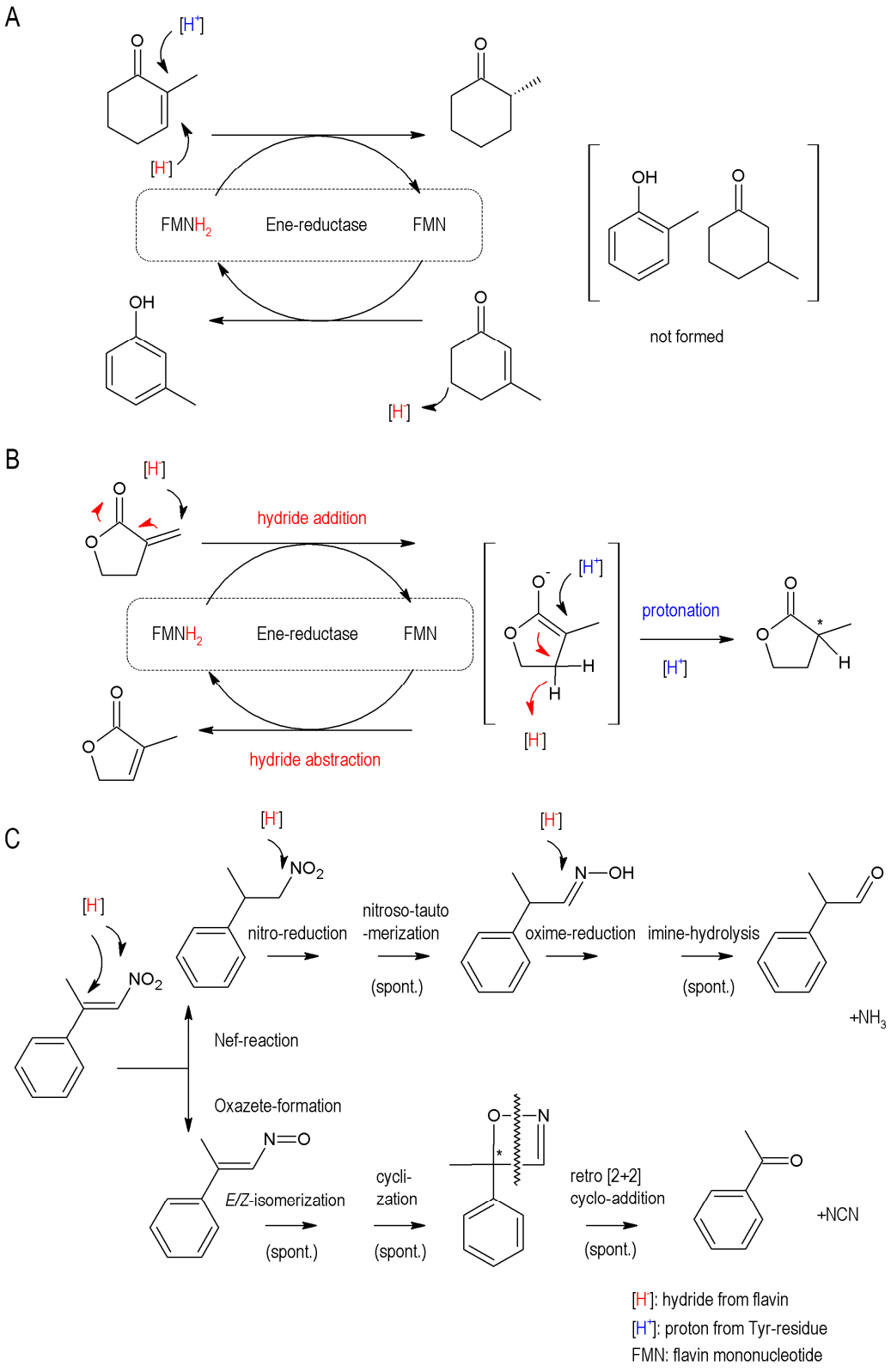

Figure 3.15 Side reactions catalyzed by ene-reductases: (A) The disproportionation reaction using 2-methylcyclohexen-1-one and 3-methylcyclohenxenone forms substituted cyclohexanone and phenol. (B) The isomerization of α,β-unsaturated γ-butyrolactones competitive to the reduction of C=C bonds to form the saturated product. (C) The reductive conversion of a β-β-disubstituted nitroalkene via the Nef-pathway versus the oxazete formation. Reaction schemes were adapted from Stueckler et al. (2010), Durchschein et al. (2012b) and Durchschein et al. (2011).

3.4.3 Substrate spectrum and stereoselectivities

As the reduction of alkenes bearing an electron-withdrawing group is the main reaction catalyzed by ERs from the OYE-family, the following section focuses on the diversity of activated alkenes and their acceptance by ERs.

The substrate spectrum of these enzymes comprise α,β-unsaturated ketones (enones), aldehydes (enals), carboxylic acids or esters, as well as imides, nitroalkenes and nitriles.

Enones, e.g. substituted cyclohexenones or cyclopentenones, are generally considered as reactive substrates. Thereby, size and position of substituents strongly influenced the enzyme activity (Swiderska and Stewart 2006). Prominent substrates of commercial interest are ketoisophorone and carvone (Winkler et al. 2012). The reduction of ketoisophorone by ERs furnished (R)-levodione, which is used as a precursor for the production of carotinoids, for example zeaxanthin and cryptoxanthin (Leuenberger et al. 1976). (R)- and (S)-carvone belonging to the group of terpenes due to their isoprene subunits are converted to (2R,5R)- and (2R,5S)-dihydrocarvone, respectively. These reduction products are key intermediates in the production of natural products, antimalarial drugs and valuable chiral building blocks (Choi et al. 1998; de Rouville et al. 2009; Lowe et al. 2009).

Enals are quickly converted into saturated aldehydes by ERs. A prominent example is citral (also a terpene), which is reduced to (S)-citronellal, a valuable precursor for the production of (-)-menthol (Müller et al. 2006).

Cyclic imides, e.g. maleimides and derivatives, are reduced with high reaction rates (Hall et al. 2008b; Mueller et al. 2010a).

α,β-Unsaturated nitroalkenes are also readily reduced by ERs to corresponding chiral nitroalkanes (Hall et al. 2008a; Toogood et al. 2008), but often furnishing a product mixture due to catalytic promiscuity of ERs as shown in Figure 3.15C (Durchschein et al. 2011; Durchschein et al. 2010).

The acceptance of *α,β-unsaturated carboxylic acids or esters* (enoic acids or enoates) by ERs depends on their degree of electronic activation. Mono-carboxylic esters are typically not easily accepted by members from the OYE family (Yanto et al. 2011). Higher electronic activation by an additional halogen atom, a second ester or nitrile group is required for the catalysis by ERs (Brenna et al. 2011a; Brenna et al. 2011b; Brenna et al. 2012c; Stueckler et al. 2007; Winkler et al. 2013). In case of α,β-unsaturated carboxylic esters, an additional α-

halogen atom as substituent promotes the enzyme activity (Brenna et al. 2011a; Tasnádi et al. 2012). On the contrary, a cyano group turned out to be a poor activating group on the α-position (Tasnádi et al. 2012), but supporting on the β-position (Winkler et al. 2013). In addition, β-alkyl or β-aryl lowered the reactivity of non-halogenated substrates (Tasnádi et al. 2012).

Overall, the degree of C=C polarization based on the electro-withdrawing group in combination with steric effects of substituents, especially at the Cβ-position, strongly influenced the catalytic efficiency (Tasnádi et al. 2012). In addition, (E/Z)-configuration of alkenes, especially enals, enoates and nitroalkenes, was shown to be crucial for the substrate recognition and the stereochemical configuration of the product (Stueckler et al. 2007; Toogood et al. 2008).

In general, the (R)-product is formed in the reduction of C=C bonds catalyzed by the majority of ERs (Toogood et al. 2010). But, in order to gain access to both stereoisomers of a desired product, e.g. in the drug discovery stage, several strategies were developed. On the one side, different enzymes can be applied to achieve the desired enantiomer, which is termed as enzyme-based stereocontrol. In the reduction of 1-nitro-2-phenylpropene, OPR1 from *Lycopersicon esculentum* formed the (R)-product, whereas OPR3, also from *Lycopersicon esculentum*, as well as Yqjm from *Bacillus subtilis* yielded the (S)-product (Hall et al. 2008a). A structural investigation revealed a correlation of observed stereospecificities with the distance of two residues within the enzymes´ active site (Oberdorfer et al. 2011). Nevertheless, the enzyme-based stereocontrol is limited to several ERs and substrate groups. On the other side, the stereochemical outcome can be controlled by substrate-engineering through size-variation of the substituents and by employing stereochemically pure (E)-or (Z)-isomers as substrate. This strategy is denoted as substrate-based stereocontrol and mainly applied for nitroalkenes, α,β-unsaturated carboxylic acids or esters, α,β-unsaturated alkoxy ketones and open-chain α-alkyl-β-aryl-alkenes (Brenna et al. 2013a; Brenna et al. 2012a; Brenna et al. 2012c; Stueckler et al. 2007; Winkler et al. 2010; Yanto et al. 2011).

The diastereomeric and enantiomeric excess of the product depend on the enzyme properties and reaction conditions.

- First of all, the stereoselectivity strongly depends on the nature of the active site of the enzymes, which varies substantially between ERs (Hall et al. 2008a; Toogood et al. 2010). Thereby, enzyme-catalyzed racemization results in low selectivities.
- Racemization can also proceed by basic amino acid groups located on the enzyme surface either of the catalyzing biocatalyst or cofactor-regeneration enzymes (Fryszkowska et al. 2009).
- In most cases, the decrease of enantiopurities is derived from non-enzymatic, chemical racemization, which strongly depends on the nature of the substance and present reaction conditions (Fryszkowska et al. 2009). Additionally, decomposition of the product can occur (Toogood et al. 2008).
- Reaction conditions, such as pH, temperature, reaction time, buffer composition or even oxygen, can influence the stereoselectivity of the process (Fryszkowska et al. 2009; Fryszkowska et al. 2012). Additionally, the choice of reaction systems, e.g. monophasic aqueous solutions with or without water-miscible solvents, biphasic systems with water-immiscible solvents or addition of adsorbents, can strongly improve the stereoselectivities (Brenna et al. 2012d; Yanto et al. 2011).

Especially molecules with a stereogenic centre at the Cα position are prone to racemization. Thereby, the rate of the racemization process depends on the nature of the compound (Brenna et al. 2012b; Fryszkowska et al. 2009; Toogood et al. 2008).

3.4.4 Preparative bioreduction of alkenes

Baker´s yeast mediated biotransformation

In the past, bioreduction of activated alkenes was predominantly performed using wild-type baker´s yeast. Though the process might be convenient due to its simplicity and cost-efficiency, the setup suffers from several drawbacks (Bechtold et al. 2012; Brenna et al. 2012e):

- Only low substrate loading is feasible due to low concentration tolerance by the microorganism, which leads to low-to-modest productivities ($< 0.5\ g\ L^{-1}\ d^{-1}$) and long reaction times.
- Separation of the product from the biomass is required, complicating the downstream process.

- Incomplete conversion or side reactions by endogenous enzymes result in a mixture of products that demand extensive and costly subsequent purification steps.
- Competing enzyme reactions can decrease the stereoselectivity of the process.

Especially in case of the reduction of activated alkenes bearing a carbonyl function, competing carbonyl reduction by endogenous alcohol dehydrogenases or carbonyl reductases during baker´s yeast-mediated biotransformation is considered to be a major problem (Silva et al. 2012). Thereby, both the formation of allylic alcohols by substrate depletion and alcohols by product depletion can occur (Kergomard et al. 1982). An example is shown in Figure 3.16. The extent of side reactions and the resulting product distributions depend on the relative reaction rates of the competing ERs and carbonyl reductases. In general, enals are more affected by competing carbonyl reductions than enones, because of higher reaction rates of *prim*-alcohol dehydrogenases compared to *sec*-alcohol dehydrogenases in relation to the ER activity (Hall et al. 2006). Additionally, in case of unsaturated esters, hydrolysis is a common side reaction when using whole cells (Utaka et al. 1989). Side-activities and further drawbacks as low productivities and long reaction times are also present in asymmetric hydrogenation with other wild-type yeast strains, bacteria (e.g. cyanobacteria) or cultured plant cells (e.g. *Nicotiana tabacum*) (Goretti et al. 2011; Goretti et al. 2009; Hirata et al. 2005; Müller et al. 2006; Shimoda et al. 2004).

In order to improve the productivity and selectivity of the wild-type biotransformations, either reaction conditions have to be controlled strictly or a second phase for substrate supply and product removal has to be applied. These methods were successfully applied in the reductions of ketoisophorone and citral, respectively (Leuenberger et al. 1976; Müller et al. 2006; Silva et al. 2012). The use of substrate and product adsorption on hydrophobic resin as an *in situ* substrate feeding product removal (SFPR) technology is a promising method to prevent toxic effects on biocatalysts due to low concentrations in the aqueous phase, as well as promote yield and stereoselectivity (Vicenzi et al. 1997). Nevertheless, achieved productivities in baker´s yeast mediated biotransformations are still unsatisfactory and competing carbonyl reduction cannot be avoided in all cases (Brenna et al. 2009).

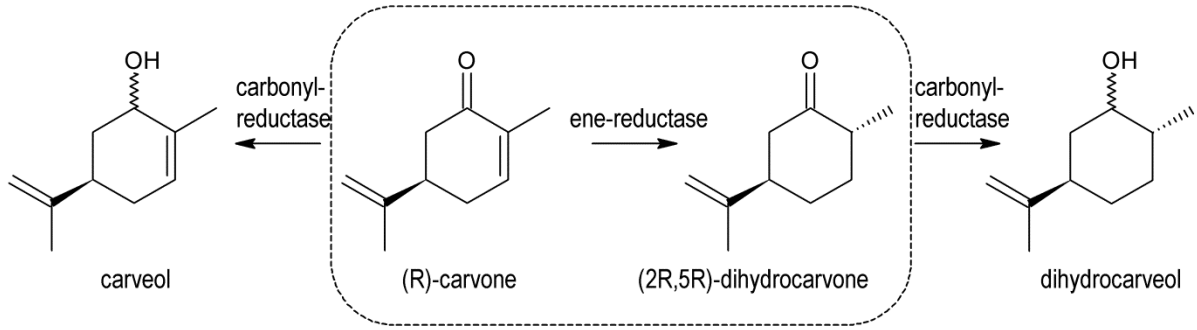

Figure 3.16 Possible side reactions by competing carbonyl reductases in case of the reduction of (R)-carvone to (2R,5R)-dihydrocarvone. Carveols (by overreduction of (R)-carvone) and dihydrocarveols (by overreduction of (2R,5R)-dihydrocarvone) can be formed as side products.

Biocatalysis using isolated ene-reductases

Recently, the application of isolated ERs, which can enhance the productivity and stereoselectivity of the biocatalytic process and possibly circumvent competitive side reactions, is considered as the favored choice (Bechtold et al. 2012; Bougioukou et al. 2010; Brenna et al. 2012e; Winkler et al. 2013). This is supported by the fact that protein purification technologies have been evolved in the last years resulting in lower costs for purified enzymes (Lichty et al. 2005). Due to the requirement of the regeneration of nicotinamide-cofactors, substrate-coupled or enzyme-coupled cofactor regeneration has to be employed (Wichmann and Vasic-Racki 2005).

Prominent enzyme-coupled cofactor regeneration strategies comprise the use of formate dehydrogenases (FDH), glucose dehydrogenases (GDH) and glucose-6-phosphate dehydrogenases (G6PDH), FDH is often considered as the most suitable enzyme since it fulfills conditions necessary for industrial standards (Tishkov and Popov 2006; Wichmann and Vasic-Racki 2005). However, bioreductions with ERs coupled with commercially supplied FDH preparations showed a notable degree of carbonyl reduction due to *prim*-alcohol dehydrogenases as impurities in commercial crude enzyme preparations (Hall et al. 2007). Therefore, GDH was in most cases selected for recycling (Bougioukou et al. 2010; Brenna et al. 2012e), though this system is accompanied by high enzyme cost, difficult product isolation and the requirement of pH regulation (Tauber et al. 2011). Alternatively, alcohol dehydrogenase (ADH)-coupled recycling systems were established for ER-based bioreductions, which are based on the oxidation of inexpensive isopropanol to the volatile acetone, thereby overcoming thermodynamic limitations. However, using ADH did not solve the problem of formation of alcohols as side products due to the activity of ADH

towards ketones and aldehydes. Though side products were marginal using enone-type substrates, this approach is not applicable for enal-type substrates (Brenna et al. 2012d; Tauber et al. 2011; Winkler et al. 2013). In conclusion, unless highly purified enzyme preparations are used for cofactor recycling, competitive side reactions cannot be avoided for all substrate types (Paul et al. 2012).

An innovative strategy is the use of synthetic, functional mimics of natural nicotinamide cofactors which were preferably accepted by ERs due to their cofactor promiscuity, but revealing low catalytic efficiency with wild-type alcohol dehydrogenases. Though unwanted side reactions can be eluded and thus crude enzyme preparations can be employed, the development of *in situ* regeneration strategies for synthetic cofactors, which is crucial for industrial applications, is still missing (Paul et al. 2012). The nicotinamide-independent and substrate-coupled approach based on the disproportionation activity of ERs has the potential to solve problems such as carbonyl reduction due to the absence of competing enzymes. But the removal of phenol as byproduct of this reaction is still challenging (Stueckler et al. 2010).

In terms of reaction engineering at preparative-scale using isolated ERs, monophasic reaction systems are accompanied by issues of low substrate solubility, low stability of both ER and the cofactor-regeneration enzyme and possible decomposition or racemization of substrate and product (Bougioukou et al. 2010; Brenna et al. 2012e; Swiderska and Stewart 2006). The application of biphasic systems with a second water-miscible organic phase allows higher substrate loading as well as protection from decomposition or racemization processes, but the enzyme stability is mostly impaired by phase and molecular toxicity (Bougioukou et al. 2010; Vermuë et al. 1993). Alternatively, the resin-based substrate feeding product removal (SFPR) technology can be applied to combine high substrate loading with high productivity and stereoselectivity. An appropriate substrate concentration in the aqueous phase suitable for biocatalyst stability, reaction rate and stereoselectivity can be adjusted by the resin to substrate ratio (Vicenzi et al. 1997). In fact, though only few examples of preparative biotransformations with ERs are published in the literature, most approaches were performed using resin-based SFPR with isolated enzymes (Bechtold et al. 2012; Brenna et al. 2012e).

Whole-cell bioreduction by recombinant Escherichia coli

Applying engineered strains with higher amount of active desired enzymes and an additional internal cofactor regeneration system can remarkably enhance the productivity and stereoselectivity of a biocatalytic process and combine benefits from both isolated enzymes and wild-type microorganisms as biocatalysts (Richter et al. 2010). While higher stability of enzymes is ensured by the natural environment and the protective cell membrane, the reaction rate of the process can be improved by higher protein expression (Kratzer et al. 2011; Richter et al. 2010). In addition, the production cost for whole-cell biocatalysts is still up to 70-fold lower compared to crude enzyme preparations with cost increasing with higher purification grade (Tufvesson et al. 2010). Numerous successful examples have been shown in case of biocatalytic ketone reductions (Goldberg et al. 2007). Thereby, *Escherichia coli* as host strain proved to be favorable due to the lower activity of endogenous ADHs compared to yeast (Hildebrandt et al. 2002).

In case of alkene reduction, alcohol formation due to competing side reactions in biotransformations using wild-type or even multiple-deletion *E. coli* strains often prevent the use of whole-cell biotransformations (Bechtold et al. 2012). However, if the rate of the desired reaction catalyzed by the overexpressed enzyme in the engineered cell is sufficient, side reactions are negligible (Goldberg et al. 2007). This was shown for whole-cell biotransformation of several enal-type substrates (i.a. citral) by Muller et al. (2007). While bioreduction using the wild-type *E. coli* strain resulted in alcohol formation, side products were below the detection limit using a recombinant *E. coli* overexpressing OYE 2 from *S. cerevisiae* (Muller et al. 2007).

As for all whole-cell bioprocesses, issues of substrate toxicity and low substrate solubility can be overcome by a second water-immiscible phase or using resin-based SFPR techniques (Bräutigam et al. 2009; Goldberg et al. 2007; Hilker et al. 2008). The substrate concentration in the aqueous phase should ensure a high reaction rate, but must not lead to cell membrane damage. Especially hydrocarbons can accumulate in the cell membrane, which can cause a loss of membrane integrity and cofactor leakage (Bräutigam et al. 2009; Sikkema et al. 1995).

4 Material and Methods

4.1 Materials

4.1.1 Chemicals and equipment

All used equipment and consumables are listed in the Appendix A.1. Substrates, reference materials and other chemicals were purchased from different commercial suppliers and also given in the Appendix A.2. 2-Methylmaleimide and *rac*-2-methylsuccinimide were synthesized as reported previously and resulting NMR spectra were in accordance with those reported in the literature (Hall et al. 2008b; Mehta et al. 1960). The composition of buffers and cultivation media are listed in the Appendix A.4. Programs used in this thesis are also described in the Appendix A.1.

4.1.2 Biological materials

Enzymes and other materials for molecular cloning are shown in the Appendix A.2. Primers were synthesized by Metabion (Martinsried, Germany) and listed in the Appendix A.3.1. Vectors and genomic DNAs are listed in the Appendix A.3.2. *Escherichia coli* (*E. coli*) DH5α (Invitrogen, Carlsbad, CA, USA) was used for cloning and *E. coli* BL21(DE3) (Novagen, San Diego, USA) for protein expression. *E. coli* strains used in this study are given in the Appendix A.3.3.

4.2 Molecular cloning

4.2.1 Polymerase chain reaction

Polymerase chain reaction (PCR) was applied for amplifying DNA fragments for subsequent cloning using the Phusion® High-Fidelity DNA Polymerase in a three-step PCR cycle. The reaction mix (50 µL or 20 µL) contained 2 µL genomic or plasmid DNA, 0.5 µM primers, 0.2 mM deoxyribonucleotide triphosphates (dNTPs) and 1 U Phusion™ DNA polymerase or 2.5 U *Tag* DNA polymerase in the respective reaction buffer. The temperature programs were chosen according to the manufacturer´s instructions. The selection of the annealing temperature and the extension time was based on the used oligonucleotides (Appendix A.3.1).

Amplification of the ER genes by PCR was performed with the genomic DNA from the listed cyanobacterial strains as templates. The genomic DNA had been isolated in previous studies (Hölsch and Weuster-Botz 2010) and was kindly provided by K. Castiglione.

4.2.2 Isolation of plasmid DNA from *Escherichia coli*

The isolation of plasmids from *E. coli* DH5α strains was performed with a 5 mL overnight cell culture using the GenElute™ HP Plasmid Miniprep Kit following the spin method according to the manufacturer´s instruction.

4.2.3 Agarose gel electrophoresis

Analytical and preparative separation of DNA were conducted on a 1% (w/v) agarose gel containing 0.4 µg mL^{-1} ethidium bromide allowing a separation range of 0.3 to 10 kilobases (kb). The electrophoresis was performed in 1 x TAE buffer at 120 V.

4.2.4 DNA purification

Subsequent to PCR reactions and agarose gel electrophoresis, the DNA fragments were purified using the GenElute™ PCR Clean-Up Kit or the GenElute™ Gel Extraction Kit according to the manual.

4.2.5 Restriction and ligation of DNA

10 U of restriction enzymes was used to digest either 30 µL of purified plasmid for 2 – 3 h or 40 µL of PCR product for 1 – 2 h at 37 °C according to the manufacturer´s instructions. Digested plasmids were dephosphorylated using 5 U Antarctic phosphophase for 1 h at 37 °C. Subsequently, restricted plasmids and DNA fragments were purified using the GenElute^{TM} PCR Clean-Up Kit. The ligation was conducted by adding 20 U T4 DNA ligase and ATP over night at 16 °C according to the supplier´s instructions.

4.2.6 Site-directed mutagenesis

Site-directed mutagenesis was performed using the QuikChange Lightning Site-Directed Mutagenesis Kit according to the given instructions. The primers used are listed in the Appendix A.3.1.

4.2.7 Preparation of chemically competent cells

Chemically competent *E. coli* cells were obtained following subsequent procedure. A 5 mL Luria Broth (LB) preculture inoculated with the respective *E. coli* strain was incubated over night at 37 °C and then subcultured into 100 mL LB in 500 mL shake flasks without baffles. The cell culture was incubated at 37 °C and 250 rpm until an optical density at 600 nm (OD_{600}) of 0.4 to 0.6 was reached. Subsequently, cells were harvested by centrifugation for 10 min at 3220 x g and 4 °C. Cells were then resuspended in 20 mL pre-cooled TfB1 medium and incubated on ice for 15 min. After a second centrifugation step (10 min, 3220 x g, 4°C), cells were resuspended in 2 mL pre-cooled TfBII medium and incubated on ice for further 15 min. The obtained competent cells were stored in 200 µL aliquots at −80 °C.

4.2.8 Transformation of chemically competent cells

Chemically competent *E. coli* cells were thawed on ice and mixed with either 1 µL plasmid or 20 µL ligation preparation. Cells were incubated for 30 min on ice and subsequently heat-shocked at 42 °C for 30 s with immediate cooling on ice for 2 min. 600 µL of pre-heated LB medium was added and cells were incubated at 37 °C for 1 h with gentle agitation. Afterwards, cells were either concentrated by centrifugation or directly plated out on a LB

agar plate supplemented with the respective antibiotic. Agar plates were incubated overnight at 37 °C.

In case of site-directed mutagenesis, XL10-Gold ultracompetent *E coli* cells provided in the QuikChange Lightning Site-Directed Mutagenesis Kit were transformed according to the supplier´s instructions.

4.2.9 Colony polymerase chain reaction

The colony-PCR was applied for the evaluation of the transformation. Hereby, a swab of a colony was suspended in 100 µL dd-H_2O and 1 µL of this suspension was directly used for PCR. The reaction mix contained 1 µL cells, 0.5 µM primers, 0.2 mM dNTPs and 2.5 U *Tag* DNA polymerase in the respective reaction buffer. The temperature programs were chosen according to the manufacturer´s instructions. The selection of the annealing temperature and the extension time was based on the used oligonucleotides (Appendix A.3.1).

4.2.10 DNA sequencing

The accuracy of the constructed vectors was confirmed by DNA sequencing performed either by GATC (Konstanz, Germany) or Eurofins MWG Operon (Ebersberg, Germany) according to the given instructions.

4.3 Microbiological methods

4.3.1 Strain mantainance

For the availability of respective *E. coli* strains, cells were either stored on LB agar plates supplemented with the corresponding antibiobic for a maximum of three weeks or frozen as cryo stocks for prolonged storage. Thereby, cells were grown in 5 mL LB medium supplemented with the respective antibiotic over night at 30 – 37 °C and 200 rpm. The cell culture was mixed with sterilized glycerol in a final concentration of 15 % (v/v) and stored at −80 °C.

4.3.2 Cultivation in shake flasks

A 5 mL LB preculture supplemented with 34 mg L^{-1} kanamycin or 50 mg L^{-1} ampicillin and inoculated with a single colony from an agar plate or with 5 µL from a cryo stock was incubated over night at 37 °C. Next, 1 mL from the preculture was added to 200 mL Terrific Broth (TB) medium in 1000 mL shake flasks without baffles. Protein expression was induced by the addition of 1 mM isopropyl β-D-1-thiogalactopyranoside (IPTG) at a cell density OD_{600} of 0.6 – 0.8. Afterwards, cells were incubated overnight for 18 – 20 h at 20 °C and 160 rpm in case of subsequent use for protein purification. If cells were applied as whole cell biocatalysts, the protein expression duration was set to 20 h.

Recombinant *E. coli* cells used for protein purification were harvested by centrifugation at 4528 x g for 15 min. Cell pellets were either stored at −20 °C or directly used for protein purification. In case cells were produced for whole-cell biotransformation, obtained cell pellets after centrifugation were directly used for biotransformation unless indicated otherwise.

4.3.3 Cultivation at the 3 L scale

Large-scale production of the whole-cell biocatalyst was performed in a 3 L fed-batch process in a stirred tank bioreactor with a nominal volume of 7.5 L (Figure 4.1). The reactor was equipped with three six-blade Rushton turbines fixed a height of 2, 8 and 16 cm from the stirrer tip. The cultivation was conducted in a minimal medium described by Wilms et al. (2001) following a modified protocol provided by Sun et al. (2013). The composition of the

minimal medium is given in the Appendix A.4.1. The feed medium contained 500 g L^{-1} glucose and 99 g L^{-1} $(NH_4)_2HPO_4$, which were autoclaved separately.

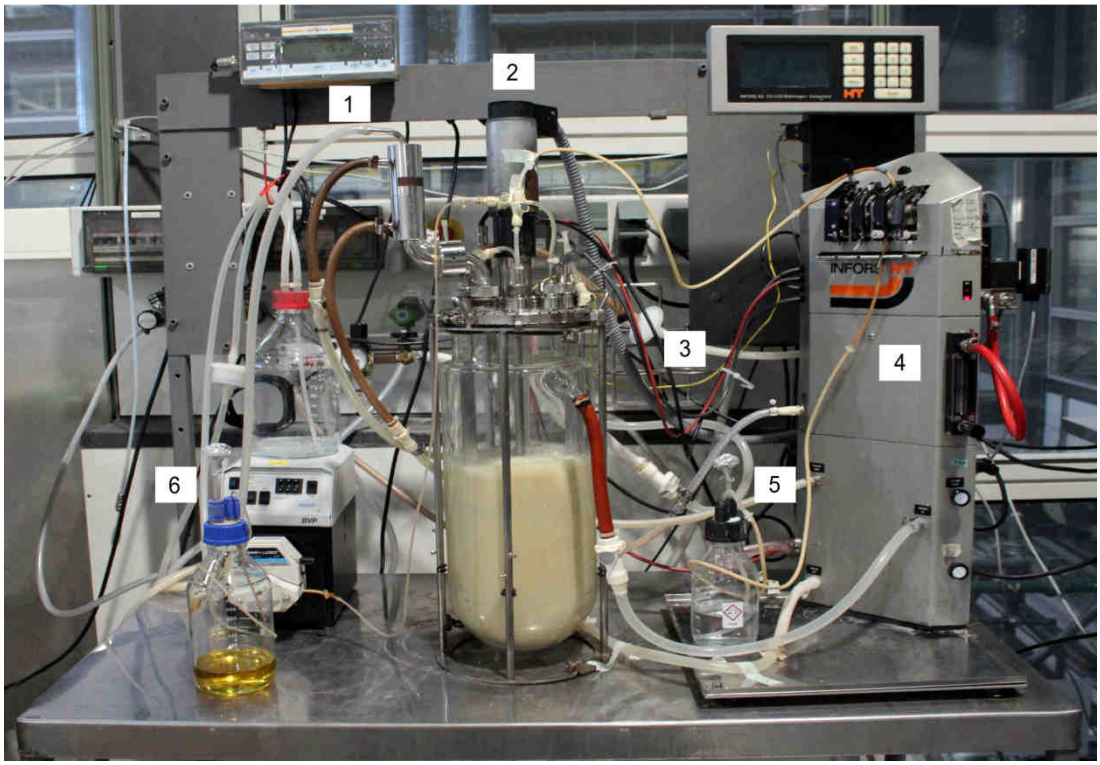

Figure 4.1 Stirred-tank reactor with a nominal volume of 7.5 L used for the cultivation of whole-cell biocatalysts in fed-batch mode: control station (1), stirrer (2), air outlet (3), pH, pO_2 and temperature probes (4), base for pH control (5) and feed (6).

The pre-culture contained 200 mL minimal medium supplemented with 3 g L^{-1} glucose and 34 mg L^{-1} kanamycin and was incubated over night at 37 °C and 250 rpm. The bioreactor was filled with 2.8 L minimal medium also supplemented with 3 g L^{-1} glucose and 34 mg L^{-1} kanamycin and inoculated with 200 mL pre-culture. The pH was controlled at pH 7.0 throughout the cultivation by addition of 25 % (v/v) NH_4OH. The fed-batch cultivation process can be divided in three steps, as described in the following:

i. During the batch phase, the temperature was set to 37 °C and dissolved oxygen (DO) was maintained above 30 % saturation by adjusting the stirrer speed. The air flow was set to 2 L min^{-1}.
ii. The exponential feeding phase was initiated at the time of complete glucose consumption. The temperature was decreased to 30 °C and a feed containing glucose, nitrogen and phosphate was added to the culture according to Equation 3.11. The growth rate was set to 0.15 h^{-1}. The aeration was increased to 5 L min^{-1} and dissolved oxygen was kept above 20 %. After 19 h, the temperature was set to 20 °C and one hour later, the protein expression phase was started.

iii. The protein expression phase was initialized by adding IPTG in a final concentration of 0.5 mM. The growth rate was set to 0.06 h^{-1} by reducing the feed rate and the temperature was kept at 20 °C for 24 h.

After cell cultivation, adequate amount of cells was mixed with glycerol to a final concentration of 15 % (v/v), subsequently shock-frozen with liquid nitrogen and stored at −58 °C.

4.3.4 Determination of optical density

The optical density of cell cultures was measured in cuvettes with an optical path length of 10 mm using a single beam photometer at a wavelength of 600 nm. Samples were appropriately diluted with PBS buffer and measured at least in triplicates.

4.3.5 Determination of cell dry weight

The cell dry weight (CDW) of *E. coli* cultures was determined gravimetrically in triplicates. A given volume (1 mL) of cell suspension was added in previously dried and weighted 1.5 mL- Eppendorf Safe-Lock Tubes™. Cells were centrifuged for 10 min at 13000 min^{-1} in a benchtop centrifuge and the supernatant was discarded. After drying at 80 °C to a constant weight, the vials were weighted again. The cell dry weight was calculated using Equation 4.1.

$$c_x = \frac{m_{full} - m_{empty}}{V} \qquad \text{Eq. 4.1}$$

c_x	cell dry weight, g_{CDW} L^{-1}
m_{full}	mass of vial with cells after drying, g
m_{empty}	mass of empty vial, g
V	volume of the sample, L

The cell dry weight of a cell suspension is directly proportional to the optical density of the sample (Equation 4.2). The correlation factor (f_x) was calculated based on OD and CDW measured for different cell suspensions.

$$c_x = f_x \cdot OD_{600} \qquad \text{Eq. 4.2}$$

c_x	cell dry weight, $g_{CDW}\ L^{-1}$
f_x	correlation factor, $g_{CDW}\ L^{-1}$
OD_{600}	optical density at 600 nm, -

4.3.6 Cell lysis

Cell lysis was conducted previous to protein purification or enzyme activity measurements. Cells were mechanically disrupted using glass beads (Ø 0.25 – 0.5 mm), which were added in a volume fraction of 50 % to the respective cell suspension. For inhibition of protease activity, 1 mM phenylmethylsulfonyl fluoride (PMSF) was added to the cell suspension. Cells were lysed for 6 min or 3 min in case of protein purification at 1800 min^{-1} in a mixer mill and subsequently centrifuged at 4 °C for 20 min at 40827 x g. The supernatant was used for enzyme activity assays or protein purification.

4.4 Protein purification and analytics

4.4.1 Immobilized metal affinity chromatography

His_6-tagged proteins (ene-reductases, formate dehydrogenase and glucose dehydrogenase), as well as the His_6-tagged tabacco etch virus (TEV) protease (a S219V mutant for improved performance, Kapust et al. (2001)) were purified using immobilized metal affinity chromatography.

After cell harvest by centrifugation, cell pellets were resuspended in pre-cooled binding buffer in a ratio of 1 g cell weight to 5 mL buffer. Cell lysis was performed according to the description in Section 4.3.6. Supernatant fractions were collected, filtered (0.45 µm, Minisart HF) and loaded onto an equilibrated 1 mL HisTrap FF crude column at a flow rate of 1 mL min^{-1}. Protein purification was performed according to the manufacturer´s specifications at 4 °C in an automatized Fast Protein Liquid Chromatography device. Online detection of proteins was enabled using the absorbance at 280 nm. The elution of His_6-tagged proteins was initiated by a linear gradient from 0 % to 100 % elution buffer containing 500 mM imidazole over 20 column volumes (CVs), while 2 mL fractions were

collected. The absorbance at 280 nm revealed the fractions containing the target protein. Respective protein fractions were pooled, dialyzed and concentrated by ultracentrifugation using a Vivaspin ultrafiltration device (molecular weight cutoff: 5 kDa). The solution was diluted to ≤ 1 mM imidazole.

In order to obtain ene-reductases without affinity tags, the enzyme was constructed as a His_6-maltose binding protein (MBP)-tagged protein. Protein purification was performed according to the standard protocol. Protein fractions were concentrated at least 10-fold. Afterwards, purified TEV proteases were added to the solution in a ratio of 1 TEV protease to 30 fusion protein based on absorbance at 280 nm for removal of the His_6-MBP tag. The cleavage was performed over night at 4 °C in the TEV reaction buffer. Subsequently, the reaction mix was diluted to an imidazole concentration of 40 mM and loaded to a 1 mL HisTrap FF crude column. Both the His_6-MBP tag cleaved from the fusion protein and the His_6-tagged TEV protease bound onto the column, while purified ene-reductases without the affinity tag was obtained.

4.4.2 Storage of protein preparations

Enzymes used in this project were stored in 25 % (v/v) glycerol at –80 °C after shock freezing using liquid nitrogen. As enzymes were highly concentrated (~1.5 – 2.3 mg mL^{-1}), minimal concentrations of glycerol remained after respective dilution for subsequent use.

4.4.3 Sodium dodecyl sulfate polyacrylamide gel electrophoresis

Sodium dodecyl sulfate polyacrylamide gel electrophoresis (SDS-PAGE) was performed using 3 % and 12.5 % Bis-Tris gels. Protein samples were supplemented with 5 x Laemmli buffer and incubated at 95 °C for 5 min for complete denaturation. The protein standards Roti®-Mark Standard (14 – 212 kDa) and Perfect Protein™ Marker (10 – 225 kDa) were used for estimation of molecular mass of proteins. SDS-PAGEs were run at 30 mA in Tris-glycine running buffer.

SDS-gels were stained according to Fairbanks et al. (1971). Thereby, the gels were boiled and incubated for 5 min in sequence in Fairbanks solutions A, B and C, which are listed in the Appendix A.4. Alternatively, SDS-gels were stained using Roti®-Blue colloidal coomassie staining solutions according to manufacturer´s instructions.

4.4.4 Determination of protein concentration

Bicinchoninic acid (BCA) assay

Protein concentration was determined at least in triplicates using the BCA Protein Assay (Thermo Fisher Scientific) according to the manufacturer´s specifications. Protein samples were diluted with sodium phosphate buffer (100 mM, pH 7.0) to ensure protein concentrations within the given range of 20 and 2000 mg L^{-1}.

UV absorption at 280 nm

Protein concentrations were estimated using the UV absorption at 280 nm. The molar extinction coefficients (ε) of the proteins were calculated using the program GENtle.

4.5 Enzyme characterization

4.5.1 Enzyme activity assay

Enzyme activities were determined by photometric assays monitoring the oxidation of NAD(P)H at 340 nm using a molar absorption coefficient of 6.22 mM^{-1} cm^{-1}. In case of ketoisophorone and 3-phenyl 2-methylpropenal the assay was performed at 365 nm using a molar absorption coefficient of 3.51 mM^{-1} cm^{-1}. All reactions were performed on a 200 µL scale in sodium phosphate buffer (100 mM, pH 7.0) at 30 °C or 25 °C using microplate spectrometers (EL808, BioTek Instruments and infinite M200, Tecan). Appropriate controls were included and experiments were conducted at least in triplicates. One unit of enzyme activity was defined as the oxidation of 1 µmol NAD(P)H per minute. Background oxidase activity was measured in the absence of alkenes and subtracted from the specific activity. The conditions for standard enzymatic assays with ene-reductases, formate dehydrogenases and glucose dehydrogenases are summarized in Table 4.1. The applied enzyme concentrations were adapted to ensure measurement of initial reaction rates within a linear range of NAD(P)H variation.

Table 4.1 Standard conditions for enzymatic assays involving ene-reductases (ER), formate dehydrogenases (FDH) and glucose dehydrogenases (GDH). Assays were performed on a 200 µL scale in sodium phosphate buffer (100 mM, pH 7.0).

	ER	**FDH**	**GDH**
Cofactor	0.5 mM NAD(P)H	0.5 mM $NAD(P)^+$	0.5 mM $NAD(P)^+$
Substrate	10 mM various alkenes	250 mM sodium formate	250 mM glucose

Investigation of the substrate spectrum using various ERs was conducted with 0.5 mM NADPH using substrates at a concentration of 10 mM (added as an ethanol solution, < 5 % (v/v) final ethanol concentration). Assays for enzyme characterization were in general performed with 10 mM maleimide and 0.5 mM NADPH, unless stated otherwise. For evaluation of the enzyme activity of whole-cell biocatalysts, 10 mM (R)-carvone was used as substrate to determine ER activity, as the (R)-carvone reduction was focused in that case.

Specific activities of purified enzymes and whole-cell biocatalysts were calculated based on the Lambert-Beer relation given in Equation 4.3.

$$EA_x = \frac{\Delta c_{\mathrm{NAD(P)H}} \cdot V_R}{\Delta_\mathrm{t} \cdot V_\mathrm{x} \cdot c_P} = \frac{\Delta A_{340} \cdot V_R \cdot 10^6}{\Delta_\mathrm{t} \cdot \varepsilon_{\mathrm{NAD(P)H}} \cdot d \cdot V_x \cdot c_P} \qquad \text{Eq. 4.3}$$

EA_x	specific enzyme activity, U mg^{-1} or specific biocatalyst activity, U g_{CDW} L^{-1}
$\frac{\Delta c_{\mathrm{NAD(P)H}}}{\Delta_\mathrm{t}}$	variation of NAD(P) concentration over time, µM min^{-1}
V_R	reaction volume, µL (here: 200 µL)
V_x	sample volume, µL
c_P	protein concentration, mg L^{-1} or biocatalyst concentration, g_{CDW} L^{-1}
$\frac{\Delta A_{340}}{\Delta_\mathrm{t}}$	variation of the absorption at 340 nm over time, min^{-1}
$\varepsilon_{NAD(P)H}$	molar extinction coefficient, 6220 L mol^{-1} cm^{-1}
d	path length, cm (here 0.59 cm)

4.5.2 Determination of kinetic parameters

Kinetic parameters were determined for ene-reductases, formate dehydrogenases and glucose dehydrogenases at 30 °C. As all three enzymes catalyze two-substrate-two-product reactions, either the substrate or the cofactor had to be supplied in excess to achieve pseudo-first order reaction conditions, which is needed for the application of Michaelis-Menten kinetics (Bisswanger 2008).

Kinetic parameters for NADH and NADPH of ene-reductases were determined using a constant concentration of 10 mM maleimide, while the concentration of NAD(P)H was varied between 0.01 mM and 0.6 mM. In case of the enzyme kinetics of FDH and GDH, substrate and cofactor concentrations were applied up to at least five-fold of the half-saturation constant K_M.

Kinetic parameters were estimated according to the Michaelis-Menten equation (Bisswanger 2008) and data were analyzed using non-linear regression analysis (Sigma Plot 8.0, SPSS).

4.5.3 Determination of factors influencing enzyme activity

Determination of temperature optima

Temperature optima were determined in 50 mM sodium phosphate buffer at pH 7.0, as sodium phosphate buffers generally display a low temperature coefficient (Perrin and Dempsey 1974). Enzyme samples were incubated at various temperatures and the specific activities were measured in photometric assays. Experiments were performed at least in triplicates.

The activation energy was calculated following the Arrhenius equation (Equation 4.4).

$$k = A \cdot e^{-\frac{E_A}{RT}} \qquad \text{Eq. 4.4}$$

k	rate constant, s^{-1}
A	*Arrhenius* factor, s^{-1}
E_A	activation energy, J mol^{-1}
R	gas constant, 8.314472 J mol^{-1} K^{-1}
T	absolute temperature, K

Determination of pH optima

Buffers for the investigation of the pH profile were 50 mM sodium citrate, 50 mM sodium phosphate, 50 mM 3-(N-morpholino)propanesulfonic acid (MOPS) and 50 mM Tris–HCl applied in a pH range of pH 5.5 – 9.5. Enzyme activities were measured in photometric assays in triplicates at 25 °C.

Investigation of the effect of organic solvents and salts

The effect of organic solvents on the activity of ERs was studied using ethanol, 1-propanol, iso-propanol and *N*,*N*-dimethylformamide (DMF) in volume fractions of 5 – 20 % (v/v). The influence of different concentrations of sodium chloride, sodium formate and ammonium formate on the ER activity was investigated for up to 3 mol L^{-1}. All studies were performed in photometric assays in triplicates at 25 °C.

4.5.4 Evaluation of enzyme stability

Enzyme stabilities were determined by measuring the enzyme activity at regular intervals during an appropriate period of time, whilst incubated in sodium phosphate buffer (100 mM, pH 7.0) under defined conditions (e.g. at different temperature or in solvents). Purified enzymes were applied for all stability studies.

Half-lives were calculated based on Equation 4.5 and 4.6.

$$EA = EA_0 \cdot e^{-k_i t} \qquad \text{Eq. 4.5}$$

EA	enzyme activity at time t, U mg^{-1}
EA_0	enzyme activity at time t=0, U mg^{-1}
k_i	inactivation constant, h^{-1}
t	time, h

$$\tau = \frac{\ln 2}{k_i} \qquad \text{Eq. 4.6}$$

τ	half-life, h
k_i	inactivation constant, h^{-1}

Half-lives were measured for ERs at different temperatures (30 °C, 40 °C, 50 °C). Enzyme preparations were adapted to a temperature of 25 °C for photometric measurement.

Solvent stabilities of ERs were determined in biphasic reaction systems containing 20 % (v/v) water-immiscible solvents. Thereby, the organic solvents *n*-hexane, toluene, methyl *tert*-butyl ether (MTBE) and diethyl ether, as well as the ionic liquids [HMPL][NTF], [HMIM][PF_6] and [HPYR][NTF] were selected for investigation. To ensure comparative conditions as for enzymatic bioconversions, experiments were performed at 30 °C in glass vials positioned on a shaking tray at 300 rpm.

Operational stabilities of ERs were measured in the bioreactor unit developed by Weuster-Botz et al. (2005). The miniaturized stirred-tank bioreactors were equipped with S-stirrers developed by Riedlberger and Weuster-Botz (2012) and operated at 400 rpm or 1500 rpm. The reaction volume was set to 10 mL, either as monophasic reaction system with 10 µg mL^{-1} ER in sodium phosphate buffer (100 mM, pH 7.0) or as biphasic reaction system containing 20 % (v/v) [HMPL][NTF].

Studies of enzyme stabilities of FDH and GDH were performed according to the standard procedure using the respective substrate and cofactor. Defined FDH or GDH solutions were incubated at 30 °C in presence of different (R)-carvone concentrations (10 – 100 mM).

4.6 Bioconversions using purified enzymes

4.6.1 Enzymatic bioconversion without cofactor regeneration system

For evaluation of the stereoselectivity of ERs, bioreductions of 2-methyl-2-cyclopenten-1-one, 3-methyl-2-cyclohexen-1-one, 2-methylmaleimide, ketoisophorone, (R)- and (S)-carvone were conducted without cofactor regeneration in 1 mL scale using 1.5 mL Eppendorf Safe-Lock Tubes™. Reactions contained 5 mM substrates (added as a DMF solution, < 2% (v/v) final DMF concentration), 15 mM NADH and 84 – 136 µg mL^{-1} purified ERs (except for GloeoER with 35 µg mL^{-1}) in sodium phosphate buffer (100 mM, pH 7.0). All reactions were agitated at 30 °C and 300 rpm (Thermomixer comfort, Eppendorf) for 24 h followed by extraction with ethyl acetate (1:1) containing 36 mM (R)-limonene as internal standard and subsequent GC analysis. Experiments were performed in triplicates.

4.6.2 Enzymatic bioconversion with cofactor regeneration system

ER-mediated bioconversions with enzyme-coupled cofactor regeneration were generally performed with a formate dehydrogenase C145S/D221Q/C255V triple mutant (FDH_{3M}) from *Mycobacterium vaccae* N10, unless stated otherwise. This triple mutant exhibited increased $NADP^+$ activity and chemical stability (Hoelsch et al. 2012).

To investigate the effect of different organic solvents on the bioreduction of ketoisophorone by the ER from *Synechococcus* sp. PCC 7942 (Syn7942ER), bioconversions were

conducted in 1 mL-scale with FDH_{3M}-coupled cofactor regeneration. Reactions contained 5 – 20 % (v/v) ethanol, iso-propanol or DMF, 250 mM sodium formate, 0.5 mM $NADP^+$, 10 mM ketoisophorone and 25 µg mL^{-1} Syn7942ER in sodium phosphate buffer (100 mM, pH 7.0) and were incubated for 6 h at 30 °C and 150 rpm (WiseCube, Witeg Labortechnik). Reactions were stopped by extraction with ethyl acetate (1:1) containing 36 mM (R)-limonene as internal standard for further GC analysis.

4.7 Characterization of reaction systems

4.7.1 Determination of distribution coefficients

The distribution coefficients of relevant substances involved in biphasic reaction systems consisting of two immiscible liquid phases are essential for its characterization. In this project, liquid-liquid biphasic reaction systems generally contained 80 % (v/v) sodium phosphate buffer (100 mM, pH 7.0) and 20 % (v/v) organic solvents or ionic liquid, unless stated otherwise. As the bioreduction of (R)-carvone to (2R,5R)-dihydrocarvone was focused, the properties of these compounds in biphasic reaction systems were investigated. It has to be noted that commercially supplied dihydrocarvone used for this investigation composed of a mixture of ~77 % (2R,5R)-dihydrocarvone and ~20 % (2S,5R)-dihydrocarvone. Experiments were performed at 1 mL scale in gas-tight sealed glass vials with a nominal volume of 1.5 mL.

In case of water-immiscible organic solvents, concentrations of (R)-carvone and dihydrocarvone were determined in both phases after phase separation by centrifugation (4528 x g, 15 min) and calculated according to Equation 3.14. Thereby, the aqueous phase was extracted with ethyl acetate (1:1) and the organic phase was diluted in ethyl acetate for further GC analysis (Section 4.9). GC samples contained 7.2 mM (R)-limonene as internal standard.

Determination of distribution coefficients for (R)-carvone and dihydrocarvone in the ionic liquids [HMPL][NTF], [HMIM][PF_6] and [HPYR][NTF] was performed in triplicates according to a protocol described by Hölsch (2009).

(R)-Carvone and dihydrocarvone were separately dissolved at a concentration of 100 mM in *n*-hexane and subsequently extracted with the respective ionic liquid in a volume ratio of 4:1

at 1800 min^{-1} for 1 h in a mixer mill. After phase separation by centrifugation (4528 x g, 15 min), the concentration of the substances in *n*-hexane, as well as the initial concentrations in *n*-hexane were determined by GC. The concentration in the IL was calculated based on the concentration in *n*-hexane before and after the extraction according to Equation 4.7.

The distribution coefficient between the ionic liquid and the aqueous buffer phase was determined by mixing the previously loaded ionic liquid with a sodium phosphate buffer (100 mM, pH 7.0) in a volume ratio of 1:4 followed by extraction for 1 h at 1800 min^{-1}. After phase separation by centrifugation (4528 x g, 15 min), the substance concentration in the aqueous phase was measured by GC. The distribution coefficient of the substance between the ionic liquid and the aqueous phase was calculated according to Equation 4.8.

$$c_{IL} = (\varphi_{IL}^{-1} - 1) \cdot \left(c_{hexane,0} - c_{hexane}\right) \quad \text{Eq. 4.7}$$

c_{IL}	concentration in the IL after extraction with *n*-hexane, mol L^{-1}
$c_{hexane,\,0}$	initial concentration in *n*-hexane, mol L^{-1}
c_{hexane}	equilibrium concentration in *n*-hexane after extraction, mol L^{-1}
φ_{IL}	volume fraction of the ionic liquid in the extraction step, -

$$logD_{IL/aq} = log_{10}\frac{c_{IL} - (\varphi_{IL}^{-1} - 1) \cdot c_{aq}}{c_{aq}} \quad \text{Eq. 4.8}$$

$logD_{IL/aq}$	decadic logarithm of the distribution coefficient of a substance between the ionic liquid and the aqueous phase, -
c_{aq}	equilibrium concentration in the aqueous buffer after the extraction, mol L^{-1}
c_{IL}	concentration in the IL after extraction with *n*-hexane, mol L^{-1}
φ_{IL}	volume fraction of the ionic liquid in the extraction step, -

In a last step, the ionic liquid after extraction with the buffer phase was again extracted with *n*-hexane in a ratio of 1:4 (v/v) for 1 h at 1800 min^{-1}. After phase separation by centrifugation (4528 x g, 15 min), the substance concentration in *n*-hexane was again measured by GC. Thus, the distribution coefficient of the substances between water saturated ionic liquid and *n*-hexane was calculated according to Equation 4.9.

$$logD_{IL/hexane} = log_{10}\frac{\left(c_{IL} - (\varphi_{IL}^{-1} - 1) \cdot c_{aq}\right) - (\varphi_{IL}^{-1} - 1) \cdot c_{hexane}}{c_{hexane}} \quad \text{Eq. 4.9}$$

$logD_{IL/hexane}$	decadic logarithm of the distribution coefficient of a substance between the ionic liquid and the *n*-hexane, -
c_{aq}	equilibrium concentration in the aqueous buffer after the extraction, mol L^{-1}
c_{IL}	concentration in the IL after extraction with *n*-hexane, mol L^{-1}
c_{hexane}	equilibrium concentration in *n*-hexane after extraction, mol L^{-1}
φ_{IL}	volume fraction of the ionic liquid in the extraction step, -

4.7.2 Determination of the moisture content of adsorbent resins

In case of resin-based solid-liquid reaction systems, the mass ratio of resin to substrate determines the rate and extent of the adsorption. Adsorbent resins Amberlite™ XAD4, XAD7 and XAD1180 were selected for preliminary studies, and XAD4 was chosen for further characterization.

The moisture content of XAD4 was determined gravimetrically. A defined wet mass (1 g) of resin was added in previously dried and weighted 15 mL reaction tubes. The adsorbent resin was dried at 80 °C to a constant weight in the reaction tubes and weighted again. The moisture content was calculated according to Equation 4.10.

$$\%\ water = \frac{m_{resin,wet} - m_{resin,dry}}{m_{resin,wet}} \cdot 100\ \% \quad \text{Eq. 4.10}$$

% water	moisture content of resin, %
$m_{resin,wet}$	mass of wet resin, g
$m_{resin,dry}$	mass of dry resin, g

For convenience, wet resin was used for experiments and the mass ratio of resin to substrate refers to the mass of wet resin.

4.7.3 Determination of the adsorbent isotherm

The capability of the adsorbent resin Amberlite^{TM} XAD4 in solid-liquid reaction systems was characterized by the determination of adsorbent isotherms. Thereby, different amount of (R)-carvone and dihydrocarvone (0.009 – 0.075 g) were separately mixed with a defined wet mass of resin (0.154 g) in 5 mL sodium phosphate buffer (100 mM, pH 7.0). The mass ratio of wet resin to substrate was in a range of 2.1 to 16.7 in case of (R)-carvone and 2.0 to 16.4 in case of dihydrocarvone. The residual concentration in the aqueous phase was for all setups below the maximal solubility of (R)-carvone or dihydrocarvone. The decadic logarithm of the solute concentration per unit mass of adsorbent was plotted against the decadic logarithm of the residual solute concentration in the aqueous phase according to the Freundlich isotherm described by Equation 3.17.

4.8 Whole-cell batch biotransformations

4.8.1 Preparation of the whole-cell biocatalyst

E. coli cells used for whole-cell biotransformation were prepared and stored as described in Section 4.3. In case of cultivation in shake flasks, cells were directly used for biotransformation after cell harvest by centrifugation (4528 x g, 15 min) and subsequent resuspension in sodium phosphate buffer (100 mM, pH 7.0). In case of liter scale cultivation and subsequent storage at −58 °C, cells were gently thawed on ice. The glycerol was removed by washing the cells two times with sodium phosphate buffer (100 mM, pH 7.0) in two centrifugation steps (4528 x g, 15 min). The cell suspension was then adjusted to the desired optical density and the biotransformation was started by the addition of biocatalyst.

4.8.2 Preliminary studies at 5 mL scale

Preliminary studies of whole-cell biotransformation involving ERs were performed in gas-tight sealed glass vials with a nominal volume of 10 mL (Figure 4.2). For biotransformation, the reaction vials were placed on a multi-stirrer plate. The mixing was enabled by a magnetic stirrer operated at 550 rpm. Experiments were performed in triplicates at room temperature (25 ± 1 °C).

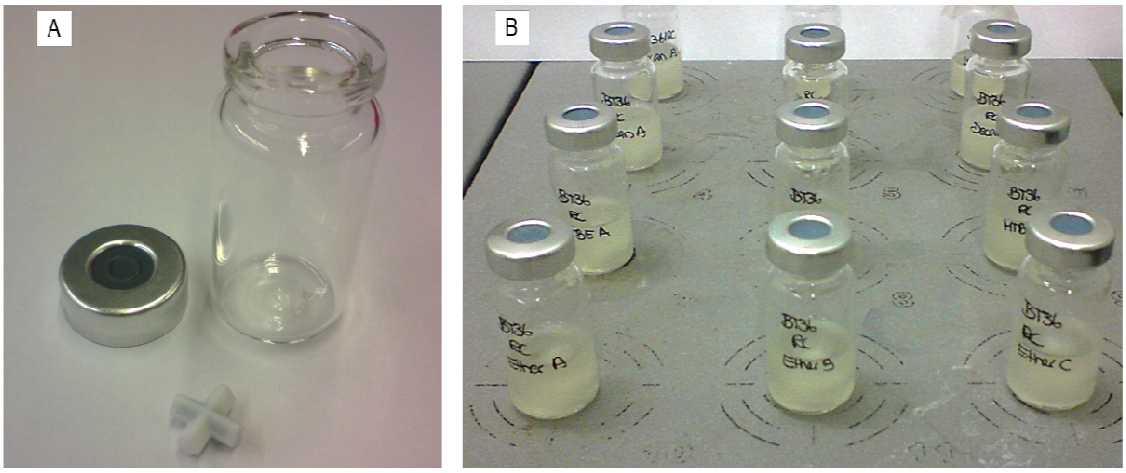

Figure 4.2 Whole-cell batch biotransformations at 5 mL scale. (A) Gas-tight sealed glass vials of a nominal volume of 10 mL and the magnetic stirrer were used. (B). Reaction vials were placed on a multi-stirrer plate during the biotransformation.

This reaction system was selected for evaluation of the monophasic reductions as well as preliminary biphasic reductions of (R)-carvone, because the evaporation was minimized in this reaction system (data not shown). Reactions were performed in a working volume of 5 mL.

Monophasic biotransformations were conducted in sodium phosphate buffer containing 8.8 g_{CDW} L^{-1} biocatalyst and 10 mM (R)-carvone added as ethanol solution (5 % (v/v) final ethanol concentration). In case a FDH was overexpressed in the cells, 250 mM sodium formate was added. Samples of 200 µL volume were taken using single-use needles (Ø 0.90 mm, Sterican®, Braun), followed by extraction (1:1) with ethyl acetate and subsequent GC analysis. Biphasic reaction systems contained 20 % (v/v) organic solvents (*n*-hexane, *n*-decane, MTBE, diethyl ether) or ionic liquids [HMPL][NTF], [HPYR][PF_6] and [HMIM][NTF] with 50 mM (R)-carvone dissolved in this phase. The aqueous phase contained 2 – 2.8 g L^{-1} biocatalyst and 250 mM formate. The reaction was stopped after 24 h by phase separation (4528 x g, 15 min) and subsequent GC analysis of the organic solvent and the ionic liquid.

4.8.3 General proceedings for biphasic whole-cell batch biotransformations with ionic liquids

Biphasic whole-cell batch biotransformation with IL as a second water-immiscible phase was performed in 12 mL, 200 mL and 1 L scale, which is further described in Sections 4.8.5 – 4.8.7. The reaction system was composed of an aqueous sodium phosphate buffer phase and 20 % (v/v) [HMPL][NTF]. The molarity and pH of the sodium phosphate buffer as well as the formate and biocatalyst concentration in this phase varied dependent on the requirements of the experiment. Prior to use, the formate stock was adjusted to the desired pH of the buffer and (R)-carvone was dissolved to the adequate concentration in the IL. Due to the high viscosity of [HMPL][NTF], the loaded IL was weighted directly in the miniaturized bioreactor or in other vessels based on the calculated density of the IL/substrate mixture. A sample of the initial IL phase was taken as control. Reactions were started by biocatalyst addition. Samples of 1 mL volume were taken using a pipette or single use syringe and needles (Ø 2.1 mm, Sterican®, Braun) followed by subsequent phase separation in Eppendorf Safe-Lock Tubes™ (13000 min^{-1}, 5 min) and GC-analysis of the IL according to Section 4.9.

All indicated concentrations of the biocatalyst and formate refer to the aqueous phase, whereas all substrate and product concentrations refer to the IL phase, unless noted otherwise. As standard conditions, 250 mM sodium formate and 8 g_{CDW} L^{-1} biocatalyst were used in 100 mM sodium phosphate buffer (pH 7.0) with 250 mM (R)-carvone dissolved in 20 % (v/v) [HMPL][NTF]. The reaction temperature was kept at 25 ± 1 °C (ambient temperature), unless indicated otherwise.

4.8.4 General proceedings for whole-cell batch biotransformations with adsorbent resins

Whole-cell batch biotransformations with adsorbent resin for *in situ* substrate supply and product removal were also performed in 12 mL, 200 mL and 1 L scale. Thereby, the reaction system composed of an aqueous sodium phosphate buffer phase and a defined mass of wet resins loaded with a respective mass of substrate. The molarity and pH of the sodium phosphate buffer as well as the substrate, formate and biocatalyst concentration varied dependent on requirements of the experiment. The mass ratio of wet resin and substrate was defined for each biotransformation. Prior to use, adsorbent resins XAD4 were weighted either directly in the reactor or using 50 mL reaction tubes. For substrate adsorption, adequate amounts of (R)-carvone were added to the adsorbent resins in the respective reactors mixed with a defined volume of sodium phosphate buffer (5 – 380 mL for 12 mL – 1 L scale). The solid-liquid suspensions were sealed using Parafilm® or the respective reactor cover and incubated for 2 h. In case of substrate adsorption in the miniaturized bioreactor or 50 mL reaction tubes, these were placed on a shaking tray at 600 rpm. In case the substrate adsorptions were performed directly in the reactors, the impeller speed was set to 600 rpm for 200 mL scale and 400 rpm for 1 L scale biotransformation. Biotransformations were started by addition of the biocatalyst. Samples of 1 mL volume were taken using a pipette or single use syringe and needles (Ø 2.1 mm, Sterican®, Braun). After phase separation in Eppendorf Safe-Lock Tubes™ by centrifugation (13000 min^{-1}, 5 min), adsorbent resins were prepared for GC analysis according to Section 4.9.

All indicated substrate, formate and biocatalyst concentrations refer to the aqueous phase. Unless stated otherwise, the standard operation setup was 50 mM (R)-carvone, 250 mM sodium formate and 8 g_{CDW} L^{-1} biocatalyst in 100 mM sodium phosphate buffer (pH 7.0).

4.8.5 Biotransformations at the 12 mL scale

Biphasic whole-cell batch biotransformations either with ionic liquid as a second water-immiscible phase or hydrophobic adsorbent resins were characterized and optimized in the bioreactor unit developed by Weuster-Botz et al. (2005) (Figure 4.3). Equipped with miniaturized stirred-tank bioreactors, up to 48 reactions can be operated in parallel at defined process conditions. Agitation was enabled by magnetically driven impellers allowing comparable process characteristics for further scale up (Hortsch and Weuster-Botz 2010; Riedlberger and Weuster-Botz 2012). Though the control of temperature, pH and monitoring of dissolved oxygen, as well as sampling and feeding was possible if integrated into a liquid-handling system (Puskeiler et al. 2005), only the temperature was controlled during the reaction. For both biphasic processes with ILs and adsorbent resins, biotransformations were performed in a reaction volume of 12 mL at 25 ± 1 °C for 5 h. The head space cooling was set to 4 °C for decreased evaporation. Baffled miniaturized bioreactors were equipped with S-impellers developed by Riedlberger and Weuster-Botz (2012) operated at 1500 rpm. Experiments were performed in triplicates.

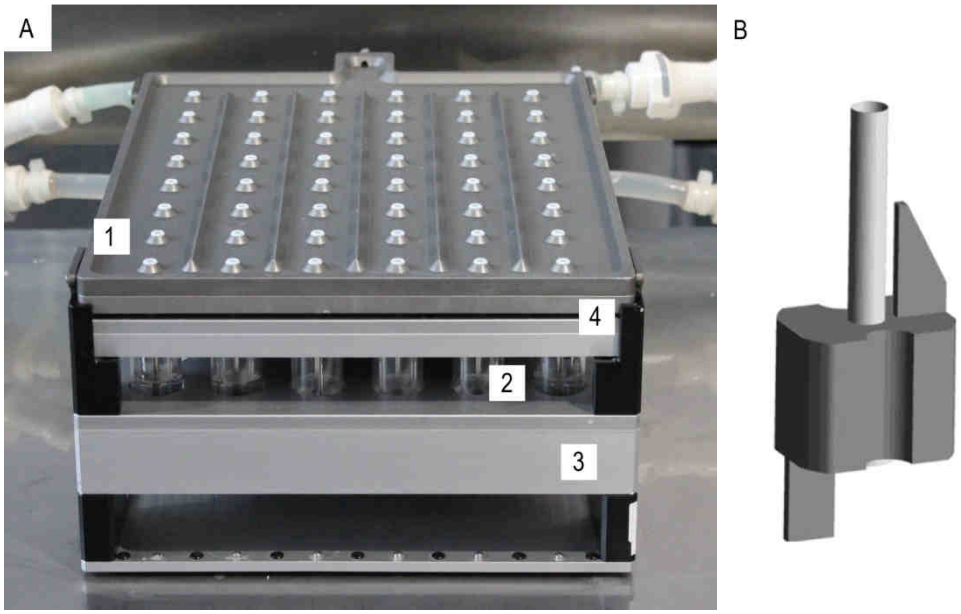

Figure 4.3 Bioreactor unit with the 48 parallel milliliter stirred-tank bioreactors for whole-cell batch biotransformations at the 12 ml scale. The bioreactor unit is presented in (A): cover equipped with 48 stirrers and the sampling openings (1), bioreactor (2), magnetic stirrer drive and temperature control (3) and head space cooling (4). A scheme of the applied S-impeller developed by Riedlberger and Weuster-Botz (2012) is shown in (B) (Riedlberger et al. 2012).

4.8.6 Biotransformations at the 200 mL scale

Whole-cell batch biotransformations at the 200 mL scale were performed in a stirred bubble column developed by Weuster-Botz et al. (2002) (Figure 4.4). The reactor with a nominal volume of 400 mL was equipped with three baffles (width 15 mm). Agitation was enabled by a magnetically driven six-blade Rushton turbine with blades possessing a square geometry of 8 x 8 cm. The impeller speed was fixed to 600 rpm, unless indicated otherwise. The reaction was performed for 8 – 10 h.

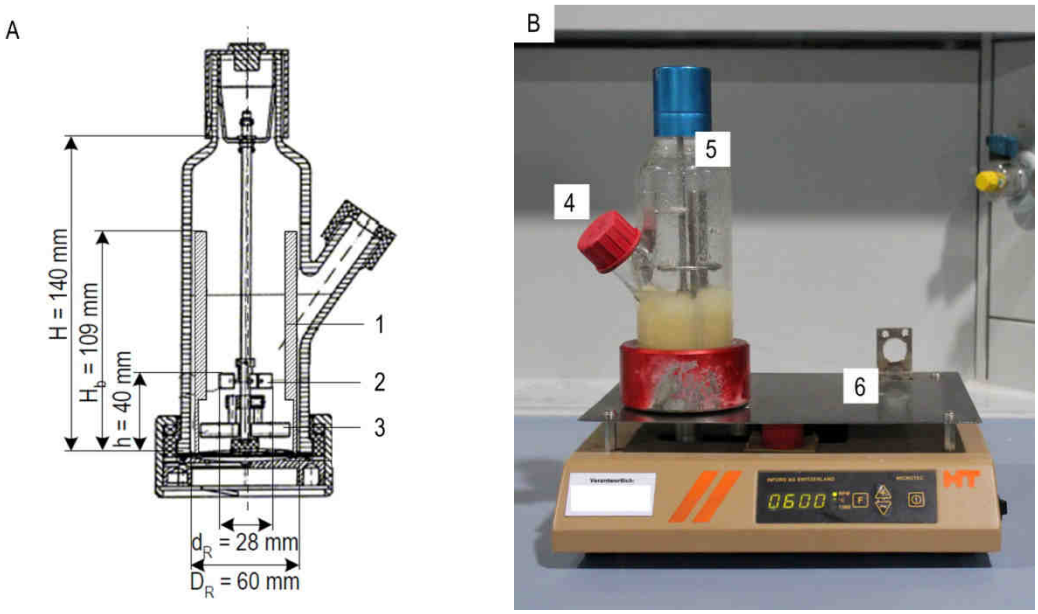

Figure 4.4 Biotransformation at the 200 mL scale in the stirred bubble column. A scheme of the bioreactor (Pfründer 2005) is given in (A) and a picture of the reactor during biotransformation is shown in (B): baffles (1), six-blade rushton turbine (2), magnetic drive inside the reactor (3), sampling opening (4), stirrer axis (5) and support with main magnetic drive (6).

4.8.7 Biotransformations at the liter scale

The scale-up of whole-cell batch biotransformation to the 1 L scale was performed in a stirred-tank bioreactor with a nominal volume of 1.2 L (Figure 4.5). It was equipped with two six-blade Rushton turbines fixed at a height of 2 cm and 6 cm from the stirrer tip. The impeller speed was set to 450 rpm for biphasic biotransformations with IL and 500 rpm for resin-based biotransformations. In general, pH was monitored but not controlled during the biotransformation. The temperature was controlled at 25 °C, unless stated otherwise.

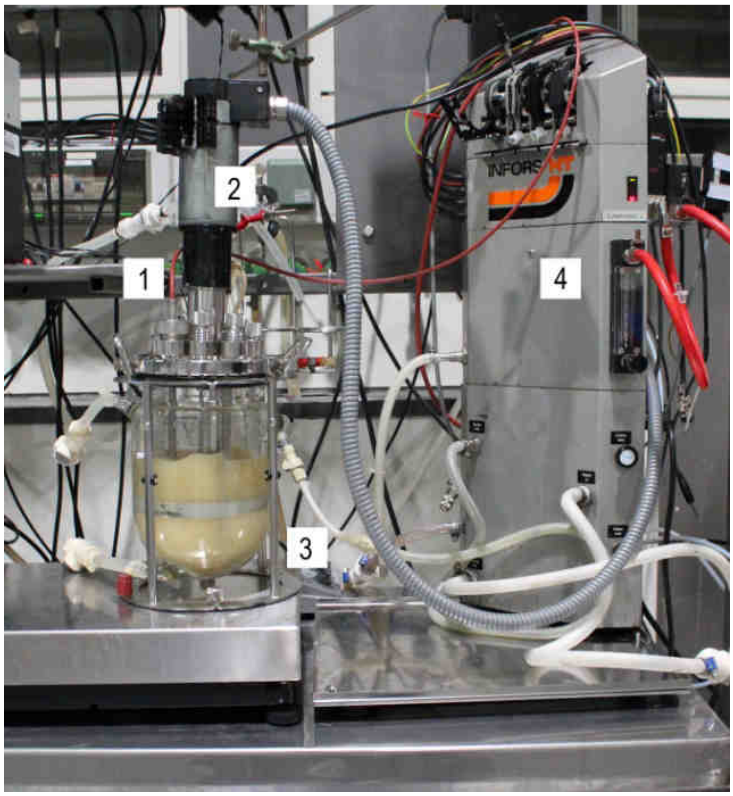

Figure 4.5 Biotransformation at the liter scale: temperature and pH probes (1), stirrer (2), bioreactor (3) and control station (4). In this picture the temperature control was not applied during biotransformation.

4.8.8 Response Surface Methodology

Selected process variables of the biphasic whole-cell batch biotransformations with water-immiscible IL were characterized using the Response Surface Methodology (RSM). In contrast to single factor experiments, multiple variables and their interacting influences can be investigated and optimized. The natural variables ξ_1, ξ_2,…ξ_k with particular influences are normalized to coded variables x_1, x_2,…x_k. The response η is given as a function of the coded variables x_1, x_2,…x_k (Equation 4.11) (Montgomery 2009).

$$\eta = f(x_1, x_2, \dots, x_k) \qquad \text{Eq. 4.11}$$

η	response, -
x_k	coded variables, -

To describe the function based on an empirical data set, a second order polynomial model was applied as presented in Equation 4.12.

$$\eta = \beta_0 + \sum_j \beta_j x_j + \sum_j \beta_{jj} x_j^2 + \sum_i \sum_j \beta_{ij} x_i x_j \qquad \text{Eq. 4.12}$$

η	predicted response (relative conversion) , -
x_j	variables under study, -
β_j	linear coefficient, -
β_{ij}	quadratic coefficient, -
β_{jj}	interaction coefficient, -

The coefficients β_j β_{ij} β_{jj} describing linear, quadratic and interacting influences were determined by the regression method of least squares using the program MATLAB (Mathworks).

For experimental design, a central composite circumscribed design (CCC) was chosen. Thereby, the center of the design space is surrounded by factorial points with a distance of ± 1 unit for each factor and star points with a distance of ± α with |α| > 1. The value of α depends on the experimental design and the numbers of factor involved (Equation 4.13) (Montgomery 2009). In case of a three factorial experimental design, the value of α was 1.682.

$$\alpha = 2^{\frac{k}{4}}$$ Eq. 4.13

α	distance to the star point, -
k	number of factors, -

The selected three process variables and borders for optimization were (R)-carvone concentration in the IL phase (100 – 600 mM), formate concentration in the aqueous phase (100 – 800 mM) and pH of the buffer (pH 5.7 – 7.2). Experiments were performed in triplicates at 12 mL scale in the bioreactor unit. Both conversions and the calculated product concentrations in the IL after 3 h and 5 h were used as response. For model validation, 12 randomly chosen operational points were created within the border used for model generation.

4.9 Analytics

4.9.1 Sample preparation for analysis by gas chromatography

As columns used for gas chromatography (GC) are generally sensitive to water and ionic liquids, samples had to be appropriately prepared before GC analysis. All organic solvents (ethyl acetate, *n*-hexane) applied for GC analysis were dried using 20 % (w/v) potassium carbonate for ~12 h. (R)-Limonene was selected as internal standard and was dissolved in dry ethyl acetate in a stock concentration of 36 mM.

Aqueous samples, which were obtained in enzymatic bioconversions or after phase separation of biphasic samples, were extracted with ethyl acetate at a ratio of 1:1 (v/v) in a mixer mill (15 min, 1800 min^{-1}). After phase separation in a benchtop centrifuge at 13000 min^{-1} for 3 min, the organic phase was diluted with dry ethyl acetate in a ratio of 1:3 (v/v). At last, 36 mM (R)-limonene dissolved in dry ethyl acetate was added as internal standard in a dilution of 1:4 (v/v) resulting in a final concentration of 7.2 mM in the GC sample. It should be noted that the determined concentrations by GC analysis were not significantly influenced whether the internal standard was added before or after the extraction.

In case of biphasic samples consisting of an aqueous phase and an ionic liquid phase, separation of the phases (5 min at 13000 min^{-1} in a benchtop centrifuge) was generally

performed prior to sample preparation. The ionic liquid phase was then extracted with *n*-hexane at a ratio of 1:4 (v/v) in a mixer mill for 1 h at 1800 min^{-1}. After another centrifugation step (15 min, 4528 x g), the organic phase was diluted with dry ethyl acetate and 36 mM (R)-limonene in a volume ratio of 1:3:1 for GC analysis. If the biphasic samples contained an organic solvent (e.g. *n*-hexane, *n*-decane), this phase was diluted in the same manner.

Solid-liquid samples containing adsorbent resins and an aqueous phase were centrifuged at 13000 min^{-1} for 5 min to separate both phases. The aqueous phase was then removed and a defined volume of ethyl acetate (300 µL) was added to the adsorbent resins. The extraction was conducted in a mixer mill for 15 min at 1800 min^{-1}. After centrifugation (13000 min^{-1} for 3 min), the organic phase was diluted with dry ethyl acetate and 36 mM (R)-limonene in a volume ratio of 1:3:1 for GC analysis.

4.9.2 Gas chromatography methods

Analysis of conversion and enantiomeric/diastereomeric excess was performed using a Varian CP-3800 gas chromatograph equipped with a flame ionization detector (FID). In case Lipodex E was applied as GC column, the injector temperature was set to 250 °C and the FID temperature to 250 °C. In case of the Astec Chiraldex B-TA column, the injector temperature and FID temperature was fixed at 200 °C and 250 °C, respectively.

The applied GC methods were listed in the following.

<u>(R)-carvone and (2R,5R)-/ (2S,5R)-dihydrocarvones</u>

Column	Lipodex E (25 m, 0.25 mm)
Internal standard	7.2 mM (R)-limonene
Injection	5 µL, split 50
Column flow	3.0 mL min^{-1}, helium 5.0
Oven temperature	30 °C hold for 2 min, to 150 °C at 3 °C min^{-1}
Typical retention times	(R)-limonene: 10.9 min, (2R,5R)-dihydrocarvone: 22.1 min, (2S,5R)-dihydrocarvone: 23.6 min (R)-carvone: 24.6 min

(R)-/ (S)-carvones and (2R,5R)-/ (2S,5R)-/ (2R,5S)-dihydrocarvones

Column	Astec Chiraldex-B-TA (40 m, 0.25 mm)
Internal standard	7.2 mM (R)-limonene
Injection	5 µL, split 100
Column flow	1.0 mL min^{-1}, helium 5.0
Oven temperature	80 °C hold for 2 min, to 110 °C at 10 °C min^{-1}, hold for 20 min; to 120 °C at 10 °C min^{-1}, hold for 10 min; to 180 °C at 10 °C min^{-1}, hold for 1 min
Typical retention times	(R)-limonene: 7.7 min, (2R,5R)-dihydrocarvone: 20.9 min, (2S,5R)-dihydrocarvone: 21.4 min, (2R,5S)-dihydrocarvone: 22.0 min, (R)-carvone: 27.3 min; (S)-carvone: 27.8 min

2-methylcyclopenten-1-one, (R)-/ (S)-2-methylcyclopentanone

Column	Astec Chiraldex-B-TA (40 m, 0.25 mm)
Internal standard	7.2 mM (R)-limonene
Injection	5 µL, split 50
Column flow	1.0 mL min^{-1}, helium 5.0
Oven temperature	70 °C hold for 8 min, to 80 °C at 10 °C min^{-1}, hold for 2 min; to 180 °C at 15 °C min^{-1}, hold for 2 min
Typical retention times	(R)-limonene: 13.3 min, (R)-2-methylcyclopentanone: 14.1 min, (S)-2-methylcyclopentanone: 14.1 min, 2-methylcyclopenten-1-one: 16.2 min

3-methylcyclohexen-1-one, (R)-/ (S)-3-methylcyclohexanone

Column	Astec Chiraldex-B-TA (40 m, 0.25 mm)
Internal standard	7.2 mM (R)-limonene
Injection	5 µL, split 50
Column flow	1.0 mL min^{-1}, helium 5.0
Oven temperature	80 °C hold for 17 min, to 180 °C at 15 °C min^{-1}, hold for 2 min
Typical retention times	(R)-limonene: 12.5 min, (R)-3-methylcyclohexanone: 20.5 min, (S)-3-methylcyclohexanone: 20.8 min, 3-methylcyclohexen-1-one: 24.6 min

2-methylmaleimide, (R)-/ (S)-2-methylsuccinimide

Column	Astec Chiraldex-B-TA (40 m, 0.25 mm)
Internal standard	7.2 mM (R)-limonene
Injection	5 µL, split 50
Column flow	1.0 mL min^{-1}, helium 5.0
Oven temperature	80 °C, to 130 °C at 10 °C min^{-1}, hold for 2 min, to 160 °C at 10 °C min^{-1}, hold for 6 min
Typical retention times	(R)-limonene: 5.9 min, (R)-2-methylsuccinimide: 10.5 min, 2-methylmaleimide: 14.2 min

ketoisophorone, (R)-/ (S)-levodione

Column	CP-Chirasil-Dex CB (25 m, 0.32 mm)
Internal standard	7.2 mM (R)-limonene
Injection	5 µL, split 50
Column flow	3.0 mL min^{-1}, helium 5.0
Oven temperature	90 °C, hold for 2 min, to 115 °C at 4 °C min^{-1}, hold for 2 min, to 180 °C at 20 °C min^{-1}, hold for 2 min
Typical retention times	(R)-limonene: 4.4 min, ketoisophorone: 9.7 min, (R)-levodione: 10.6 min, (S)-levodione: 10.82 min

4.9.3 Gas chromatography-mass spectrometry

Gas chromatography-mass spectrometry (GC-MS) was performed in the laboratory of Prof. Kühn (Institute of Inorganic Chemistry, Technische Universität München). Samples were prepared as described in Section 4.9.1 and analyzed in a CP3800 gas chromatograph (Varian) equipped with an ion trap MS detector.

(R)-carvone, dihydrocarvone, dihydrocarveol

Column	OPTIMA®-WAXplus (30 m, 0.32 mm)
Internal standard	7.2 mM (R)-limonene
Injection	2 µL, split 45
Column flow	3.0 mL min^{-1}, helium 5.0
Oven temperature	80 °C, hold for 1 min, to 100 °C at 10 °C min^{-1}, hold for 3 min, to 120 °C at 5 °C min^{-1}, hold for 5 min, to 200 °C at 10 °C min^{-1}, to 280 °C at 20 °C min^{-1}, hold for 4 min
Typical retention times	(R)-limonene: 3.1 min, (2R,5R)-dihydrocarvone: 10.1 min, (2S,5R)-dihydrocarvone: 10.6 min (R)-carvone: 13.9 min

4.9.4 Fluorescence-activated cell sorting

Fluorescence-activated cell sorting (FACS) was used to investigate cell damages induced by storage conditions or biotransformations. Cell samples were adjusted to OD_{600} 1.0 and subsequently diluted 1000-fold using phosphate buffered saline (PBS) to a particle density of ~10^9 particles mL^{-1}. This enabled a working range of 1000 signals s^{-1} at a flow of 1 mL s^{-1}. Cells (1 mL sample) were stained with 3 mM N-(3-triethylammoniumpropyl)-4-(4-(4-(diethylamino)phenyl)butadienyl)pyridinium-dibromid (RH414) and 0.75 mM bis-(1,3-dibutylbarbituric acid)trimethine oxonol ($Dibac_4[3]$). RH414 was applied to minimize background signals caused by cell debris, as this dye binds to the cell membrane. The membrane potential dye $Dibac_4[3]$ enters depolarized cells and binds to intracellular proteins or membranes (Suller and Lloyd 1999). By plotting the fluorescence of $Dibac_4[3]$ against the forward scatter, which indicates the particle size, cells can be classified as living or disrupted cells (Langemann et al. 2010).

4.9.5 Preparative purification of products

The liter-scale whole-cell biotransformation using adsorbent resins was terminated by separation the resins from the cell suspension using filtration (filter: Ø ~0.5 mm). The reactor was rinsed with ~400 mL destilled water to obtain the residual resins by a further filtration step. Obtained resins were extracted four-times using 400 – 500 mL ethyl acetate. Fractions of organic phases were pooled and subsequently transferred to a rotary evaporator LABOROTA 4003 (Heidolph). The organic phases were heated up to 40 °C under reduced pressure of 180 mbar to remove ethyl acetate. As boiling temperatures of both (R)-carvone and dihydrocarvone were ~230 °C, the temperature was increased to 100 °C and the pressure was reduced to 60 mbar to remove other possible contaminants. The obtained product was analyzed by GC, GC-MS and ^{1}H-NMR (Bruker Avance UltraShield 400 MHz spectrometer, 300 K). NMR spectroscopy was performed in collaboration with the laboratory of Prof. Kühn (Institute of Inorganic Chemistry, Technische Universität München).

5 Characterization of an novel ene-reductase from *Synechococcus* sp. PCC 7942[1]

5.1 Cloning, protein expression and purification

The ene-reductase from the cyanobacterium *Synechococcus* sp. PCC 7942 (RefSeq ID: YP_399492) was identified using the basic local alignment search tool (BLAST) of the National Center for Biotechnology Information (NCBI) databank (Altschul et al. 1990). The amino acid sequence exhibited a high similarity to OPR1 from *Oryza sativa* (51 % identity, 66 % similarity) and NemR from *E. coli* (49 % identity, 62 % similarity). In contrast, the similarity to OYE1 from *Saccharomyces carlsbergensis* and OYE2, OYE3 from *Saccharomyces cerevisiae* was lower (40 – 42 % identity, 56 – 57 % similarity). A sequence alignment with other OYE homologues demonstrated that Syn7942ER belongs to the so-called "classic ERs" according to the classification by Toogood et al. (2010). In addition, Syn7942ER is considered to be a monomeric protein based on the P-[LM]-T-R-X-R pattern in the loop β1 region and the G-[FYW]-X(3)-P-G-[ILV]-[FHYW] pattern in the loop β2 region according to Oberdorfer et al. (2011). The sequence alignment is shown in the Appendix A.5.2.

Cloning of the ER gene enabled the expression of a protein with a C-terminal His_6-tag (Syn7942ER-His_6) as well as a native protein without an affinity tag (Syn7942ER), which was obtained by the removal of the N-terminal His_6-maltose-binding- protein (His_6-MBP) tag from a His_6-MBP-Syn7942ER fusion protein. Typical yields after protein purification were about 5.6 mg protein per gram dry cell weight (mg g_{DCW}^{-1}) for Syn7942ER-His_6 and 0.5 mg g_{DCW}^{-1} for Syn7942ER. A SDS-PAGE analysis of purified Syn7942ER is presented

[1] Parts of the results have already been published in Fu Y, Hoelsch K, Weuster-Botz D. 2012. A novel ene-reductase from *Synechococcus* sp. PCC 7942 for the asymmetric reduction of alkenes. Process Biochemistry 47(12):1988-1997.

in the Appendix A.5.1. Purified enzymes were used for the characterization of the substrate spectrum, cofactor preference and stereoselectivity, as well as the enzyme properties with regard to the effect of temperature, pH and organic solvents.

5.2 Evaluation of catalytic efficiency and stereoselectivity

5.2.1 Substrate spectrum

The substrate spectrum of Syn7942ER was studied using 22 alkenes from different substance classes. The results are presented in Table 5.1. Syn7942ER showed high activities for maleimide derivatives (1.35 – 2.30 U mg^{-1}). In addition, cyclic enones were accepted with good rates (0.26 – 1.16 U mg^{-1}). Ketoisophorone, a molecule possessing two carbonyl groups, led to a higher activity (1.16 U mg^{-1}) compared to enones with one carbonyl group (< 0.75 U mg^{-1}). In contrast to 2-cyclohexen-1-one, a 2.9-fold lower reaction rate was shown for the enone with a smaller ring size (2-cyclopenten-1-one, 0.26 U mg^{-1}). Syn7942ER accepted (R)- and (S)-carvone with a slight preference for the (R)-enantiomer (0.61 U mg^{-1} and 0.37 U mg^{-1}, respectively). Both carbonyl and nitro groups were accepted equally as the electron-withdrawing activating group (0.75 U mg^{-1} for 2-cyclohexen-1-one compared to 0.83 U mg^{-1} for 1-nitrocyclohexene). No enzyme activity was detected using ß-substituted cyclic enones (3-methyl-2-cyclopenten-1-one, 3-methyl-2-cyclohexen-1-one), enones with exocyclic C=C bonds ((S)-/ (R)-pulegone) and dicarboxylic acids (itaconic acid, mesaconic acid).

The substrate spectrum was also investigated for Syn7942ER-His_6 with all 22 compounds. The C-terminal His_6-tag resulted in an overall reduction of the specific activity by an average factor of 2.7 ± 0.9, though it did not influence the preference for specific substrate types (data not shown).

Table 5.1 Substrate spectrum of Syn7942ER. Specific activities were determined at 25 °C using 10 mM substrate and 0.5 mM NADPH. n.d. = not detected.

Substrate	Products[a]	Specific activity, U mg^{-1}
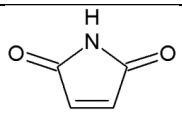 maleimide	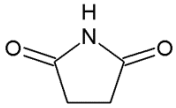 succinimide	1.35 ± 0.16
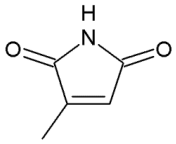 2-methylmaleimide	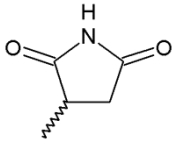 2-methylsuccinimide	2.30 ± 0.20
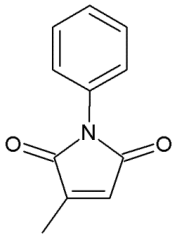 2-methyl-*N*-phenylmaleimide	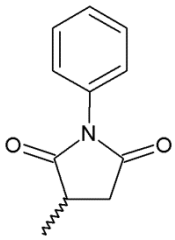 2-methyl-*N*-phenylsuccinimide	1.61 ± 0.12
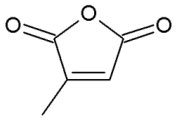 citraconic anhydride	–	n.d.
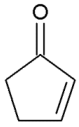 2-cyclopenten-1-one	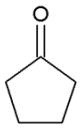 2-cyclopentanone	0.26 ± 0.13
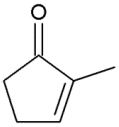 2-methyl-2-cyclopenten-1-one	–	n.d.
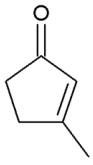 3-methyl-2-cyclopenten-1-one	–	n.d.
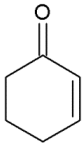 2-cyclohexen-1-one	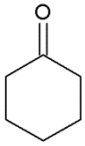 2-cyclohexanone	0.75 ± 0.03

Substrate	Products[a]	Specific activity, U mg^{-1}
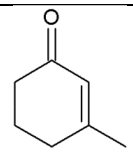 3-methyl-2-cyclohexen-1-one	–	n.d.
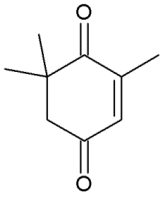 ketoisophorone	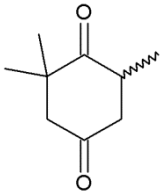 levodione	1.16 ± 0.02
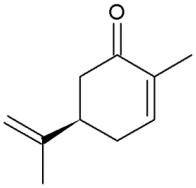 (5R)-carvone	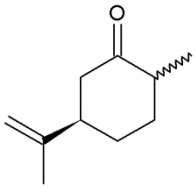 (5R)-dihydrocarvone	0.61 ± 0.18
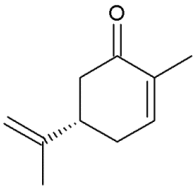 (5S)-carvone	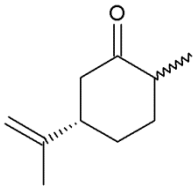 (5S)-dihydrocarvone	0.37 ± 0.10
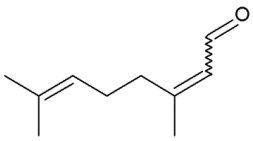 citral (*cis/trans*)	–	n.d.
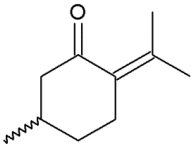 (R) or (S)-pulegone	–	n.d.
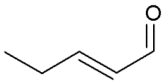 *trans*-2-penten-1-al	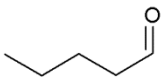 *trans*-2-pentanal	1.31 ± 0.09
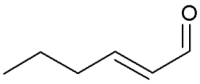 *trans*-2-hexen-1-al	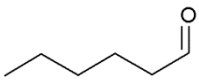 *trans*-2-hexanal	1.57 ± 0.10
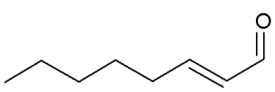 *trans*-2-octen-1-al	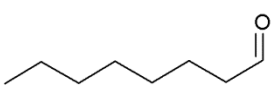 *trans*-2-octanal	1.45 ± 0.16

Substrate	Products[a]	Specific activity, U mg^{-1}
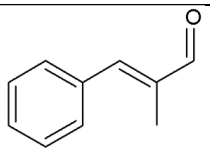	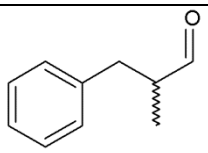	
3-phenyl-2-methylpropenal	3-phenyl-2-methylpropanal	0.19 ± 0.01
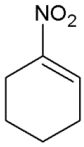	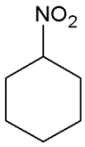	
1-nitrocyclohexene	1-nitrocyclohexane	0.83 ± 0.03
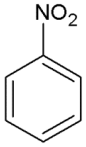		
nitrobenzene	–	n.d.
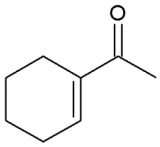		
1-acetyl-1-cyclohexene	–	n.d.
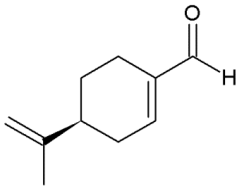	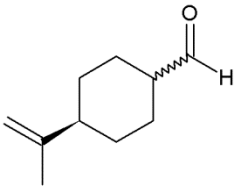	
(S)-perillaldehyde	dihydro-perillaldehyde	0.52 ± 0.06
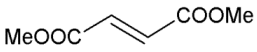	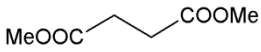	
dimethyl maleate	dimethyl succinate	0.55 ± 0.02
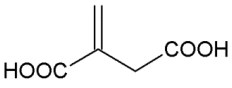		
itaconic acid	–	n.d.
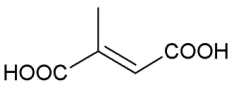		
mesaconic acid	–	n.d.

[a] As results were obtained from photometric assays, products were not determined. The displayed substances represent the expected products.

5.2.2 Cofactor specificity and kinetic parameters

Since the preference for the cofactors NADPH and NADH differs within the members of the OYE family (Chaparro-Riggers et al. 2007; Williams et al. 2004), the cofactor specificity of the Syn7942ER was investigated. Syn7942ER preferred NADPH over NADH with a activity ratio of 22:1. The apparent K_m and v_{max} for NADPH with maleimide as substrate were 0.36 ± 0.06 mM and 2.80 ± 0.29 U mg^{-1}, respectively. The C-terminal His_6-tag did not change the cofactor preference (NADPH to NADH activity ratio: 18:1), but it had a substantial impact on the apparent kinetic constants for NADPH, lowering the v_{max} 3.1-fold and the K_m 3.6-fold.

5.2.3 Conversion and stereoselectivity

The stereoselectivity of Syn7942ER was evaluated using 2-methyl-2-cyclopenten-1-one, 3-methyl-2-cyclohexen-1-one, (R)-carvone, 2-methylmaleimide and ketoisophorone (Table 5.2). The five substrates were chosen as representatives for the substance classes: maleimide derivatives, terpenoids and enones. In addition, both (R)-carvone and ketoisophorone are commercially interesting prochiral substrates (Winkler et al. 2012).

Syn7942ER reduced 2-methylmaleimide with high rate and stereoselectivity forming (R)-methylsuccinimide (> 99 % conversion and 99 % enantiomeric excess (ee)). (R)-carvone was converted in a *trans*-fashion yielding (2R,5R)-dihydrocarvone with an excellent stereoselectivity of 98 % diastereomeric excess (de). Reduction of 2-methyl-2-cyclopenten-1-one resulted in the (S)-enantiomer with low-to-modest optical purity (76 % ee). In case of ketoisophorone, the reduction over 24 h furnished (R)-levodione with a low enantiomeric excess (17 % ee). The low enantiopurity was caused by product racemization in aqueous solutions (Fryszkowska et al. 2009), given that molecules with a stereogenic centre at the Cα position are prone to racemise (Bechtold et al. 2012; Brenna et al. 2012d; Brenna et al. 2012e). This was supported by the fact that the reduction of the enantiomeric excess occured after a reaction time of 3 h, reaching 97 % ee at 93 % conversion of ketoisophorone.

No significant influence of the C-terminal His_6-tag was observed on the stereoselectivity of Syn7942ER. Thus, the C-terminal His_6-tag did not seem to impact the binding mode of substrates prior to the hydride transfer from FMN.

Table 5.2 Bioreduction with Syn7942ER. Assays contained 86 µg mL^{-1} (2.1 µM) purified ER, 15 mM NADH and 5 mM substrates (2-methyl-2-cyclopenten-1-one, 3-methyl-2-cyclohexen-1-one, (R)-carvone, 2-methylmaleimide and ketoisophorone). Reactions were performed for 24 h at 30 °C. Conversions (Conv., %) and enantiomeric excesses (ee, %) / diastereomeric excesses (de, %) were determined by chiral GC.

Substrate	Product	Conv. , %	ee/ de, %
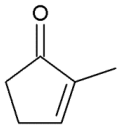	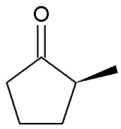		
2-methyl-2-cyclopenten-1-one	(S)-2-methylcyclopentanone	70	76 ee
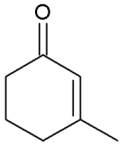	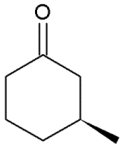		
3-methyl-2-cyclohexen-1-one	(S)-2-methylcyclohexanone	2	72 ee
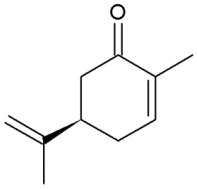	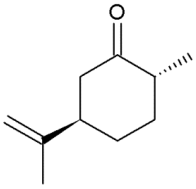		98 de
(R)-carvone	(2R,5R)-dihydrocarvone	> 99	99 ee
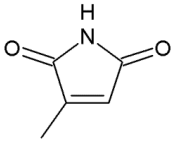	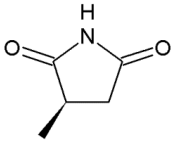		
2-methylmaleimide	2-methylsuccinimide	> 99	99 ee
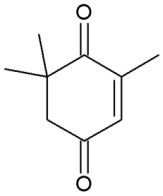	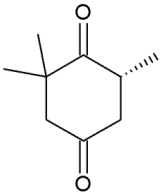		
ketoisophorone	(R)-levodione	> 99 93 (3 h)	17 97 (3 h)

5.3 Evaluation of reaction conditions

5.3.1 Temperature and pH optima

Syn7942ER was characterized with regard to the effect of temperature and pH on the enzyme activity using maleimide as substrate (Figure 5.1). A broad temperature optimum was determined ranging from 40 °C to 47 °C. An activation energy of 63.76 kJ mol^{-1} was calculated following the Arrhenius equation. The pH optimum for Syn7942ER was identified between pH 7.6 and pH 8.6 with the highest activity achieved using Tris-HCl buffer.

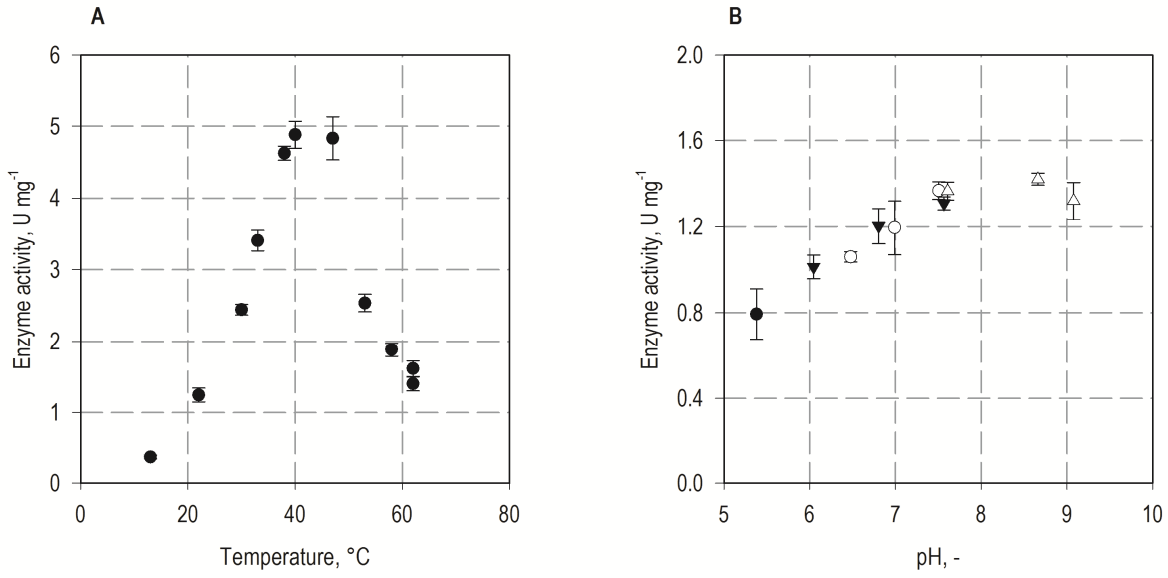

Figure 5.1 Temperature and pH optima of Syn7942ER. (A) Effect of temperature on the enzyme activity of Syn7942ER. (B) pH profile of Syn7942ER using 50 mM sodium citrate (black circle), 50 mM sodium phosphate (white circle), 50 mM 3-(N-morpholino)propanesulfonic acid (MOPS) (black triangle), and 50 mM Tris–HCl (white triangle). Reactions were performed with 10 mM maleimide and 0.5 mM NADPH.

5.3.2 Effect of salts and organic solvents

The effect of salts and co-solvents on the reaction rate of Syn7942ER was studied in assays with maleimide. The enzyme activity was not significantly influenced by concentrations of up to 0.3 M sodium phosphate (data not shown) and 1 M sodium chloride (Figure 5.1A). However, 3 M sodium chloride resulted in a reduction of the enzyme activity by 31 %. The effect of water miscible solvents on the enzyme activity of Syn7942ER was investigated using ethanol, 1-propanol, iso-propanol and DMF (Figure 5.1B). Ethanol appeared to be the

best solvent, since the enzyme acitivity was not impaired by 5 % (v/v) ethanol and 80 % of the enzyme activity was retained in the presence of 20 % (v/v) ethanol. In contrast, 20 % (v/v) DMF led to a reduction of the enzyme activity by 75 %.

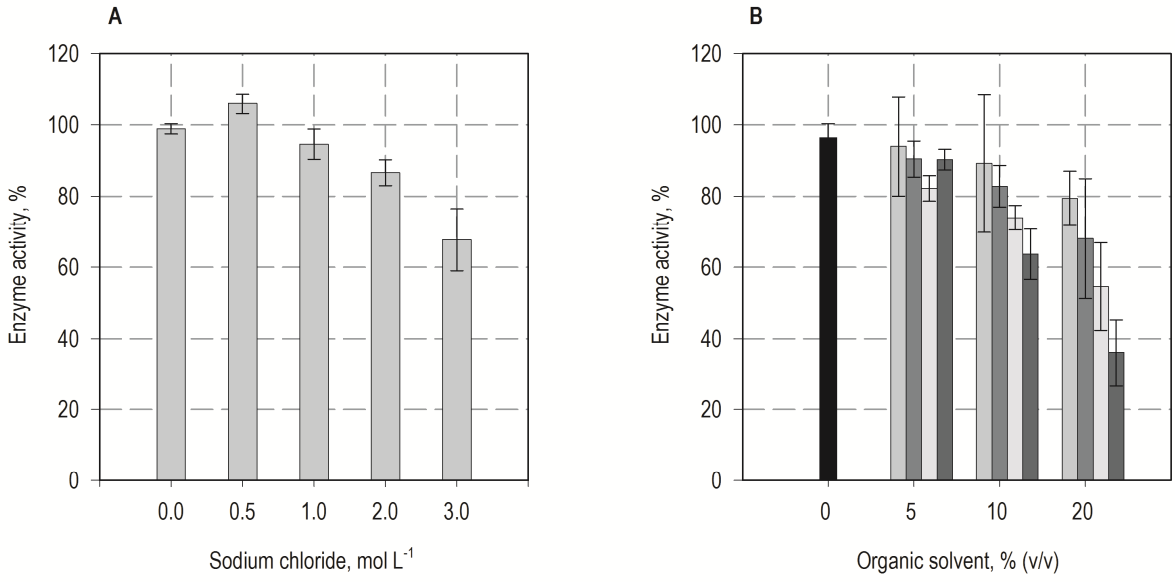

Figure 5.2 Effect of salts and organic solvents on the activity of Syn7942ER. (A) Dependence of the enzyme activity of Syn7942ER on 0 – 3 M sodium chloride concentration. (B) Impact of 0 – 20 % (v/v) organic solvents on the enzyme activity of Syn7942ER: reference (■), ethanol (■), 1-propanol (■), iso-propanol (■), dimethylformamide (■). Specific activities were determined using 10 mM maleimide and 0.5 mM NADPH.

In addition, the catalytic performance of Syn7942ER was investigated in presence of 5 – 20 % ethanol, iso-propanol and DMF during the bioreduction of ketoisophorone in mL-scale (Figure 5.2). Increasing amounts of organic solvents resulted in lower conversions. The highest conversions were achieved using 5 – 10 % (v/v) ethanol and iso-propanol. At 20 % (v/v), the reaction with iso-propanol yielded a 17 % lower conversion compared to ethanol. In contrast, conversions were reduced by 13 % to 23 % at the same concentrations of DMF compared to iso-propanol and ethanol, which is consistent with the results of the activitiy assays. Therefore, the enzymatic reaction rate is determined by the concentration and choice of the organic solvent, which can impair the catalytic structure and enzyme stability (Hollmann et al. 2011; Yanto et al. 2011).

Syn7942ER exhibited a high stereoselectivity in the formation of (R)-levodione, if the non-enzymatic racemization of the product in aqueous medium is minimized (Table 5.2). The results indicated that the enantiopurity of (R)-levodione decreased with higher conversions. Fryszkowska et al. (2009) showed that the enantiomeric excess of (R)-levodione depends on

the relative rates of the enzymatic reaction and the non-enzymatic racemization. When the reaction rate decreases with increasing conversion, the racemization process increases proportionally to the product concentration (first-order reaction), resulting in lower enantiopurities at higher conversions. The reactions with DMF resulted in significant lower stereoselectivities at similar conversions compared to the reactions with ethanol and iso-propanol. This result indicates that organic solvents might also influence the stereoselectivity of the enzyme or the water-mediated racemization (Hollmann et al. 2011; Yanto et al. 2011).

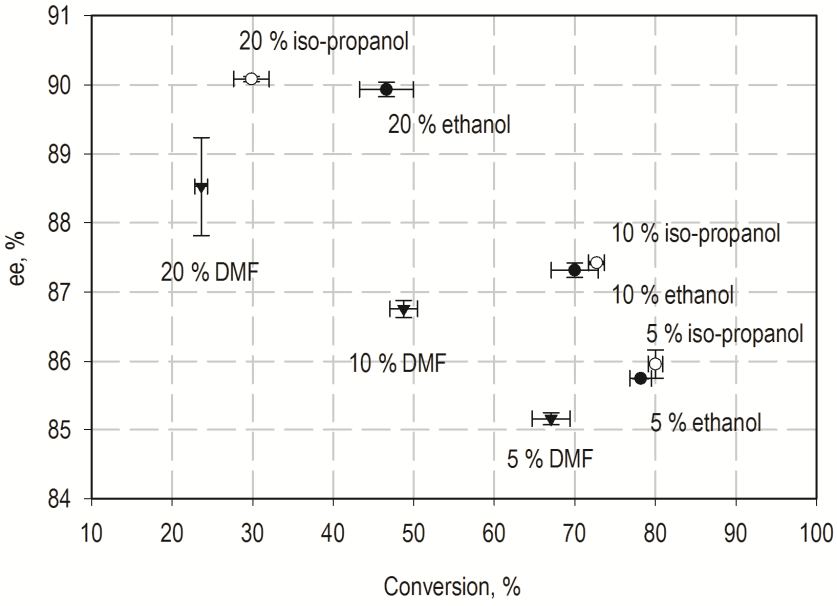

Figure 5.3 Bioreduction of ketoisophorone by Syn7942ER with 5 %, 10 % and 20 % (v/v) co-solvents: ethanol (black circle), iso-propanol (white circle) and dimethylformamide (black triangle). Reactions were performed at the mL scale with 57 µg mL^{-1} (1.2 µM) NADP$^+$-dependent FDH C145S/D221Q/C255V from *Mycobacterium vaccae* N 10, 250 mM sodium formate, 0.5 mM NADP$^+$, 10 mM ketoisophorone and 25 µg mL^{-1} (0.6 µM) Syn7942ER for 6 h at 30 °C and 150 rpm. Conversions and enantiomeric excesses (ee) were determined by chiral GC.

5.4 Discussion

Biocatalysis is considered as a valuable option for the stereoselective reduction of activated C=C bonds. Not only molecules with high optical purities can be produced using ERs, also the stereochemical outcome of the reaction can be controlled by the choice of substrate or enzyme (Hall et al. 2008b; Hall et al. 2007; Stueckler et al. 2007; Winkler et al. 2010). Although ERs show similarities regarding the stereochemistry of the product, both reaction rates and optical purities of the product vary between homologous enzymes (Toogood et al. 2010). This promotes the search for new biocatalysts performing highly stereoselective reactions.

In this section, the characterization of a novel ER from *Synechococcus* sp. PCC 7942 with respect to its biocatalytic potential for the asymmetric hydrogenation was presented. The impact of a C-terminal His_6-tag, which is useful for convenient protein purification, was studied. A significant reduction in enzyme activity was observed for Syn7942ER-His_6 without a clear preference for a specific substrate type. The K_m for NADPH was increased 3.6-fold, whereas the stereoselectivity was not influenced. Therefore, the affinity tag did not seem to alter the binding mode of alkenes, but probably the hydride transfer from NADPH to FMN. Strong structural and functional impairments due to a C-terminal tag has been observed for Yqjm from *Bacillus subtilis* of the dimeric "thermophilic-like" group (Fitzpatrick et al. 2004), which is based on the role of highly conserved C-terminal residues in the formation of the active site and dimer-dimer interfaces (Kitzing et al. 2005). In case of PETNR from *Enterobacter cloacae* st. PB2, a member of the monomeric "classical" group, which Syn7942ER can also be assigned to, a C-terminal tag did not affect the kinetic properties at all (Hulley et al. 2010). Consequently, the effect of C-terminal affinity tags cannot be predicted based on the structural differences of the two proposed groups.

The current commercial interest in ERs has been derived from their ability of generating industrial relevant compounds with high optical purities (Winkler et al. 2012). Syn7942ER showed moderate enzyme activities using maleimides (1.35 – 2.30 U mg^{-1}) and enones (0.26 – 1.16 U mg^{-1}), which are highly valuable building blocks for polymerization processes or synthons for pharmaceutical drug synthesis (Toogood et al. 2010). Ketoisophorone, an important intermediate for the production of carotenoids, such as zeaxanthin and xanthoxin (Leuenberger et al. 1976), was converted with a reaction rate of 1.16 U mg^{-1}. The reduction of carvones followed reaction rates in the range of 0.37 to 0.61 U mg^{-1} yielding

dihydrocarvones, that can be used for the synthesis of shape memory polyesters (Lowe et al. 2009), antimalarial drugs and natural products (Winkler et al. 2012). In case of (R)-carvone and ketoisophorone, the activities are comparable to those of KYE from *Kluyveromyces lactis* ATCC 8585 and XenA from *Pseudomonas putida* (Chaparro-Riggers et al. 2007).

The notable similarity of homologous ERs regarding the stereochemical outcome of the products (Toogood et al. 2010) was also observed for the novel Syn7942ER. The reduction of ketoisophorone, 2-methylmaleimide and (R)-carvone furnished (R)-enantiomers. (S)-products were derived in case of 2-methyl-2-cyclopenten-1-one and 3-methyl-2-cyclohexen-1-one, which is similar to the enantiopreference of PETNR (Fryszkowska et al. 2009), OYE1-3 (Hall et al. 2008b) or NemR (Mueller et al. 2010b). Syn7942ER reduced 2-methylmaleimide with a high enantiomeric excess of > 99 % ee, consistent with published data from other ERs (Fryszkowska et al. 2009; Hall et al. 2008a; Hall et al. 2008b; Mueller et al. 2010b). Low enantiomeric purities resulted from the reduction of 2-methyl-2-cyclopenten-1-one. This has been also observed for other ERs and explained by a flipped docking mode due to the smaller ring size of the molecule (Barna et al. 2001; Fryszkowska et al. 2009). Additionally, it is noteworthy that (2R,5R)-dihydrocarvone was produced with the highest enantiopurity of 98 % de by the reduction of (R)-carvone using Syn7942ER compared to published ERs from the literature (16 % de – 97 % de for PETNR (Fryszkowska et al. 2009), MorR from *Pseudomonas putida* M10, EBP1 from *Candida albicans*, NemR (Mueller et al. 2010b) and wild type OYE1 (Padhi et al. 2009)). Only mutants of OYE1 and LacER from *Lactobacillus casei* showed the same diastereomeric excess of 98 % de (Gao et al. 2012; Padhi et al. 2009).

Compared to the catalytic properties of *Synechococcus* sp. PCC 7942 as a whole-cell biocatalyst, similar preferences of substrate types were observed (Hirata et al. 2005; Shimoda et al. 2004). In whole-cell biotransformations, the cyanobacterium showed high conversion towards maleimide derivatives and α-methylated enones, whereas β-substituted enones led to low reaction rates (Hirata et al. 2005; Shimoda et al. 2004). Similar to the reactions with isolated Syn7942ER, (R)-enantiomers were obtained with > 99 % ee using maleimide derivatives (Hirata et al. 2005). In contrast to Syn7942ER, which reduced (R)-carvone and ketoisophorone furnishing (R)-enantiomers, corresponding (S)-enantiomers were produced during whole-cell biotransformations (Shimoda et al. 2004). Hence, other enzymes besides Syn7942ER might be involved in the reduction of activated alkenes in *Synechococcus* sp. PCC 7942.

In conclusion, the ability of Syn7942ER to reduce a variety of activated alkenes in a highly stereoselective manner revealed the potential of cyanobacterial ERs for asymmetric reduction. Thus, the capability of additional ERs from cyaobacteria was evaluated next.

6 Comparative characterization of ene-reductases from cyanobacteria[2]

6.1 Cloning, protein expression and purification

Putative ERs from various cyanobacterial strains, which were identified using the basic local alignment search tool (BLAST) of the National Center for Biotechnology Information (NCBI) databank (Altschul et al. 1990), were evaluated regarding their ability of asymmetric reduction of activated C=C bonds. A list of the ERs under study is shown in Table 6.1. During preliminary studies using cell lysates of ERs overexpressed in *E. coli*, putative ERs from *Synechococccus* sp. PCC 7335 (NCBI-RefSeq: ZP_05035623.1) and *Nostoc* sp. PCC 7120 (NCBI-RefSeq: NP_484870.1) did not show any activity towards maleimide, carvone or ketoisophorone (data not shown). Therefore, these enzymes were not characterized further. All other ERs were purified and characterized with regard to their substrate spectrum, cofactor specificity and stereoselectivity. A sequence alignment of all cyanobacterial ERs (Appendix, A.5.2) revealed differences in sequence patterns and active site residues, allowing an assignment to the two different subclasses proposed by Toogood et al. (2010) and Oberdorfer et al. (2011) All candidates can be assigned to the "classical" ERs, except for AnabaenaER3 and GloeoER, which belong to the group of "thermophilic-like" ERs. A SDS-PAGE with all ERs under study is shown in the Appendix A.5.1.

[2] Parts of the results have already been published in Fu Y, Castiglione K, Weuster-Botz D. 2013. Comparative characterization of novel ene-reductases from cyanobacteria. Biotechnol Bioeng 110(5):1293-301.

Table 6.1 List of studied ERs from cyanobacteria.

Abbreviation	NCBI-refSeq.	Cyanobacterial strain	Habitat	Taxonomic order
CyanothER1	YP_002370366.1	*Cyanothece* sp. PCC 8801	limnic	*Chroococcales*
CyanothER2	YP_002371879.1	*Cyanothece* sp. PCC 8801	limnic	*Chroococcales*
LyngbyaER1	ZP_01620253.1	*Lyngbya* sp. PCC 8106	euryhaline	*Oscillatoriales*
NospuncER1	YP_001869478.1	*Nostoc punctiforme* PCC 73102	limnic	*Nostocales*
NostocER1	NP_485905.1	*Nostoc* sp. PCC 7120	limnic	*Nostocales*
AcaryoER1	YP_001519129.1	*Acaryochloris marina* MBIC11017	marine	*Unclassified*
AcaryoER3	YP_001522070.1	*Acaryochloris marina* MBIC11017	marine	*Unclassified*
AnabaenaER3[a]	YP_320425.1	*Anabaena variabilis* ATCC 29413	limnic	*Nostocales*
GloeoER[a]	NP_926774.1	*Gloeobacter violaceus* PCC 7421	terrestrial	*Gloeobacterales*

[a] AnabaenaER3 and GloeoER belong to the group of "thermophilic-like" ene-reductases, whereas the other enzymes can be assigned to the "classical" ERs.

6.2 Evaluation of catalytic efficiency and stereoselectivity

6.2.1 Substrate spectrum

In order to obtain a comprehensive picture of the substrate spectrum, enzyme activities of the cyanobacterial ERs were studied using representatives from different substance groups (enones, maleimides, terpenoids and nitroalkenes). The results are depicted in Figure 6.1 and data are listed in the Appendix A.5.3. All cyanobacterial ERs showed activities in a range of 0.90 – 29.58 U mg^{-1} with maleimide as substrate (Figure. 6.1A). A slight modification of the molecule by an additional methyl-group (2-methylmaleimide) significantly influenced the reaction rates in case of CyanothER2, AcaryoER3 and LyngbyaER1. In contrast to maleimide and its derivative, the ER activities towards enones and aldehydes were throughout lower. *Trans*-1-hexen-1-al was reduced with rates of 0.27 U mg^{-1} to 2.32 U mg^{-1}, whereas the more sterically demanding aldehyde 3-phenyl-2-methylpropenal was reduced with lower rates in the range of 0.02 – 0.54 U mg^{-1} (Figure 6.1B). 2-Cyclohexen-1-one was reduced with higher reaction rates by all cyanobacterial ERs compared to 2-cyclopenten-1-one, which possesses a smaller ring size (0.30 – 2.03 U mg^{-1} vs. 0 – 1.19 U mg^{-1}) (Figure 6.1C and 6.1D). The preference of the electron-withdrawing group (carbonyl group vs. nitro group) was evaluated by comparison of the

activity towards 2-cyclohexen-1-one and 1-nitrocyclohexene (Figure 6.1C). The carbonyl group was preferably accepted by most cyanobacterial ERs. Only NostocER1, LyngbyaER1 and GloeoER showed 1.2- to 2.1-fold higher activities towards nitrohexene. The terpenoids (R)- and (S)-carvone were reduced with reaction rates of up to 1.09 U mg^{-1} (Figure 6.1E and 6.1F). The reduction of ketoisophorone was catalyzed with activities from 0.09 U mg^{-1} to 2.16 U mg^{-1} (Figure 6.1E). No enzyme activity was detected using ß-substituted cyclic enones (3-methyl-2-cyclopenten-1-one, 3-methyl-2-cyclohexen-1-one) and enones with exocyclic C=C bonds ((S)-/ (R)-pulegone) (data not shown).

AnabaenaER3 and GloeoER, the two ERs from the "thermophilic-like" subclass, exhibited different substrate preferences compared to the cyanobacterial ERs from the classical group. AnabaenaER3 and GloeoER showed a notably higher activity for 2-cyclopenten-1-one compared to the other ERs (1.01 – 1.19 U mg^{-1} vs. 0 – 0.51 U mg^{-1}) (Figure 6.1D). Whereas activities for 2-methyl-2-cyclopenten-1-one were almost undetectable for most of the cyanobacterial ERs, AnabaenaER3 and GloeoER showed activities of 0.26 U mg^{-1} and 0.27 U mg^{-1}, respectively. Differences were also observed in the reduction of the ketoisophorone and (R)-carvone. All cyanobacterial ERs from the group of "classical" ERs reduced ketoisophorone with higher reaction rates compared to the reaction using (R)-carvone, only the two members of the "thermophilic-like" subgroup reduced (R)-carvone with higher activities (Figure 6.1E). The highest reaction rates were achieved using AcaryoER1 (2.00 U mg^{-1}) and NostocER1 (2.16 U mg^{-1}) in the reduction of ketoisophorone and using AnabaenaER3 (1.09 U mg^{-1}) in case of (R)-carvone.

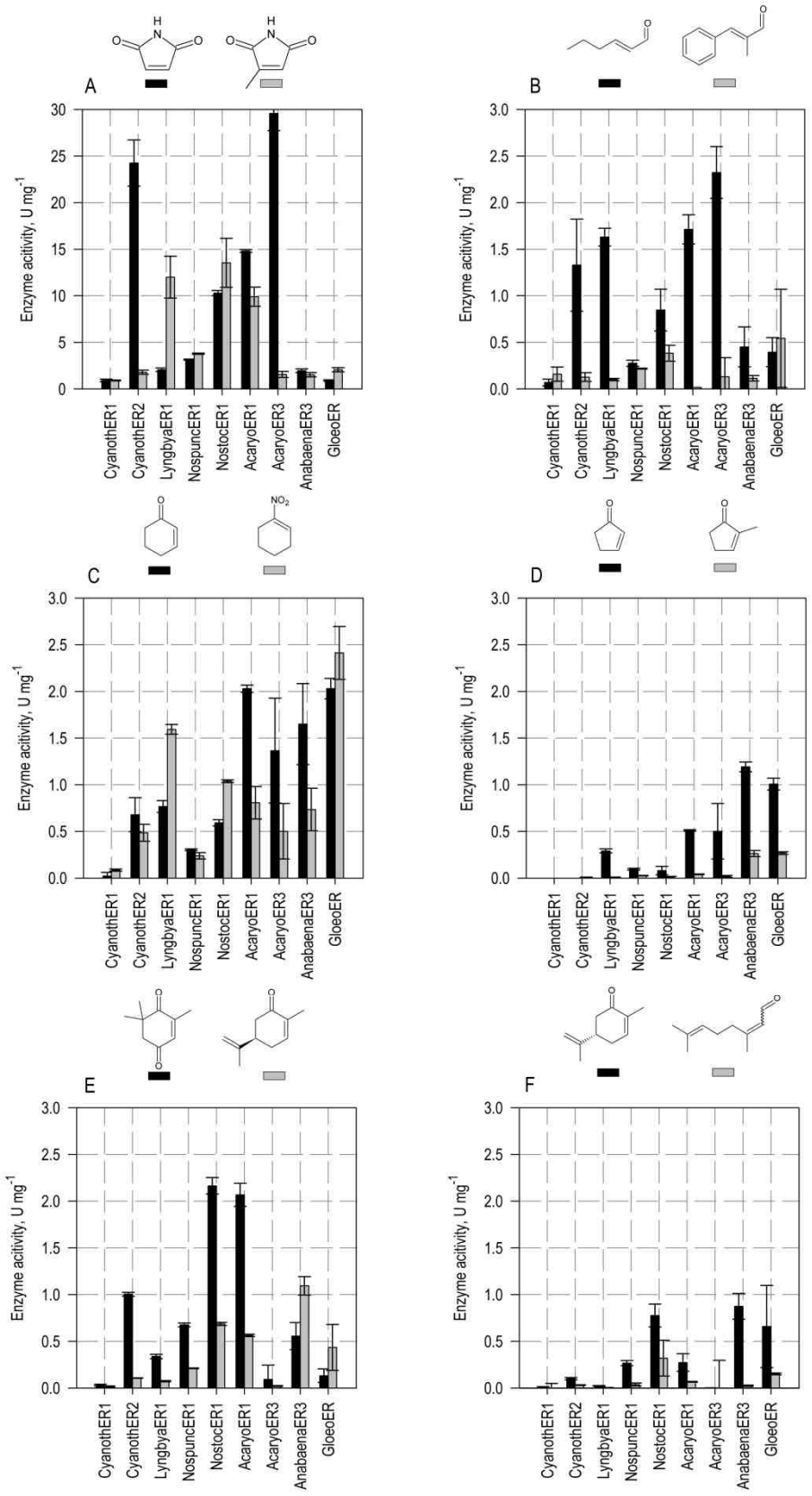

Figure 6.1 Substrate spectra of cyanobacterial ERs. Specific activities are displayed for the reduction of (A) maleimide (black) and 2-methylmaleimide (grey), (B) trans-2-hexen-1-al (black) and 3-phenyl-2-methylpropenal (grey), (C) 2-cyclohexen-1-one (black) and 1-nitrocyclohexene (grey), (D) 2-cyclopenten-1-one (black) and 2-methyl-2-cyclopenten-1-one (grey) (E) ketoisophorone (black) and (R)-carvone (grey), (F) (S)-carvone (black) and citral (grey). Assay conditions: 500 µM NADPH, 10 mM substrate, 100 mM sodium phosphate (pH 7.0), 25 °C.

6.2.2 Cofactor specificity and kinetic parameters

The cofactor preference is one major aspect when evaluating nicotinamide-dependent enzymes, because the cofactor and its regeneration influence the economy of the biocatalytic process. Similar to most ERs described in the literature (Toogood et al. 2010) all cyanobacterial ERs preferred NADPH over NADH with apparent K_m for NADPH varying between 52.2 µM and 383 µM (except for CyanothER1 and GloeoER, Table 6.2). As NAD(H) is clearly the better choice with respect to cost and stability (Wichmann and Vasic-Racki 2005) enzyme activities were determined using up to 500 µM NADH (Table 6.2). A cofactor concentration of up to 500 µM matches the basic requirements for economically feasible biotransformations (Hollmann et al. 2011). The studied ERs showed identical or up to 12.3-fold lower activity using NADH instead of NADPH. In the reduction of maleimide using AcaryoER1, AcaryoER3, AnabaenaER3 and CyanothER1, enzyme activities were identical or up to 2.5-fold lower (40 – 100 % of the original enzyme activity). AcaryoER3, which showed an enzyme activity of 35.53 U mg^{-1} using NADPH, catalyzed the same reaction with 16.73 U mg^{-1} using NADH.

Table 6.2 Half-saturation constants (Km), specific enzyme activities and cofactor preference of the cyanobacterial ERs under study. Assay conditions: 10 mM maleimide, 100 mM sodium phosphate buffer (pH 7.0), 30 °C. n.d.= not detected.

ER	K_m (NADPH), µM	500 µM NADPH, U mg^{-1}	500 µM NADH, U mg^{-1}	NADPH:NADH activity ratio 500 µM (200 µM)[a], -
CyanothER1	< 5	1.25 ± 0.24	1.25 ± 0.16	1.0 (0.9)
CyanothER2	108.7 ± 8.1	32.75 ± 3.12	12.01 ± 0.34	2.7 (5.3)
AnabaenaER3	383.0 ± 20.0	3.01 ± 0.02	2.05 ± 0.06	1.5 (1.6)
LyngbyaER1	170.7 ± 17.6	4.26 ± 0.42	0.38 ± 0.05	12.3 (39.4)
NostocER1	92.2 ± 8.3	10.50 ± 1.22	1.36 ± 0.04	7.7 (17.2)
NospuncER1	121.5 ± 8.8	4.26 ± 0.25	1.28 ± 0.04	3.3 (5.0)
AcaryoER1	109.4 ± 6.6	26.33 ± 2.18	10.45 ± 0.92	2.5 (3.5)
AcaryoER3	52.2 ± 4.6	35.53 ± 1.65	16.73 ± 0.39	2.3 (4.2)
GloeoER	< 10	1.06 ± 0.08	n.d.	n.d.

[a] The ratio of the activity with NADPH and NADH used for the estimation of cofactor preference depends on the half-saturation constants of both cofactors. Therefore, the NADPH to NADH activity ratio using 200 µM cofactor is additionally shown.

Because both AnabaenaER3 and AcaryoER1 showed acceptable activities towards (R)-carvone and ketoisophorone using NADPH as cofactor (Figure 6.1E) and a good NADH acceptance (Table 6.2) as well, the enzyme activities were determined for these two enzymes with 500 µM NADH and four other substrates ((R)-carvone, 2-methyl-2-

cyclopenten-1-one, 2-cyclopenten-1-one and ketoisophorone). The results are shown in Table 6.3. Using NADH as cofactor, a specific activity of 1.32 U mg^{-1} was achieved in the reduction of ketoisophorone by AcaryoER1 and 0.81 U mg^{-1} in the reduction of (R)-carvone by AnabaenaER3.

Table 6.3 Specific activities of AnabaenaER3 and AcaryoER1 using NADH as cofactor. Assay conditions: 10 mM substrate, 500 µM cofactor, 100 mM sodium phosphate buffer (pH 7.0), 25 °C.

	AnabaenaER3 (NADH), U mg^{-1}	**AcaryoER1 (NADH), U mg^{-1}**
Maleimide	1.45 ± 0.02	6.59 ± 0.30
(R)-Carvone	0.81 ± 0.06	0.23 ± 0.01
2-Methylcyclopentenone	0.25 ± 0.02	0.06 ± 0.003
2-Cyclopentenone	0.81 ± 0.02	0.39 ± 0.02
Ketoisophorone	0.32 ± 0.42	1.32 ± 0.10

6.2.3 Conversion and stereoselectivity

Next, the stereoselectivities of the cyanobacterial ERs were studied with six exemplarily chosen prochiral enones. The results are depicted in Table 6.4. For all ERs, 2-methylmaleimide was an excellent substrate, as it was completely converted to (R)-methylsuccinimide with high enantiomeric excesses (ee) of > 99 % ee. After 24 h, 26 % to 99 % 2-methyl-2-cyclopenten-1-one was converted in a *cis*-specific fashion yielding (S)-2-methylcyclopentan-1-one with 75 % to 81 % ee. Though no activity was detectable for 3-methyl-2-cyclohexen-1-one in photometric assays, the bioreduction assay revealed low conversions (2 – 12 %) at moderate ee-values (26 – 87 % (S) ee). The *cis*-specific fashion of both reactions is typical for ERs (Toogood et al. 2010) and can be explained by the flipped docking mode of the molecules (Barna et al. 2001). In most cases, (R)-carvone was completely converted to (2R,5R)-dihydrocarvone with high diastereomeric excesses (de) of 97 – 98 % de. Reduction of (S)-carvone resulted in (2R,5S)-dihydrocarvone with diastereomeric excesses in the range of 87 % to 91 % de. Ketoisophorone was converted > 99 % using most ERs. Low optical purities of (R)-levodione (17 – 46 % ee) can be explained by product racemization in an aqueous environment (Fryszkowska et al. 2009). In fact, during the reduction of ketoisophorone by NostocER1 using a $NADP^+$-dependent FDH mutant for the cofactor regeneration (Hoelsch et al. 2012), (R)-levodione was formed with an optical purity of 94 % ee after 2 h (Table 6.5). After 24 h, the conversion reached > 99 %, though the optical purity was reduced to 32 % ee.

Table 6.4 Asymmetric bioreduction by cyanobacterial ERs using different prochiral enones. Assay conditions: 5 mM substrate, 15 mM NADH, 100 mM sodium phosphate buffer (pH 7.0), 30 °C for 24 h. Conv. = conversion, ee = enantiomeric excess. n.c. = no conversion, n.d. = not detected.

ER	**2-Methyl-2-cyclopenten-1-one**		**3-Methyl-2-cyclohexen-1-one**		**(R)-Carvone**		**(S)-Carvone**		**2-Methyl-maleimide**		**Ketoisophorone**	
	Conv, %	ee, %	Conv, %	ee, %	Conv, %	de, %	Conv, %	de, %	Conv, %	ee, %	Conv, %	ee, %
CyanothER1	0.7	99 (S)	nc	nd	29	99 (R)	29	n.d.	99	99 (R)	40	38 (R)
CyanothER2	32	83 (S)	2	79(S)	99	97 (R)	99	87 (R)	99	99 (R)	99	16 (R)
LyngbyaER1	88	81 (S)	6	63(S)	99	98 (R)	99	91 (R)	99	99 (R)	99	18 (R)
NospuncER1	3.8	77 (S)	7	26(S)	99	98 (R)	99	89 (R)	99	99 (R)	99	19 (R)
NostocER1	89	80 (S)	5	43(S)	99	97 (R)	99	87 (R)	99	99 (R)	82	17 (R)
AcaryoER1	26	75 (S)	12	87(S)	99	97 (R)	99	89 (R)	99	99 (R)	99	17 (R)
AcaryoER3	n.c.	n.d.	9	30 (S)	45	97 (R)	22	89 (R)	99	99 (R)	88	34 (R)
AnabaenaER3	99	78 (S)	n.c.	n.d.	99	97 (R)	99	86 (R)	99	99 (R)	76	24 (R)
GloeoER	1.5	n.d.	n.c.	n.d.	24	34 (R)	16	99 (R)	38	99 (R)	11	46 (R)

Table 6.5 Bioreduction of ketoisophorone by NostocER1 using a cofactor-regeneration system. Assay conditions: 21 µg mL^{-1} NostocER1, 21 µg mL^{-1} FDH C145S/D221Q/C255V from *Mycobacterium vaccae* N 10, 500 µM $NADP^+$, 250 mM sodium formate, 5 mM ketoisophorone, 30 °C. Conv. = conversion, ee = enantiomeric excess.

Time	Conv., %	ee, %
2 h	58	94 (R)
3 h	74	90 (R)
24 h	> 99	32 (R)

6.2.4 Discussion

The major advantage of ERs is the capability of reducing a broad range of alkenes in a *trans*-specific fashion yielding molecules with high optical purities, thus, complementing or substituting strategies of (organo)chemical synthesis. Much effort has been directed towards the establishment of these enzymes in industrial biocatalysis including the investigation of catalytic activity, substrate spectrum and stability of various ERs (Winkler et al. 2012) Nevertheless, drawbacks of these enzymes exist. On the one hand, some ERs have to be applied under strict anaerobic conditions. A prominent example is PETNR from *Enterobacter cloacae* st. PB2, which showed reduced activity of up to 48 % in presence of oxygen (Fryszkowska et al. 2009). On the other hand, most ERs strongly depend on NADPH as cofactor. For example, activities of XenA from *Pseudomonas putida* and YersER from *Yersinia bercovieri* were up to 22-fold lower using NADH (Chaparro-Riggers et al. 2007). Only few ERs from the literature, for example MR from *Pseudomonas putida* M10 or LacER from *Lactobacillus casei*, preferred NADH as cofactor, but these enzymes often exhibit a narrow substrate range and low activity (French and Bruce 1994; Gao et al. 2012; Mueller et al. 2010b)

In this thesis, nine cyanobacterial ERs of different taxonomic orders and habitats were characterized with the aim of finding novel ERs with the capability of overcoming these limitations. The results revealed several ERs with high activities in presence of oxygen and outstanding properties regarding NADH acceptance and stereoselectivities. Taxonomic orders and habitats did not correlate with the activity, cofactor preference and stereoselectivity of the enzymes.

Enzyme activities of three selected cyanobacterial ERs are compared with ERs from the literature in Table 6.6. With NADPH, activities of the cyanobacterial ERs were comparable

or higher than the activities of ERs described in the literature. AcaryoER3 showed an excellent activity towards maleimide compared to other ERs under similar conditions (29.58 U mg^{-1} vs. 2.04 – 25.82 U mg^{-1} using KYE1 from *Kluyveromyces lactis*, XenA and YersER). The activities of AnabaenaER3 and AcaryoER1 with the commercially relevant compounds (R)-carvone and ketoisophorone (1.09 U mg^{-1} and 2.00 U mg^{-1}) using NADPH as cofactor were comparable with the activities of other ERs (0.7 – 10.11 U mg^{-1}). In contrast to the ERs from the literature, which exhibited strong NADPH preferences, the three cyanobacterial ERs showed good reaction rates with NADH as cofactor as well. The good NADH acceptance of AcaryoER1, AcaryoER3 and AnabaenaER3 is pointed out by a NADPH to NADH activity ratio of 1.5 to 4.2 compared to ratios in the range of 7 to 22 in case of KYE, XenA and YersER. Maleimide was reduced with a rate of 16.7 U mg^{-1} using NADH by AcaryoER3, whereas ERs from the literature showed activities lower than 1.50 U mg^{-1}. AnabaenaER3 and AcaryoER1 converted (R)-carvone and ketoisophorone using NADH with reaction rates of 0.81 U $mg^{-1}$and 1.32 U mg^{-1}, respectively.

Table 6.6 Comparison of cyanobacterial ERs with ERs from the literature regarding enzyme activity (U mg^{-1}) and cofactor specificity in the reduction of maleimide, (R)-carvone and ketoisophorone. Cofactor preference was presented using the NADPH to NADH activity ratio. n.a. = not available, n.d. = not detected.

ER	**maleimide**		**(R)-carvone**		**ketoisophorone**		**NADPH:NADH activity ratio[e]**
	NADPH	NADH	NADPH	NADH	NADPH	NADH	
AcaryoER3[a]	29.58	16.7[b]	0.02	n.a.	0.09	n.a.	2.3 – 4.2
AnabaenaER3[a]	1.95	1.45	1.09	0.81	0.56	0.32	1.5 – 1.6
AcaryoER1[a]	14.80	6.59	0.56	0.23	2.00	1.32	2.3 – 3.5
KYE1[c]	2.04	n.d.	0.73	n.a.	1.33	n.a.	> 7
XenA[c]	25.82	1.50	0.00	n.a.	1.84	n.a.	18
YersER[c]	18.88	n.d.	2.54	n.a.	10.11	n.a.	> 22
LacER[d]	0.00	0.00	0.00	0.16	na	n.a.	NADH-dependent

[a] Assay conditions: 100 mM sodium phosphate, pH 7.0, 10 mM substrate, 500 µM cofactor, 25 °C.
[b] Assay conditions: 100 mM sodium phosphate, pH 7.0, 10 mM substrate, 500 µM cofactor, 30 °C.
[c] Chaparro-Riggers et al. (2007).
[d] Gao et al. (2012).
[e] The NADPH to NADH activity ratio is shown as the ratio of activity using 200 µM to 500 µM cofactor and maleimide at 30 °C in this study. The values in the reference Chaparro-Riggers et al. (2007) were measured with 200 µM cofactor.

The stability of the biocatalyst in presence of oxygen and the acceptance of NADH are both favorable attributes for large-scale applications, enhancing the economy of the process. Biocatalytic reactions under strict anaerobic conditions are constrained to lab-scale due to the current limitations in the development of anaerobic bioreactors or handling of these

biocatalysts (Toogood et al. 2010). Cofactor costs are 4- to 18-fold lower using NAD(H) compared to NADP(H) (commercial suppliers). In addition, NADH exhibited up to 7-fold higher stability (half-life) compared to NADPH depending on the pH and ionic strength of the reaction system (Wu et al. 1986).

In addition to the reaction rate, stereochemical outcome and stereoselectivity are crucial for the evaluation of a biocatalyst, especially in case of asymmetric reductions. High selectivity and specificity are the most important benefits of using enzymes in synthetic chemistry (Hollmann et al. 2011). Due to the catalytic mechanism of ERs, most reductions proceed in a *trans*-specific fashion, resulting in a similar stereochemistry of the product for the majority of homologous enzymes (Toogood et al. 2010). This can be confirmed by the obtained results, as the stereochemical outcome of reactions was identical among all cyanobacterial ERs under study (Table 6.4). On the contrary, the diastereomeric and enantiomeric excess of the product depends on the nature of the active site of the enzyme and varies substantially between ERs (Toogood et al. 2010) (Table 6.7). However, the enantiopurity of the product can be influenced by racemization in aqueous medium. Especially in case of ERs, reduction products often possess a stereogenic centre at Cα position, which is prone to racemization (Brenna et al. 2012e; Fryszkowska et al. 2009). The rate of racemization depends on the nature of the compound. In case of levodione, the racemization proceeded with approximately −3 % ee per hour (Fryszkowska et al. 2009). Therefore, obtained data of enantiomeric excesses of (R)-levodione after a 24 h reaction cannot be associated with the catalytic performance of the biocatalysts, though most selectivity data in the literature were determined after 24 h or 48 h (Fryszkowska et al. 2009; Hall et al. 2008a; Hall et al. 2008b; Mueller et al. 2010b). Nevertheless, the optical purity of 94 % ee for NostocER1 after a reaction of 2 h (Table 6.5) indicated high stereoselectivity of the cyanobacterial ERs in the reduction of ketoisophorone.

In contrast, the effect of product racemization was minimal in the reduction of (R)-carvone and 2-methyl-2-cyclopenten-1-one (Fryszkowska et al. 2009). Thus, Table 6.7 compares the stereoselectivities of selected ERs from cyanobacteria with OYE-homologues from the literature for these two reactions. The cyanobacterial ERs exhibited excellent stereoselectivities with regard to the reduction of (R)-carvone in comparison with ERs from the literature. Whereas (2R,5R)-dihydrocarvone was formed in diastereomeric excesses of 16 % to 97 % de by ERs from the literature, up to 98 % de and 99 % conversion were achieved by NospuncER1 and LyngbyaER1. Bioconversion using CyanothER1 even

reached product purities of 99 % de, though the conversion was moderate. The bioreduction of 2-methyl-2-cyclopenten-1-one by AnabaenaER3, CyanothER2 and LyngbyaER1 resulted in higher conversions (up to 99 %) and enantiomeric excesses (up to 83 % ee) compared to literature data from ER homologues (< 72 % conversion and < 64 % ee).

Table 6.7 Comparison of conversion (Conv, %) and diastereomeric excesses / enantiomeric excesses (de % / ee %) in the reduction of (R)-carvone and 2-methylcyclopenten-1-one with NAD(H) as cofactor using cyanobacterial ERs with ERs from literature. n.a. = not available, n.d. = not detected.

ER	**(R)-Carvone**		**2-Methylcyclopenten-1-one**	
	Conv., %	de, %	Conv., %	ee, %
CyanothER1[a]	26	99 (R)	0.7	99 (S)
LyngbyaER1[a]	99	98 (R)	88	81 (S)
NospuncER1[a]	99	98 (R)	3.8	77 (S)
AnabaenaER3[a]	99	97 (R)	99	78 (S)
AcaryoER1[a]	99	97 (R)	26	75 (S)
CyanothER2[a]	99	97 (R)	32	83 (S)
NCR[b]	n.a.	n.a.	80	15 (S)
OYE 1-3[b]	98[c]	97 (R)[c]	40-46	*rac* – 5 (S)
OPR1/OPR3[d]	n.a.	n.a.	58/ 27	61/ 45 (S)
Yqjm[d]	n.a.	n.a.	50	55 (S)
PETNR[e]	95	94 (R)	48	64 (S)
NemR[e]	97	92 (R)	72	59 (S)
MR[e]	25	16 (R)	< 1	n.d.
EBP1[e]	11	95 (R)	14	38 (S)
LacER[f]	99	98 (R)	n.a.	n.a.

[a] Assay conditions: 100 mM sodium phosphate, pH 7.0, 5 mM substrate, 15 mM NADH, 30 °C, 24 h.
[b] Hall et al. (2008b).
[c] OYE1, Padhi et al. (2009).
[d] Hall et al. (2007), Hall et al. (2008a).
[e] Mueller et al. (2010).
[f] Gao et al. (2012)

6.3 Enzyme stability and process capability of selected ene-reductases

Selected ene-reductases were characterized regarding their stability towards temperature and solvents. The performance of these enzymes under operational conditions was of special interest with respect to the application in biocatalytic processes. The results are presented in the following.

6.3.1 Storage stability

The evaluation of the storage conditions was carried out for AcaryoER1, AnabaenaER3, NostocER1 and CyanothER2. The enzyme activities were not impaired using 25 % (v/v) glycerol after a shock freezing process using liquid nitrogen and subsequent storage at −80 °C for at least 3 months (data not shown). Enzymes were stored in high concentrations (~1.5 – 2.3 mg mL^{-1}) resulting in < 1 % (v/v) glycerol after dilution and subsequent use for activity assays or enzymatic conversions.

6.3.2 Temperature stability

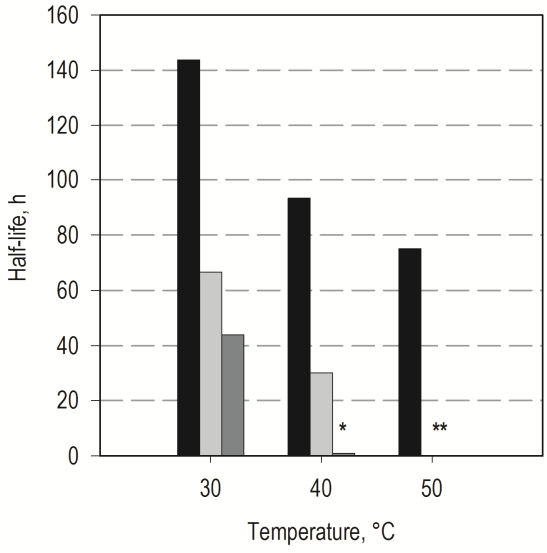

Figure 6.2 Temperature stability of ERs. Half-lives of AnabaenaER3 (black), NostocER1 (grey) and AcaryoER1 (dark grey) were determined at the respective temperature at 200 rpm in Eppendorf Safe-Lock Tubes. (*) 0.91 h for AcaryoER1, (**) 0.15 h for NostocER1 and 0.21 h for AcaryoER1.

The temperature stability of AnabaenaER3, Nostoc ER1 and AcaryoER1 was studied using half-life measurements (Figure 6.2). The half-lives of the three enzymes were between 44 h and 144 h at 30 °C. The presumably dimeric AnabaenaER3 showed a notably higher temperature stability compared to the presumably monomeric enzymes NostocER1 and AcaryoER1. At 30 °C, the half-life of AnabaenaER3 was three-fold higher compared to AcaryoER1. At 50 °C, only AnabaenaER3 showed a half-life of 75 h, whereas the half-lives of NostocER1 and AcaryoER1 were 0.15 h and 0.21 h, respectively.

6.3.3 Solvent stability

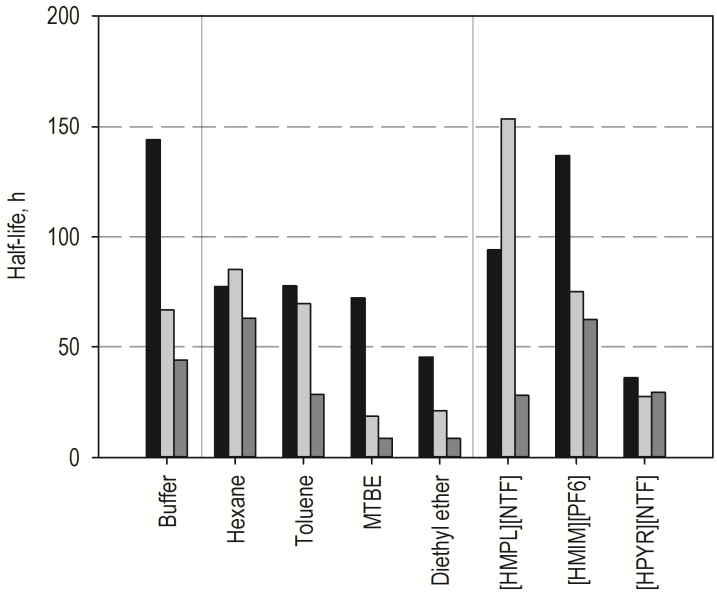

Figure 6.3 Solvent stabilities of ERs under process conditions. Half-lives were measured for AnabaenaER3 (black), NostocER1 (grey) and AcaryoER1 (dark grey) incubated in sodium phosphate buffer (100 mM, pH 7.0) containing 20 % (v/v) water-immiscible organic solvents or ionic liquids at 30 °C in glass vials positioned on a shaking tray at 200 rpm. References were measured in 100 mM sodium phosphate buffer (pH 7.0) under the same conditions.

AnabaenaER3, NostocER1 and AcaryoER1 were studied with regard to their stability in biphasic reaction systems containing 20 % (v/v) organic solvents and ionic liquids in 100 mM sodium phosphate buffer (pH 7.0). Enzyme preparations were positioned on a shaking tray at 200 rpm at 30 °C (Figure 6.3). Due to the rotating movement of the reaction system, enzymes were exposed to both molecular and phase toxicity.

Under this condition, AnabaenaER3 showed (again) higher stabilities with in most biphasic reaction systems and in the reference without the addition of solvents. In a biphasic reaction system with 20 % (v/v) organic solvents, the stabilities of NostocER1 and AcaryoER1 were

more impaired by solvents possessing lower log*P* such as MTBE (log*P* 0.93) and diethyl ether (log*P* 0.89) compared to solvents with higher log*P* such as *n*-hexane (log*P* 3.9) and toluene (log*P* 2.73). For example, the half-life of NostocER1was decreased to 19 h using MTBE in contrast to a half-life of 85 h using *n*-hexane. A superior stability of AnabaenaER3 was not observed using 20 % (v/v) ionic liquids as a second phase. Using [HMPL][NTF] as a second water-immiscible phase, the half-lives of AnabaenaER3 and NostocER1 were 94 h and 154 h, respectively.

The hydrophobicity of organic solvents, quantified by the log*P* value, is considered as the key determinant for enzyme activity and stability. Using more hydrophobic solvents, the distortion of the essential water from the enzyme surface can be mostly prevented, which makes organic solvents of log*P* > 2 more favorable for biocatalytic applications (Laane et al. 1987; Vermue and Tramper 1995). This log*P* concept was confirmed for the stabilities of NostocER1 and AcaryoER1. In contrast, the half-life of AnabaenaER3 was not decreased using MTBE with lower log*P*. This indicated an additional influence on the enzyme stability by the molecular structure and functionality of the organic solvent and rules out the log*P* as the only criterion. This effect was also observed for other enzymes (Hölsch 2009)

In case of ionic liquids, the miscibility with water and toxicity cannot be easily concluded from the log*P*. In general, higher log*P* of IL also implies stronger hydrophobicity and often a better biocompatibility (Zhao 2012). However, the complicated mechanism and interaction of the anions or cations with the enzymes have to be taken into account. The interference depends on the enzyme and catalytic mechanism (Gamenara et al. 2012).

6.3.4 Stability under process conditions

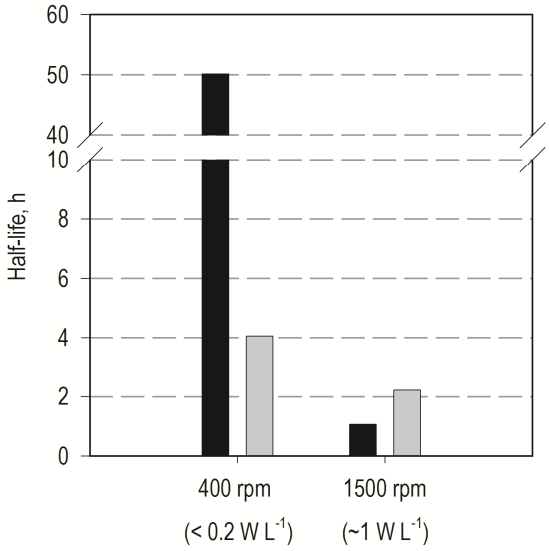

Figure 6.4 Stability of ERs under defined process conditions. Half-lives were determined with NostocER1 in the 48-parallel bioreactor system at 30 °C. Unbaffled reactors equipped with S-stirrers were used with a reaction volume of 10 mL. Enzymes (10 µg mL^{-1}) were incubated in sodium phosphate buffer (100 mM, pH 7.0, black) or a biphasic system with 20 % (v/v) [HMPL][NTF] in sodium phosphate buffer (100 mM, pH 7.0, grey). The volumetric power consumptions at 400 rpm and 1500 rpm were estimated based on Riedlberger (2012) and given in brackets.

The stability of NostocER1 at increased hydrodynamic shear stress and in presence of gas-liquid interfaces was studied under process conditions in a 48- parallel bioreactor unit in unbaffled reactors equipped with S-stirrers, which were developed for enzymatic hydrolysis and homogenization of suspended particles (Riedlberger and Weuster-Botz 2012). Enzyme stability was evaluated at different stirrer speeds in a monophasic setup and in a biphasic setup with 20 % (v/v) of the water-immiscible ionic liquid [HMPL][NTF]. The results are shown in Figure 6.4.

For both reaction setups, the half-life of NostocER1 was strongly decreased at higher stirrer speed. Whereas the half-life was 50 h at 400 rpm, it was reduced to 1 h at 1500 rpm in the monophasic system. This deactivation can be induced by both the hydrodynamic shear stress and increased gas-liquid interface area leading to structural changes, which is commonly reported for cellulases or lipases (Ghadge et al. 2003). When using a biphasic setup with 20 % (v/v) IL instead of a monophasic system, the half-life of NostocER1 was reduced from 50 h to 4 h at 400 rpm. Thereby, the increased phase toxicity due to the mixing of the two liquid phases can be considered as the main cause for enzyme deactivation.

6.3.5 Discussion

Three selected ene-reductases AnabaenaER3, NostocER1 and AcaryoER1 were investigated regarding thermal stability, tolerance of organic solvents and ionic liquid and agitation under process conditions. Enzyme stability, especially under operational conditions, is one of the key criteria for an efficient and economically feasible biocatalytic process (Hollmann et al. 2011).

Both the evaluation of the stability towards high temperature and organic solvents revealed the presumably dimeric AnabaenaER3 from the "thermophilic-like" subgroup of the OYE family as the enzyme with the highest stability. The stability was up to three-fold higher compared to the presumably monomeric enzymes NostocER1 and AcaryoER1. Further, a half-life of 75 h was measured for AnabaenaER3 at 50 °C, whereas the stability of NostocER1 and AcaryoER1 decreased up to 0.15 h. With regard to the organic solvents, the superior stability of AnabaenaER3 compared to NostocER1 and AcaryoER1 was in particular observed using organic solvents with lower log*P* (MTBE, diethyl ether). Deactivation by phase toxicity seemed to be similar for all three studied ERs. Acceptable half-lives of ≥ 70 h were achieved for both AnabaenaER3 and NostocER1 using 20 % (v/v) ionic liquids and organic solvents with log*P* ≥ 2.7 (*n*-hexane, toluene).

In general, the rigidity of the enzyme structure determines the resistance of enzymes towards high temperature, which correlates with the stability in organic solvents (Reich et al. 2013). For the same reason, enzymes from thermophilic organisms required higher temperature for sufficient flexibility in their structure to gain full activity (Adalbjornsson et al. 2010; Schittmayer et al. 2011). Whereas the protein core is often highly conserved in mesophilic and thermophilic enzymes, differences in the surface loops can influence the enzyme stability. In case of ene-reductases, members of the "thermophilic-like" subgroup possess shorter surface loops compared to those in the "classical" group. These shorter surface loops are considered to be responsible for the higher enzyme stability due to increased protein rigidity (Reich et al. 2013). In addition, members from the "thermophilic-like" subgroup are presumed to be multimeric enzymes, which are generally considered to be more rigid and stable than monomeric enzymes (Iyer and Ananthanarayan 2008). Consequently, the superior stability of AnabaenaER3 may be derived from the higher rigidity due to the shorter surface loops and the multimeric structure.

A comparison of the stability of the three characterized ERs from cyanobacteria with described ERs from the literature is shown in Table 6.8.

Table 6.8 Comparison of the thermal stability of ene-reductases from cyanobacteria with ene-reductases described in the literature.

ER	**Half-life at 30 °C, h**	**Half-life at 45 °C* / 50 °C, h**
AnabaenaER3	144	75
NostocER1	67	< 0.15
AcaryoER1	44	< 0.21
KYE1[a]	19	< 0.08*
XenA[a]	10 / 63[b]	< 0.08*
Yers-ER[a]	> 36	< 1.95*

[a] Chaparro-Riggers et al. (2007).
[b] Yanto et al. (2011).

Compared to XenA from *Pseudomonas putida*, KYE1 from *Kluyveromyces lactis*, and Yers-ER from *Yersinia bercovieri* (Chaparro-Riggers et al. 2007), the stability of the three ERs from cyanobacteria was notably higher. Especially AnabaenaER3 displayed an outstanding stability with an up to 14-fold increased half-life at 30 °C, as well as a half-life of 75 h at 50 °C. In contrast, the half-lives of XenA, KYE1 and Yers-ER were already reduced to ≤ 1.95 h at 45 °C. This difference in stability may also be derived from the protein structure, because XenA, KYE1 and Yers-ER belong to the monomeric members from the “classical” subgroup.

Regarding the industrial application of AnabaenaER3, NostocER1 and AcaryoER1 in enzymatic bioprocesses, a careful evaluation of operational conditions is required to ensure sufficient enzyme activity and stability over the process time. The stirring rate revealed to be crucial, because it affects the enzyme stability by hydrodynamic shear stress or exposure to gas-liquid interfaces in monophasic systems. An increased agitation in the milliliter bioreactor system from 400 rpm to 1500 rpm reduced the half-life of NostocER1 from 50 h to 1 h. In case of biphasic reaction systems, the extent of the phase toxicity is increased at higher stirrer speed. When 20 % (v/v) IL was applied as a second liquid phase, the half-life decreased to 4 h at 400 rpm compared to 50 h in monophasic systems.

7 Whole-cell biotransformation using ene-reductases

7.1 Evaluation of the applicability of whole-cell biotransformation using ene-reductases

Presently, an efficient strategy for large-scale application of ene-reductases was not established yet due to several problems. Using purified ene-reductases for biocatalysis, the enzymatic process was limited by the enzyme stability (Bougioukou et al. 2010; Yanto et al. 2010), the requirement of cofactor regeneration (Durchschein et al. 2012a), high demand on the purity of enzyme preparation to avoid side reactions (Hall et al. 2008a) and high costs for protein purification (Tufvesson et al. 2010). On the contrary, the application of cost-efficient wild-type microorganisms such as baker´s yeast was accompanied by low volumetric productivity, toxic effects of the substrate and side reactions by endogenous enzymes, e.g. alcohol dehydrogenases (ADHs) and carbonyl reductases (CRs) (Goretti et al. 2009).

To overcome these limitations, the applicability of recombinant resting whole cells overexpressing ene-reductases from cyanobacteria for alkene reduction was evaluated. *Escherichia coli* was chosen as host strain due to the lower activity of endogenous ADHs compared to yeast (Hildebrandt et al. 2002). The reduction of (R)-carvone to (2R,5R)-dihydrocarvone was selected as example for evaluating the applicability of recombinant whole-cell biocatalyst. (2R,5R)-Dihydrocarvone is a key intermediate in the production of natural products, antimalarial drugs and valuable chiral building blocks (Winkler et al. 2012). (R)-carvone is a volatile and hydrophobic terpenoid with a boiling point at 230 °C and a water-solubility of 8.8 mM (Fichan et al. 1999; Goretti et al. 2013; Schlyter et al.

2004). A reaction scheme with all possible side products by overreduction is depicted in Figure 7.1.

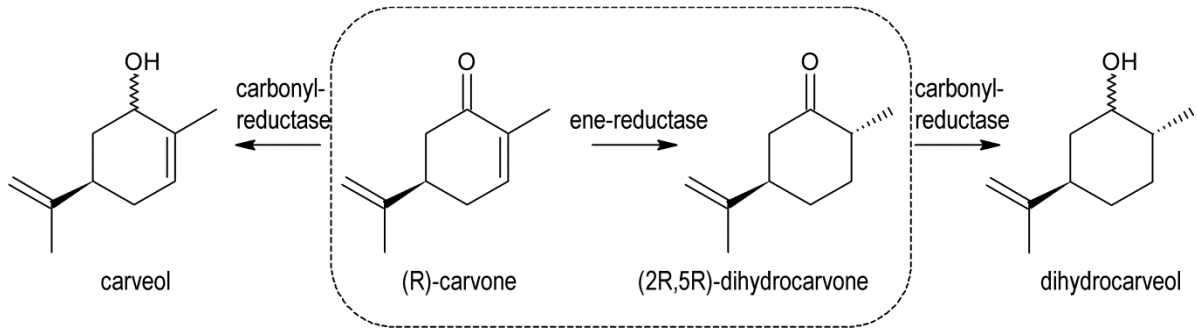

Figure 7.1 Possible side reactions by competing carbonyl reductases in case of the reduction of (R)-carvone to (2R,5R)-dihydrocarvone. Carveols (by overreduction of (R)-carvone) and dihydrocarveols (by overreduction of (2R,5R)-dihydrocarvone) can be most likely formed as side products.

7.1.1 Effect of substrate and product on *Escherichia coli*

The toxicity of (R)-carvone and dihydrocarvone on *Escherichia coli* was evaluated in growth studies. The determined growth curves in presence of 0 mM to 4 mM (R)-carvone and dihydrocarvone are shown in Figure 7.2.

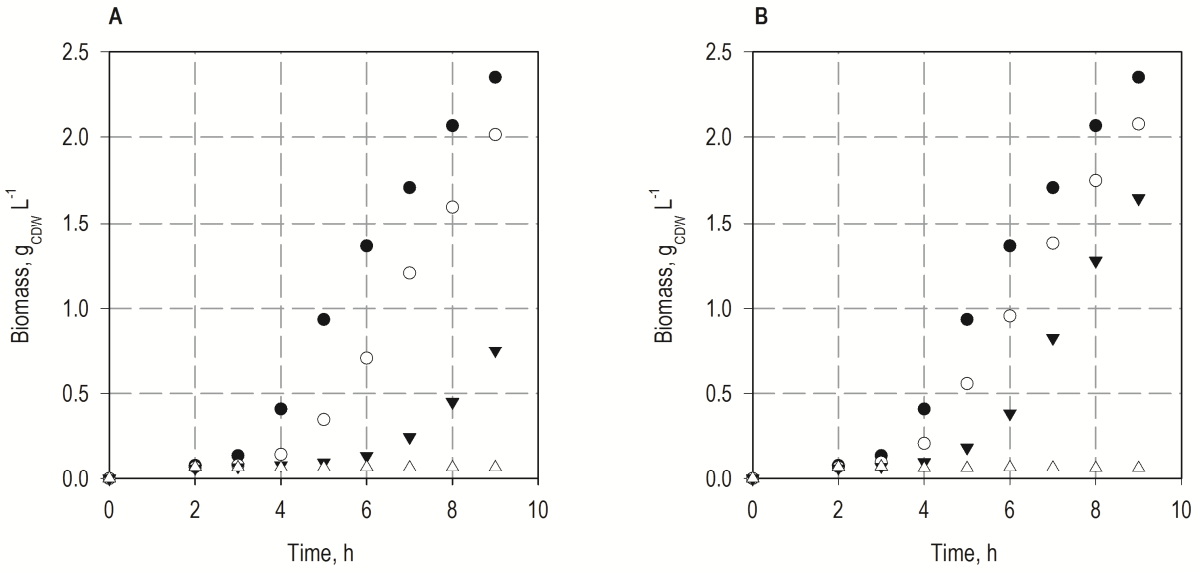

Figure 7.2 Cell growth in presence of substrate and product. The growth *E. coli* BL21 (DE3) containing a empty pET28 vector is shown in presence of (A) (R)-carvone and (B) dihydrocarvone in a concentration of 0 mM (black dots), 1 mM (white dots), 2 mM (black triangles) and 4 mM (white triangles). Cells were incubated at 37 °C and 250 rpm.

Both substances inhibited cell growth at concentrations ≥ 1 mM, which was indicated by the reduced specific growth rate and the prolonged lag-phase. The minimal inhibition concentration (MIC), which is defined as the required concentration for a complete inhibition of cell growth, was determined at 4 mM for both (R)-carvone and dihydrocarvone. At this concentration, the cell membrane has probably lost its integrity and the intracellular pH homeostasis is impaired due to the dissipation of the proton motive force (Sikkema et al. 1995). In fact, various reports confirmed the antimicrobial and repellent effect of carvones. For that reason, carvones are often used as antifeedants and antimicrobial agents (de Carvalho and da Fonseca 2006; Schlyter et al. 2004).

7.1.2 Whole-cell batch biotransformation in monophasic reaction systems

The comparative characterization of the ERs from cyanobacteria revealed AnabaenaER3 from *Anabaena variabilis* ATCC 29413 and NostocER1 from *Nostoc* sp. PCC 7102 as efficient biocatalysts for the reduction of (R)-carvone. Though AnabaenaER3 showed a higher specific activity for (R)-carvone (1.09 U mg^{-1}), *E. coli* with overexpressed NostocER1 (0.69 U mg^{-1}) displayed a higher volumetric activity due to the 2-fold higher protein expression of NostocER1 (data not shown). In addition, the lower K_M for NADPH of NostocER1 (92.2 µM compared to 383.0 µM for AnabaenaER3) can be beneficial for the activity of the ER inside cells. The reduction of (R)-carvone was compared using two *E. coli* strains overexpressing NostocER1 and AnabaenaER3, respectively. To improve the cell intern cofactor regeneration, the formate dehydrogenase mutant D221G from *Mycobacterium vaccae* N 10 (further denoted as FDH_{1M}), was overexpressed in the recombinant strains as well. This FDH mutant was engineered for enhanced $NADP^+$ activity and displayed a maximal reaction rate v_{max} of 1.24 U mg^{-1} using $NADP^+$ and a half-saturation constant K_M of 0.51 mM at pH 7.0 (Liu et al. 2013). The biotransformation was performed using 18.3 g_{CDW} L^{-1} cells, 10 mM (R)-carvone and 250 mM sodium formate in 100 mM phosphate buffer (pH 7.0). After 3 h, the conversion obtained using the *E. coli* strain overexpressing NostocER1 and FDH_{1M} was 2.7-fold higher compared to the strain with AnabaenaER3 and FDH_{1M} (85.1 % vs. 31.0 %). The stereoselectivity were similar for both biocatalysts (74 % de and 77 % de). Consequently, the recombinant *E. coli* strain overexpressing NostocER1 and FDH_{1M} was selected for the whole-cell biotransformation of

(R)-carvone to (2R,5R)-dihydrocarvone. This biocatalyst is further denoted as *E. coli* pET28NosFDH$_{1M}$.

The evaluation of whole-cell biotransformation of (R)-carvone in a monophasic reaction system is exemplarily presented using the wild-type *E. coli* strain, a recombinant *E. coli* strain with overexpressed NostocER1 and *E. coli* pET28NosFDH$_{1M}$. An initial substrate concentration of 10 mM (R)-carvone dissolved using 5 % ethanol was applied. The conversion and diastereomeric excess of the reactions are shown in Figure 7.3.

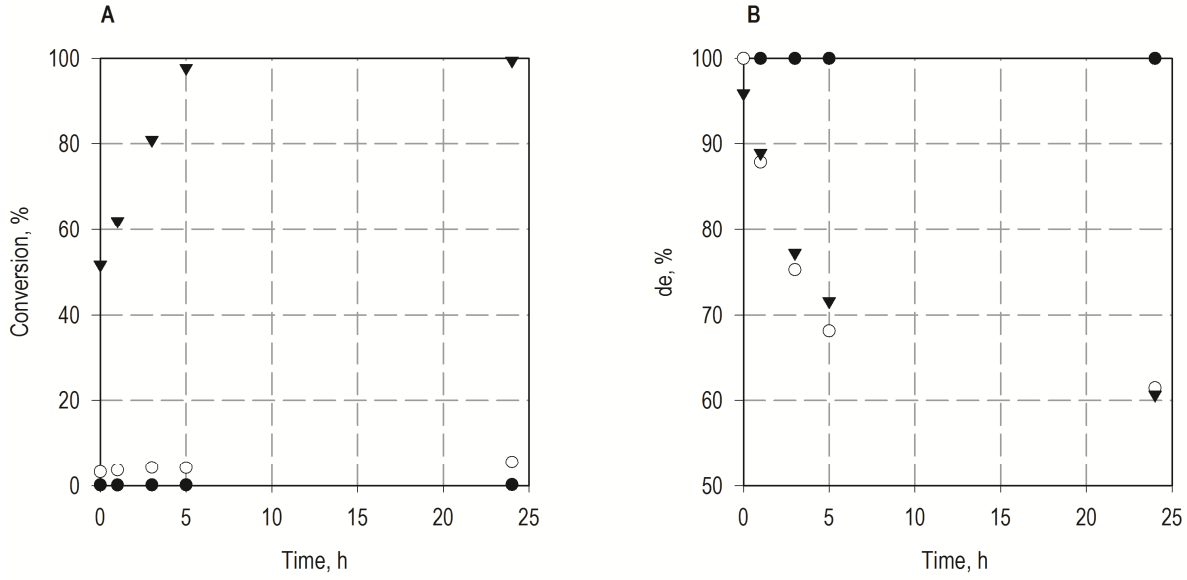

Figure 7.3 Whole-cell bioreduction of (R)-carvone in a monophasic buffered reaction system. The conversion and diastereomeric excesses (% de) of different recombinant strains were evaluated: wild-type *E. coli* (BL21) (black circles), *E. coli* with overexpressed NostocER1 (white circles), *E. coli* with overexpressed NostocER1 and FDH$_{1M}$ (black triangles). Bioconversions were performed in 5 mL-scale in glass vials with 8.8 g_{CDW} L^{-1} biocatalyst with 250 mM formate and 10 mM (R)-carvone in sodium phosphate buffer (100 mM, pH 7.0) at 25 °C and 550 rpm.

Whereas a minimal amount of dihydrocarvone was furnished using wild-type *E. coli* and *E. coli* with overexpressed NostocER1 (0.3 % and 5.6 % conversion after 24 h), over 97.8 % conversion was obtained after 5 h using the *E. coli* strain overexpressing both NostocER1 and FDH$_{1M}$. The full conversion was observed after 24 h.

However, the diastereomeric excess of both *E. coli* with overexpressed NostocER1 and *E. coli* pET28NosFDH$_{1M}$ was decreased to ~61 % de within 24 h, as (2S,5R)-dihydrocarvone was formed as the major side product. The low stereoselectivity was not caused by NostocER1, because (2R,5R)-dihydrocarvone was obtained with 97 % de using purified NostocER1 (Section 6.2). Thus, endogenous enzymes from the host cell might be responsible for the decreased stereoselectivity.

The decrease of the diastereomeric excess was independent from the reaction rate of the whole-cell biocatalyst and the biocatalyst itself. The stereoselectivity of the reaction could not be circumvented by overexpressing of other ene-reductases from cyanobacteria (e.g. AnabaenaER3), the integration of other enzyme-coupled cofactor regeneration systems (GDH, FDH mutants), or using cell lysate for the bioconversion (data not shown).

7.1.3 Whole-cell batch biotransformation in biphasic reaction systems

To cope with side reactions, *in situ* substrate feeding and product removal (SFPR) strategies can be applied in form of a liquid-liquid or solid-liquid reaction system. Thereby, a second water-immiscible phase serves as substrate reservoir and *in situ* product extractant and the biocatalytic reaction is performed in the aqueous phase.

Biphasic whole-cell bioreduction of (R)-carvone was investigated using 20 % (v/v) water-immiscible organic solvents or ionic liquids (ILs) and the biocatalyst *E. coli* pET28NosFDH$_{1M}$. Results are presented in Figure 7.4.

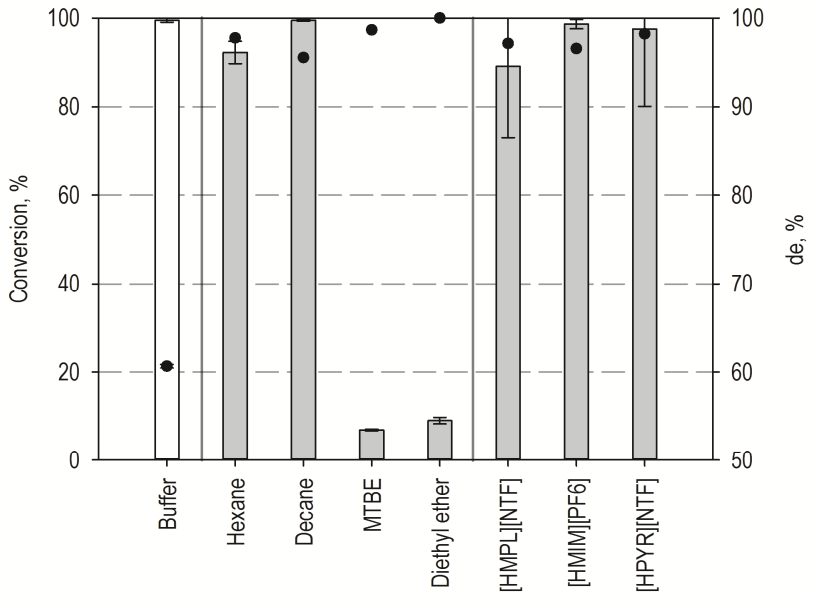

Figure 7.4 Whole-cell batch biotransformations in biphasic reaction systems with 20 % (v/v) organic solvents or ionic liquids. The reaction mixture contained 2.0 – 2.8 $g_{CDW}\,L^{-1}$ *E. coli* overexpressing NostocER1 and FDH$_{1M}$, 250 mM formate and either 10 mM (R)-carvone in the monophasic reference (buffer) or 50 mM in the water-immiscible phase. Reactions were performed in sodium phosphate buffer (100 mM, pH 7.0) at 25 °C and 550 rpm and incubated for 24 h.

High conversions (> 90 %) were achieved in the biphasic reaction systems using organic solvents with higher log*P* (*n*-hexane log*P* 3.7, *n*-decane log*P* 5.0) and the three selected ILs ([HMPL][NTF], [HMIM][PF_6], [HPYR][NTF]) after 24 h. The conversions were comparable to the results obtained in the monophasic reaction system (> 99 % conversion). Low conversions in case of MTBE and diethyl ether can be explained by biocatalyst damages induced by solvent toxicity, as these organic solvents exhibited lower partition coefficients (log*P* 0.93 and log*P* 0.89).

But in contrast to the low diastereomeric excess of ~60 % de in the monophasic reference, (2R,5R)-dihydrocarvone was furnished with 95 – 98 % de in all biphasic reaction systems. This confirmed that higher stereoselectivities can be achieved by minimizing side reactions in biphasic reaction systems.

For further characterization of the biphasic reaction systems, distribution coefficients of (R)-carvone and dihydrocarvone between the water-immiscible solvents and sodium phosphate buffer (100 mM, pH 7.0) were determined and shown in Table 7.1. An adequate selection of water-immiscible solvents offering appropriate partition coefficients for substrate and product is essential to enable efficient biotransformation processes.

Table 7.1 Distribution coefficients (log*D*) of (R)-carvone and dihydrocarvone between various water-immiscible organic solvents and ionic liquids and sodium phosphate buffer (100 mM, pH 7.0).

	$\log D_{\text{(R)-carvone}}$, -	$\log D_{\text{dihydrocarvone}}$, -
n-Hexane	2.57	2.15
n-Decane	2.67	2.05
MTBE	2.66	1.99
Diethyl ether	2.50	2.19
[HMPL][NTF]	2.64	2.97
[HPYR][NTF]	2.62	2.71
[HMIM][PF_6]	2.93	2.87

Higher distribution coefficients of (R)-carvone and dihydrocarvone were measured in presence of ILs (log*D* 2.62 – 2.97) compared to those determined for organic solvents (log*D* 1.99 – 2.67). In general, distribution coefficients for substrate and product between the water-immiscible and the aqueous phase in a order of 2 or 3 decades are recommended ensuring non-toxic conditions for the biocatalyst and facilitating subsequent product recovery (Weuster-Botz 2007).

With due regard to the achieved conversion and stereoselectivity using IL as a second phase, the higher distribution coefficients for substrate and product, and better biocompatibility of

ILs shown by Weuster-Botz (2007), biphasic biotransformations with ILs were considered to be superior compared to reactions involving organic solvents. As the ionic liquid [HMPL][NTF] was thoroughly investigated in biphasic whole-cell biotransformations in previous studies by Dennewald (2011), it was chosen for further characterization and process optimization.

7.1.4 Evaluation of side reactions

The formation of side products using whole-cell biocatalysts is considered as one major disadvantage compared to enzymatic processes. In particular in the reduction of (R)-carvone, the formation of alcohols by endogenous alcohol dehydrogenases or carbonyl reductases was observed in various biotransformations with wild-type microorganisms (Goretti et al. 2013; Silva et al. 2012). Thus, carveol and dihydrocarveol as possible side products were investigated using chiral GC and GC-MS.

Neither carveol, nor dihydrocarveol could be detected by GC and GC-MS during whole-cell biotransformations using *E. coli* pET28NosFDH$_{1M}$ or other recombinant *E. coli* strains applied in both monophasic and biphasic reaction systems (data not shown). It has to be noted, that in case of the monophasic reaction setup, the formation of alcohols might be below the detection level of GC and GC-MS, because low product concentrations were obtained due to the limited substrate loading. In case of biphasic reaction systems, the formation of alcohols could be ruled out even at high substrate loadings.

Nevertheless, the fact that no alcohol could be detected points out the benefit of using *Escherichia coli* as host cell with its low endogenous ADH or CR activities (Hildebrandt et al. 2002). Further, overexpressing ene-reductases and enzymes for cofactor regeneration might have supported the outcompeting of carbonyl reductions.

In summary, with the elimination of alcohols as side products, (2S,5R)-dihydrocarvone was determined as the major side product, resulting in notably decreased diastereomeric excess in monophasic reactions.

7.1.5 Discussion

First alkene reductions involving ene-reductase activity were described for baker´s yeast-mediated biotransformations (Leuenberger et al. 1976). In most cases, a product mix was obtained comprised of saturated and unsaturated ketone and respective alcohols which were formed by the overreduction of the carbonyl group of substrate and product catalyzed by endogenous ADHs or CRs. In addition, the desired product was often furnished with decreased diastereomeric or enantiomeric excesses (Goretti et al. 2009; Kawai et al. 1996; Sakai et al. 1992). However, the desired product could be obtained in a sufficient quality by extensive reaction control coupled with elaborate product purification (Leuenberger et al. 1976).

Presently, enzymatic reductions using purified ene-reductases are mostly preferred for the reduction of activated alkenes in order to circumvent the competitive reactions during whole-cell biotransformations (Bechtold et al. 2012; Brenna et al. 2013a; Brenna et al. 2012e; Winkler et al. 2013). Nevertheless, higher process costs derived from the demand for enzyme purification and possible enzyme deactivation during the biocatalytic process have to be considered.

In this project, the applicability of whole-cell biotransformations involving ERs from cyanobacteria overexpressed in *E. coli* as host cell was investigated with respect to the reduction of (R)-carvone to (2R,5R)-dihydrocarvone. Whereas alcohols as side products were not detected, (2S,5R)-dihydrocarvone was formed in a substantial quantity, resulting in a low diastereomeric excess of 61 % de (R) in monophasic reaction system.

Low stereoselectivities in whole-cell biotransformations can be caused by different factors: (i) racemization of the product in aqueous environment, (ii) feature of the biocatalyst (ene-reductase) itself, (iii) interference with the cofactor-regeneration system, (iv) other competing enzyme present in the host cell catalyzing the same reaction with an opposite preference of the stereochemical outcome of the product, and (v) other enzymes in the host cell catalyzing the isomerisation reaction.

The isomerisation of (2R,5R)-dihydrocarvone induced by the aqueous environment can be considered as negligible, because the rate of the decrease in diastereomeric excess was determined as −0.12 % de h^{-1} in sodium phosphate buffer (100 mM, pH 7.0, 30 °C, data not shown) and a rate of approximately −6.2 % de h^{-1} was observed in monophasic reactions. As high stereoselectivities of > 97 % de were achieved in enzymatic bioreductions using

purified NostocER1 with FDH_{3M} for cofactor recycling (data not shown), the decrease of the diastereomeric was not caused by the property of the catalyzing enzyme. Similarly, interference with the FDH-based cofactor regeneration system could be excluded as the same enzyme was used for cofactor recycling in enzymatic reactions. Endogenous enzymes of the *E. coli* host cell which could be responsible for competing reactions comprise enzymes catalyzing similar reactions (e.g. ene-reductases) and enzymes catalyzing isomerisation reactions. In fact, *E. coli* itself possesses an ene-reductase, which is denoted as NemR in the literature (Mueller et al. 2010a). However, NemR was reported to reduce (R)-carvone to (2R,5R)-dihydrocarvone with a stereoselectivity of 92 % de. Thus, the substantial decrease in stereoselectivity might be caused by other endogenous enzymes catalyzing isomerization reactions.

Compared to the literature data, a similar decreased diastereomeric excess was reported during biotransformations with crude lysate of recombinant *E. coli* overexpressing the ene-reductase EBP1, resulting in 59 % de after 24 h (Mueller et al. 2010b). This supported the assumption of competing reactions by endogenous *E. coli* enzymes.

The decrease in stereoselectivity was prevented using biphasic reaction systems with a second water-immiscible organic solvent or ionic liquid phase. Due to high distribution coefficients, low concentrations of (R)-carvone and dihydrocarvone were present in the aqueous phase as substrates and products were *in situ* supplied and removed.

The application of biphasic reaction systems offers various advantages regarding the whole-cell reduction of (R)-carvone. First, toxic effects on the biocatalyst can be prevented due to low substrate concentrations in the aqueous phase. This was in particular critical, as (R)-carvone prohibited cell growth at concentrations $\geq$ 4 mM. Furthermore, this hydrophobic substance is known to accumulate in the cell membrane causing loss of the membrane integrity and subsequent cofactor leakage (Sikkema et al. 1994a). Though the substrate concentration in the aqueous phase also influence the mass transport through the cell membrane, the inactivation of whole-cell biocatalysts by induced loss of membrane integrity was considered as more critical for the biotransformation (Bräutigam et al. 2009; Dennewald 2011). Second, in contrast to organic solvents, the good biocompatibility with *E. coli* cells in case of ionic liquid as the second phase was proven in various studies (Bräutigam et al. 2009; Weuster-Botz 2007). Moreover, IL-based biphasic whole-cell biotransformation processes were intensely characterized and scaled up for ketone reduction in previous studies (Dennewald 2011). Most importantly, the stereoselectivity in the whole-

cell biotransformation of (R)-carvone was notably improved using biphasic processes, resulting in diastereomeric excesses of > 95 % de.

As whole-cell reduction of (R)-carvone in IL-based biphasic reaction systems furnished the desired product (2R,5R)-dihydrocarvone with high diastereomeric excess and purity without carveol or dihydrocarveol as side products, this strategy seemed to circumvent both disadvantages of yeast-mediated biotransformations and enzymatic bioconversions.

The formation of alcohols as side products was especially reported for yeast-based biotransformations (Goretti et al. 2011; Goretti et al. 2009; Goretti et al. 2013; Silva et al. 2012), but also in biotransformations using other cell types including bacteria, fungi, plant cells and microalgae (Hamada et al. 1997; Hook et al. 2003). Though enals are more affected by competing carbonyl reductions than enones due to higher reaction rates of *prim*-alcohol dehydrogenases compared to *sec*-alcohol dehydrogenases (Hall et al. 2006), substantial formation of alcohols was also observed in (R)-carvone reductions. Thereby, dihydrocarveol furnished by the carbonyl reduction of dihydrocarvone was generally detected as side product whereas the formation of carveol was not observed (Goretti et al. 2013; Silva et al. 2012).

When using *E. coli* as host strain, only limited formation of alcohols as side products was reported (Hirata et al. 2009; Muller et al. 2007; Swiderska and Stewart 2006). In whole-cell biotransformations of (R)-carvone using wild-type *E. coli* and a recombinant *E. coli* with overexpressed ER from *Nicotiana tabacum* no alcohol was detected as side product (Hirata et al. 2009). Even in case of whole-cell biotransformation of enals (e.g. citral), alcohols were only formed using the wild-type *E. coli*, but did not occur using a recombinant *E. coli* with overexpressed OYE2. Thereby, side reactions were probably outcompeted by the higher reaction rate of OYE2 (Muller et al. 2007). These results combined with the results obtained using recombinant *E. coli* overexpressing NostocER1 in this project confirmed the applicability of recombinant *E. coli* for the reduction of activated alkenes.

7.2 Strain development

Since the applicability of whole-cells for the reduction of (R)-carvone was proven in the preliminary studies and the formation of side products could be minimized using a biphasic reaction system for *in situ* substrate feeding and product removal, the development and optimization of the whole-cell biotransformation was focused next.

Both the development of strain and process are key elements for achieving high efficiency and productivity in a biocatalytic reaction. Hereby, the strain development was based on the biocatalyst *E. coli* pET28NosFDH$_{1M}$. The plasmid in this recombinant strain incorporated an expression cassette, where both NostocER1 and FDH$_{1M}$ genes are inserted downstream the T7 promoter. The strain development was focused on optimization of the vector construct and adequate selection of FDH mutants. For the evaluation of the generated biocatalysts, biphasic whole-cell batch biotransformations with 20 % (v/v) [HMPL][NTF] were performed at the 12 mL scale in the parallel bioreactor unit.

7.2.1 Evaluation of different vector systems

Vectors were constructed with different orders of the NostocER1 and FDH$_{1M}$ genes inserted into expression cassettes of standard cloning vectors and an additional T7 promoter for enhanced transcription and translation. A simplified scheme of the vectors is presented in Figure 7.5. Corresponding recombinant *E. coli* strains were evaluated regarding the enzyme activity and biphasic whole-cell bioreduction of (R)-carvone. The results are shown in Figure 7.6.

In the bioreduction of (R)-carvone, the highest conversion was achieved by *E. coli* pET28NosT7FDH$_{1M,}$ which contained a vector with the FDH$_{1M}$ gene inserted downstream from an additional T7 promoter. With 98.2 % after 5 h, the conversion was about 7 % higher compared to the reference strain *E. coli* pET28NosFDH$_{1M}$ without the second T7 promoter. An inversion of the orders of the NostocER1 and FDH$_{1M}$ genes on the expression cassette was presented in the vector of *E. coli* pET21FDH$_{1M}$Nos, but resulted in 18 % lower conversion compared to the reference strain *E. coli* pET28NosFDH$_{1M.}$ The lowest conversion was obtained using *E. coli* pCOLANosT7FDH$_{1M}$ despite of the second T7 promoter of the pCOLA-Duet1 vector within the *E. coli* cell. All four recombinant strains displayed high stereoselectivities of > 98.6 % de.

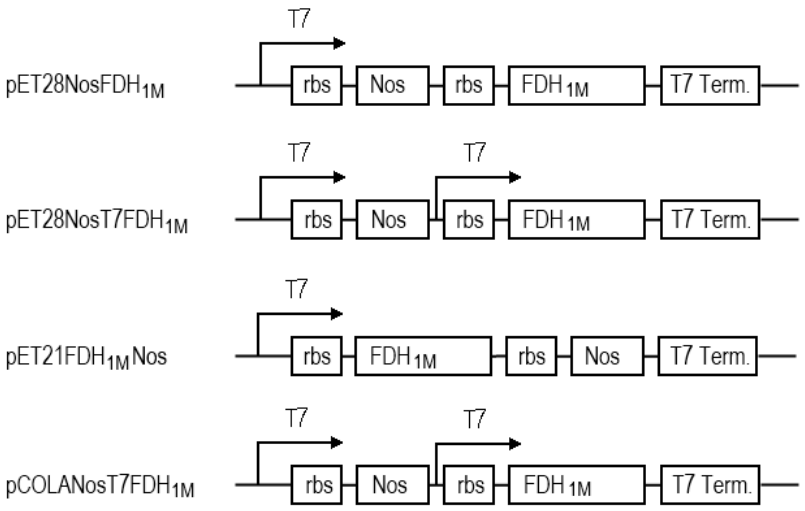

Figure 7.5 Schemes of the expression cassettes with NostocER1 (Nos1) and FDH_{1M} genes, T7 promotor (T7), T7 terminator (T7 Term.) and ribosomal binding sites (rbs) integrated in different cloning vectors (pET28a(+), pET21a(+), pCOLA-Duet).

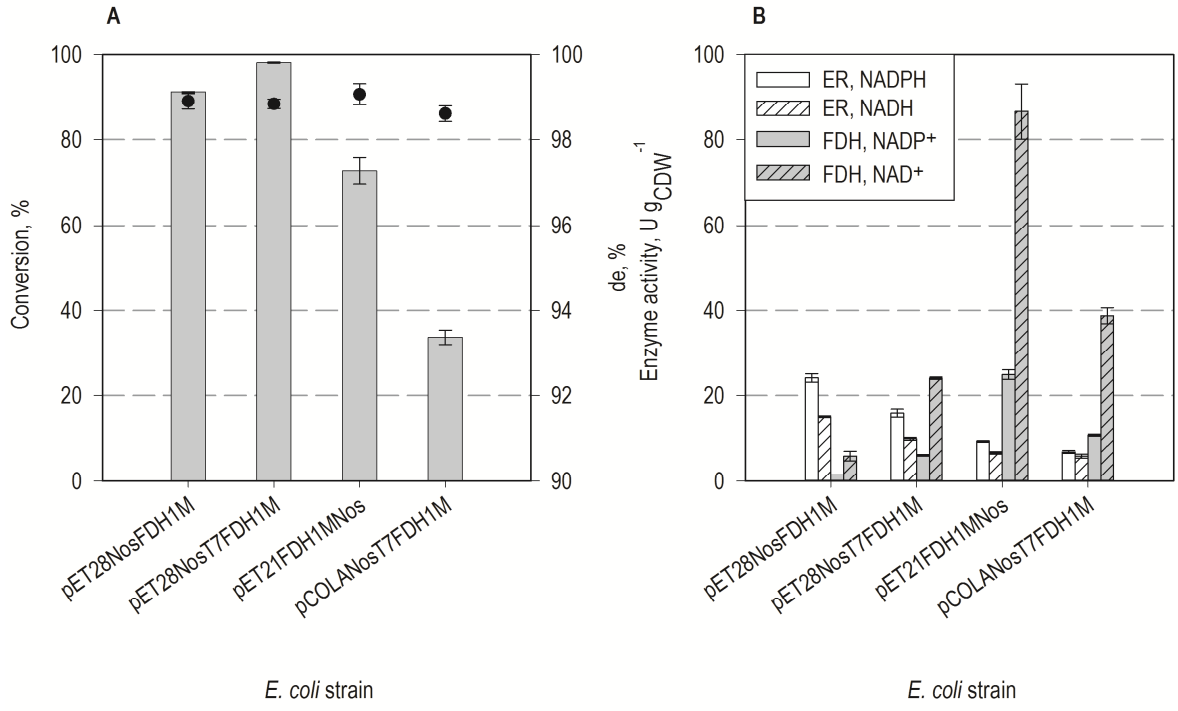

Figure 7.6 Characterization of recombinant whole-cell biocatalysts containing different vector constructs with regard to (A) bioconversion of (R)-carvone after 5 h and (B) specific enzyme activities. Enzyme activities were measured with cell lysate at 25 °C and 340 nm using 0.5 mM NADP(H) or NAD(H), 10 mM (R)-carvone or 250 mM sodium formate. Biotransformations were performed at the 12 mL scale at 25 °C in reactions containing 8 g_{CDW} L^{-1} biocatalyst, 250 mM formate in sodium phosphate buffer (100 mM, pH 7.0) and 250 mM (R)-carvone in 20 % (v/v) [HMPL][NTF].

The conversions of the recombinant strains can be explained by differences in the protein expression of NostocER1 and FDH_{1M}, leading to divergent biocatalyst activities with regard

to alkene reduction and cofactor recycling. In case of the reference strain *E. coli* pET28NosFDH$_{1M}$ the reaction rate was limited by the FDH activity, which was 1.5 U g_{CDW}^{-1} compared to 24.1 U g_{CDW}^{-1} for NostocER1 using NADP as cofactor. Conversely, with the inverted gene orders in *E. coli* pET21FDH$_{1M}$Nos, higher FDH activity of 24.9 U g_{CDW}^{-1} was obtained, but the ER activity decreased to 9.3 U g_{CDW}^{-1}. As the reduction of (R)-carvone is directly connected to the ER activity, a lower conversion was achieved with this strain. A more balanced activity ratio was obtained by introducing a second T7 promoter in case of *E. coli* pET28NosT7FDH$_{1M}$. This resulted in enzyme activities of 15.9 U g_{CDW}^{-1} for NostocER1 and 6.1 U g_{CDW}^{-1} for FDH$_{1M}$, as well as the highest conversion in the reduction of (R)-carvone. The lower reaction rate using *E. coli* pCOLANosT7FDH$_{1M}$ may be derived from lower protein expression due to the lower copy number of the pCOLA_Duet1 vector. In contrast, both pET28a(+) and pET21a(+) vectors are medium copy number plasmids.

In summary, the pET28a(+) vector providing two separate T7 promoters for the ene-reducase and the FDH as cofactor-regeneration enzyme was identified as beneficial for the whole-cell biotransformation of (R)-carvone.

7.2.2 Evaluation of FDH mutants for cofactor regeneration

The FDH D221G mutant from *Mycobacterium vaccae* N 10 (FDH$_{1M}$) was included so far for cofactor regeneration in whole-cell biotransformations. Though this enzyme displayed a higher activity for $NADP^+$ ($v_{max,\ NADP^+}$: 1.24 U mg^{-1}, $K_{M,\ NADP^+}$: 0.51 mM, pH 7.0) compared to the wild-type FDH (Liu et al. 2013), the activity can be further enhanced by additional directed mutations. Hoelsch et al. (2012) had developed various FDH mutants for enhanced $NADP^+$ activity and chemical stability. Eleven pET21a(+) vectors incorporating different FDH mutants were kindly provided by Dr. K. Castiglione for subsequent cotransformations with a pCOLA-Duet1 vector containing the NostocER1 gene into *E. coli* BL21(DE3). Schemes of the expression cassettes of both vectors are presented in Figure 7.7. The enzyme activity and capability of whole-cell bioreductions of the eleven recombinant strains overexpressing different FDH mutants were investigated and the results are shown in Figure 7.8.

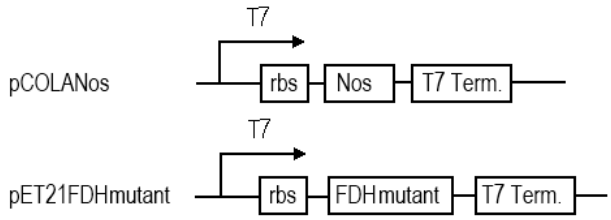

Figure 7.7 Schemes of the expression cassettes in the two plamids pCOLANos and pET21FDHmutant which were cotransformed in *E. coli.* The expression cassettes comprised of the T7 promoter, the ribosome binding site (rbs), the gene of NostocER1 (Nos) or the respective FDH mutant (FDH mutant) and the T7 terminator (T7 Term.).

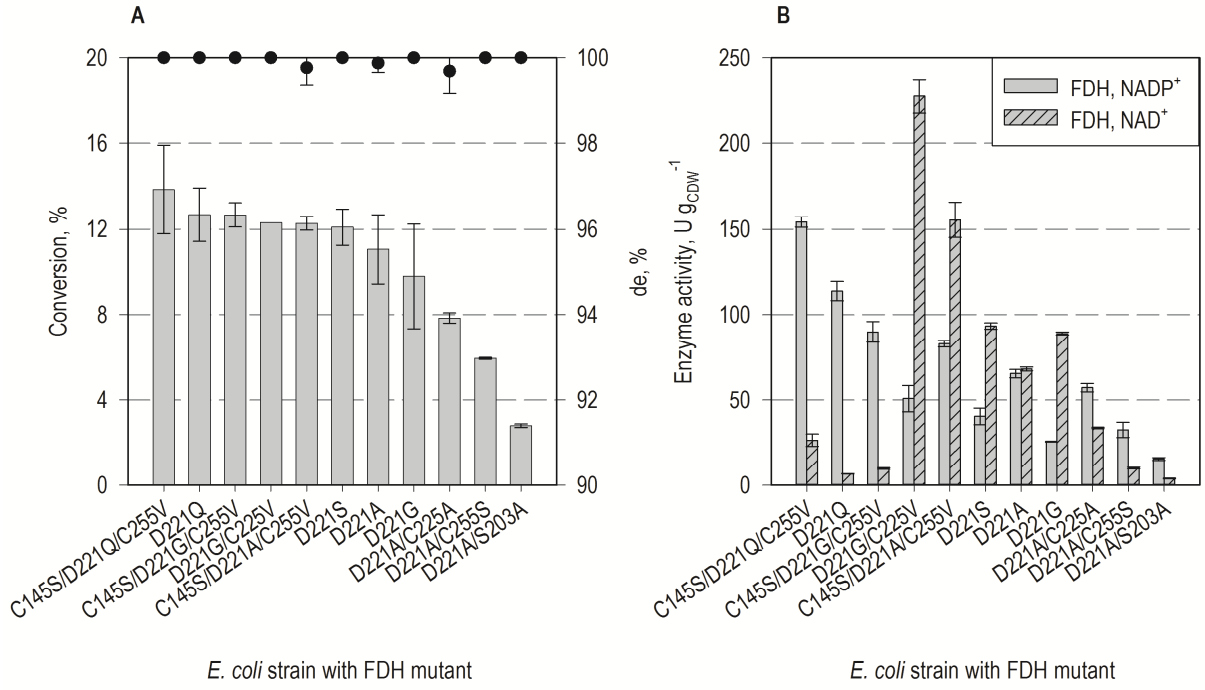

Figure 7.8 Characterization of recombinant whole-cell biocatalysts cotransformed with pCOLANos and pET21 FDHmutant. The bioconversion of (R)-carvone after 5 h (A) and the specific enzyme activities (B) are shown. Enzyme activities were measured with cell lysate at 25 °C and 340 nm using 0.5 mM NADP(H) or NAD(H), 10 mM (R)-carvone or 250 mM formate. The ER activities were below 2 U g_{CDW}^{-1} and thus not displayed. Batch biotransformations were performed at the 12 mL scale at 25 °C in reactions containing 8 g_{CDW} L^{-1} biocatalyst, 250 mM formate in sodium phosphate buffer (100 mM, pH 7.0) and 250 mM (R)-carvone in 20 % (v/v) [HMPL][NTF].

As the NostocER1 gene had to be inserted into pCOLA-Duet1, a medium copy number vector, to be compatible with the pET21a(+) vectors with the integrated FDH mutant genes, the ER activity was relatively low (< 2 U g_{CDW}^{-1}) for all eleven recombinant strains due to low protein expression levels. Thus, the whole-cell biotransformation was limited by the ER activity for all tested strains. Nevertheless, effects of the different FDH mutants on the bioconversion could be observed. Hereby, the conversion after 5 h varied between 2.8 % and 13.8 %.

The highest conversion of 13.8 % was obtained using the FDH C145/D221Q/C255V triple mutant. Recombinant strains with FDH D221Q and FDH C145S/ D221G/C225V achieved both 12.7 % conversion after 5 h. With regard to the enzyme activities, higher $NADP^+$ activities were generally observed for strains obtaining higher conversions in the biotransformations. The three strains exhibited the highest FDH activity with $NADP^+$ of 154.3, 113.8 and 89.9 U g_{CDW}^{-1}, respectively. However, lower $NADP^+$ activities were measured with the strains containing FDH D221G/C225V, FDH D221S and FDH D221G, though comparable conversions in a range of 9.8 – 12.3 % were obtained. In these cases, the cofactor supply was probably compensated by a high FDH activity with NAD^+ (88.9 – 227.3 U g_{CDW}^{-1}), as NostocER1 also accepted NAD^+ as cofactor (Section 6.2).

Previous studies revealed an increased chemical stability of the FDH C145S/D221Q/C255V triple mutant in presence of high (R)-carvone concentrations in addition to the higher activity for $NADP^+$ (39.6 h with 100 mM (R)-carvone compared to 0.07 h for $FDH_{1M,}$ data not shown). As this superior stability was also expected to be beneficial for the whole-cell bioreduction of (R)-carvone, the FDH C145S/D221Q/C255V triple mutant (further denoted as FDH_{3M}) was chosen for further investigation.

7.2.3 Combination of favorable vector construct and FDH mutant

To combine the results from the investigation of the vector construct and FDH mutants, the point mutations of the FDH_{3M} gene were inserted into the favorable vector construct comprising two separate T7 promoters for each NostocER1 and FDH (pET28NosT7FDH_{1M}). As the FDH point mutations D221Q, C145S and C255V were introduced in sequence, recombinant strains containing the respective pET28NosT7FDHmutant vectors as depicted in Figure 7.9, were studied regarding the (R)-carvone reduction (Figure 7.10).

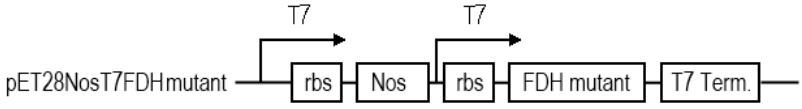

Figure 7.9 Scheme of the expression cassette of the pET28NosT7FDHmutant vector containing two T7 promoters (T7), the gene of NostocER1 (Nos), the ribosome binding site (rbs), the selected FDH mutants genes (FDH mutant) and the T7 terminator (T7 Term.)

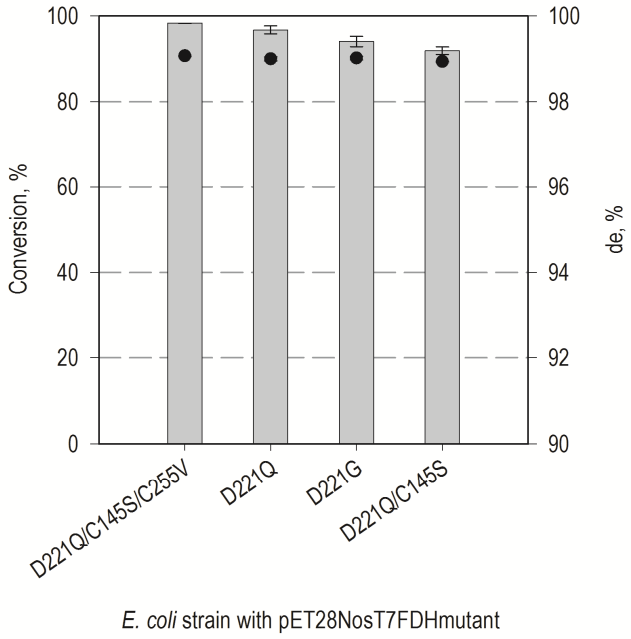

Figure 7.10 Characterization of the effect of different FDH point mutations introduced into the pET28NosT7FDHmutant vector on the (R)-carvone reduction. The reactions were performed at 12 mL scale using 8 g L^{-1} biocatalyst, 250 mM formate in sodium phosphate buffer (100 mM, pH 7.0) and 250 mM (R)-carvone in 20 % (v/v) [HMPL][NTF] at 25 °C for 5 h.

Consistent to the previous results, recombinant strains containing the FDH D221Q and the D221Q/C145S/C255V triple FDH mutant showed a slightly increased conversion of 2.8 % and 4.6 % in comparison to the strain with the FDH D221G mutant. The best results were achieved with the FDH_{3M} triple mutant. Thereby, 98.3 % conversion of (R)-carvone with a diastereomeric excess of 99.1 % de for (2R,5R)-dihydrocarvone was obtained after 5 h.

In conclusion, the *E. coli* strain with a vector comprising separate T7 promoters for the NostocER1 and the FDH D221Q/145S/C255V triple mutant (FDH_{3M}) was identified as the best biocatalyst for whole-cell biotransformation of (R)-carvone.

7.2.4 Evaluation of different biocatalysts at the 200 mL scale

As previous strain development studies were performed at the 12 mL scale and conversions after 5 h were used for evaluation, only limited information about the different biocatalysts could be gathered. A detailed view of the reaction rates of the different biocatalysts was enabled by biphasic whole-cell bioconversion of (R)-carvone at the 200 mL scale. The reference strain *E. coli* pET28NosFDH$_{1M}$ was thereby compared to the strain with a second T7 promoter (*E. coli* pET28NosT7FDH$_{1M}$), as well as the biocatalyst *E. coli*

pET28NosT7FDH$_{3M}$ with FDH triple mutant, which achieved the highest conversion in 12 mL-scale studies. The evolution of conversion and stereoselectivity during the biotransformation is depicted in Figure 7.11. In addition, the maximal volumetric productivity was calculated for each biocatalyst and presented in Figure 7.12.

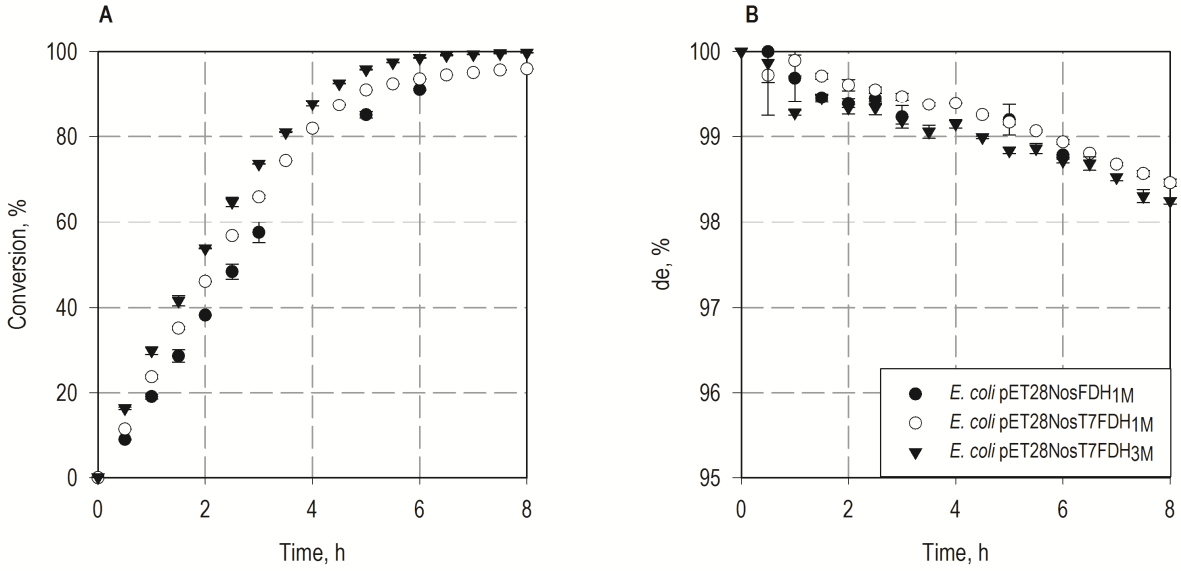

Figure 7.11 Comparison of different whole-cell biocatalysts at the 200 mL scale. Batch biotransformation of (R)-carvone was investigated using *E. coli* pET28NosFDH$_{1M}$ (black dots), *E. coli* pET28NosFDH$_{1M}$ (white dots) and *E. coli* pET28NosT7FDH$_{3M}$ (black triangles). Reactions contained 8 g_{CDW} L^{-1} biocatalyst, 250 mM sodium formate in sodium phosphate buffer (100 mM, pH 7.0) and 250 mM (R)-carvone in 20 % (v/v) [HMPL][NTF] and were performed at 25 °C. Conversions are shown in (A) and the diastereomeric excesses are displayed in (B).

Consistent to the results obtained from the 12 mL-scale biotransformations, the biocatalyst *E. coli* pET28NosT7FDH$_{3M}$ was confirmed as the best candidate for (R)-carvone reduction. A complete conversion (> 99.8 %) was solely achieved by *E. coli* pET28NosT7FDH$_{3M}$ after 8 h. In contrast, the reaction rate of *E. coli* pET28NosT7FDH$_{1M}$ was reduced with increasing reaction time without accomplishing a complete conversion after 8 h. Using *E. coli* pET28NosT7FDH$_{3M}$, a maximal volumetric productivity of 14.9 mmol L^{-1} h^{-1} was achieved compared to 9.6 mmol L^{-1} h^{-1} in case of the reference strain *E. coli* pET28NosFDH$_{1M}$.

With regard to the stereoselectivity, the choice of biocatalyst did not significantly affect the diastereomeric excess of the produced (2R,5R)-dihydrocarvone. For all three recombinant strains, the stereoselectivity decreased following a linear trend with increasing reaction time. In case of the *E. coli* pETNosT7FDH$_{3M}$, (2R,5R)-dihydrocarvone was furnished with 98.3 % de at time of the complete conversion.

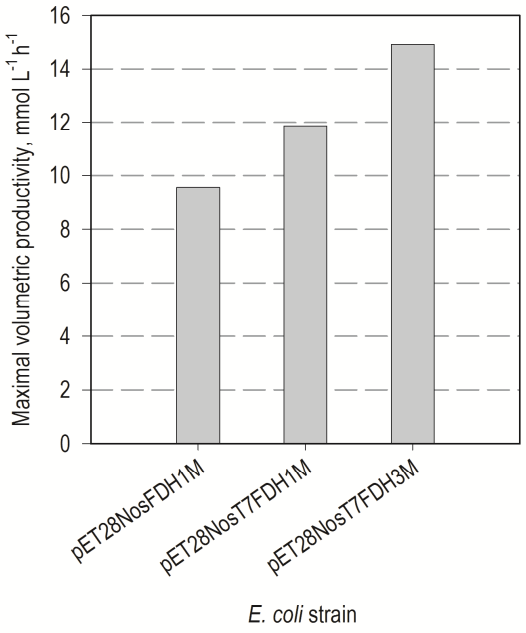

Figure 7.12 Comparison of the maximal volumetric productivities obtained in whole-cell biotransformations of (R)-carvone using different *E. coli* strains. The biocatalysts *E. coli* pET28NosFDH$_{1M}$, *E. coli* pET28NosFDH$_{1M}$ and *E. coli* pET28NosT7FDH$_{3M}$ were investigated. Reactions contained 8 g_{CDW} L^{-1} biocatalyst, 250 mM sodium formate in sodium phosphate buffer (100 mM, pH 7.0) and 250 mM (R)-carvone in 20 % (v/v) [HMPL][NTF]. Reactions were performed at 25 °C.

7.2.5 Discussion

The whole-cell biocatalyst *E. coli* pET28NosFDH$_{1M}$ was improved regarding the ER and FDH activity for efficient biotransformation of (R)-carvone. Thereby, the composition within the expression cassette and the selection of beneficial FDH mutants was focused.

Improved transcription and translation of the FDH gene was achieved by introducing a second T7 promoter, leading to higher FDH amount and overall FDH activity. The developed strain *E. coli* pET28NosT7FDH$_{1M}$ exhibited indeed an improved conversion, which confirmed the FDH activity as the rate-limiting step then using the previous strain.

The evaluation of different FDH mutants exhibiting diverging preferences for NAD^+ and $NADP^+$, kinetic properties and stability developed by Hoelsch et al. (2012) revealed a higher relevance of NADPH supply for the (R)-carvone reduction catalyzed by NostocER1. This was concluded as recombinant biocatalysts showing higher conversions mostly displayed a higher FDH activity for $NADP^+$. The primary influence of the NADPH supply for the overall reaction rate can be explained by the kinetic property of NostocER1. This ene-reductase displayed a clear preference for NADPH over NADH, pointed out by a

NADPH to NADH activity ratio of at least 2. In addition, the half-saturation constant for NADPH was substantially lower compared to the corresponding constant for NADH (0.09 mM vs > 0.5 mM). As the NADH/ NADPH concentrations inside *E. coli* cells were expected to be below ~0.5 mM (Bennett et al. 2009; Zhang et al. 2012), it can be proposed that NADPH was predominately involved in the overall catalytic reaction.

The FDH C145S/D221Q/C255V triple mutant (FDH_{3M}) was selected for the integration in the optimized vector providing increased NADPH regeneration by higher protein expression and specific activity within the recombinant *E. coli* cell overexpressing NostocER1. In comparison to the previous strains containing FDH_{1M}, notably higher initial apparent reaction rates were enabled using the optimized biocatalyst containing FDH_{3M}. In addition, a complete conversion was solely achieved by *E. coli* pET28NosT7FDH_{3M}, whereas the decreasing reaction rate indicated a biocatalyst inactivation in case of the corresponding strain with $FDH_{1M.}$

The inactivation of the biocatalysts with overexpressed FDH_{1M} might be explained by the low chemical stability of purified FDH_{1M} in presence of (R)-carvone. A half-life of 11.6 h was measured for purified FDH_{1M} in presence of 10 mM (R)-carvone, a half-life of 4.3 h with 50 mM (R)-carvone and 0.07 h with 100 mM (R)-carvone. On the contrary, purified FDH_{3M} exhibited a half-life of 39.6 h in presence of 100 mM (R)-carvone (data not shown). Thus, the superior performance of best biocatalyst *E. coli* pET28NosT7FDH_{3M} was probably supported by both higher NADPH supply and superior chemical stability of $FDH_{3M.}$

7.3 Production and storage of the whole-cell biocatalyst

7.3.1 Cultivation of the whole-cell biocatalyst at liter-scale

After identifying *E. coli* pET28NosT7FDH$_{3M}$ as the best biocatalyst for (R)-carvone reduction, the biocatalyst was produced at the 3 L scale allowing a better availability for biotransformation.

E. coli pET28NosT7FDH$_{3M}$ was cultivated in a 3 L fed-batch process in a minimal medium developed by Wilms et al. (2001) following a modified protocol described by Sun et al. (2013). A typical evolution of the biomass concentration as a function of time is shown in Figure 7.13. The process parameters are exemplarily shown in the Appendix A.5.4. The cultivation process was divided into three steps:

i. At the beginning of the *batch phase*, the minimal medium was supplemented with 3 g L^{-1} glucose, which was completely consumed by the cells within 3 h. The biomass increased with a specific growth rate of 0.71 h^{-1} up to 1.2 g_{CDW} L^{-1} after 3 h.
ii. During the *fed-batch phase*, the growth rate was set to 0.15 h^{-1} and the temperature was decreased to 30 °C, resulting in an increase of biomass up to 18.8 g_{CDW} L^{-1} within the next 20 h. The achieved biomass concentration was close to the expected value of 19.2 g_{CDW} L^{-1} calculated by Equation 4.12.
iii. The *protein expression phase* was subsequently induced by adding IPTG in a final concentration of 0.5 mM. The growth rate was set to 0.06 h^{-1} and the temperature was reduced to 20 °C. Cells were harvested after 24 h of protein expression with a biomass concentration of 42.8 g_{CDW} L^{-1}, which was equate to an optical density OD_{600} of 94.8.

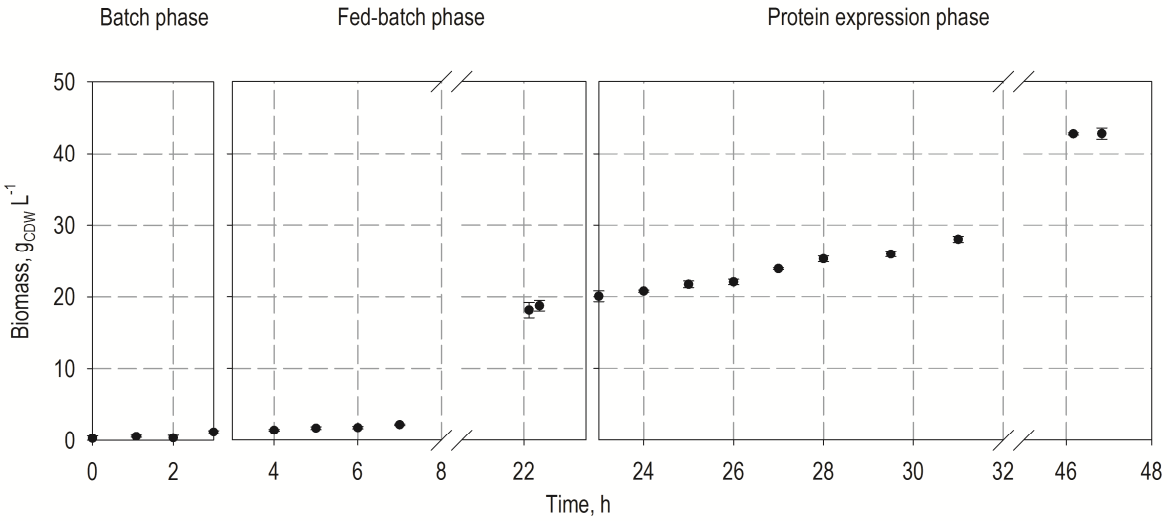

Figure 7.13 Evolution of biomass concentration during the cultivation of *E. coli* pET28NosT7FDH$_{3M}$ in a 3 L scale. The cultivation process was divided into three steps: (i) batch phase (3 h), (ii) fed-batch phase (20 h), (iii) protein expression phase (24 h).

The evolution of the NostocER1 and FDH$_{3M}$ activity in the biocatalyst after induction of the protein expression is presented in Figure 7.14. During the protein expression phase, the specific enzyme activities increased following an almost linear trend achieving a FDH$_{3M}$ activity of 30.0 U g_{CDW}^{-1} and a NostocER1 activity of 32.9 U g_{CDW}^{-1} using NADP(H) at the end of the cultivation.

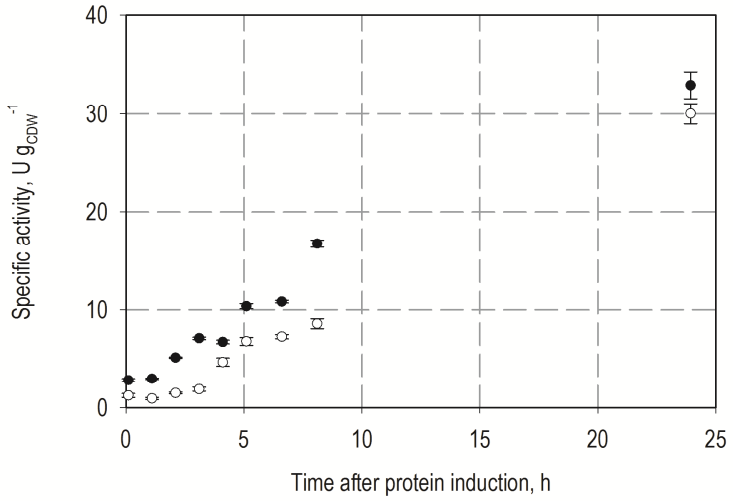

Figure 7.14 Evolution of the biocatalyst activity during the protein expression phase. The specific activity of NostocER1 (black dots) and FDH$_{3M}$ (white dots) measured after cell disruption of the biocatalyst *E. coli* pET28NosT7FDH$_{3M}$ are presented. Enzyme activities were measured using 0.5 mM NADP(H) at 25 °C and 340 mM. 10 mM (R)-carvone was used as substrate for NostocER1 and 250 mM sodium formate was applied in case of FDH$_{3M.}$

In conclusion, the biocatalyst production on a liter scale was successfully established yielding high concentrations of the biocatalysts with acceptable activities. As the cultivation process on a liter scale was entirely different compared to the conditions in shaking flasks, a reasonable comparison of the biocatalyst activities is not possible.

7.3.2 Storage of the whole-cell biocatalyst

With regard to the quality and performance of the whole-cell biocatalyst during whole-cell biotransformations, the storage of cells may even play a more important role compared to the level of protein expression and enzyme activity after cultivation. Inappropriate storage procedure can lead to the damage of the cell membrane and cofactor leakage could occur during the biotransformation process, resulting in reduced reaction rate and conversion. For example, multiple cycles of freezing and thawing cell suspensions is commonly used to obtain permeabilized cells (Chen 2007). Furthermore, the cofactor regeneration enzyme inside the cell might be deactivated by higher concentrations of substrate or product in the cells enabled by facilitated transport through permeablized cell membranes. On the contrary, the activity of the catalyzing enzyme could be increased by higher substrate concentrations depending on the respective K_M.

In previous studies, storage of whole-cell biocatalysts at 4 °C resulted in up to ~80 % decrease of the conversion (data not shown). In addition, if the cell suspension was frozen without the addition of glycerol and stored at −20 °C, the reaction rate was decreased by at least 20 % (data not shown). Consequently, 15 % (v/v) glycerol was added in subsequent experiments and cells were shock-frozen using liquid nitrogen. A storage temperature of −58 °C was chosen.

E. coli pET28NosFDH$_{1M}$ harvested from the cultivation in shaking flasks and *E. coli* pET28NosT7FDH$_{1M}$ obtained from the cultivation at the 3 L scale were applied for the evaluation of different storage conditions. As the cell membrane properties are assumed to be predominantly affected by different storage procedures, the presented results should also be valid for other whole-cell biocatalysts such as the *E. coli* pET28NosT7FDH$_{3M}$ with the FDH triple mutant.

For the investigation of storage procedures, cells were harvested by centrifugation and either resuspended in fresh TB medium or sodium phosphate buffer (100 mM, pH 7.0) containing

15 % (v/v) glycerol for subsequent shock-freezing and storage, or directly frozen as cell pellet. In case of *E. coli* pET28NosFDH$_{3M}$ from the liter-scale cultivation, 15 % (v/v) glycerol were also directly added into the cultivation medium followed by shock-freezing and storage at −58°C. The results of the bioconversion of (R)-carvone using these differently prepared biocatalysts are summarized in Figure 7.15.

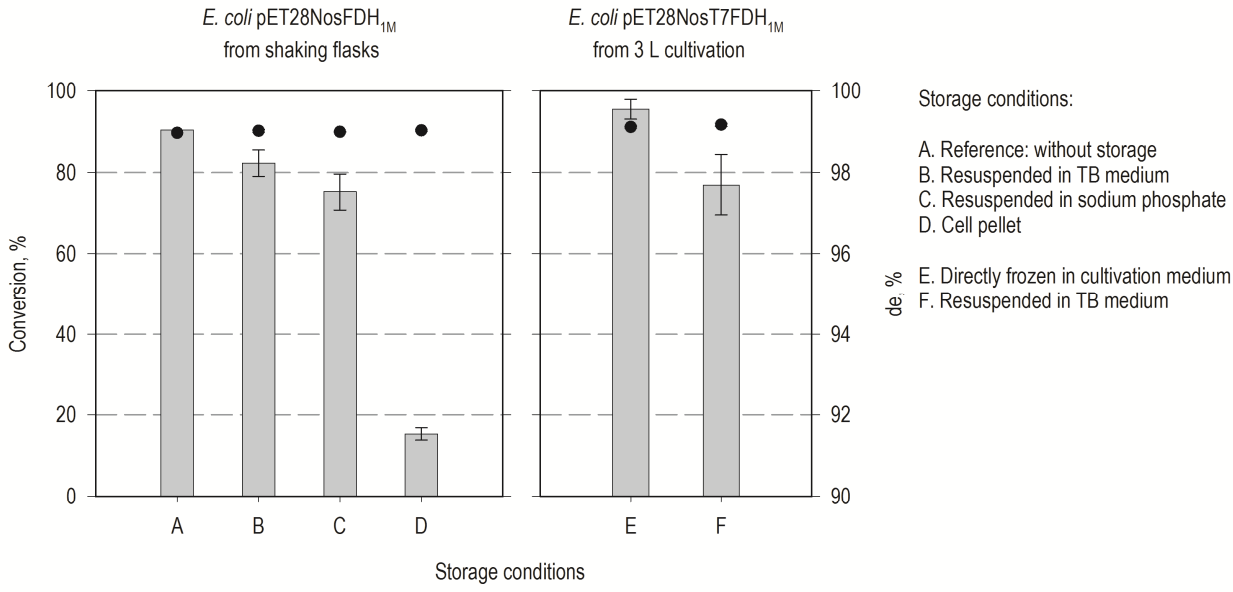

Figure 7.15 Evaluation of different storage procedures with regard to the performance in whole-cell biotransformations. Experiments were performed using *E. coli* pET28NosFDH$_{1M}$ and *E. coli* pET28NosT7FDH$_{1M}$ harvested from cultivations in shaking flasks and in a liter bioreactor, respectively. The biotransformation was conducted at the 12 mL scale at 25 °C using 8 g_{CDW} L^{-1} biocatalyst and 250 mM sodium formate, in sodium phosphate buffer (100 mM, pH 7.0) and 250 mM (R)-carvone in 20 % (v/v) [HMPL][NTF]. The conversion and diastereomeric excess after 5 h are presented.

The whole-cell biotransformation was severely impaired using biocatalysts stored as cell pellet, as 83.1 % decreased conversion was determined. When cells were harvested by centrifugation and resuspended in TB medium or phosphate buffer, the conversion was reduced by up to 19 % for both strains obtained from shaking flasks and 3 L cultivation. The best results were achieved using either fresh cells or by adding 15 % (v/v) glycerol directly to the cultivation medium followed by subsequent shock-freezing and storage at −58 °C.

As lower conversion was generally observed using cells harvested by centrifugation with subsequent medium exchange, it can be assumed, that cells or in particular the cell membranes were probably damaged during this procedure. This might be caused by either mechanical stress or osmotic stress in case of using phosphate buffer.

For a detailed investigation of the membrane integrity, oxidized forms of nicotinamide cofactors were added during whole-cell biotransformations with *E. coli*

pET28NosT7FDH$_{1M}$. If cells are intact, pyridine nucleotides are not able to pass through the cell membrane (De Smet et al. 1978). With disintegrated membrane structures, a permeation of the nicotinamide cofactors into the cell is possible, thereby increasing the enzymatic reaction rate. The results are shown in Figure 7.16.

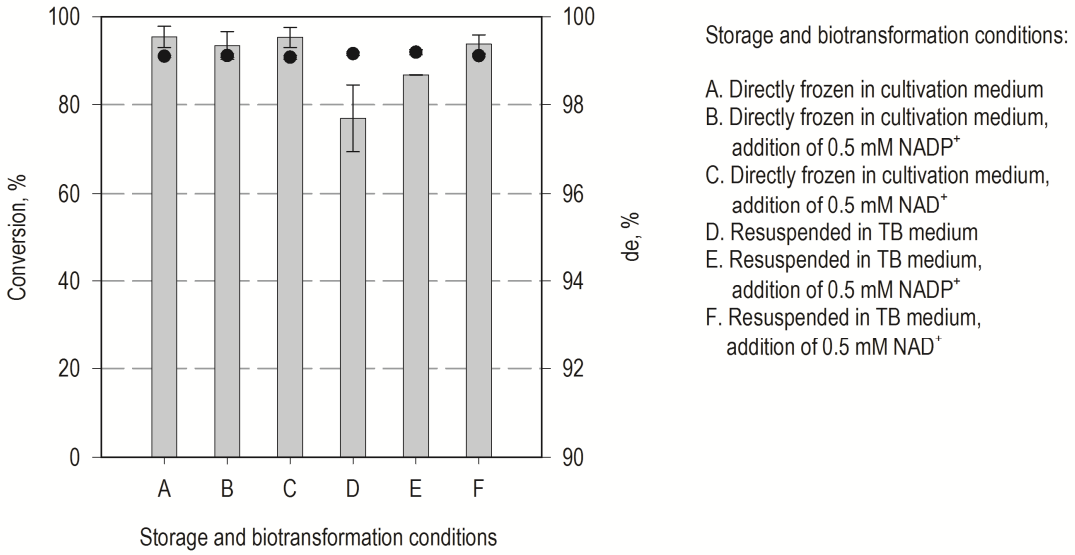

Figure 7.16 Investigation of the membrane integrity during biotransformation by adding nicotinamide cofactors. *E. coli* pET28NosT7FDH$_{1M}$ was harvested from the 3 L cultivation and stored either directly in the cultivation medium or in fresh TB medium, both supplemented with 15 % (v/v) glycerol. Cells were shock-frozen and stored at −58 °C. For investigation of the membrane integrity, either NAD^+ or $NADP^+$ in a final concentration of 0.5 mM was added to the biotransformation reaction mixture containing 8 g_{CDW} L^{-1} biocatalyst and 250 mM sodium formate in sodium phosphate buffer (100 mM, pH 7.0) and 250 mM (R)-carvone in 20 % (v/v) [HMPL][NTF]. Reactions were performed at the 12 mL scale at 25 °C. Conversions after 5 h (grey bars) as well as the diastereomeric excess after 5 h (de, dots) are presented.

If the cell harvest by centrifugation is avoided by directly adding glycerol and subsequent freezing and storage, the addition of NAD^+ or $NADP^+$ as cofactor did not influence the reaction rate of the biotransformation. This proved that the integrity of the cell membrane was preserved within the reaction time. In contrast, using biocatalysts that underwent the procedure of centrifugation and medium exchange, the conversion was reduced by 19.4 % without cofactor addition. Supplementation of NAD^+ or $NADP^+$ in the reaction mixture significantly increased the conversion of (R)-carvone by up to 21.9 %.

Without the addition of cofactors, the available cofactor concentration within the cell was probably reduced due to loss of the membrane integrity and subsequent cofactor leakage. This effect could be compensated by adequate supply with NAD^+ or $NADP^+$. Thereby, higher reaction rates can be explained by the uptake of the cofactors through the cell

membrane allowing higher cofactor availability for the biocatalytic reaction, which could only possible in case of disintegrated cell membrane.

The superior effect by the addition of NAD^+ compared to $NADP^+$ was contrary to the fact that $NADP^+$ was identified as more important for the reduction by NostocER1 within the cells. But this effect might be derived from the higher stability of NAD^+ compared to $NADP^+$ under the reaction condition (Wu et al. 1986).

The visualization of the disintegrated cell membrane by fluorescence-activated cell sorting (FACS) was further investigated. Cells were stained with the membrane potential dye bis-(1,3-dibutylbarbituric acid) trimethine oxonol ($Dibac_4[3]$), which enters depolarized cells and binds to intracellular proteins or membranes, thereby exhibiting enhanced fluorescence (Suller and Lloyd 1999). The fluorescence of $Dibac_4[3]$ was plotted against the forward scatter, which indicated the particle size. The results are shown for the cells stored in cultivation medium (Figure 7.17A), resuspended in fresh medium (Figure 7.17B), as well as the state of the membrane integrity after 5 h of whole-cell biotransformation of (R)-carvone (Figure 7.17C). Cells were classified in intact, living cells (R1) and disrupted, dead cells (R2).

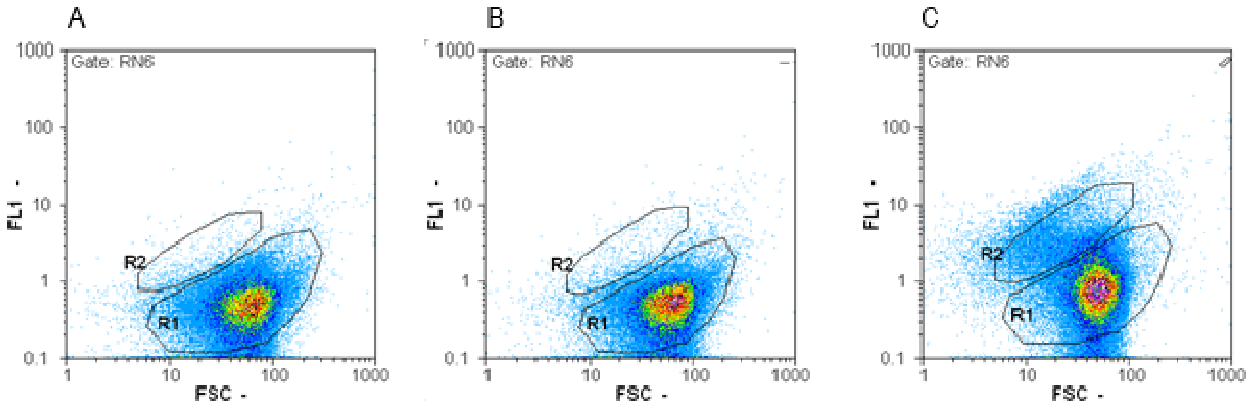

Figure 7.17 Fluorescence-activated cell sorting (FACS) analysis of whole-cell biocatalyst during storage and biotransformation. The membrane integrity of *E. coli* $NosT7FDH_{1M}$ cells were investigated under different conditions: (A) Cells were directly frozen in cultivation medium containing 15 % (v/v) glycerol and stored at −58°C, (B) Cells were resuspended in fresh medium containing 15 % (v/v) glycerol and stored at −58 °C, (C) Cells after 5 h biotransformation using intact cells at the beginning.

No differences with regard to the membrane potentials of cell populations were observed for the two storage conditions (Figure 7.17A, 7.17B). However, cells after a 5 h biphasic biotransformation of (R)-carvone revealed a disintegration of the cell membrane indicated by an increase in the population of dead cells exhibiting increased fluorescence of $Dibac_4[3]$.

The loss of membrane integrity with increasing process time might be induced by prolonged accumulation of (R)-carvone in the cell membrane, as well as toxicity effects of the applied ionic liquid.

7.3.3 Discussion

The production and storage of the whole-cell biocatalyst can have strong impact on the biotransformation, as it defines the enzymatic activity and the cell membrane properties of the biocatalyst. Especially in biphasic whole-cell biotransformations involving oxidoreductases, the intactness of the cell membrane during biotransformation is critical for cell intern cofactor regeneration without any cofactor loss (Bräutigam et al. 2009; Weuster-Botz 2007). Otherwise, the apparent cofactor concentration inside the cell would be significantly reduced, resulting in decreased reaction rates of the cofactor-depending enzymes inside the cell. Disintegrated cell membrane further allows increased fluxes of substrate and product through the cell membrane, which can either increase the enzyme activity due to higher substrate availability or inactivate the respective enzyme activity and stability.

In some cases, the loss of membrane integrity is even desired to enable an improved substrate transport enhancing the reaction rate of the process (Kratzer et al. 2011; Müller et al. 2006; Schmolzer et al. 2012). This can be accomplished by permeabilization of cell membranes using solvent and detergent treatment (e.g. toluene, EDTA), additives (e.g. polymyxin B) and multiple freeze and thaw cycles (Chen 2007). Hereby, an addition of the nicotinamide cofactor is required to obtain acceptable reaction rates. However, if possible, intact cells enabling intracellular cofactor regeneration without cofactor addition is preferred with regard to the improved cofactor turnover number, increased enzyme stabilities within the cell and lower costs (Richter et al. 2010).

With reference to the biphasic whole-cell bioconversion of (R)-carvone, it was demonstrated, that the cell membrane had to be intact at least at the begin of the biotransformation to obtain high reaction rates. Inappropriate storage procedures involving medium exchange resulted in cells with disintegrated cell membrane achieving notably lower conversions compared to reactions with intact cells. Addition of nicotinamide cofactors increased the conversion significantly which indicated that the decreased reaction rate was caused by cofactor leakage.

It should be noted that whole-cell biotransformations using recombinant biocatalysts harboring a glucose dehydrogenase from *Bacillus subtilis* supported the assumption of intact cell membranes at begin of the biotransformation. Thereby, limited conversion of (R)-carvone was measured (data not shown). This can be explained by the fact that glucose was phosphorylated during the transport into the cell and could not serve as substrate for the glucose dehydrogenase (Hilt et al. 1991; Kratzer et al. 2011).

Though disintegrated cell membrane permeable for nicotinamide cofactors could not be detected using fluorescence activated cell sorting (FACS), a significant change in the cell membrane integrity was observed for cells used in IL-based biphasic biotransformations after a process time of 5 h. This indicated a progressive disintegration of the cell membrane with increasing process time. As (R)-carvone is known to accumulate in the cell membrane, disturbing the cell membrane integrity (Sikkema et al. 1994a), the observed cell membrane damage can be partly explained by the interference with the hydrophobic substrate and product. In fact, cells were completely damaged, when incubated in monophasic reaction systems with 50 mM (R)-carvone (data not shown). Furthermore, the membrane integrity of *E. coli* cells was decreased to ~30 % after 5 h incubation in 20 % (v/v) [HMPL][NTF] (Weuster-Botz 2007). Hence, prolonged interactions with the ionic liquid might also support the disintegration of the cell membrane. A loss of the cell membrane integrity during whole-cell biotransformation induced by 2-octanone was also observed in biphasic whole-cell biotransformations with 20 % [HMPL][NTF] (Dennewald 2011).

7.4 Optimization and scale-up of biphasic batch biotransformations with ionic liquids

The objective was to develop an efficient biphasic whole-cell biotransformation process under optimized operation conditions, thereby achieving a complete conversion in proper reaction time and high stereoselectivity. First, process variables with significant influence on the biotransformation were identified and various factors critical for the process were analyzed. In the next step, the bioconversion of (R)-carvone was optimized with regard to these process variables. At last, the whole process was scaled up under optimized operation conditions.

7.4.1 Identification of relevant process variables

Preliminary to a model-based optimization of whole-cell biotransformation of (R)-carvone, process variables with significant influence were identified and the boundaries for the experimental design were estimated.

Effect of pH and buffer molarity

The influence of pH on the (R)-carvone bioconversion was investigated in a range of pH 6.0 to pH 8.0 in 100 mM sodium phosphate buffer using the optimized biocatalyst *E. coli* pET28NosT7FDH$_{3M}$. Thereby, the pH was adjusted at the beginning of the biotransformation and was not controlled during the biotransformation to keep the process simple. The results are presented in Figure 7.18A.

The highest conversion (97.9 %) was achieved at pH 6.0 after 5 h. Alkaline pH conditions (pH 7.5 – 8.0) decreased the conversion by up to 35.4 %, resulting in 64.6 % conversion at pH 8.0. The stereoselectivity was not affected by the pH, as diastereomeric excesses of ≥ 99.2 % de were achieved for all conditions.

During the biotransformation in 100 mM phosphate buffer, the pH increased by 1 unit within 5 h (data not shown). Thus, different buffer molarities in a range of 100 mM to 500 mM were evaluated to minimize the pH drift. However, even with buffer molarities of ≥ 300 mM, the pH was still raised by ~0.4 units (data not shown). The influence of the buffer molarity on the biotransformation is shown in Figure 7.18B.

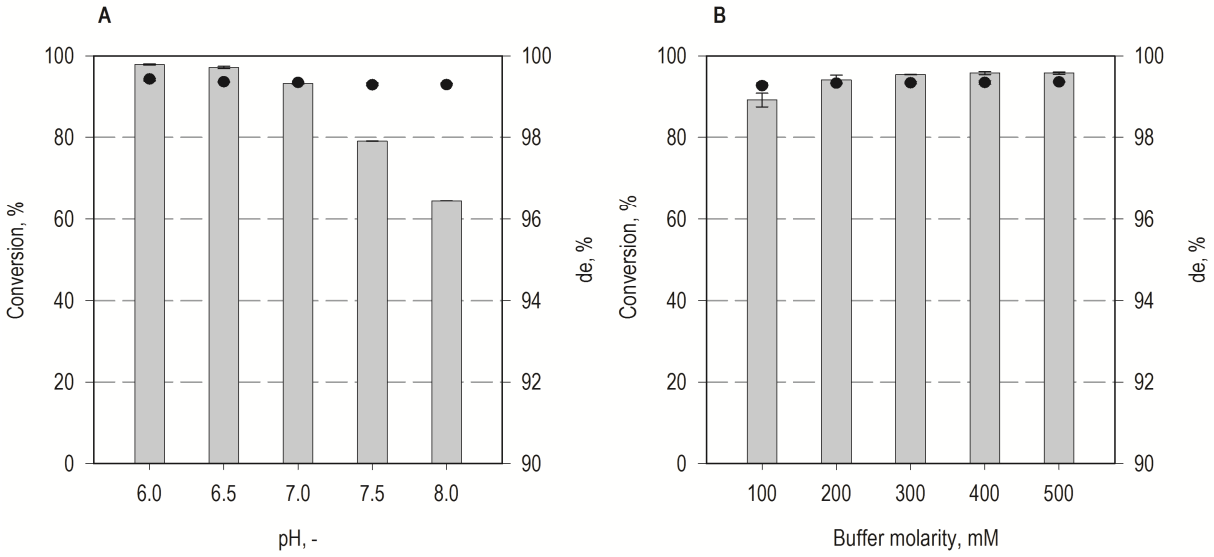

Figure 7.18 Effect of initial pH and buffer molarity on the whole-cell batch biotransformation using *E. coli* pET28NosT7FDH$_{3M}$. The reactions contained 8 g_{CDW} L^{-1} biocatalyst and 250 mM sodium formate in phosphate buffer with the respective pH and 250 mM (R)-carvone in 20 % (v/v) [HMPL][NTF] (A). Sodium phosphate buffers with the respective buffer molarities at pH 7.0 were applied (B). The biotransformation was performed at the 12 mL scale at 25 °C. The conversion and diastereomeric excess after 5 h are presented.

Compared to the reference reaction in 100 mM buffer, the conversion was enhanced by 7 % obtaining a value of 95.5 % using 300 mM sodium phosphate buffer. A further increase of the buffer molarity had no significant influence on the reaction rate (even with respect to the conversions achieved after 1 h, data not shown). With regard to the stereoselectivity of the process, (2R,5R)-dihydrocarvone was obtained in ≥ 99.2 % de. Thus, the buffer molarity had no influence on the stereoselectivity of the process.

As a result, a slightly acidic pH at pH 6.0 – 6.5 turned out to be beneficial for the bioconversion of (R)-carvone at 100 mM buffer molarity, as reactions with pH increased above pH 7.5 seemed to diminish the reaction rate. Using higher buffer capacity by increasing the buffer molarity, a drift to alkaline pH could be minimized, enabling high conversions also at pH 7.0. Thus, the pH should be kept below pH 7.0 during the reaction to ensure high reaction rates.

It has to be further noted that an increase of sodium ions in the reaction or substitution of sodium ions by using e.g. ammonium formate or potassium phosphate buffer instead of sodium formate and sodium phosphate buffer had no significant influence on the biotransformation (data not shown).

Effect of substrate, formate and biocatalyst concentrations

The concentration of (R)-carvone in the aqueous phase in a biphasic buffer/[HMPL][NTF] system is defined by the distribution coefficient of log*D* 2.64. For the standard concentration of 250 mM (R)-carvone in the IL phase, a concentration of 0.57 mM (R)-carvone is present in the aqueous phase. An increased (R)-carvone concentration in the aqueous phase could enhance the reaction rate but also lead to biocatalyst inactivation due to increased accumulation in the cell membrane.

The formate concentration in the reaction system can affect the reaction rate of the biocatalyst by either influencing the reaction rate of the FDH or NostocER1. The applied FDH_{3M} displayed a K_M of 113 mM for formate (Hoelsch et al 2012). In contrast, the activity of NostocER1 was decreased by 49.6 % in presence of 1000 mM sodium phosphate (data not shown). To enable complete conversions, formate has to be provided at least in an equimolar amount with reference to the initial substrate concentration.

In general, a complete conversion of high substrate amount is desired. Consequently, the reaction time has to be extended at low biocatalyst concentrations, or the biocatalyst amount has to be increased.

All three process variables were found to significantly influencing the reaction rate and stereoselectivity in preliminary studies (data not shown). As the optimal substrate concentration correlates with the concentration of both formate and biomass, a combined investigation was preferred.

7.4.2 Optimization of initial process conditions

Based on previous considerations and experiments, several process variables (pH, substrate, cosubstrate and biocatalyst concentration) were assumed to exhibit interacting influences on the batch biotransformation. Thus, the whole-cell biotransformation of (R)-carvone to (2R,5R)-dihydrocarvone using the best biocatalyst *E. coli* pET28NosT7FDH$_{3M}$ was optimized in two steps.

First, response surface methodology (RSM) was applied for optimization of initial pH, substrate and cosubstrate concentrations at a defined biocatalyst concentration. Thereby the central composite circumscribed design (CCC) was chosen for optimal experimental design. Separately, the biocatalyst concentration was further adapted to higher substrate loadings. The results are presented in the following.

Empirical model-based optimization of (R)-carvone reduction

The following process variables and boundaries were chosen for a model-based statistical experimental design:

i. *Substrate* concentrations (x_1) within boundaries of 200 mM to 600 mM (R)-carvone in the ionic liquid were selected. Though a high substrate loading was desired, the increased concentration in the aqueous phase might inactivate the biocatalyst.
ii. *Cosubstrate* concentrations (x_2) within boundaries of 100 mM to 800 mM formate in the aqueous phase were chosen, as higher formate concentrations might be required for the conversion of higher substrate concentrations.
iii. Various *pH* set points (x_3) at the beginning of the biotransformation were set with pH 5.7 and pH 7.2 as boundaries, as the pH optimum was expected to be around pH 6.0, but the buffer capacity of phosphate buffer was limited to pH 5.7.

For all reactions, the pH was not controlled during the batch biotransformation process and a sodium phosphate buffer at a concentration of 300 mM was applied. A volume ratio of 20 % (v/v) [HMPL][NTF] as the second IL phase was kept constant, as it was proven to be favorable for biphasic whole-cell biotransformations (Bräutigam et al. 2009; Dennenwald 2011). A biocatalyst concentration of 8 g_{CDW} L^{-1} was chosen. The reaction temperature was set to 25 °C. Experiments were performed in parallel using the bioreactor unit at a 12 mL scale according to the central composite circumscribed design (CCC). The operation conditions and the conversions after 3 h and 5 h are shown in Table 7.2.

Table 7.2 Experimental design and results of triplicates for the creation of the empirical model based on central composite design. The measured conversion is compared with the predicted conversion after 3 h and 5 h of biotransformation using *E. coli* pET28NosT7FDH$_{3M.}$ All experiments were conducted in 300 mM sodium phosphate buffer with 20 % (v/v) [HMPL][NTF] using 8 g_{CDW} L^{-1} biocatalyst at 25 °C.

Exp. No.	Variables			Conversion 3 h, %		Conversion 5 h, %	
	pH, -	Substrate, mM	Formate, mM	Experiment	Model	Experiment	Model
1	6.0	201.4	241.9	93.4 ± 0.4	81.0	99.6 ± 0.0	92.6
2	6.0	201.4	658.1	89.2 ± 0.9	85.0	99.0 ± 0.1	100.0
3	6.0	498.7	241.9	51.6 ± 1.2	33.2	76.0 ± 1.7	58.0
4	6.0	498.7	658.1	44.9 ± 0.5	35.0	64.1 ± 1.0	56.7
5	6.9	201.4	241.9	92.7 ± 0.0	81.4	99.4 ± 0.0	92.6
6	6.9	201.4	658.1	90.4 ± 1.4	79.7	99.2 ± 0.2	94.0
7	6.9	498.7	241.9	47.0 ± 1.2	33.6	67.3 ± 1.2	58.1
8	6.9	498.7	658.1	37.5 ± 1.0	29.6	52.3 ± 1.1	45.5
9	5.7	350.0	450.0	62.6 ± 1.7	52.7	87.5 ± 0.3	81.0
10	7.2	350.0	450.0	58.6 ± 1.8	48.6	81.6 ± 2.1	71.7
11	6.5	100.0	450.0	98.7 ± 0.1	100.0	99.8 ± 0.1	100.0
12	6.5	600.0	450.0	37.7 ± 0.9	24.0	55.2 ± 1.4	36.0
13	6.5	350.0	100.0	65.0 ± 0.6	56.1	85.3 ± 0.3	81.2
14	6.5	350.0	800.0	66.4 ± 0.9	56.1	90.1 ± 0.6	81.2
15	6.5	350.0	450.0	70.4 ± 1.1	57.7	93.2 ± 0.5	89.6

The measured conversions after 3 h and 5 h were separately fitted to two second-order polynomial models based on Equation 4.12. The models were refined using regression analysis and removing of non-significant parameters according to the exhibited *p* values.

As a result, model equations for relative conversions after 3 h and 5 h were obtained and presented in Equation 7.1 and 7.2. Corresponding coefficients and *p* values (*t* test) are listed in Table 7.3. The two models exhibited good coefficients of determination (R^2 = 0.969, 0.958) and adjusted coefficients of determination ($\bar{R}^2$ = 0.939, 0.916).

$$\eta_{3h} = 0.697 - 0.210x_1 - 0.013x_3 - 0.012x_1x_2 - 0.016x_1x_3 + 0.002x_1^2 - 0.007x_2^2 - 0.025x_3^2 \quad \text{Eq. 7.1}$$

$$\eta_{5h} = 0.933 - 0.156x_1 - 0.022x_3 - 0.033x_1x_2 - 0.026x_1 - 0.057x_1^2 - 0.021x_2^2 - 0.032x_3^2 \quad \text{Eq. 7.2}$$

Table 7.3 Identified coefficients β and p values of the second-order polynomial for the estimation of the conversion after a process time of 3 h and 5 h.

Coefficient	Parameter 3 h	*p* value (*t* test)	Parameter 5 h	*p* value (*t* test)
β_0	0.697	3.223e-06	0.933	2.406e-07
β_1	−0.210	1.598e-06	−0.156	6.753e-06
β_3	−0.013	0.383	−0.022	0.131
β_{12}	−0.012	0.536	−0.033	0.099
β_{13}	−0.016	0.427	−0.026	0.177
β_{11}	0.002	0.919	−0.057	0.023
β_{22}	−0.007	0.769	−0.021	0.323
β_{33}	−0.025	0.289	−0.032	0.146

The obtained models describing the conversions after 3 h and 5 h are visualized in Figure 7.19A, 7.19B. Corresponding product concentrations (referred to the IL phase) formed after 3 h and 5 h were calculated based on the Equations 7.1 and 7.2 and the initial substrate concentrations. These results are presented in Figure 7.19C and 7.19D.

As the conversion generally depended on the substrate loading, the obtained product concentrations revealed more information regarding the reaction rate of the biotransformation. Because a complete conversion was achieved for most operation settings at low substrate loading ($\leq$ 200 mM in IL), the influences of the process variables under study were more apparent at higher substrate concentrations. It has to be noted that a stereoselectivity of $\geq$ 99.1 % de was obtained for all conditions under study (data not shown).

Enhanced product formation was observed for conditions at pH 6.1 – 6.5, which was expected with regard to the preliminary studies. The reaction rate was notably decreased at higher pH.

The influence of formate concentrations on the biotransformation was less significant for conditions with low substrate loading. However, at higher substrate concentrations ($\geq$ 500 mM) an interacting negative effect of higher formate concentrations ($\geq$ 700 mM) and higher pH ($\geq$ pH 7.0) on the conversion and formed product concentration was observed. This indicated influences of both formate and pH in this operation range. A higher FDH activity is expected at increased formate concentration ($K_{M,formate}$ for FDH_{3M} of 113 mM), which would result in a stronger accumulation of sodium hydroxide and subsequent pH drift

towards alkaline pH (Kaup et al. 2009). This might have caused a decreased reaction rate under this condition.

With regard to the substrate loading in the IL phase, complete conversions was accomplished for (R)-carvone concentrations below 200 mM in the IL phase independently from pH and formate concentrations. For high (R)-carvone concentrations up to 600 mM in the IL, high product concentration was obtained at $\leq$ pH 6.5 and $\leq$ 500 mM formate. An inactivation of biocatalyst was not observed under this conditions within the given process time of 5 h.

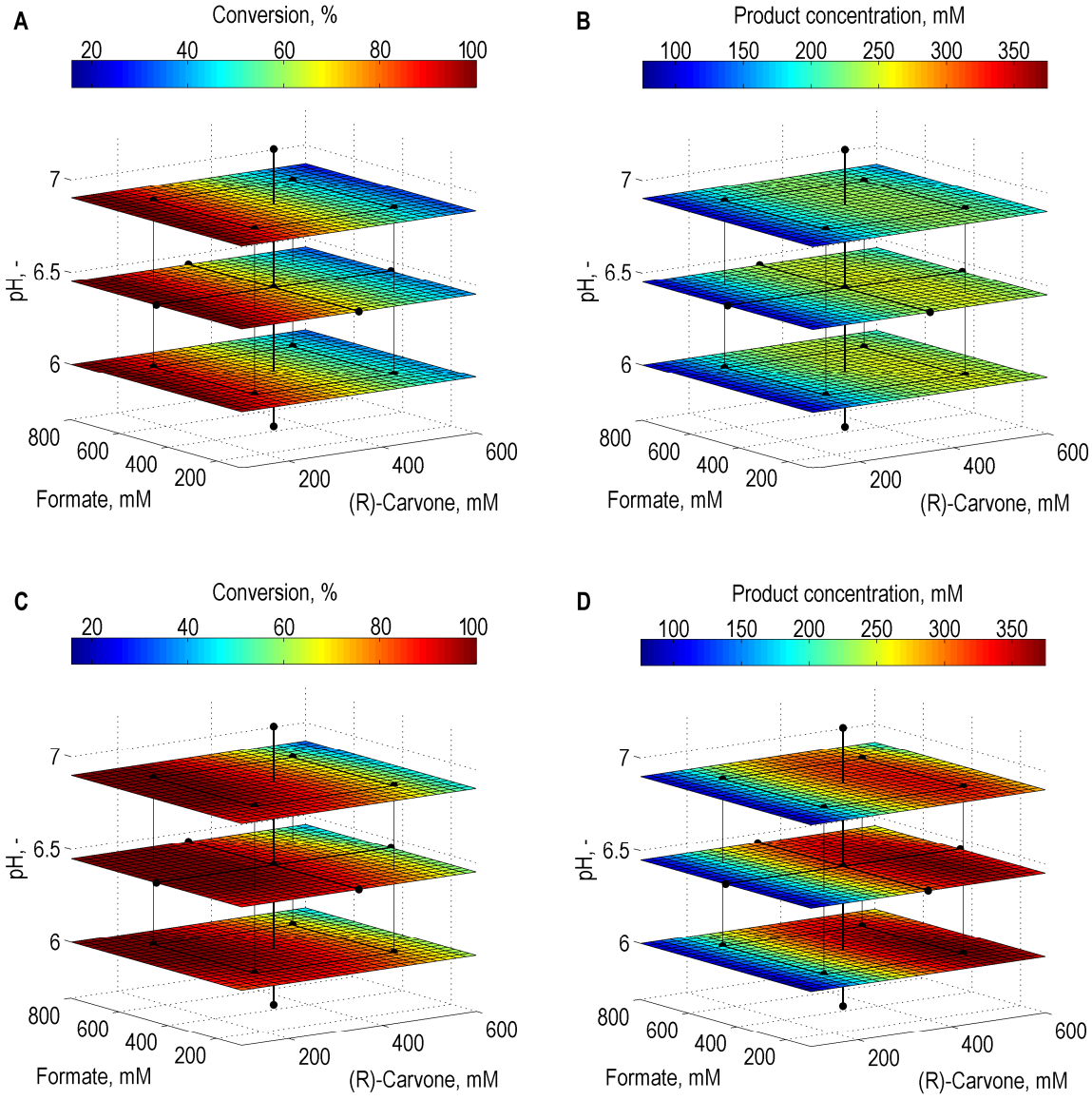

Figure 7.19 Simulation of whole-cell biotransformation of (R)-carvone at different pH, formate and substrate concentrations. The conversions after 3 h (A) and 5 h (C), as well as the calculated product concentrations after 3 h (B) and 5 h (D) are shown. The substrate and product concentrations refer to the ionic liquid phase.

Model validation

Subsequent to the creation of an empirical model, a careful validation is essential to ensure data accuracy. Both models obtained from data after 3 h and 5 h were verified by 12 randomly generated operation points within the designed space. The resulted experimental data and the predicted data from the models are summarized in Table 7.4.

Table 7.4 Randomly created operation points and experimental data for model validation. All experiments were conducted in 300 mM sodium phosphate buffer with 20 % (v/v) [HMPL][NTF] using 8 g_{CDW} L^{-1} *E. coli* pET28NosT7FDH$_{3M.}$ at 25 °C.

Exp. No.	**Variables**			**Conversion 3 h, %**		**Conversion 5 h, %**	
	pH, -	Substrate, mM	Formate, mM	Experiment	Model	Experiment	Model
1	6.0	241.9	201.3	87.2 ± 0.2	80.9	99.0 ± 0.1	93.0
2	6.5	450.0	350.0	57.4 ± 1.8	55.9	82.7 ± 1.4	80.9
3	6.9	166.5	281.7	95.6 ± 0.0	92.8	99.9 ± 0.0	97.3
4	6.6	426.1	172.8	58.4 ± 0.3	57.5	82.2 ± 0.8	80.6
5	6.3	212.3	682.0	90.6 ± 0.2	89.5	99.1 ± 0.0	100.0
6	6.2	543.1	388.9	47.4 ± 1.4	44.3	69.7 ± 1.5	66.7
7	6.9	170.6	228.4	96.0 ± 0.2	90.9	99.9 ± 0.0	94.5
8	6.5	515.6	624.6	46.1 ± 1.0	44.7	67.5 ± 1.3	63.9
9	6.6	543.7	569.2	45.3 ± 0.3	40.1	64.9 ± 0.1	58.0
10	5.9	537.2	431.0	49.0 ± 0.9	44.2	72.0 ± 0.8	67.0
11	6.0	340.4	736.2	70.9 ± 0.9	69.0	93.6 ± 0.4	89.8
12	6.0	441.3	405.2	61.5 ± 1.6	56.9	86.3 ± 1.5	82.6

The predicted conversion is plotted against the observed conversion in Figure 7.20. The correlation of the predicted and measured data was well for both models with $R^2 = 0.977$ for the conversion after 3 h and $R^2 = 0.955$ for a process time of 5 h.

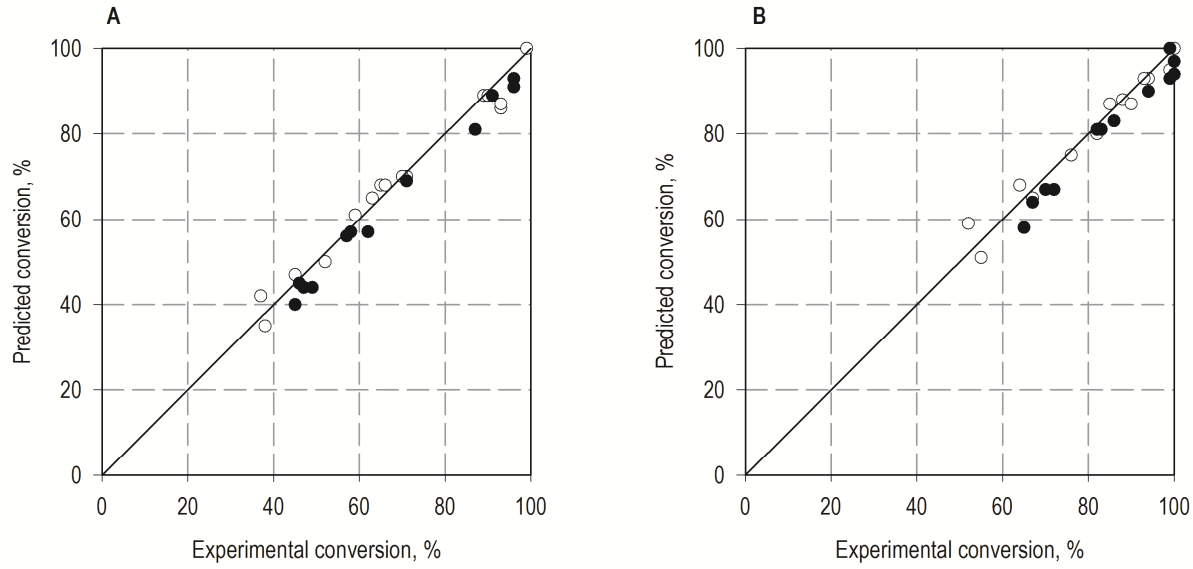

Figure 7.20 Validation of the empirical model by correlation of the predicted and experimental conversions. The data used for parameter identification to create the model (black dots) and for model validation (white dots) are presented for biotransformation after 3 h (A) and 5 h (B). All experiments were conducted at 25 °C in 300 mM sodium phosphate buffer with 20 % (v/v) [HMPL][NTF] using 8 g_{CDW} L^{-1} *E. coli* pET28NosT7FDH$_{3M}$.

Optimum search

The created second-order polynomials were explored to maximal product concentrations at a given minimum conversion threshold. The optimal operation points are presented in Table 7.5.

Table 7.5 Optimal operation states resulting in maximal product concentrations at a given minimum conversion threshold or without a given minimum conversion threshold. Other process variables such as temperature (25 °C), biocatalyst concentration (8 g_{CDW} L^{-1}) and the reaction buffer (300 mM sodium phosphate buffer) with 20 % (v/v) [HMPL][NTF] were kept constant.

Model	Threshold, %	Model prediction		Process conditions		
		Conversion, %	Product, mM	pH, -	Substrate, mM	Formate, mM
3 h	-	58.7	254.2	6.3	433.3	333.3
	≥ 95	97.5	158.5	6.5	162.5	683.3
	≥ 99	-	-	-	-	-
5 h	-	75.5	374.5	6.1	495.8	304.2
	≥ 95	95.7	315.0	6.4	329.2	479.2
	≥ 99	99.2	285.2	6.4	287.5	508.3

After a process time of 3 h, no operation conditions could be identified for achieving 99 % conversion. The highest product concentration of 374.5 mM was obtained after 5 h using 495.8 mM (R)-carvone in the IL phase and 304.2 mM formate in the aqueous phase at

pH 6.1. Thereby, (R)-carvone was converted by 75.5 %. To gain at least 99 % conversion after 5 h, a start concentration of 287.6 mM (R)-carvone in the IL phase with 508.3 mM formate at pH 6.4 was proposed as favorable condition. This operation point was further applied for process scale-up (Section 7.4.3).

Optimization of initial substrate and biocatalyst concentrations

The objective of the batch process development for (R)-carvone reduction was a complete conversion of high initial substrate amount within a given reaction time, thereby achieving high diastereomeric excess of the product. Thus, high initial biocatalyst concentrations are required adequately to the substrate amount. The influence of the substrate and biocatalyst concentration was evaluated with process conditions based on a bifactorial experimental design, as this allowed an adequate allocation of process conditions within the experimental boundaries. The boundaries given for the (R)-carvone concentration in the IL were 100 mM – 1000 mM. The boundaries of biocatalyst concentrations were set to 4 $g_{CDW}\,L^{-1}$ and 38 $g_{CDW}\,L^{-1}$. *E. coli* pET28NosT7FDH$_{3M}$ was selected for the investigation. 100 mM sodium phosphate buffer (100 mM, pH 7.0) was chosen to allow comparability to the reference experiments. The obtained product concentrations in the IL phase and the diastereomeric excesses after 5 h are shown in Figure 7.21 and Table 7.6.

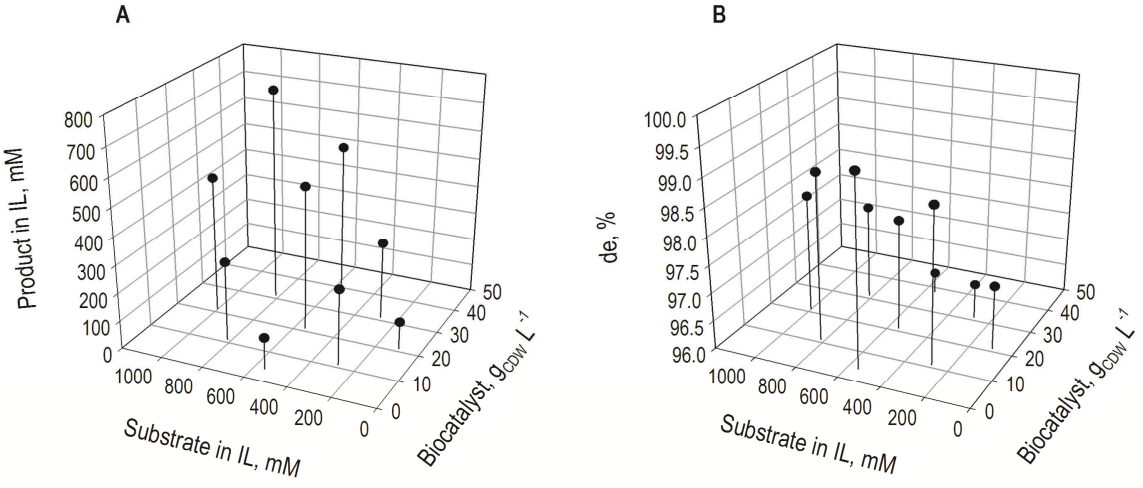

Figure 7.21 Whole-cell batch biotransformation of (R)-carvone at different initial biocatalyst and substrate concentrations. Reactions contained 250 mM formate at various substrate concentrations in a range of 100 – 1000 mM in 20 % (v/v) [HMPL][NTF] and biocatalyst concentrations in a range of 4 – 38 $g_{CDW}\,L^{-1}$ in sodium phosphate buffer (100 mM, pH 7.0). *E. coli* pET28NosT7FDH$_{3M}$ was used for the 12 mL-scale biotransformations conducted at 25 °C. Product concentrations in IL (A) and diastereomeric excesses (de) (B) after 5 h are presented.

Table 7.6 Effect of different biocatalyst and substrate concentrations on the whole-cell batch biotransformation of (R)-carvone. Reactions were performed in sodium phosphate buffer (100 mM, pH 7.0) with 20 % (v/v) [HMPL][NTF] at 25 °C. *E. coli* pET28NosT7FDH$_{3M}$ was used and 250 mM formate was added. IL = ionic liquid, de = diastereomeric excess.

Exp.	Variables		Results				
No.	Biocatalyst, $g_{CDW}L^{-1}$	Substrate , mM in IL	Conversion (5 h), %	Product. mM in IL	de (5 h), %	Space-time yield, mmol L^{-1} h^{-1}	de decrease, % de h^{-1}
1	10.9	282.4	96.2	271.7	98.8	10.9	−0.24
2	10.9	817.6	34.9	285.4	99.0	11.4	−0.20
3	31.1	282.4	99.8	281.7	96.6	11.3	−0.67
4	31.1	817.6	93.0	760.5	97.7	30.4	−0.46
5	4.0	550.0	20.8	114.5	99.4	4.6	−0.12
6	38.0	550.0	99.9	549.6	96.4	22.0	−0.72
7	21.0	100.0	99.5	99.5	97.2	4.0	−0.57
8	21.0	1000.0	49.2	491.7	98.1	20.7	−0.40
9	21.0	550.0	94.1	517.5	98.0	19.7	−0.37

In general, (R)-carvone reductions with higher initial biocatalyst concentrations yielded higher product concentrations. However, the stereoselectivity of the process decreased with higher product formation facilitated by higher biocatalyst amount. An initial substrate concentration in the IL of 818.6 mM was converted by 93.0 % furnishing (2R,5R)-dihydrocarvone in 97.7 % de after 5 h using 31 g_{CDW} L^{-1} biocatalyst.

A detailed view of the reaction rate and the evolution of the stereoselectivity dependent on substrate loading and biocatalyst concentration are given by the space-time yield as a function of the initial biocatalyst concentration and the rate of diastereomeric excess decrease as a function of the space-time yield (Figure 7.22). Thereby, operational conditions achieving complete conversions (≥ 99.4 %) were left out the correlation.

A linear correlation of space-time yield and biocatalyst concentration was found. An increase of the initial biocatalyst concentration of 10 g_{CDW} L^{-1} led to an increase of the space time yield by ~10 mmol L^{-1} h^{-1}. Higher space-time yield was achieved in reactions with higher substrate and biocatalyst concentrations. With regard to the stereoselectivity, the decrease of de proceeded faster with increasing space-time yield, which resulted in an increased product concentration in the aqueous phase. The de decreased with a rate between −0.12 % de h^{-1} and −0.46 % de h^{-1}.

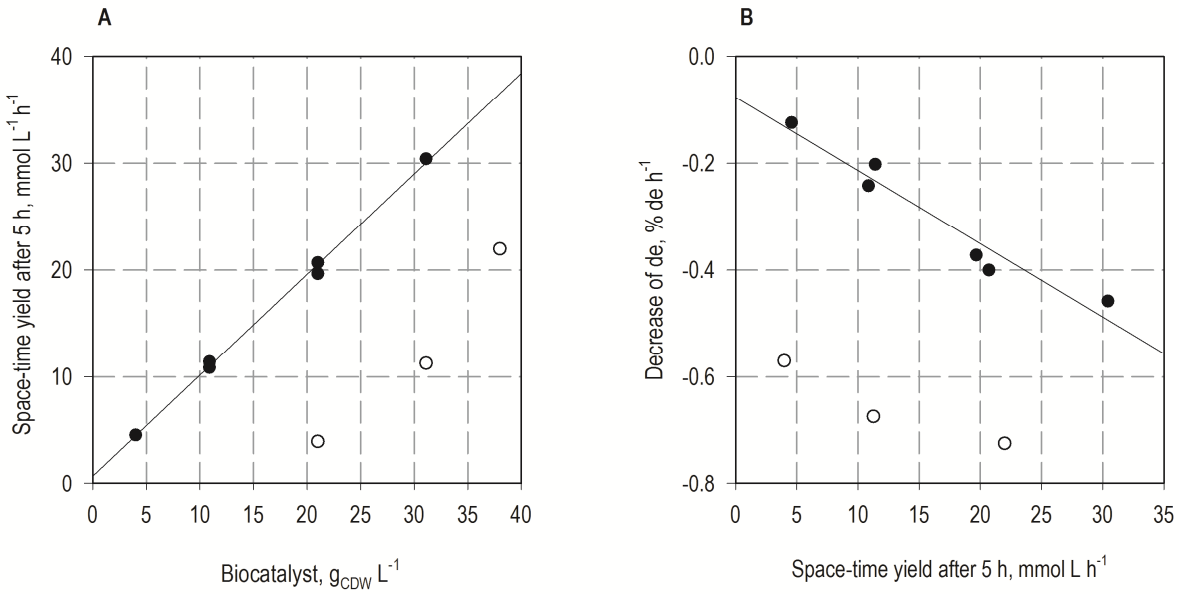

Figure 7.22 Correlation of biocatalyst concentrations with the space-time yield (A) and correlation of the rate of decrease in diastereomeric excess with the space time yield (B) at different biocatalyst and substrate concentrations. Reactions contained 250 mM formate at various substrate concentrations in a range of 100 – 1000 mM and biocatalyst concentrations in a range of 4 – 38 $g_{CDW}\,L^{-1}$ in sodium phosphate buffer (100 mM, pH 7.0) with 20 % (v/v) [HMPL][NTF]. *E. coli* pET28NosT7FDH$_{3M}$ was used for the 12 mL-scale batch biotransformations conducted at 25 °C. The white dots indicate the process conditions, where ≥ 99.4 % conversion was obtained within 5 h.

7.4.3 Scale-up of biphasic whole-cell batch biotransformations

In this section, the scale-up of the biotransformation process is focused. In previous studies by Dennewald (2011), the process scale-up of biphasic whole-cell biotransformations was successfully demonstrated based on constant maximal energy dissipation (ε_{max}). To ensure comparable mass transfers during the biphasic batch biotransformation, the drop size distribution should be similar for different reaction scales. This was enabled by keeping constant maximal local energy dissipations in the reactors.

In this thesis, the same scale-up strategy was pursued for process scaling of biphasic (R)-carvone biotransformations. The three studied process scales were 12 mL scale in the milliliter bioreactor unit (Weuster-Botz 2005), 200 mL scale in a stirred bubble column (Weuster-Botz et al. 2002) and 1 L scale in a standard laboratory stirred-tank bioreactor.

Scale-up between the 12 mL and 200 mL scale

Whole-cell batch biotransformations on a 12 mL scale were performed in the miniaturized stirrered-tank reaction system equipped with S-impellers developed by Riedlberger and

Weuster-Botz (2012). The S-impellers were originally designed for homogenization of solids in enzymatic hydrolysis (Riedlberger and Weuster-Botz 2012), but also recommended by Dennewald et al. (2012) for biphasic reaction systems with ionic liquids.

Biphasic biotransformations with ILs at the 200 mL scale in the stirred bubble column were favorable at a maximal energy dissipation of 10 W kg^{-1}, which was present at a stirrer speed of 600 rpm (Dennewald et al. 2012). Unfortunately, no data regarding the maximal energy dissipation in baffled reactors equipped with S-impellers was available, thus a direct correlation based on constant ε_{max} was not possible. Nevertheless, correlations of the volumetric power consumption and the maximal energy dissipation with regard to a standard liter-scale stirred-tank bioreactor and the gas-inducing impeller for the miniaturized stirred-tank bioreactor were provided by Hortsch and Weuster-Botz (2010). As this correlation depends on the ratio between the diameter of the impeller and the diameter of the reactor (Henzler 2000), the relation for the S-impeller applied in miniaturized stirred-tank bioreactors was assumed to be in a similar range compared to the gas-inducing impeller. Thus, the required volumetric power consumption was expected to be in a range of 1 W L^{-1} to 3 W L^{-1}, which was facilitated with an impeller speed of 1500 rpm in miniaturized baffled bioreactor equipped with S-impellers at a reaction volume of 12 mL (Riedlberger 2012). Consequently, the milliliter scale biotransformations were performed using this setup.

A comparison of the biphasic bioreduction of (R)-carvone on a 12 mL scale and 200 mL scale is given in Figure 7.23 using the biocatalyst *E. coli* pET28NosT7FDH$_{3M.}$ Because of the reduced working volume in the miniaturized bioreactors, only two samples were taken within a process time of 5 h. The conversions and diastereomeric excesses obtained after 1 h and 5 h were similar for both scales.

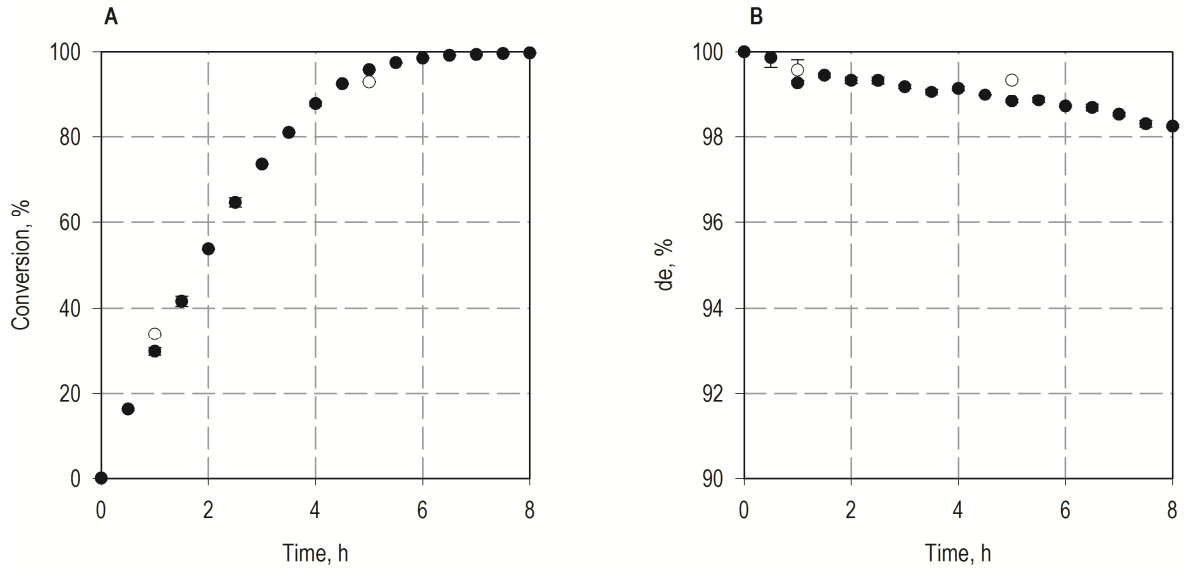

Figure 7.23 Correlation of whole-cell batch biotransformations performed in the bioreactor unit at a 12 mL scale with biotransformations performed at 200 mL scale. Experiments were performed with 8 g_{CDW} L^{-1} *E. coli* pET28NosT7FDH$_{3M}$ and 250 mM sodium formate in phosphate buffer (100 mM, pH 7.0) and 250 mM (R)-carvone in 20 % (v/v) [HMPL][NTF]. The impeller speed was set to 1500 rpm in case of the reactions performed at 12 mL scale and to 600 rpm in the reaction system at 200 mL scale. The reaction temperature was set to 25 °C. The conversion (A) and diastereomeric excess (de, B) for the 12 mL scale (white dots) and 200 mL scale (black dots) are presented.

Scale up to the liter scale

Optimal process conditions derived from the RSM optimization (287.5 mM (R)-carvone in the 20 % [HMPL][NTF], 8 g_{CDW} L^{-1} biocatalyst and 508.3 mM formate in 300 mM sodium phosphate buffer at pH 6.4) for the highest product yield and 99 % conversion after 5 h in the miniaturized bioreactors were transferred to both 200 mL and 1 L scale using *E. coli* pET28NosT7FDH$_{3M}$.

Preliminary studies in 200 mL scale showed a notable increase in the reaction rate when the process (ambient) temperature was decreased from 25 °C to 20 °C (Figure 7.24). The maximal reaction rate was increased from 13.2 mmol L^{-1} h^{-1} to 15.8 mmol L^{-1} h^{-1}. In addition, a higher diastereomeric excess of 99.3 % de was obtained at 20 °C after 8 h compared to 98.8 % de at 25 °C.

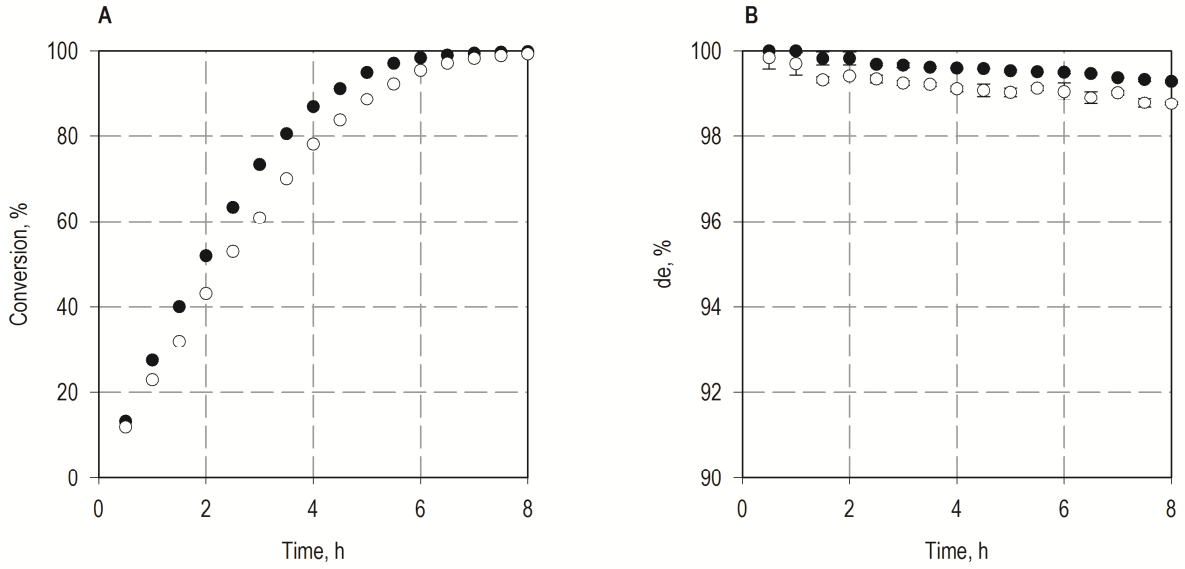

Figure 7.24 Whole-cell batch biotransformation of (R)-carvone at different temperatures. The conversion (A) and diastereomeric excess (B) are shown for the biotransformation of (R)-carvone using 8 g_{CDW} L^{-1} *E. coli* pET28NosT7FDH$_{3M}$ in a biphasic system with 20 % (v/v) [HMPL][NTF] containing 287.5 mM (R)-carvone and 508.3 mM formate in sodium phosphate buffer (300 mM, pH 6.4). The temperature was set to 20 °C (black dots) and 25 °C (white dots). The impeller speed was set to 600 rpm.

Thus, further scale-up to 1 L scale was performed at 20 °C (ambient temperature). Thereby, biotransformations at the 200 mL and 1 L scale were performed simultaneously using the same biocatalyst batch to guarantee the same process conditions. The optimized process conditions were applied for both scales. Based on constant maximal energy dissipations (~10 W kg^{-1}), an impeller speed of 450 rpm was chosen for the 1 L scale compared to 600 rpm at 200 mL scale (Dennewald, 2011). The conversion and stereoselectivity during biotransformation at the 200 mL and 1 L scale are presented in Figure 7.25.

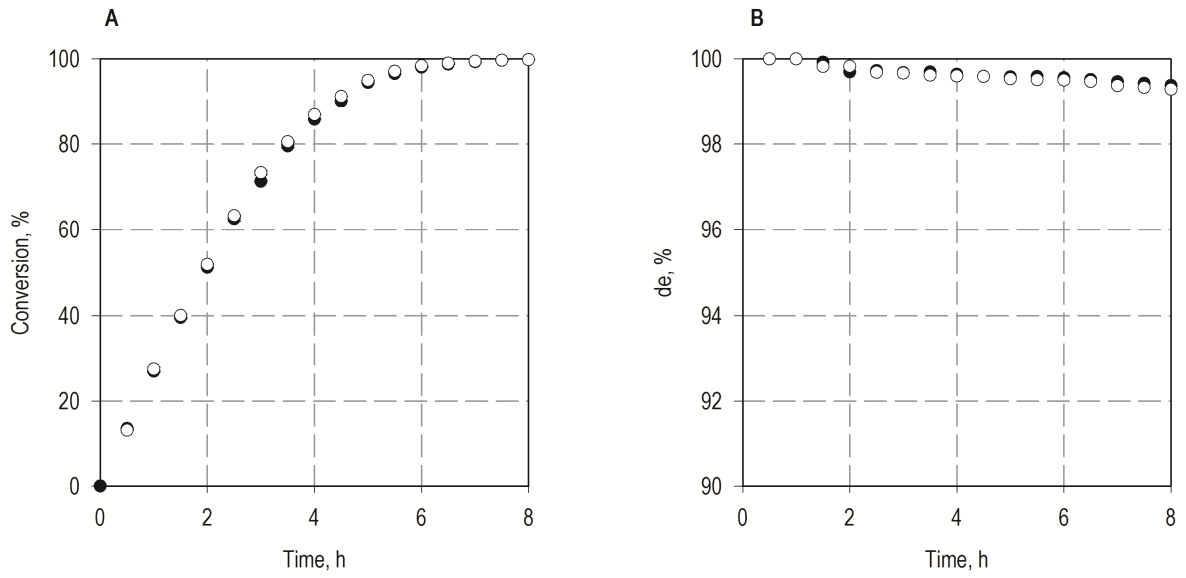

Figure 7.25 Scale-up of the batch biotransformation of (R)-carvone from the 200 mL to the 1 L scale. The conversion (A) and diastereomeric excess (B) are shown for the biotransformation of (R)-carvone using 8 g_{CDW} L^{-1} *E. coli* pET28NosT7FDH$_{3M}$ in a biphasic system with 20 % (v/v) [HMPL][NTF] containing 287.5 mM (R)-carvone and 508.3 mM formate in sodium phosphate buffer (300 mM, pH 6.4). The ambient temperature was 20 °C for both biotransformations. The impeller speed was set to 600 rpm in case of the 200 mL-scale biotransformation (white dots) and 450 rpm for the 1 L-scale biotransformation (black dots).

The evolution of conversion and diasteromeric excess were in excellent agreement for both scales. The maximal (initial) reaction rate was at 15.8 mmol L^{-1} h^{-1} for both scales and ≥ 99.4 % conversion was achieved after 8 h furnishing 57 mmol (2R,5R)-dihydrocarvone with a purity of 99.2 % de. In conclusion, the scale up of the biphasic whole-cell biotransformation of (R)-carvone under optimized process conditions was successful.

At last, the whole-cell (R)-carvone reduction was aimed at higher substrate concentrations. As preliminary results showed an inactivation of the biocatalyst after 8 – 10 h applied at 8 g_{CDW} L^{-1} (data not shown), a complete conversion within 8 h was aimed using higher biocatalyst concentrations. Whole-cell biotransformation of 800 mM (R)-carvone in the IL phase (equal to a theoretical overall concentration of 160 mM) was performed with 36 g_{CDW} L^{-1} *E. coli* pET28NosT7FDH$_{3M}$ on a liter scale using optimized process conditions. Thereby, the reaction was performed at the standard temperature of 25 °C to enable comparable conditions with previous experiments. The evolution of the biotransformation is presented in Figure 7.26.

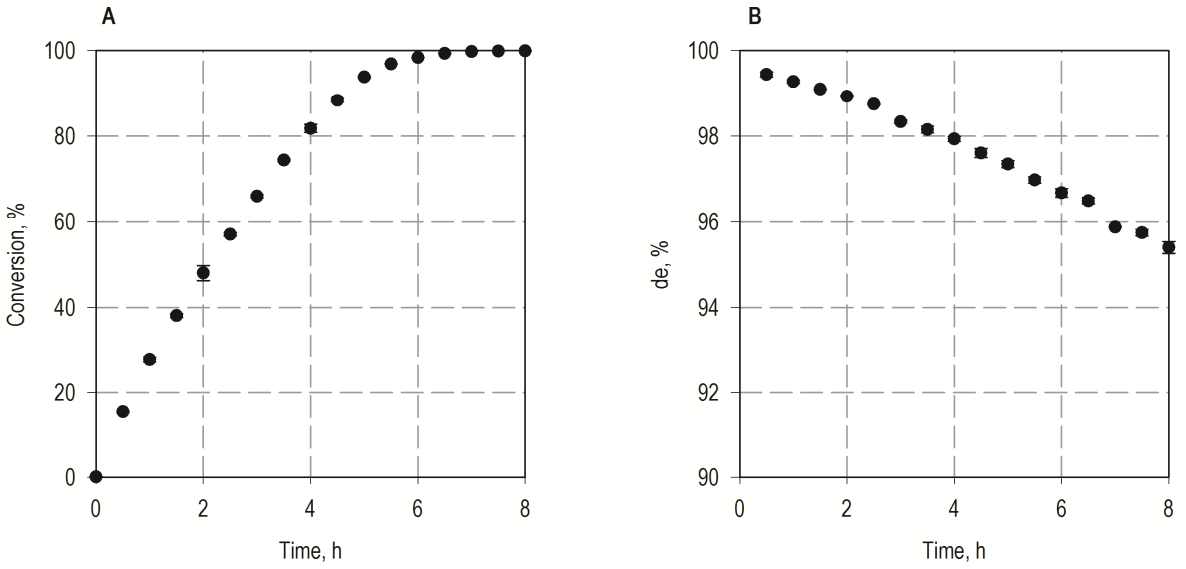

Figure 7.26 Whole-cell batch biotransformation of (R)-carvone on a 1 L scale at high substrate loading. The reaction contained 800 mM (R)-carvone dissolved in 20 % (v/v) [HMPL][NTF] and 400 mM formate in sodium phosphate buffer (300 mM, pH 6.4). The temperature was controlled at 25 °C and the impeller speed was set to 450 rpm.

After a reaction time of 6.5 h, 99.3 % conversion was obtained furnishing (2R,5R)-dihydrocarvone with a diastereomeric excess of 96.5 % de. The space-time yield after 6.5 h was 24.5 mmol L^{-1} h^{-1}. A complete conversion was achieved after 8 h (≥ 99.9 % conversion, 95.4 % de). The achieved low stereoselectivity was in accordance with the stereoselectivities obtained at the milliliter scale using high substrate and biocatalyst concentrations (Section 7.4.2).

7.4.4 Discussion

For adequate optimization of a biocatalytic process, a deep understanding of the influence of significant process variables is essential. The biphasic whole-cell batch biotransformation of (R)-carvone was characterized in detail with subsequent optimization and scale up to 1 L. The effect of various process variables including the interactions thereof are summarized and discussed in the following.

The ***pH and buffer capacity*** were identified as critical process variables. An initial acidic pH in a range of pH 6.1 – 6.5 was preferable for the whole-cell bioreduction of (R)-carvone. It was of particular importance that the pH did not increase over pH 7.0 during the biocatalytic reaction, as this resulted in decreased reaction rates. Under process conditions without pH control, as it was the case for the studied (R)-carvone reductions, a higher buffer

capacity can indeed reduce the pH drift into the alkaline range, but not prevent it completely. Higher buffer molarities (300 mM – 1000 mM) could be applied without inhibition of the biocatalytic reaction. The increasing pH with progressing reaction time was caused by the accumulation of sodium hydroxide formed by the oxidation of sodium formate to carbon dioxide catalyzed by the overexpressed formate dehydrogenase inside the recombinant *E. coli* cells. This effect was generally reported for biotransformations involving formate dehydrogenases (Ernst et al. 2005; Kaup et al. 2004).

The lower reaction rate of the whole-cell biotransformation at alkaline pH might be caused by a decreased enzyme activity of the ER or FDH_{3M} or limited formate transport into the cell. Though in growing *E. coli* cells the intracellular pH can be regulated within a range of pH 7.4 – 7.8 over an external pH range of pH 5.0 – 9.0 (Slonczewski et al. 1981; Wilks and Slonczewski 2007), the intracellular pH in the applied biocatalysts was unknown under the operated conditions. Regarding ERs, a pH optimum at neutral to slight alkaline pH was mostly observed (Chaparro-Riggers et al. 2007). This was also the case for Syn7942ER from cyanobacteria as described in Section 6.1. In contrast, FDH_{1M} displayed a lower reaction rate at pH 8.0 compared to pH 7.0. In addition, the half-saturation constant for $NADP^+$ was increased about 2-fold at pH 8.0 (Liu et al. 2013). This would indicate a reduced reaction rate induced by the FDH at alkaline pH. Apart from that, the availability of intracellular formate clearly influences the FDH activity. In particular, the FDH_{3M} chosen for the studied biotransformations, exhibited a high K_M of 113 mM for formate (Hoelsch et al. 2012). High intracellular formate concentrations depend on the extracellular formate concentrations as well as the efficiency of formate transport through the cell membrane. The formate transporter FocA, which is reported to mediate the import and export of formate, displayed a strong pH dependence (Lü et al. 2011). At high external pH, FocA act as a passive export channel for formate. At low pH, FocA functions as an active formate/H^+ symport facilitating rapid formate uptake (Lü et al. 2011). The switch point for the pH-dependent gating was determined at pH 6.8 in growth studies (Sawers 2005). Thus, higher reaction rates at acidic pH might be supported by increased formate transport into the cell.

With regard to the **formate concentration** in the aqueous phase, decreased reaction rates were only observed at high concentrations in combination with higher pH. Thus, the pH change seemed to be more critical for the biotransformation than the formate concentration itself. In fact, possible enzyme inactivation can only occur at high formate concentrations inside the cell. Though NostocER1 was shown to display reduced activity in presence of

high formate concentration (50 % reduction in activity in presence of 1000 mM sodium formate, data not shown), this effect was not observed in the reaction rate of the whole-cell biotransformations.

The influence of the **biocatalyst concentration** and the **substrate concentration** on the reaction rate of the whole-cell reduction of (R)-carvone was tightly connected. Increased biocatalyst concentration resulted in proportionally higher volumetric productivity of the biotransformations. (R)-carvone concentrations in the IL phase in a range of 100 mM to 600 mM, did not significantly affect the space-time yield after 5 h batch biotransformation. Consequently, the mass transport of (R)-carvone from the IL phase into the aqueous phase could not be the rate-limiting step of the reaction. This implied that the substrate transport into the cell or the enzymatic transformation within the cell could be the rate-limiting steps of the whole-cell (R)-carvone reduction.

A linear decrease of the **diastereomeric excess** was observed with progressing reaction time. The stereoselectivity of the reaction was additionally influenced by the product formation, which was coupled to the biocatalyst concentration. The decrease of diastereomeric excess was accelerated with higher product concentration in the aqueous phase. Thus, the stereoselectivity was decreased for biotransformations at high substrate and biocatalyst concentration. The process temperature was determined as one major influencing factor for the stereoselectivity. Lowering the temperature from 25 °C to 20 °C resulted in an increase of the diastereomeric excess by 0.5 % de.

The optimized biphasic whole-cell reduction of (R)-carvone was successfully scaled up to 1 L based on constant maximal local energy dissipations, demonstrating the capability of (2R,5R)-dihydrocarvone production in larger scales.

7.5 Biphasic batch biotransformation with adsorbent resins

In this section, the applicability of the resin-based substrate feeding and product removal method (resin-based SFPR) method was evaluated with regard to the (R)-carvone reduction using recombinant whole-cell biocatalysts. First, suitable adsorbent resins were selected and further characterized regarding adsorption and desorption properties. Afterwards, the resin-based whole-cell biotransformation was characterized and optimized on a 12 mL scale in the bioreactor unit, as well as at 200 mL in the stirred bubble column. At last, the process was scaled up to the liter scale. Hereby, the objective was again a complete conversion of high initial substrate concentration with high reaction rate within a given reaction time in a batch process.

7.5.1 Selection and characterization of resin

In preliminary studies, the adsorbent resins Amberlite^{TM} XAD4, XAD7 and XAD1180 (DOW, Rohm and Haas) were investigated regarding the adsorption and desorption of (R)-carvone and dihydrocarvone. These polymeric adsorbents displayed different properties regarding the structure matrix, surface area and porosity (DOW, Rohm and Haas) and have been applied in various biocatalytic and adsorption reactions (Bechtold et al. 2012; Bilgili 2006; Brenna et al. 2013b; Brenna et al. 2012e; Vicenzi et al. 1997). The characteristics of the adsorbent resins are summarized in Table 7.7.

Whole-cell batch biotransformations were performed using these adsorbent resins. The mass ratio of resin to substrate is defined by the ratio of wet resin mass to the substrate mass. At the same resin to substance mass ratio of 3, (R)-carvone and dihydrocarvone concentrations in the aqueous phase using XAD7 and XAD1180 were at least 1.4-fold higher compared to XAD4 (data not shown). This means that a higher resin amount was required using XAD7 and XAD1180 to ensure the same limited substrate concentration in the aqueous phase, which indicated an insufficient adsorbent capacity of XAD7 and XAD1180. This was further confirmed in whole-cell bioreductions of (R)-carvone in presence of resin to substrate mass ratios of 2 to 10. Thereby, similarly high conversions were obtained in case of a high mass ratio of 10 for XAD7 and moderate mass ratios in a range of 3 to 5 for XAD4 (data not shown). Thus, further investigations concentrated on XAD4 as favorable adsorbent resin for whole-cell (R)-carvone reduction.

Table 7.7 Characteristics of the selected adsorbent resin. Data were obtained from the manufacturer Rohm and Haas (DOW).

Feature	XAD4	XAD7	XAD1180
Chemistry	polystyrene–divinylbenzene[a]	aliphatic ester	polystyrene–divinylbenzene
Matrix	macroreticular crosslinked aromatic polymer	macroreticular aliphatic crosslinked polymer	macroreticular crosslinked aromatic polymer
Surface area, $m^2\ g^{-1}$	750 (min)	380 (min)	500 (min)
Porosity, mL mL^{-1}	≥ 0.50	≥ 0.50	≥ 0.60
Particle size, mm	0.3 – 1.2	0.2 – 1.9	0.3-1.2
Pore envelope, Å	55 - 80	400 – 450	450 – 500
Moisture content, %	54 – 60 (55.4[b])	61 – 69	61 – 67
Density, g mL^{-1}	1.02	1.07	1.02

[a] The structure is given in Figure 3.12 (Section 3.2.8).

[b] The moisture content was separately determined for the used resin batch.

For a detailed characterization of XAD4 adsorption isotherms were determined for (R)-carvone and dihydrocarvone. The obtained correlation of the quantity of adsorbed solute per quantity adsorbent (q_S) and the residual concentration of solute in the aqueous phase (C_S) were analyzed according to the Freundlich isotherm equation (Equation 3.17). Linearized Freundlich adsorption isotherms are depicted in Figure 7.27 and the identified Freundlich parameters are shown in Table 7.8.

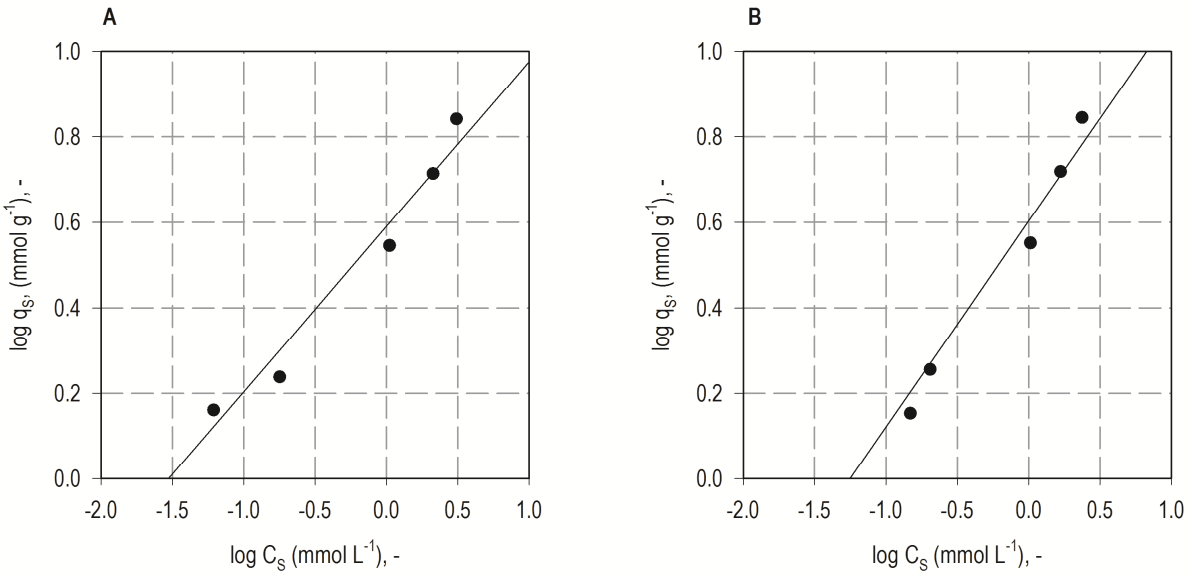

Figure 7.27 Linearized Freundlich adsorption isotherms at 25 °C and experimental equilibrium data are shown for (R)-carvone (A) and dihydrocarvone (B).

Table 7.8 Freundlich parameters determined for XAD4 with (R)-carvone and dihydrocarvone. The correlation coefficients (R^2) are also indicated.

	K_F	b_F	R^2
(R)-Carvone	3.89	0.385	0.981
Dihydrocarvone	4.03	0.485	0.979

The Freundlich constant K_F indicates the adsorption capacity of the adsorbent and b_F represents the adsorption intensity. The adsorption capacity was similar and only slightly higher for dihydrocarvone compared to (R)-carvone. This indicated a higher affinity of the adsorbent for dihydrocarvone at a defined residual concentration. A similar dimensionless constant b_F was obtained with dihydrocarvone, indicating a comparable change in effectiveness at different residual concentrations. In general, XAD4 can be considered as effective for the adsorption of (R)-carvone and dihydrocarvone.

Substrate and product concentrations in the aqueous buffer phase, where the biocatalysis occurs, are expected to be critical for the evolution of the reaction, as it was the case in the biphasic biotransformations with a second water-immiscible ionic liquid phase Thus, concentrations of (R)-carvone and dihydrocarvone in the aqueous phase obtained in equilibrium experiments are plotted against the resin to substrate mass ratio in Figure 7.28. As wet resin was used for biotransformation for convenience (and referred to in further experiments), but dry resin provided actual information about adsorbent property, both variables are given.

Concentrations of (R)-carvone and dihydrocarvone in the aqueous phase decreased with higher resin to substance mass ratio. This was expected as a higher amount of adsorbent is always correlated with an increased adsorption area, resulting in lower substance concentrations in the aqueous phase. Thus, non-toxic environment for whole-cell biocatalysts by adjusting an appropriate substrate concentration in the aqueous phase can be enabled by variation of the resin to substrate ratio.

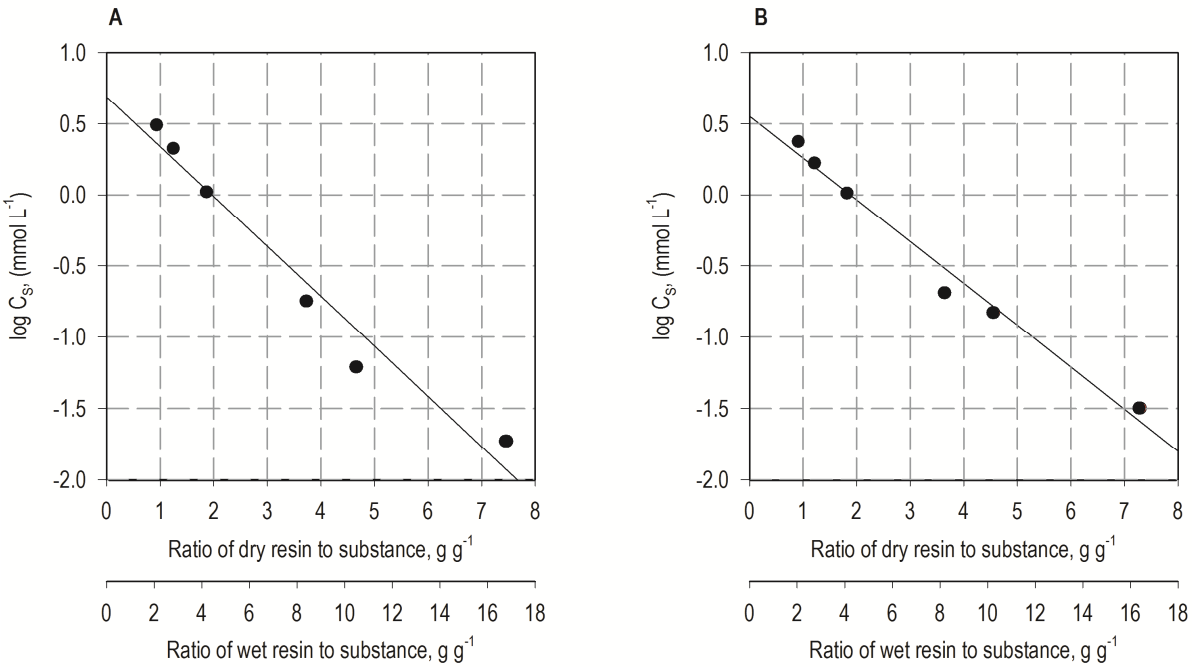

Figure 7.28 Decadic logarithm of the residual concentrations in the aqueous phase (C_S) at different resin to substrate mass ratios obtained in equilibrium experiments at 25 °C for (R)-carvone (A) and dihydrocarvone (B).

7.5.2 Process optimization

Resin-based whole-cell biotransformations for (R)-carvone reduction were generally performed using the optimized biocatalyst *E. coli* pET28NosT7FDH$_{3M}$ unless indicated otherwise. The objective of the investigation was to characterize and optimize process parameters with major importance for the evolution of the batch biotransformation. Process characterization and optimization were performed at both 12 mL and 200 mL scales.

For reactions at 12 mL scale in the miniaturized stirred-tank bioreactors, baffled reactors equipped with S-impellers developed by Riedlberger and Weuster-Botz (2012) were applied at an impeller speed of 1500 rpm. This setup was proven to be advantageous in comparison to unbaffled reactors or gas-inducing impellers (data not shown). Reactions at 200 mL scale were conducted at 600 rpm using a stirred bubble column as previously described for IL-based biphasic biotransformations.

Influence of pH, formate, substrate and biocatalyst concentrations

Though the effect of pH and buffer molarity was expected to be similar for IL- and resin-based biphasic biotransformations, this was verified in 12 mL scale experiments using a resin to substrate mass ratio of 4. Similar to the results obtained from the biphasic reactions with IL, the reaction rate of the biotransformation was improved at pH 6.1 – pH 6.5 and higher buffer molarities of ≥ 300 mM sodium phosphate (data not shown).

Whereas the substrate/product concentration in the aqueous phase depends on the distribution coefficients in biphasic biotransformations with IL as a second phase, the concentration in the aqueous phase using adsorbent resins is defined by the mass ratio of resin to substrate. In theory, the amount of resin can be increased with the substrate amount to enable constant low substrate concentrations in the aqueous phase ensuring the biocatalyst integrity. The effect of substrate, formate and biocatalyst concentrations was evaluated at 12 mL scale in the milliliter bioreactor system.

Preliminary studies using high (R)-carvone concentrations up to 400 mM and biocatalyst concentrations up to 64 $g_{CDW}\,L^{-1}$ revealed operational boundaries given by the milliliter bioreactor system. At high substrate concentrations, the required amount of adsorbent resin had to be notably raised to ensure a constant resin to substrate ratio. High resin amount in combination with high biocatalyst concentrations resulted in severely increased viscosity of the reaction mix leading to limited mass transfers caused by aggregation of resin and biomass on the impeller. This is exemplarily shown in Figure 7.29.

Figure 7.29 S-impellers after 5 h batch biotransformation using 64 $g_{CDW}\,L^{-1}$ *E. coli* pET28NosT7FDH$_{3M}$, 400 mM (R)-carvone and 500 mM formate at a resin to substrate mass ratio of 4.

Consequently, the maximal substrate concentration was limited to 300 mM (R)-carvone. The effect of different biocatalyst concentrations (8, 32, 48 $g_{CDW}\,L^{-1}$) at various formate concentrations (300 mM to 1000 mM) on the resin-based biotransformation was investigated. The resin to substrate mass ratio was kept constant at 4 for all conditions. The conversions after 5 h are shown in Figure 7.30.

The best conversion was obtained with 48 $g_{CDW}\,L^{-1}$ biocatalyst and 400 mM formate, reaching 94.8 % conversion and 98.5 % de after 5 h in the batch process. The reaction rate was not significantly influenced within a formate concentration range of 300 – 500 mM. Decreased conversions at 1000 mM formate might be derived from increased pH, as the initial pH was set to pH 7.0. This was also observed in biphasic biotransformations with IL (Section 7.4). Hence, the correlation of the biocatalyst concentration with the space-time yield and the rate of decreasing diastereomeric excess were performed for reactions at 300 – 500 mM formate (Figure 7.31).

A 4-fold increase of the biocatalyst concentration (from 8 $g_{CDW}\,L^{-1}$ to 32 $g_{CDW}\,L^{-1}$) resulted in 4-fold higher maximal space-time yield (determined after 1 h). But if a 6-fold increased biocatalyst concentration was applied (48 $g_{CDW}\,L^{-1}$), the reaction rate was raised only 5-fold. This might be explained by mass transfer limitations due to increased viscosity in the reaction systems. The decrease of the stereoselectivity accelerated with increased product formation at higher biocatalyst concentrations similar to the IL-based biotransformations (Section 7.4).

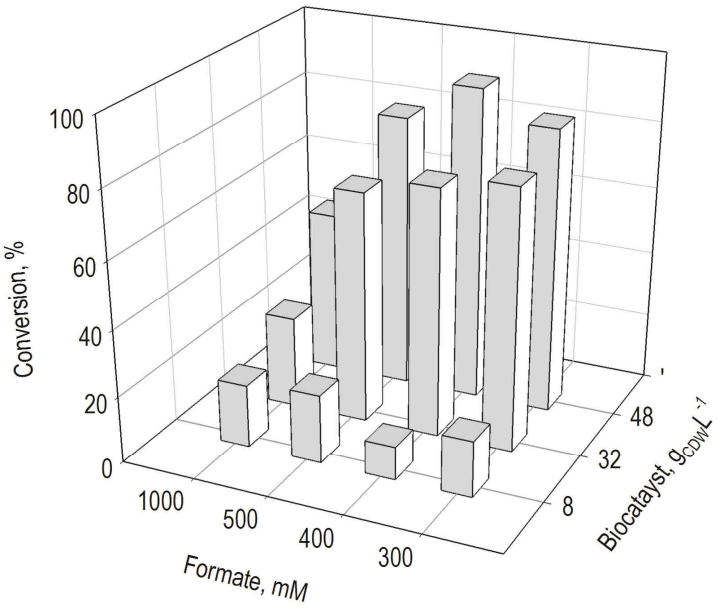

Figure 7.30 Optimization of the biocatalyst and formate concentrations for resin-based batch bioreduction of (R)-carvone. All reactions were performed using *E. coli* pET28NosT7FDH$_{3M}$ at a constant resin to substrate mass ratio of 4 at 25 °C and 1500 rpm at the 12 mL scale using the bioreactor unit equipped with S-impellers. The reactions contained 300 mM (R)-carvone in sodium phosphate buffer (100 mM, pH 7.0) and different concentrations of formate and biocatalyst. The substrate concentration was 300 mM for all conditions. Conversions after a process time of 5 h are presented.

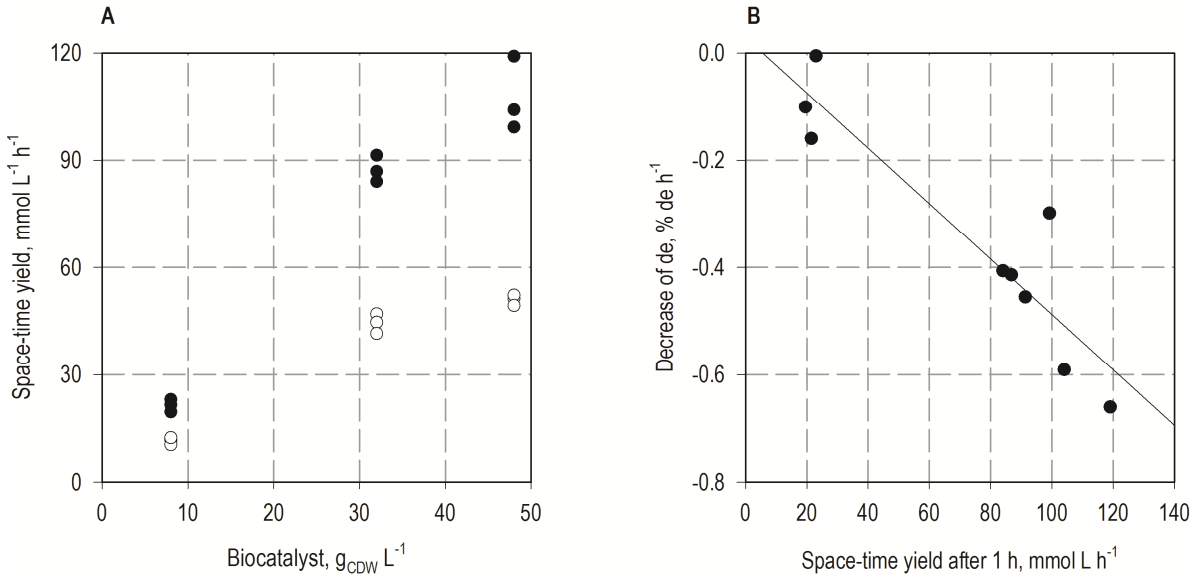

Figure 7.31 Space-time yield and stereoselectivity in resin-based batch biotransformation with increased biocatalyst concentrations. Space-time yield after 1 h (black dots) and 5 h (white dots) are presented in (A). A correlation of the decrease of diastereomeric excess with the space-time yield after 1 h is given in (B). Reactions were performed using different biocatalyst concentrations with 300 – 500 mM formate and 300 mM (R)-carvone in sodium phosphate buffer (100 mM, pH 7.0) at a resin to substrate mass ratio of 4 and 25 °C.

Influence of the resin to substrate mass ratio

A particular feature of the resin-based substrate feeding and product removal method is the possibility of adjusting the appropriate substrate concentration in the aqueous phase by applying different resin to substrate mass ratios. This effect was investigated in 200 mL scale batch biotransformations and the results are shown in Figure 7.32.

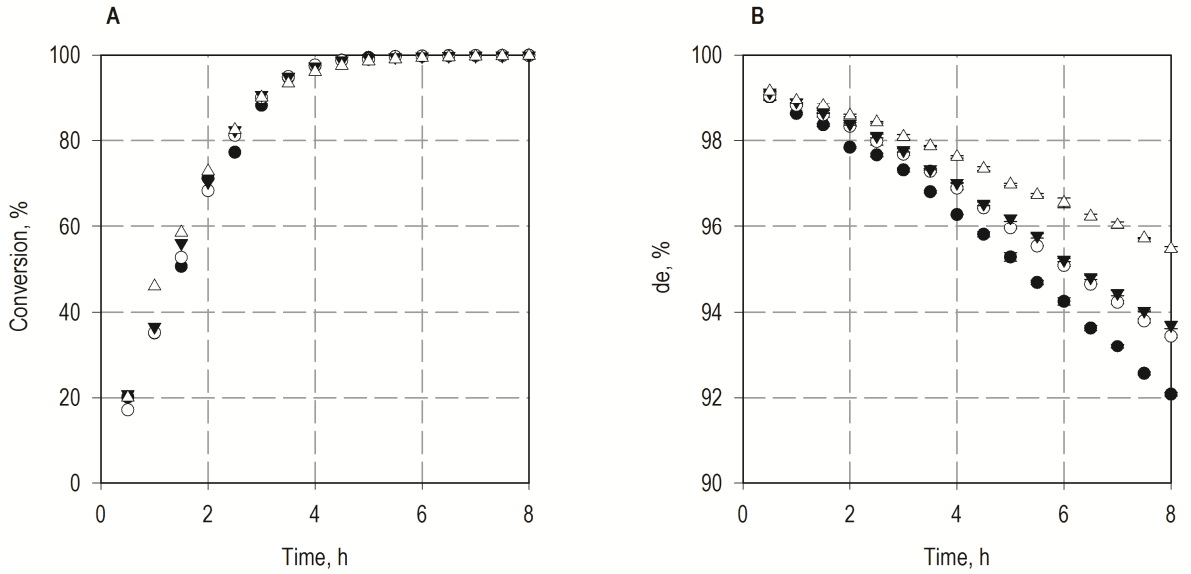

Figure 7.32 Influence of different resin to substrate ratios on conversion and stereoselectivity of the (R)-carvone reduction. Whole-cell batch biotransformations were performed at the 200 mL scale with 50 mM (R)-carvone, 250 mM formate and 8 g_{CDW} L^{-1} *E. coli* pET28NosT7FDH$_{3M}$ in sodium phosphate buffer (100 mM, pH 7.0) at 25 °C and 600 rpm. Resin to substrate mass ratios of 3.5 (black dots), 4 (white dots), 4.5 (black triangles) and 5 (white triangles) were investigated. Conversions (A) and diastereomeric excesses (B) are presented.

Within the range of wet resin to substrate mass ratio of 3.5 to 5, no significant alteration in the evolution of the batch biotransformation was observed. For all conditions with 50 mM (R)-carvone as initial substrate concentration, ≥ 99 % conversion was obtained after 5 h. In contrast, the stereoselectivity of the process was clearly affected by different resin to substrate ratios. With increasing mass ratio of resin to substrate, notably higher diastereomeric excesses were obtained for the product. Thereby, the diastereomeric excess after 8 h deviated from 92.1 % de in case of a ratio of 3.5 to 95.5 % de in case of a ratio of 5. The evolution of stereoselectivity was improved from −1.06 % de h^{-1} to −0.50 % de h^{-1}.

Influence of impeller speed

The influence of higher power input on the biotransforamtion induced by increased impeller speed was evaluated at 200 mL scale under standard conditions with 8 g_{CDW} L^{-1} biocatalyst. Thereby, impeller speeds in a range of 600 rpm to 800 rpm were tested. This corresponded to a maximal local energy dissipation of 10 – 20 W kg^{-1} and a volumetric power consumption of 0.4 – 0.6 W L^{-1} (Dennewald et al. 2012; Weuster-Botz et al. 2002). The results are presented in Figure 7.33.

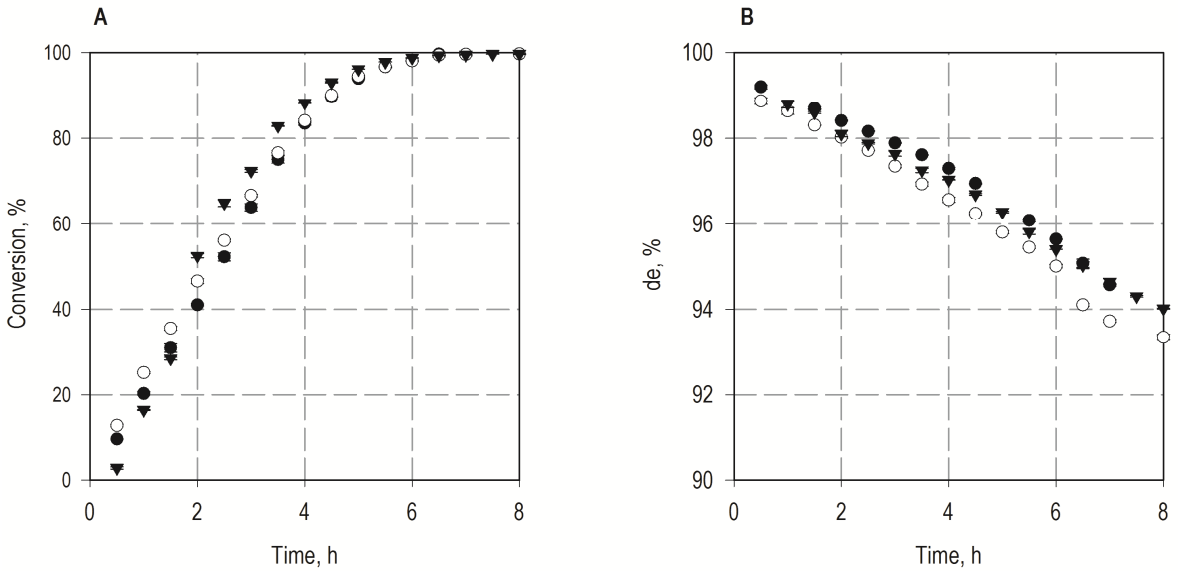

Figure 7.33 Influence of the impeller speed on the resin-based whole-cell batch biotransformation of (R)-carvone. Reactions were performed at the 200 mL scale with 50 mM (R)-carvone, 250 mM formate and 8 g_{CDW} L^{-1} *E. coli* pET28NosT7FDH$_{1M.}$ at 25 °C at a resin to substrate ratio of 4. The tested impeller speeds were 600 rpm (black dots), 700 rpm (white dots) and 800 rpm (black triangles). Conversions (A) and diastereomeric excesses (B) are presented.

An increase of the impeller speed from 600 rpm to 800 rpm did not significantly affect the bioconversion and the stereoselectivity of the whole-cell process. A conversion of ≥ 99.5 % was obtained for all reactions after 7 h. The rate of de decrease were similar at −0.8 % de h^{-1}

7.5.3 Scale-up to the liter scale

After investigation of the relevant process variables, the whole-cell reduction of (R)-carvone using adsorbent resins for *in situ* substrate supply and product removal was transferred into the 1 L scale.

Using a low biocatalyst concentration and a high substrate concentration (8 g_{CDW} L^{-1} *E. coli* pET28NosT7FDH$_{3M,}$ 300 mM (R)-carvone) at a resin to substrate mass ratio of 5, the reaction stopped after 20 h at 25 % conversion without further product formation within the next 20 h (data not shown). This might be caused by the inactivation of the whole-cell biocatalyst. Thus, a higher biocatalyst concentration was chosen.

The biocatalyst concentration was adapted to 36 g_{CDW} L^{-1} for enhanced conversion within a process time of 9 h. The optimized biocatalyst *E. coli* pET28NosT7FDH$_{3M}$ was selected for biotransformation. Due to the expected higher viscosity of the reaction mix, an impeller speed of 500 rpm was chosen for the biotransformation at 1 L scale, which correlated with a stirrer speed of 800 rpm at 200 mL scale in terms of the maximal local energy dissipation (~20 W kg^{-1}) (Dennewald et al. 2012). The conversion and diastereomeric excess for both scales are presented in Figure 7.34.

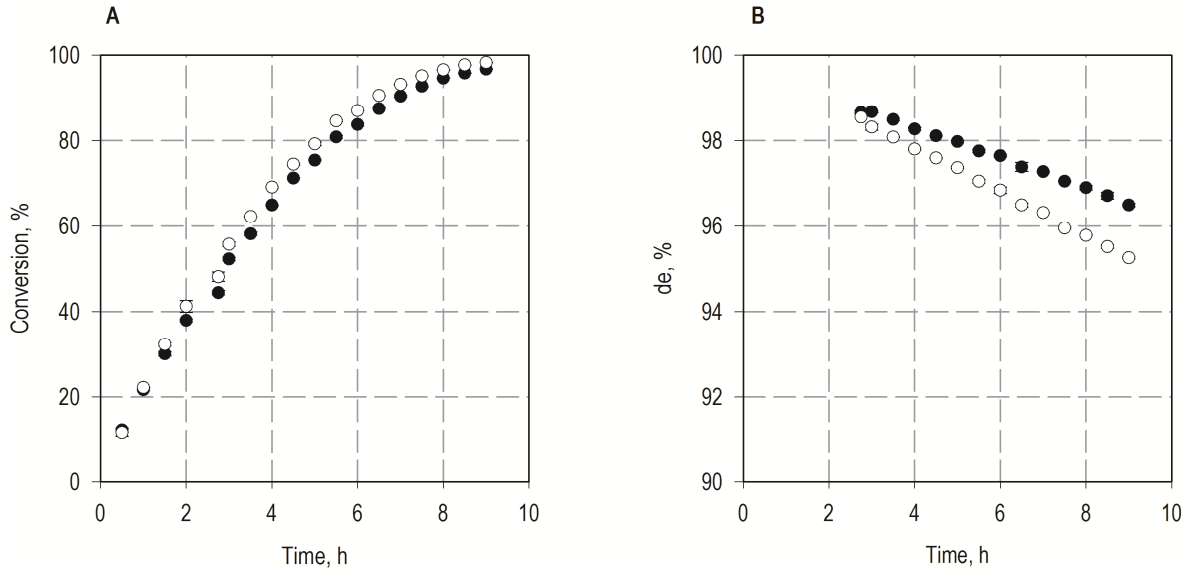

Figure 7.34 Resin-based whole-cell batch biotransformation at the 200 mL scale (white dots) and the 1 L scale (black dots) . Bioreductions of (R)-carvone were performed with 300 mM (R)-carvone, 400 mM formate and 36 g_{CDW} L^{-1} *E. coli* NosT7FDH$_{3M}$ in sodium phosphate buffer (300 mM, pH 6.3) with a resin to substrate ratio of 5 at 25 °C. An impeller speed of 800 rpm was chosen for the 200 mL scale and 500 rpm for the 1 L scale to ensure similar energy input in both systems.

The evolution of the conversion was similar for the resin-based whole-cell biotransformation of (R)-carvone at both scales. Thereby, 98.3 % conversion was obtained after 9 h in case of the 200 mL scale and 96.8 % conversion at the 1 L scale. However, the diastereomeric excesses for (2R,5R)-dihydrocarvone determined after 9 h diverged slightly (95.3 % de for 200 mL scale and 96.5 % de for 1 L scale). Maximal volumetric productivities of 81.7 mmol L^{-1} h^{-1} and 81.1 mmol L^{-1} h^{-1} were calculated for the 200 mL scale and the 1 L scale, respectively.

The slight difference between the 200 mL and 1 L scale might be explained by the diverging strategy for temperature control. The temperature was controlled at 25 °C in the 1 L scale reaction, in contrast to ~25 °C (ambient temperature) in the 200 mL scale process. Thus, whereas the measured temperature was constant at 25 °C for the 1 L process, the temperature in the 200 mL process was raised to 27 °C at the end of the reaction. As the temperature strongly affected the stereoselectivity of the (R)-carvone reduction in IL-based biotransformations (Section 7.4), this might also explain the lower stereoselectivity obtained in the 200 mL scale biotransformation. Moreover, the maximal local energy dissipation might not be the optimal scaling parameter for solid-liquid reaction systems. An impeller speed of 500 rpm in the liter scale corresponded to a volumetric power consumption of ~0.2 W L^{-1}, whereas the 200 mL scale exhibited ~0.6 W L^{-1} (Weuster-Botz et al. 2002). Though the reaction was not impaired when conducted at ~0.4 W L^{-1} (600 rpm in 200 mL scale), a volumetric power consumption of ~0.2 W L^{-1} could influence the mass transfers. In addition, the higher viscosity of the reaction system was not considered for estimation of the required stirrer speed.

Nevertheless, 96.8 % of an initial substrate concentration of 300 mM (R)-carvone was converted on a liter scale furnishing 290.4 mM (2R,5R)-dihydrocarvone after 9 h with a diastereomeric excess of 96.5 % de. Thus, a liter-scale process with adsorbent resins for *in situ* substrate supply and product removal was successfully established achieving high product concentrations within a defined process time.

Subsequent to the liter scale biotransformation, adsorbent resins were separated by filtration and extracted repeatedly with ethyl acetate. The solvent was further removed by distillation and the obtained product was analyzed using GC-MS and NMR (Appendix, A.5.5). The process yield after product isolation was 73.3 %, which might derive from loss of adsorbents during product separation (removal from the bioreactor and filtration). Beside of

(R)-carvone and (2S,5R)-dihydrocarvone, no other substance was detected in GC-MS and NMR.

7.5.4 Discussion

A resin-based *in situ* substrate feeding and product removal strategy was evaluated as an alternative method for the whole-cell biotransformation of (R)-carvone. Thereby, the same optimized biocatalyst *E. coli* pET28NosT7FDH$_{3M}$ was used.

In solid-liquid reaction systems with adsorbent resins, the substrate and product concentration in the aqueous phase can be adjusted by the adsorbent quantity. With higher **resin to substrate mass ratio**, the apparent quantity of sites available for absorption of solutes is increased and the residual concentration in the aqueous phase is reduced. Hereby, the adsorbent capacity of the resin is of importance as it defines the required amount of resin for the desired residual concentration in the aqueous phase.

Higher resin to substrate mass ratio leads to lower substrate concentration present in the aqueous phase. The extracellular substrate concentration can influence the mass transfer into the cell and the reaction rate of the enzymatic conversion. It was observed that a resin to substrate ratio of 3.5 to 5 had no impact on the time course of the conversion. Thus, the mass transfer from the adsorbent resin into the aqueous phase did not seem to be rate-limiting. Accordingly, the residual product concentration in the aqueous phase formed by the biotransformation can be decreased by applying a higher resin to substrate mass ratio in the reaction system. The aqueous product concentration can affect the rate of side reactions, e.g. isomerization reaction. In fact, whole-cell biotransformation with 50 mM (R)-carvone and 8 $g_{CDW}\,L^{-1}$ biocatalysts demonstrated that the stereoselectivity of the process was increased with higher mass ratio of resin to (R)-carvone. The time-dependent decrease of the diastereomeric excess was slowed down from -1.06 % de h^{-1} to -0.50 % de h^{-1} by increasing the resin to substrate mass ratio from 3.5 to 5. Consequently, side reactions responsible for decreasing stereoselectivity were probably reduced with lower residual product concentration in the aqueous phase.

An appropriate resin to substrate mass ratio did not only improve the stereoselectivity of the process by minimizing side activities. When the mass ratio of resin to substrate is kept constant, an equal residual concentration remains in the aqueous phase. Thus, higher initial

substrate loadings are facilitated without changing the residual concentrations in the aqueous phase and subsequently affect the reaction rate. The initial substrate concentration and the biocatalyst concentration were increased to 300 mM (R)-carvone and 36 g_{CDW} L^{-1} to allow complete conversion within a short reaction time. At the 200 mL scale, 96.6 % conversion was reached after 8 h furnishing an overall amount of ~290 mmol (2R,5R)-dihydrocarvone with a diastereomeric excess of 95.8 % de. The diastereomeric excess decreased with a similar rate of −0.53 % de h^{-1} compared to the biotransformation with lower substrate and biocatalyst concentration (50 mM (R)-carvone, 8 g_{CDW} L^{-1}, −0.50 % de h^{-1}), which was performed under comparable reaction conditions (200 mL scale, ambient temperature of 25 °C and a resin to substrate mass ratio of 5). This result confirmed that the stereoselectivity of the process can be kept constant for higher substrate loadings in resin-based biotransformations.

The stereoselectivity in the liter-scale biotransformation process with initial concentrations of 300 mM (R)-carvone and 36 g_{CDW} L^{-1} biocatalyst was even higher compared to the 200 mL-scale reactions. The diastereomeric excess decreased with a rate of −0.35 % de h^{-1} reaching 96.5 % de after 9 h process time at 96.8 % conversion. The superior stereoselectivity compared to the 200 mL-scale processes might be attributed to the applied temperature control at 25 °C in the liter-scale bioreactor. In comparison, 200 mL-scale biotransformations were performed at an ambient temperature of 25 °C without additional temperature control. The temperature was increased up to +2 °C during the biotransformation probably due to higher friction forces in solid-liquid reaction systems (data not shown).

The **agitation rate** applied during the resin-based biotransformation can influence the mass transfer from the adsorbent resin into the aqueous phase At higher stirrer speed, the thickness of the fluid film surrounding the adsorbent is reduced, resulting in an improved mass transfer from the adsorbent into the liquid phase (Paul et al. 2004). For resin-based biotransformations with low biocatalyst and substrate concentrations, agitation in a range of 600 – 800 rpm in the 200 mL-scale reaction neither influenced the rate nor the stereoselectivity of the reaction. As the overall reaction was not affected by the agitation and the substrate concentration in the aqueous phase, this supported the hypothesis that the rate-limiting step might be the substrate transport into the cell or the enzymatic biotransformation. However, as the viscosity of the reaction mixture increased with higher biocatalyst concentration and resin amount, the rate limiting step might shift to the mass

transfer from the adsorbent into the liquid phase. This was observed in the experiments with high biocatalyst, substrate and resin amount in the bioreactor unit. Consequently, an appropriate impeller speed has to be chosen for adequate mixing of the reactions at such operation conditions. However, cell damage can possibly occur at high stirrer speed by mechanical shear forces due to agitated adsorbent resin. This was reported in the literature for yeast-mediated biotransformations using adsorbent resin (Vicenzi et al. 1997). In case of the resin-based whole-cell biotransformation of (R)-carvone, inactivation of the biocatalyst induced by higher stirrer speed was not observed within the reaction time under studied conditions.

7.6 Comparison of IL- and resin-based whole-cell batch biotransformation of (R)-carvone

In this section, the characteristics of whole-cell batch biotransformation of (R)-carvone with ionic liquid and adsorbent resin as a second phase are summarized and compared. The results of selected batch biotransformation processes at the 200 mL and 1 L scale under different process conditions (biocatalyst and substrate concentrations, temperature) are shown in Table 7.9. Factors increasing the reaction rate and the stereoselectivity of IL- and resin-based whole-cell batch biotransformations are given in Table 7.10.

Table 7.9 Comparison of IL- and resin-based whole-cell batch biotransformation of (R)-carvone based on different reactions performed at the 200 mL and 1 L scale using *E. coli* pET28NosT7FDH$_{3M}$. The given substrate and product concentrations refer to the whole reaction system. The biocatalyst concentration refers to the aqueous buffer phase. Indicated conversions, diastereomeric excesses (de) and space-time yields refer to the reaction time, which is given in brackets.

	Variables			**Results**				
	Temp., °C	Bio-catalyst, $g_{CDW}\,L^{-1}$	Substrate, mM	Conversion, %	Product, mM	de, %	Space-time yield, mmol L^{-1} h^{-1}	de decrease, % de h^{-1}
IL[a,c]	25	8.0	50.0	99.4 (7.0 h)	49.7	98.7	7.1	−0.20
A[a,c]	25	8.0	50.0	99.5 (6.5 h)	49.8	96.2	7.6	−0.50
IL[a,d]	25	8.0	57.5	99.3 (8.0 h)	57.1	98.8	7.1	−0.16
IL[b,d]	20	8.0	57.5	99.8 (8.0 h)	57.4	99.4	7.2	−0.08
IL[b,d]	25	36	160	99.4 (6.5 h)	159.0	96.5	24.5	−0.55
A[a,d]	25	36	300	96.6 (8.0 h)	289.8	95.8	36.3	−0.53
A[b,d]	25	36	300	96.8 (9.0 h)	290.4	96.5	32.3	−0.35

[a] Biotransformation at the 200 mL scale at the given ambient temperature. An additional temperature control was not applied.

[b] Biotransformation at the 1 L scale with temperature control.

[c] Standard process conditions: Ionic liquid-based processes (IL): 100 mM sodium phosphate buffer, pH 7.0, 250 mM formate and 20 % (v/v) [HMPL][NTF]; Adsorbent resin-based processes (A): 100 mM sodium phosphate buffer, pH 7.0, 250 mM formate and XAD4 with a resin to substrate mass ratio of 5.

[d] Optimized process conditions: Ionic liquid-based processes (IL): 300 mM sodium phosphate buffer, pH 6.4, 508 mM formate (400 mM formate in case of 36 $g_{CDW}\,L^{-1}$ biocatalyst) and 20 % (v/v) [HMPL][NTF]; Adsorbent resin-based processes (A): 300 mM sodium phosphate buffer, pH 6.3, 400 mM formate, XAD4 with a resin to substrate ratio of 5.

Table 7.10 Summary of optimized process variables improving the space-time yield and stereoselectivity of whole-cell batch biotransformations of (R)-carvone for both ionic liquid-based and resin-based *in situ* substrate supply and product removal.

Space-time yield ↑	**Stereoselectivity ↑**
- high biocatalyst activity	- high distribution coefficient of the IL
- intact biocatalyst (high stability)	- low substrate concentration in the IL
- high biocatalyst concentration	- high resin to substrate ratio (≥ 5)
- pH 6.2 – 6.5	- low temperature (20 °C – 25 °C)
- ≥ 300 mM sodium phosphate	- short reaction time (≤ 10 h)
- 300 – 400 mM sodium formate	

The influence of pH, buffer molarity and the cosubstrate concentration was similar for both IL- and resin-based biotransformations (pH 6.2 – 6.5, ≥ 300 mM sodium phosphate, 300 – 400 mM sodium formate). This was expected, because these process variables are directly related to the biocatalyst independent from the *in situ* substrate supply or product extraction strategy. The reaction rate and the space-time yield increased proportionally with the biocatalyst concentration in both reaction systems. Solely high substrate concentrations in the IL phase (800 mM (R)-carvone in the IL and 160 mM in the entire reaction) resulted in a comparably decreased space-time yield, probably due to biocatalyst instability.

In general, the objectives of biotransformation processes are complete conversions and high stereoselectivities. At low initial substrate concentration of 57.7 mM, excellent results were achieved using 20 % (v/v) [HMPL][NTF], resulting in 99.8 % conversion after 8 h obtaining (2R,5R)-dihydrocarvone with 99.4 % de. However, a full conversion of a high initial substrate loading is preferable for biotransformations. This can be enabled by extending the reaction time when applying low biocatalyst concentrations, or by using higher biocatalyst amount for a limited reaction time. Applying low biocatalyst concentrations was not an option, as 8 $g_{CDW}\,L^{-1}$ biocatalyst was deactivated by high substrate concentrations in the IL and resin phase after ~10 h in both IL- and resin-based biotransformations, resulting in incomplete conversions. Higher biocatalyst and substrate concentration in IL-based reaction systems resulted in an increased residual product concentration in the aqueous phase, which led to an accelerated decrease of the diastereomeric excesses (−0.55 % de h^{-1} at 36 g L^{-1} biocatalyst and 160 mM (R)-carvone compared to −0.20 % de h^{-1} at 8 g L^{-1} biocatalyst and 57.7 mM (R)-carvone). The decrease of the diastereomeric excess was comparable to those obtained in the resin-based biotransformation with a resin to substrate mass ratio of 5 (−0.53 % de h^{-1}). As the resin to

substrate mass ratio was kept constant, the stereoselectivity was not affected by the substrate and biocatalyst concentrations.

This effect might be derived from differences in the *in situ* substrate supply and product removal strategy and the resulting concentrations in the aqueous phase. In case of reaction systems with IL as a second phase, the product concentration in the aqueous phase depends on the distribution coefficient between the IL and the aqueous phase. As the volume fraction of the IL was kept constant, the rising product formation by applying higher substrate and biocatalyst concentration resulted in higher product concentrations in the aqueous phase. This might have led to increased side reactions and lower diastereomeric excesses. In case of resin-based biotransformations, the residual product concentration in the aqueous phase depends on the resin to substrate mass ratio. If this mass ratio was kept constant, comparable stereoselectivities can be achieved at high substrate and biocatalyst concentrations.

To enable higher substrate loadings in IL-based biphasic reaction systems without a decrease in the stereoselectivity, either the volume fraction of the IL has to be increased or another IL with improved distribution coefficients for substrate and product has to be found. However, distribution coefficients between the IL and the aqueous phase were in many cases relatively similar for a given compound (Bräutigam et al. 2009) and the volume fraction of IL should be limited to ≤ 40 % (v/v) to avoid cell damage (Dennewald et al. 2011). In this thesis, the IL volume fraction was kept constant at 20 % to allow direct comparisons to other studies of IL-based whole-cell biotransformation (Bräutigam et al. 2009; Dennewald 2011) and assure the biocatalyst stability. An IL volume fraction of 40 % (v/v) would indeed double the overall substrate quantity in the reaction system while preserving the same product concentration in the aqueous phase. Thereby, process variables as temperature and stirrer speed and especially the biocatalyst stability during the (R)-carvone reduction have to be evaluated. In addition, a higher biocatalyst concentration could also influence the mass transfers in the reaction system depending on the applied stirrer speed.

For resin-based biotransformations, the stereoselectivity can be raised by applying a higher resin to substrate mass ratio. Thus, high substrate loadings require a respective high quantity of adsorbent resins to ensure high stereoselectivity. In combination with high biocatalyst concentrations the viscosity of the suspension increases, which could lead to mass transfer limitations. The adsorption capacity of the adsorbent resin defines the overall amount of

resin for a given concentration in the aqueous phase. As the resin XAD4 displays a density of 1.02 g mL^{-1}, a volume fraction of 22.5 % (v/v) resin is required in a liter-scale reaction system with an overall concentration of 300 mM (R)-carvone and a resin to substrate mass ratio of 5. The calculated (R)-carvone concentration in the aqueous phase would be 0.7 mM. Comparably, 1500 mM (R)-carvone in 20 % (v/v) [HMPL][NTF] representing 300 mM (R)-carvone in the overall reaction system, resulted in a calculated concentration of 3.4 mM (R)-carvone in the aqueous phase, which could lead to biocatalyst inactivation. If a volume fraction of 40 % (v/v) is applied, the (R)-carvone concentration in the IL and the aqueous phase are reduced to 750 mM and 1.7 mM, respectively. Whereas further increase of overall substrate concentration is limited to the biocatalyst stability at the given volume fraction of the IL in liquid-liquid phase reaction systems, the mass transfer can be a problem for resin-based reaction systems with high substrate loadings.

It should be noted that a low temperature (20 °C) and controlled temperature over the reaction time significantly increased the diastereomeric excess. Especially in case of resin-based reactions, sufficiently controlled temperature during the biotransformation could indeed enhance the stereoselectivity, as the reaction temperature was notably increased within 9 h process time.

The differences between the IL- and resin-based reaction systems regarding the reaction engineering, economical and ecological aspects are summarized in Table 7.11. In general, the phase toxicity can be avoided using hydrophobic resins contrary to IL-buffer reaction systems (Vicenzi et al. 1997). The separation of the IL and aqueous phase by centrifugation is replaced by a filtration step in resin-based reaction systems. However, high biomass concentration can complicate the downstream process. Though, adsorbent resins are usually considered as more cost-efficient compared to ILs, the cost for ILs strongly depends on the property and the production amount (Abdul Kholiq and Heinzle 2006). In addition, the recyclability for both resins and ILs were demonstrated reducing the overall cost of the process (Dennewald et al. 2011; Vicenzi et al. 1997).

Table 7.11 Characteristics of ionic liquids and adsorbent resins in batch biotransformations regarding process engineering, economical and ecological aspects.

	Ionic liquids	**Adsorbent resins**
Biocatalyst toxicity	Toxicity depends on the IL property. Whole-cell reaction systems are limited to ≤ 40 % (v/v) IL. Phase toxicity can be a problem.[a]	Phase toxicity is avoided. Cell damages by mechanical stress have been reported.[b]
Downstream processing	Phase separation by centrifugation, and further distillation or extraction of the product.	Phase separation by filtration and extraction of the product.
Recycling/ reuse	Demonstrated during 25 cycles of whole-cell biotransformation.[a]	Number of regeneration cycles varies between 5 – 1300 depending on application.[c]
Cost	High cost (~\$1000 kg^{-1}), depending on the produced quantity and IL property.[d]	Low cost (~\$15 L^{-1}).[b]
Environmental aspects	ILs are considered as "green" solvents due to the low volatility compared to organic solvents. However, there is a conflict between toxicity and biodegradability.[e]	As adsorbent resins are solid beads, volatility or toxicity are avoided. Biodegradability depends on the polymer structure.[b]

[a] Dennewald et al. (2011).
[b] Vicenzi et al. (1997).
[c] Daignault et al. (1988).
[d] Golding et al. (2002); Abdul Kholiq and Heinzle (2006).
[e] Pham et al. (2010).

The literature reveals several examples of (R)-carvone reduction using bacteria and yeast cells (Cramarossa et al. 2005; Goretti et al. 2013; Shimoda et al. 2004; Silva et al. 2012; van Dyk et al. 1998). Mostly, dihydrocarveol was detected as a side product (Cramarossa et al. 2005; Goretti et al. 2013; van Dyk et al. 1998). Low space-time yields (≤ 0.05 mmol L^{-1} h^{-1}) and moderate to high stereoselectivities (80 – 95 % de) were obtained using wild-type strains (Goretti et al. 2013; Shimoda et al. 2004). The baker´s yeast mediated biotransformation was optimized by addition of supplements or applying biphasic reaction systems with ionic liquids (Silva et al. 2012). Though high stereoselectivities (99 % de) were achieved, the conversions and space-time yields were moderate (≤ 70 %, ≤ 2.9 mmol L^{-1} h^{-1}) despite of a high biocatalyst concentration of 100 g_{CDW} L^{-1}. In addition, up to 6 % dihydrocarveol was detected. Using [BMIM][PF_6] as a second ionic liquid phase, 56 % conversion was obtained with a space-time yield of 2.3 mmol L^{-1} h^{-1}. The substrate loading was limited to a concentration of 16.6 mM (R)-carvone due to biocatalyst inhibition (Silva et al. 2012). In this thesis, an 11-fold higher space-time yield of 32.3 mmol L^{-1} h^{-1} and a diastereomeric excess of 96.5 % de was obtained using recombinant *E. coli* in a resin-

based reaction system. Higher stereoselectivity of 99.4 % de was achieved using 20 % (v/v) [HMPL][NTF] with a overall space-time yield of 7.2 mmol L^{-1} h^{-1}, which is 2.5-fold higher compared to the literature data. In contrast to the wild-type mediated biotransformation of (R)-carvone described in the literature (Goretti et al. 2013; Silva et al. 2012), up to 18-fold higher initial substrate concentrations (≤ 300 mM (R)-carvone) were applied in this study and alcohols as side products were not detected.

Preparative-scale biotransformation of alkenes described in the literature mostly involved isolated ERs in enzymatic reactions. An example represents the reduction of 150 mM citral by crude extract of *Pichia stipitis* OYE 2.6 and GDH for cofactor regeneration, obtaining a space-time yield of 24 mmol L^{-1} h^{-1} and 95 % de. However, enzymes were inactivated after ~20 h under the applied conditions (Bougioukou et al. 2010). Another example is the gram-scale reduction of (S)-2-ethoxy-3-(*p*-methoxyphenyl)propanoate (EEHP) by OYE3 from *Saccharomyces cerevisiae*. Using purified OYE3 with GDH for cofactor regeneration and adsorbent resins for *in situ* substrate supply and product removal, 145.5 mM (30 g L^{-1}) EEHP was converted with a space-time yield of 11.2 mmol L^{-1} h^{-1} (2.3 g L^{-1} h^{-1}) (Bechtold et al. 2012). Compared to biocatalytic reactions involving ERs and other substrates, biotransformations in this study were performed with up to 2-fold higher substrate loadings achieving 1.3 – 2.9-fold higher space-time yields.

To summarize, the liter-scale reduction of (R)-carvone by recombinant *E. coli* cells overexpressing an ER and a FDH was demonstrated for the first time. Compared to (R)-carvone reductions described in the literature (Silva et al. 2012), the initial substrate concentration of the developed biphasic whole-cell processes was increased by 18-fold achieving up to 2.5- to 11-fold higher space-time yields and high stereoselectivities (96.5 – 99.4 % de). The obtained space-time yields were even up to 2.9-fold higher compared to other preparative-scale reductions using isolated ERs described in the literature (Bechtold et al. 2012; Bougioukou et al. 2010).

8 Conclusions

The high demand for enantiopure molecules in the pharmaceutical and fine-chemical industry requires efficient strategies for the production of chiral building blocks applied as precursors in the synthesis route of active pharmaceutical ingredients. Asymmetric reduction of C=C bonds represents one of the most widely employed strategies for the production of chiral molecules, because it leads to the creation of up to two stereogenic centers (Stuermer et al. 2007). In special, the *trans*-specific reduction of alkenes by ene-reductases (ERs) from the old yellow enzyme (OYE) family offers an attractive and green way for the chiral molecule production, complementing and substituting strategies of (organo)chemical synthesis (Toogood et al. 2010).

Though various ERs have been found in bacteria, fungi and plants in the last years (Toogood et al. 2010), there are several challenges impeding the large-scale application of ERs. In particular, the insufficient enzyme stability under operational conditions (Yanto et al. 2010), the strong preference for NADPH, the requirement of cofactor recycling (Durchschein et al. 2012a; Paul et al. 2012), as well as the lack of established robust whole-cell biotransformations were predominantly stated as major hindrances (Winkler et al. 2012).

To overcome the limitations of the ER properties, a **comparative characterization** of ten ERs from cyanobacterial strains of different taxonomic orders and habitats with regard to the substrate spectrum, cofactor specificity and stereoselectivity was performed. Based on sequence motifs, two enzymes were assigned to the “thermophilic-like” group comprising multimeric ERs, whereas the others belong to the “classical” group of momomeric ERs (Toogood et al. 2010; Oberdorfer et al 2011).

The investigation of the substrate spectrum using representatives from different substance groups (i.a. enones, maleimides, terpenoids, nitroalkenes) revealed a broad substrate acceptance for the ERs from cyanobacteria. Several ERs were identified exhibiting high

activities and outstanding properties regarding the NADH acceptance and stereoselectivity (Table 8.1). With NADPH as cofactor, enzyme activities of ERs from cyanobacteria were similar or higher compared to ERs described in the literature. AcaryoER3 from *Acaryochloris marina* MBIC11017 showed an excellent activity towards maleimides compared to other ERs under similar conditions (29.58 U mg^{-1} vs. 2.04 – 25.82 U mg^{-1} for XenA from *Pseudomonas putida* M10, KYE from *Kluyveromyces lactis* and YersER from *Lactobacillus casei,* Chaparro-Riggers et al. (2007)). In addition, the NADH acceptance of cyanobacterial ERs was considerably higher compared to other ERs in the literature. This was pointed out by a lower NADPH to NADH activity ratio of 1.5 – 4.2 compared to ratios in the range of 7 – 22 in case of XenA, KYE and YersER (Chaparro-Riggers et al. 2007). Moreover, the actual enzyme activity using NADH was at least 11-fold higher (16.7 U mg^{-1} for AcaryoER3 compared to 1.50 U mg^{-1} for XenA using 0.5 mM NADH).

As the stereoselectivity is one crucial factor in biocatalysis, this was also evaluated using selected substrates. (R)-Carvone was reduced to (2R,5R)-dihydrocarvone with 99 % conversion and 98 % de using LyngbyaER1 and NospuncER1 from *Lyngbya* sp. PCC 8106 and *Nostoc punctiforme* PCC 73102, respectively. (2R,5R)-Dihydrocarvone is a key intermediate in the production of natural products, antimalarial drugs and valuable chiral building blocks (Winkler et al. 2012).

Table 8.1 Summarized comparison of the cyanobacterial ERs (AcaryoER3, AnabaenaER3 and AcaryoER1) and the ERs described in the literature (KYE1, XenA, YersER). Conv. = conversion, de = diastereomeric excess, n.a. = not available, n.d. = not detectable.

ER	Maleimide		(R)-Carvone		NADPH:NADH activity ratio[e]	Half-life at 30 °C, h
	NADPH	NADH	Conv. %	de, %		
AcaryoER3[a]	29.58	16.7[b]	45	97	2.3 – 4.2	n.a.
AnabaenaER3[a]	1.95	1.45	99	97	1.5 – 1.6	144
AcaryoER1	14.80	6.59	99	97	2.3 – 3.5	44
KYE1[c]	2.04	n.d.	n.a.	n.a.	> 7	19
XenA[c]	25.82	1.50	n.a.	n.a.	18	10[c] /63[d]
YersER[c]	18.88	n.d.	n.a.	n.a.	> 22	> 36

[a] Assay conditions: 100 mM sodium phosphate, pH 7.0, 10 mM substrate, 500 µM cofactor, 25 °C.
[b] Assay conditions: 100 mM sodium phosphate, pH 7.0, 10 mM substrate, 500 µM cofactor, 30 °C.
[c] Chaparro-Riggers et al. (2007).
[d] Yanto et al. (2010).
[e] The NADPH to NADH activity ratio is shown as the ratio of activity using 200 µM to 500 µM cofactor and maleimide at 30 °C in this study. The values in the reference Chaparro-Riggers et al. (2007) were measured with 200 µM cofactor.

Though the taxonomic orders and habitats did not correlate with the enzyme activity, cofactor preference and stereoselectivity, the affiliation of the ER and its protein structure did influence the substrate preference and particularly the enzyme stability. AnabaenaER3 from *Anabaena variabilis* ATCC 29413, a presumably dimeric ER from the "thermophilic-like" group, showed higher activities towards carvones, whereas the ERs from the "classical" group preferred ketoisophorone over carvone. More importantly, AnabaenaER3 displayed > 3-fold higher temperature stability compared to the "classical" ERs, e.g. NostocER1 from *Nostoc* sp. PCC 7120, which was also superior compared to ERs from the literature (XenA, KYE, Yers-ER). This might be explained by the presumably dimeric structure and shorter surface loops of AnabaenaER3 as typical characteristics of "thermophilic-like" ERs (Reich et al. 2013).

The second part of this thesis aimed at the development of an efficient **biotransformation process** involving ERs from cyanobacteria. The traditional application of cost-efficient wild-type microorganisms such as baker´s yeast was accompanied by low volumetric productivity, toxic effects of the substrate and side reactions by endogenous enzymes, e.g. alcohol formation by alcohol dehydrogenases and carbonyl reductases (Goretti et al. 2009). Thus, purified ERs were preferably used for small and preparative scale biocatalysis (Bechtold et al. 2012; Brenna et al. 2012e), though enzymatic processes were limited by insufficient enzyme stability (Bougioukou et al. 2010; Yanto et al. 2010), high demand on the purity of the enzyme preparation to avoid side reactions (Hall et al. 2008a), the requirement of a cofactor regeneration system (Paul et al. 2012) and high costs for protein purification (Tufvesson et al. 2010).

To overcome these limitations, the whole-cell biotransformation with recombinant *Escherichia coli* was evaluated with regard to the preparative-scale reduction of alkenes. The reduction of (R)-carvone yielding (2R,5R)-dihydrocarvone was selected as model reaction. Though AnabaenaER3 showed the highest specific activity for (R)-carvone (1.09 U mg^{-1}), NostocER1 (0.69 U mg^{-1}) was chosen due to the lower K_M for NADPH and higher protein expression resulting in a superior volumetric activity. Recombinant *E. coli* overexpressing NostocER1 and the formate dehydrogenase (FDH) D221G mutant from *Mycobacterium vaccae* N 10 was first chosen for the biotransformation.

Whereas alcohols as side products could not be detected during whole-cell batch biotransformations, the diastereomeric excess of the formed (2R,5R)-dihydrocarvone decreased to 61 % de after 24 h reaction time in the monophasic aqueous system. As

purified NostocER1 showed high stereoselectivity in the reduction of (R)-carvone forming the (2R,5R)-diastereomer with 97 % de, the lower stereoselectivity in whole-cell processes might be caused by endogenous enzymes from the *E. coli* host cell, e.g. catalyzing isomerization reactions. These side reactions were successfully minimized by applying the *in situ* substrate feeding and product removal strategy in a batch process either using ionic liquid (IL) as a second water-immiscible liquid phase or hydrophobic adsorbent resins. Though, a time-dependent linear decrease of the diastereomeric excess was observed, the stereoselectivity of whole-cell reduction of (R)-carvone in biphasic reaction systems was increased up to 99.4 % de. A typical time-course of the whole-cell biotransformation is given in Figure 8.1.

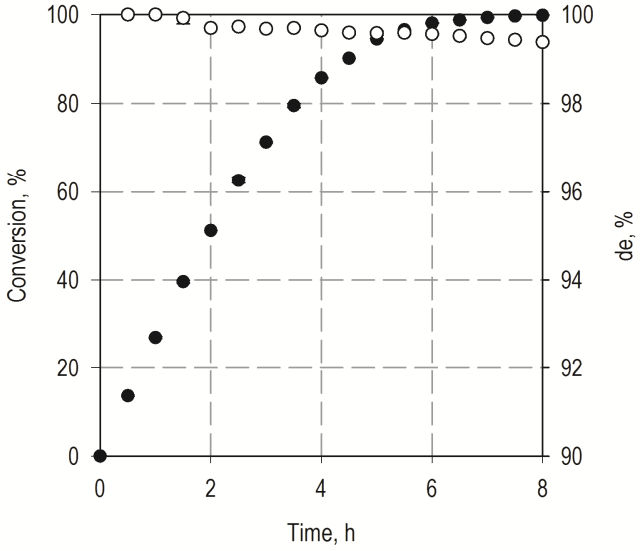

Figure 8.1 Whole-cell batch biotransformation at a liter scale using 8 g_{CDW} L^{-1} *E. coli* pET28NosT7FDH$_{3M}$ in a biphasic reaction system with 20 % (v/v) [HMPL][NTF] containing 287.5 mM (R)-carvone and 508.3 mM formate in sodium phosphate buffer (300 mM, pH 6.4). The reaction was performed at 20 °C and 600 rpm. Conversion and diastereomeric excess are presented.

Next, the focus was on the characterization and optimization of the whole-cell biocatalyst and the biotransformation process. The objective was to develop a biphasic whole-cell batch biotransformation process at a liter scale, exhibiting high volumetric productivity, complete conversion and high stereoselectivity at high substrate loadings within < 10 h process time.

The development of the whole-cell biocatalyst focused on the gene arrangement of the expression cassette of the vector and the selection of beneficial FDH mutants for improved cofactor regeneration. The resulting recombinant whole-cell biocatalyst displayed improved cofactor regeneration by introducing a second T7 promoter into the applied vector and the substitution of FDH D221G by the FDH C145S/D221Q/C225V triple mutant (FDH$_{3M}$) from *Mycobacterium vaccae* N 10, which displayed a higher activity for $NADP^+$ (Hoelsch et al.

2012). Using this optimized biocatalyst *E. coli* pET28NosT7FDH$_{3M}$, the volumetric productivity was increased by 36 % achieving > 99.7 % conversion and 98.3 % de after 8 h (250 mM (R)-carvone in 20 % (v/v) [HMPL][NTF], 8 g_{CDW} L^{-1} biocatalyst, 250 mM formate in 100 mM phosphate buffer, pH 7.0).

Batch process development was performed for both IL- and resin-based biphasic whole-cell biotransformation of (R)-carvone. In general, a slightly acidic initial pH (pH 6.2 – 6.5) in sodium phosphate buffer with a molarity of ≥ 300 mM was favorable for achieving higher space-time yields. In case of biphasic reaction systems using a second IL phase, the substrate/product concentration in the aqueous phase is defined by the distribution coefficients of the substrate/product between the IL and aqueous phase. [HMPL][NTF][3] was chosen with distribution coefficients of log*D* 2.64 for (R)-carvone and log*D* 2.97 for dihydrocarvone. At low biocatalyst and substrate concentrations (Table 8.2, A), high conversions (99.3 %) and stereoselectivities (98.8 % de at 25 °C) were achieved after 8 h with 20 % (v/v) IL. However, high biocatalyst and substrate concentrations (Table 8.2, C) resulted in a moderate stereoselectivity (96.5 % de, 25 °C) with 20 % (v/v) IL, though a complete conversion (99.4 %) was reached after 6.5 h. The lower stereoselectivity can be explained by the higher product concentration in the aqueous phase resulting in increased side reactions. Higher substrate loadings without changing the stereoselectivity might be enabled by increasing the volume fraction of the IL. However, the biocatalyst stability can be impaired in reaction systems with > 40 % (v/v) [HMPL][NTF] (Dennewald et al. 2011).

The hydrophobic adsorbent resin XAD4 was chosen for the resin-based whole-cell reduction of (R)-carvone. Provided that the resin to substrate mass ratio was kept constant, the stereoselectivity of the reaction was not decreased at higher substrate and biocatalyst concentrations. Furthermore, the stereoselectivity of the whole-cell biotransformation increased from 92 % de to 96 % de by raising the resin to substrate mass ratio from 3.5 to 5 without influencing the volumetric productivity of the reaction. At the liter scale, 96.8 % conversion of an initial substrate concentration of 300 mM (R)-carvone after 9 h yielded (2R,5R)-dihydrocarvone with a diastereomeric excess of 96.5 % de (25 °C, Table 8.2, D).

The stereoselectivity of the process can be improved by decreasing the temperature. In IL-based biphasic whole-cell biotransformation, the diastereomeric excess was enhanced from

[3] 1-Hexyl-1-methylpyrrolidinium bis(trifluoromethylsulfonyl)imide.

98.8 % de to 99.4 % de by lowering the temperature from 25 °C to 20 °C (Table 8.2, B; Figure 8.1).

Table 8.2 Comparison of IL- and resin-based whole-cell batch biotransformation of (R)-carvone based on different reactions performed at the 200 mL and 1 L scale using *E. coli* pET28NosT7FDH$_{3M}$. The given substrate and product concentrations refer to the whole reaction system. The biocatalyst concentrations refer to the aqueous phase. Indicated conversions, diastereomeric excesses (de) and space-time yields refer to the reaction time, given in brackets.

No.[a]	Variables			Results				
	Temp., °C	Bio-catalyst, g_{CDW} L^{-1}	Substrate, mM	Conversion, %	Product, mM	de, %	Space-time yield, mmol L^{-1} h^{-1}	de decrease, % de h^{-1}
A	25	8	57.5	99.3 (8.0 h)	57.1	98.8	7.1	−0.16
B	20	8	57.5	99.8 (8.0 h)	57.4	99.4	7.2	−0.08
C	25	36	160.0	99.4 (6.5 h)	159.0	96.5	24.5	−0.55
D	25	36	300.0	96.8 (9.0 h)	290.4	96.5	32.3	−0.35

[a] (A) IL-based biotransformation at 200 mL scale using 287.5 mM (R)-carvone in 20 % (v/v) [HMPL][NTF], 508 mM sodium formate, sodium phosphate buffer (300 mM, pH 6.4)
(B) IL-based biotransformation at 1 L scale using 287.5 mM (R)-carvone in 20 % (v/v) [HMPL][NTF], 508 mM sodium formate, sodium phosphate buffer (300 mM, pH 6.4)
(C) IL-based biotransformation at 1 L scale using 800 mM (R)-carvone in 20 % (v/v) [HMPL][NTF], 400 mM sodium formate, sodium phosphate buffer (300 mM, pH 6.4)
(D) Resin-based biotransformation at 1 L scale using 300 mM (R)-carvone, 400 mM sodium formate, XAD4 with a resin to substrate ratio of 5, sodium phosphate buffer (300 mM, pH 6.3)

To summarize, ten novel ERs from cyanobacteria were characterized for the asymmetric reduction of alkenes. Among these, several ERs displayed a superior NADH acceptance and higher operational stabilities, which are favorable properties for industrial applications. In addition, an efficient whole-cell batch biotransformation process involving ERs was demonstrated at a liter scale. Using recombinant *E. coli* overexpressing NostocER1 and a FDH mutant in reaction systems with ionic liquids or adsorbent resins for *in situ* substrate supply and product removal, up to 300 mM (R)-carvone were converted with high volumetric productivities (up to 32.3 mmol L^{-1} h^{-1}) within 9 h achieving high conversions (up to 99.8 %). Compared to the (R)-carvone reductions in the literature (Silva et al. 2012), the initial substrate loading was increased by 18-fold and the space-time yield was improved by 11-fold. The desired product (2R,5R)-dihydrocarvone was obtained with high stereoselectivity of up to 99.4 % de without other side products.

9 Outlook

The comparative characterization of ten ene-reductases from cyanobacterial revealed efficient biocatalysts with outstanding catalytic properties, cofactor specificities and stabilities. Based on these results, a combination of the beneficial characteristics of the ERs, e.g. the surface loops of AnabaenaER3 for better stability and the catalytic center of AcaryoER3 for higher activity using protein engineering could further improve enzyme properties. In addition, structural elements responsible for the better NADH acceptance of AnabaenaER3 might be identified by the analysis of the protein structure and improved by protein engineering. By combining the high stability, activity and enhanced cofactor specificity, biocatalysts can be created with improved properties for industrial applications.

With regard to the application of recombinant *E. coli* overexpressing an ER and a FDH for the alkene reduction, further work can focus on the optimization of the downstream process and the recycling of ionic liquids, adsorbent resins and biocatalysts. Other host strains instead of *E. coli* can be investigated for better productivity and stereoselectivity of the reaction. Furthermore, multistep reactions based on the reduction of (R)-carvone to obtain other valuable chiral compounds can be enabled by further overexpression of desired enzymes. For example, the industrial valuable compound (1S,2R,5R)-dihydrocarveol can be synthesized by further reduction of (2R,5R)-dihydrocarvone (Chen et al. 2012). At last, other challenging alkene reductions, e.g. involving the formation of side products or product racemization, can be studied using the developed reaction system.

References

Abdul Kholiq M, Heinzle E. 2006. Prozessmodellierung und Nachhaltigkeitsbewertung einer Ganzzellbiotransformation im zweiphasigen System ionische Flüssigkeit/Wasser. Chemie Ingenieur Technik 78(3):307-316.

Adalbjornsson BV, Toogood HS, Fryszkowska A, Pudney CR, Jowitt TA, Leys D, Scrutton NS. 2010. Biocatalysis with thermostable enzymes: structure and properties of a thermophilic 'ene'-reductase related to old yellow enzyme. Chembiochem 11(2):197-207.

Adams JP, Collis AJ, Henderson RK, Sutton PW. 2009. Biotransformations in small-molecule pharmaceutical development. In: Whittall J, Sutton PW, editors. Practical methods for biocatalysis and biotransformations. Chichester: John Wiley & Sons. p 1-82.

Aehle W, Eck J. 2012. Discovery of enzymes. In: Drauz K, Gröger H, May O, editors. Enzyme catalysis in organic synthesis Weinheim Wiley-VCH.

Alberts B, Johnson A, Lewis J, Raff M, Roberts K, Walter P. 2002. Energy conversion: mitochondria and chloroplasts.

Altschul SF, Gish W, Miller W, Myers EW, Lipman DJ. 1990. Basic Local Alignment Search Tool. J Mol Biol 215(3):403-410.

Bar R. 1988. Effect of interphase mixing on a water ‐ organic solvent two ‐ liquid phase microbial system: ethanol fermentation. Journal of Chemical Technology and Biotechnology 43(1):49-62.

Barna T, Messiha HL, Petosa C, Bruce NC, Scrutton NS, Moody PCE. 2002. Crystal Structure of Bacterial Morphinone Reductase and Properties of the C191A Mutant Enzyme. Journal of Biological Chemistry 277(34):30976-30983.

Barna TM, Khan H, Bruce NC, Barsukov I, Scrutton NS, Moody PC. 2001. Crystal structure of pentaerythritol tetranitrate reductase: "flipped" binding geometries for steroid substrates in different redox states of the enzyme. J Mol Biol 310(2):433-47.

Bechtold M, Brenna E, Femmer C, Gatti FG, Panke S, Parmeggiani F, Sacchetti A. 2012. Biotechnological Development of a Practical Synthesis of Ethyl (S)-2-Ethoxy-3-(p-methoxyphenyl)propanoate (EEHP): Over 100-Fold Productivity Increase from Yeast Whole Cells to Recombinant Isolated Enzymes. Organic Process Research & Development 16(2):269-276.

Behrens GA, Hummel A, Padhi SK, Schätzle S, Bornscheuer UT. 2011. Discovery and Protein Engineering of Biocatalysts for Organic Synthesis. Advanced Synthesis & Catalysis 353(13):2191-2215.

Bennett BD, Kimball EH, Gao M, Osterhout R, Van Dien SJ, Rabinowitz JD. 2009. Absolute metabolite concentrations and implied enzyme active site occupancy in Escherichia coli. Nature chemical biology 5(8):593-599.

Bilgili MS. 2006. Adsorption of 4-chlorophenol from aqueous solutions by xad-4 resin: Isotherm, kinetic, and thermodynamic analysis. Journal of Hazardous Materials 137(1):157-164.

Bisswanger H. 2008. Enzyme Kinetics. Weinheim: Wiley-VCH.

Blanch HW, Clark DS. 1997. Biochemical engineering: CRC Press.

Blehert DS, Fox BG, Chambliss GH. 1999. Cloning and sequence analysis of two Pseudomonas flavoprotein xenobiotic reductases. J Bacteriol 181(20):6254-6263.

Bonrath W, Medlock J, Schütz J, Wüstenberg B, Netscher T. 2012. Hydrogenation in the Vitamins and Fine Chemicals Industry – An Overview. Hydrogenation.

Bornscheuer UT, Huisman GW, Kazlauskas RJ, Lutz S, Moore JC, Robins K. 2012. Engineering the third wave of biocatalysis. Nature 485(7397):185-94.

Bougioukou DJ, Walton AZ, Stewart JD. 2010. Towards preparative-scale, biocatalytic alkene reductions. Chem Commun (Camb) 46(45):8558-60.

Bräutigam S, Dennewald D, Schürmann M, Lutje-Spelberg J, Pitner W-R, Weuster-Botz D. 2009. Whole-cell biocatalysis: Evaluation of new hydrophobic ionic liquids for efficient asymmetric reduction of prochiral ketones. Enzyme and Microbial Technology 45(4):310-316.

Breithaupt C, Kurzbauer R, Schaller F, Stintzi A, Schaller A, Huber R, Macheroux P, Clausen T. 2009. Structural basis of substrate specificity of plant 12-oxophytodienoate reductases. J Mol Biol 392(5):1266-77.

Brenna E, Cosi SL, Ferrandi EE, Gatti FG, Monti D, Parmeggiani F, Sacchetti A. 2013a. Substrate scope and synthetic applications of the enantioselective reduction of α-alkyl-β-arylenones mediated by Old Yellow Enzymes. Org Biomol Chem 11(18):2988-2996.

Brenna E, Fronza G, Fuganti C, Gatti FG, Manfredi A, Parmeggiani F, Ronchi P. 2012a. On the stereochemistry of the Baker's Yeast-mediated reduction of regioisomeric unsaturated aldehydes: Examples of enantioselectivity switch promoted by substrate-engineering. Journal of Molecular Catalysis B-Enzymatic 84:94-101.

Brenna E, Fronza G, Fuganti C, Monti D, Parmeggiani F. 2011a. Enantioselective C=C bond reduction of unsaturated alpha-chloro esters by old yellow enzymes. Journal of Molecular Catalysis B-Enzymatic 73(1-4):17-21.

Brenna E, Fuganti C, Gatti FG, Parmeggiani F. 2009. New stereospecific synthesis of Tesaglitazar and Navaglitazar precursors. Tetrahedron: Asymmetry 20(23):2694-2698.

Brenna E, Gatti FG, Malpezzi L, Monti D, Parmeggiani F, Sacchetti A. 2013b. Synthesis of Robalzotan, Ebalzotan, and Rotigotine Precursors via the Stereoselective Multienzymatic Cascade Reduction of α,β-Unsaturated Aldehydes. The Journal of Organic Chemistry 78(10):4811-4822.

Brenna E, Gatti FG, Manfredi A, Monti D, Parmeggiani F. 2011b. Biocatalyzed Enantioselective Reduction of Activated C=C Bonds: Synthesis of Enantiomerically Enriched α-Halo-β-arylpropionic Acids. European Journal of Organic Chemistry 2011(20-21):4015-4022.

Brenna E, Gatti FG, Manfredi A, Monti D, Parmeggiani F. 2012b. Enoate reductase-mediated preparation of methyl (S)-2-bromobutanoate, a useful key intermediate for the synthesis of chiral active pharmaceutical ingredients. Org Process Res Dev 16(2):262-268.

Brenna E, Gatti FG, Manfredi A, Monti D, Parmeggiani F. 2012c. Steric Effects on the Stereochemistry of Old Yellow Enzyme-Mediated Reductions of Unsaturated Diesters: Flipping of the Substrate within the Enzyme Active Site Induced by Structural Modifications. Advanced Synthesis & Catalysis 354(14-15):2859-2864.

Brenna E, Gatti FG, Monti D, Parmeggiani F, Sacchetti A. 2012d. Cascade Coupling of Ene Reductases with Alcohol Dehydrogenases: Enantioselective Reduction of Prochiral Unsaturated Aldehydes. ChemCatChem 4(5):653-659.

Brenna E, Gatti FG, Monti D, Parmeggiani F, Sacchetti A. 2012e. Productivity enhancement of C=C bioreductions by coupling the in situ substrate feeding product removal technology with isolated enzymes. Chem Commun (Camb) 48(1):79-81.

Brige A, Van den Hemel D, Carpentier W, De Smet L, Van Beeumen JJ. 2006. Comparative characterization and expression analysis of the four Old Yellow Enzyme homologues from *Shewanella oneidensis* indicate differences in physiological function. Biochem J 394(Pt 1):335-44.

Chaparro-Riggers JF, Rogers TA, Vazquez-Figueroa E, Polizzi KM, Bommarius AS. 2007. Comparison of three enoate reductases and their potential use for biotransformations. Adv Synth Catal 349(8-9):1521-1531.

Chen RR. 2007. Permeability issues in whole-cell bioprocesses and cellular membrane engineering. Appl Microbiol Biotechnol 74(4):730-8.

Chen X, Gao X, Wu Q, Zhu D. 2012. Synthesis of optically active dihydrocarveol via a stepwise or one-pot enzymatic reduction of (R)- and (S)-carvone. Tetrahedron: Asymmetry 23(10):734-738.

Chenault HK, Whitesides GM. 1987. Regeneration of nicotinamide cofactors for use in organic synthesis. Applied Biochemistry and Biotechnology 14(2):147-197.

Choi D-S, Huang S, Huang M, Barnard TS, Adams RD, Seminario JM, Tour JM. 1998. Revised Structures of N-Substituted Dibrominated Pyrrole Derivatives and Their Polymeric Products. Termaleimide Models with Low Optical Band Gaps. The Journal of Organic Chemistry 63(8):2646-2655.

Clish CB, Levy BD, Chiang N, Tai H-H, Serhan CN. 2000. Oxidoreductases in Lipoxin A4 Metabolic Inactivation: A Novel Role for 15-Oxoprostaglandin 13-

Reductase/Leukotriene B4 12-hydroxydehydrogenase in Inflammation. Journal of Biological Chemistry 275(33):25372-25380.

Corpet F. 1988. Multiple sequence alignment with hierarchical-clustering. Nucleic Acids Res 16(22):10881-10890.

Cramarossa MR, Nadini A, Bondi M, Messi P, Pagnoni UM, Forti L. 2005. Biocatalytic reduction of (+)- and (–)-carvone by bacteria. Comptes Rendus Chimie 8(5):849-852.

Daignault S, Noot D, Williams D, Huck P. 1988. A review of the use of XAD resins to concentrate organic compounds in water. Water Research 22(7):803-813.

de Carvalho C, da Fonseca M. 2006. Carvone: Why and how should one bother to produce this terpene. Food Chemistry 95(3):413-422.

de Rouville H-PJ, Vives G, Tur E, Crassous J, Rapenne G. 2009. Synthesis and analytical resolution of chiral pyrazoles derived from (5R)-dihydrocarvone. New Journal of Chemistry 33(2):293-299.

De Smet MJ, Kingma J, Witholt B. 1978. The effect of toluene on the structure and permeability of the outer and cytoplasmic membranes of *Escherichia coli*. Biochimica et Biophysica Acta (BBA)-Biomembranes 506(1):64-80.

Dennewald D. 2011. Biphasic Whole-cell Synthesis of R-2-octanol with Recycling of the Ionic Liquid.

Dennewald D, Hortsch R, Weuster-Botz D. 2012. Evaluation of parallel milliliter-scale stirred-tank bioreactors for the study of biphasic whole-cell biocatalysis with ionic liquids. J Biotechnol 157(1):253-257.

Dennewald D, Pitner W-R, Weuster-Botz D. 2011. Recycling of the ionic liquid phase in process integrated biphasic whole-cell biocatalysis. Process Biochemistry 46(5):1132-1137.

Dennewald D, Weuster-Botz D. 2012. Ionic Liquids and Whole-Cell–Catalyzed Processes. Ionic Liquids in Biotransformations and Organocatalysis: John Wiley & Sons, Inc. p 261-314.

Dobbs DA, Vanhessche KPM, Brazi E, Rautenstrauch V, Lenoir J-Y, Genêt J-P, Wiles J, Bergens SH. 2000. Industrial Synthesis of (+)-cis-Methyl Dihydrojasmonate by Enantioselective Catalytic Hydrogenation; Identification of the Precatalyst [Ru((−)-Me-DuPHOS)(H)(η6-1,3,5-cyclooctatriene)](BF4). Angewandte Chemie International Edition 39(11):1992-1995.

DOW. 2000. Amberlite^{TM} XAD^{TM} polymeric adsorbents. Rohm and Haas

Ducat DC, Way JC, Silver PA. 2011. Engineering cyanobacteria to generate high-value products. Trends Biotechnol 29(2):95-103.

Duetz WA, Van Beilen JB, Witholt B. 2001. Using proteins in their natural environment: potential and limitations of microbial whole-cell hydroxylations in applied biocatalysis. Curr Opin Biotechnol 12(4):419-425.

Durchschein K, Fabian WMF, Macheroux P, Zangger K, Trimmel G, Faber K. 2011. Reductive biotransformation of nitroalkenes via nitroso-intermediates to oxazetes catalyzed by xenobiotic reductase A (XenA). Org Biomol Chem 9(9):3364-3369.

Durchschein K, Ferreira-da Silva B, Wallner S, Macheroux P, Kroutil W, Glueck SM, Faber K. 2010. The flavoprotein-catalyzed reduction of aliphatic nitro-compounds represents a biocatalytic equivalent to the Nef-reaction. Green Chemistry 12(4):616-619.

Durchschein K, Wallner S, Macheroux P, Schwab W, Winkler T, Kreis W, Faber K. 2012a. Nicotinamide-Dependent Ene Reductases as Alternative Biocatalysts for the Reduction of Activated Alkenes. European Journal of Organic Chemistry 2012(26):4963-4968.

Durchschein K, Wallner S, Macheroux P, Zangger K, Fabian WM, Faber K. 2012b. Unusual C=C bond isomerization of an alpha,beta-unsaturated gamma-butyrolactone catalysed by flavoproteins from the old yellow enzyme family. Chembiochem 13(16):2346-51.

Ehira S, Teramoto H, Inui M, Yukawa H. 2010. A novel redox-sensing transcriptional regulator CyeR controls expression of an Old Yellow Enzyme family protein in *Corynebacterium glutamicum*. Microbiology 156(Pt 5):1335-41.

Ernst M, Kaup B, Müller M, Bringer-Meyer S, Sahm H. 2005. Enantioselective reduction of carbonyl compounds by whole-cell biotransformation, combining a formate dehydrogenase and a (R)-specific alcohol dehydrogenase. Appl Microbiol Biotechnol 66(6):629-634.

Evans KO. 2006. Room-temperature ionic liquid cations act as short-chain surfactants and disintegrate a phospholipid bilayer. Colloids and Surfaces A: Physicochemical and Engineering Aspects 274(1):11-17.

Evans KO. 2008. Supported phospholipid bilayer interaction with components found in typical room-temperature ionic liquids–a QCM-D and AFM study. International Journal of Molecular Sciences 9(4):498-511.

Faber K. 2011. Biotransformations in organic chemistry. Heidelberg: Springer.

Fairbanks G, Steck TL, Wallach DFH. 1971. Electrophoretic analysis of major polypeptides of the human erythrocyte membran. Biochemistry 10(13):2606-2617.

Fichan I, Larroche C, Gros JB. 1999. Water solubility, vapor pressure, and activity coefficients of terpenes and terpenoids. Journal of Chemical and Engineering Data 44(1):56-62.

Fitzpatrick TB, Amrhein N, Macheroux P. 2003. Characterization of YqjM, an Old Yellow Enzyme homolog from *Bacillus subtilis* involved in the oxidative stress response. J Biol Chem 278(22):19891-7.

Fitzpatrick TB, Auweter S, Kitzing K, Clausen T, Amrhein N, Macheroux P. 2004. Structural and functional impairment of an old yellow enzyme homologue upon affinity tag incorporation. Protein Expr Purif 36(2):280-91.

Fox KM, Karplus PA. 1994. Old yellow enzyme at 2 Å resolution: overall structure, ligand binding, and comparison with related flavoproteins. Structure 2(11):1089-1105.

French CE, Bruce NC. 1994. Purification and characterization of morphinone reductase from Pseudomonas putida M10. Biochem J 301:97-103.

Fryszkowska A, Fisher K, Gardiner JM, Stephens GM. 2008. Highly Enantioselective Reduction of β,β-Disubstituted Aromatic Nitroalkenes Catalyzed by *Clostridium sporogenes*. The Journal of Organic Chemistry 73(11):4295-4298.

Fryszkowska A, Toogood H, Sakuma M, Gardiner JM, Stephens GM, Scrutton NS. 2009. Asymmetric Reduction of Activated Alkenes by Pentaerythritol Tetranitrate Reductase: Specificity and Control of Stereochemical Outcome by Reaction Optimisation. Adv Synth Catal 351(17):2976-2990.

Fryszkowska A, Toogood HS, Mansell D, Stephens G, Gardiner JM, Scrutton NS. 2012. A surprising observation that oxygen can affect the product enantiopurity of an enzyme-catalysed reaction. FEBS J 279(22):4160-71.

Fu Y, Castiglione K, Weuster-Botz D. 2013. Comparative characterization of novel ene-reductases from cyanobacteria. Biotechnol Bioeng 110(5):1293-301.

Fu Y, Hoelsch K, Weuster-Botz D. 2012. A novel ene-reductase from *Synechococcus* sp. PCC 7942 for the asymmetric reduction of alkenes. Process Biochemistry 47(12):1988-1997.

Gamenara D, Méndez PS, Seoane G, Domínguez de María P. 2012. Ionic Liquids as (Co-)Solvents for Nonhydrolytic Enzymes. Ionic Liquids in Biotransformations and Organocatalysis: John Wiley & Sons, Inc. p 229-259.

Ganske F, Bornscheuer UT. 2006. Growth of *Escherichia coli*, *Pichia pastoris* and *Bacillus cereus* in the presence of the ionic liquids [BMIM][BF4] and [BMIM][PF6] and organic solvents. Biotechnol Lett 28(7):465-469.

Gao X, Ren J, Wu Q, Zhu D. 2012. Biochemical characterization and substrate profiling of a new NADH-dependent enoate reductase from *Lactobacillus casei*. Enzyme Microb Technol 51(1):26-34.

Gebhardt G. 2006. Charakterisierung und Optimierung der Formiat-Dehydrogenase aus *Mycobacterium vaccae* durch ein automatisiertes Screeningverfahren [Master´s Thesis]: Technische Universität München.

Ghadge RS, Sawant SB, Joshi JB. 2003. Enzyme deactivation in a bubble column, a stirred vessel and an inclined plane. Chemical Engineering Science 58(23–24):5125-5134.

Goldberg K, Edegger K, Kroutil W, Liese A. 2006. Overcoming the thermodynamic limitation in asymmetric hydrogen transfer reactions catalyzed by whole cells. Biotechnol Bioeng 95(1):192-198.

Goldberg K, Schroer K, Lutz S, Liese A. 2007. Biocatalytic ketone reduction--a powerful tool for the production of chiral alcohols-part II: whole-cell reductions. Appl Microbiol Biotechnol 76(2):249-55.

Golding J, Forsyth S, MacFarlane DR, Forsyth M, Deacon GB. 2002. Methanesulfonate and p-toluenesulfonate salts of the N-methyl-N-alkylpyrrolidinium and quaternary ammonium cations: novel low cost ionic liquids. Green Chemistry 4(3):223-229.

Goretti M, Ponzoni C, Caselli E, Marchegiani E, Cramarossa MR, Turchetti B, Forti L, Buzzini P. 2011. Bioreduction of alpha,beta-unsaturated ketones and aldehydes by non-conventional yeast (NCY) whole-cells. Bioresour Technol 102(5):3993-8.

Goretti M, Ponzoni C, Caselli E, Marchigiani E, Cramarossa MR, Turchetti B, Buzzini P, Forti L. 2009. Biotransformation of electron-poor alkenes by yeasts: Asymmetric reduction of (4S)-(+)-carvone by yeast enoate reductases. Enzyme and Microbial Technology 45(6-7):463-468.

Goretti M, Turchetti B, Cramarossa MR, Forti L, Buzzini P. 2013. Production of Flavours and Fragrances via Bioreduction of (4R)-(-)-Carvone and (1R)-(-)-Myrtenal by Non-Conventional Yeast Whole-Cells. Molecules 18(5):5736-5748.

Gröger H, Asano Y. 2012. Introduction - principles and historical landmarks of enzyme catalysis in organic synthesis. In: Drauz K, Gröger H, May O, editors. Enzyme Catalysis in Organic Synthesis. 3 ed: Wiley-VCH.

Hall M, Hauer B, Stuermer R, Kroutil W, Faber K. 2006. Asymmetric whole-cell bioreduction of an α,β-unsaturated aldehyde (citral): competing prim-alcohol dehydrogenase and C–C lyase activities. Tetrahedron: Asymmetry 17(21):3058-3062.

Hall M, Stueckler C, Ehammer H, Pointner E, Oberdorfer G, Gruber K, Hauer B, Stuermer R, Kroutil W, Macheroux P and others. 2008a. Asymmetric bioreduction of C=C bonds using enoate reductases OPR1, OPR3 and YqjM: Enzyme-based stereocontrol. Adv Synth Catal 350(3):411-418.

Hall M, Stueckler C, Hauer B, Stuermer R, Friedrich T, Breuer M, Kroutil W, Faber K. 2008b. Asymmetric bioreduction of activated C=C Bonds using *Zymomonas mobilis* NCR enoate reductase and old yellow enzymes OYE 1–3 from yeasts. European J Org Chem 2008(9):1511-1516.

Hall M, Stueckler C, Kroutil W, Macheroux P, Faber K. 2007. Asymmetric bioreduction of activated alkenes using cloned 12-oxophytodienoate reductase isoenzymes OPR-1 and OPR-3 from *Lycopersicon esculentum* (tomato): a striking change of stereoselectivity. Angew Chem Int Ed Engl 46(21):3934-7.

Hamada H, Yasumune H, Fuchikami Y, Hirata T, Sattler I, Williams HJ, Ian Scott A. 1997. Biotransformation of geraniol, nerol and (+)- and (−)-carvone by suspension cultured cells of *Catharanthus roseus*. Phytochemistry 44(4):615-621.

He YM, Fan QH. 2010. Phosphine-free chiral metal catalysts for highly effective asymmetric catalytic hydrogenation. Org Biomol Chem 8(11):2497-504.

Heipieper HJ, Weber FJ, Sikkema J, Keweloh H, de Bont JAM. 1994. Mechanisms of resistance of whole cells to toxic organic solvents. Trends Biotechnol 12(10):409-415.

Henzler H-J. 2000. Particle stress in bioreactors. Influence of Stress on Cell Growth and Product Formation: Springer. p 35-82.

Herz RS. 2009. Aromatherapy Facts and Fictions: A Scientific Analysis of Olfactory Effects on Mood, Physiology and Behavior. International Journal of Neuroscience 119(2):263-290.

Hildebrandt P, Musidlowska A, Bornscheuer UT, Altenbuchner J. 2002. Cloning, functional expression and biochemical characterization of a stereoselective alcohol dehydrogenase from *Pseudomonas fluorescens* DSM50106. Appl Microbiol Biotechnol 59(4-5):483-7.

Hilker I, Gutierrez MC, Furstoss R, Ward J, Wohlgemuth R, Alphand V. 2008. Preparative scale Baeyer-Villiger biooxidation at high concentration using recombinant *Escherichia coli* and *in situ* substrate feeding and product removal process. Nat. Protocols 3(3):546-554.

Hilker I, Wohlgemuth R, Alphand V, Furstoss R. 2005. Microbial transformations 59: First kilogram scale asymmetric microbial Baeyer-Villiger oxidation with optimized productivity using a resin-based *in situ* SFPR strategy. Biotechnol Bioeng 92(6):702-710.

Hilt W, Pfleiderer G, Fortnagel P. 1991. Glucose dehydrogenase from *Bacillus subtilis* expressed in *Escherichia coli I*: purification, characterization and comparison with glucose dehydrogenase from *Bacillus megaterium*. Biochimica et Biophysica Acta (BBA)-Protein Structure and Molecular Enzymology 1076(2):298-304.

Hirata T, Matsushima A, Sato Y, Iwasaki T, Nomura H, Watanabe T, Toyoda S, Izumi S. 2009. Stereospecific hydrogenation of the C=C double bond of enones by *Escherichia coli* overexpressing an enone reductase of *Nicotiana tabacum*. Journal of Molecular Catalysis B-Enzymatic 59(1-3):158-162.

Hirata T, Takarada A, Hegazy M-EF, Sato Y, Matsushima A, Kondo Y, Matsuki A, Hamada H. 2005. Hydrogenation of the C–C double bond of maleimides with cultured plant cells. J Mol Catal B Enzymatic 32(4):131-134.

Hoelsch K, Suhrer I, Heusel M, Weuster-Botz D. 2012. Engineering of formate dehydrogenase: synergistic effect of mutations affecting cofactor specificity and chemical stability. Appl Microbiol Biotechnol 97(6):2473-81.

Hollmann F, Arends IWCE, Holtmann D. 2011. Enzymatic reductions for the chemist. Green Chem 13(9):2285.

Hölsch K. 2009. Asymmetrische Synthesen mit neuen Oxidoreduktasen aus Cyanobakterien [PhD thesis]: Technische Universität München

Hölsch K, Havel J, Haslbeck M, Weuster-Botz D. 2008. Identification, cloning, and characterization of a novel ketoreductase from the cyanobacterium *Synechococcus* sp. strain PCC 7942. Appl Environ Microbiol 74(21):6697-702.

Hölsch K, Weuster-Botz D. 2010. New oxidoreductases from cyanobacteria: Exploring nature's diversity. Enzyme Microb Technol 47(5):228-235.

Hook IL, Ryan S, Sheridan H. 2003. Biotransformation of aliphatic and aromatic ketones, including several monoterpenoid ketones and their derivatives by five species of marine microalgae. Phytochemistry 63(1):31-36.

Hortsch R, Weuster-Botz D. 2010. Power consumption and maximum energy dissipation in a milliliter-scale bioreactor. Biotechnology progress 26(2):595-599.

Huisman GW, Liang J, Krebber A. 2010. Practical chiral alcohol manufacture using ketoreductases. Curr Opin Chem Biol 14(2):122-9.

Hulley ME, Toogood HS, Fryszkowska A, Mansell D, Stephens GM, Gardiner JM, Scrutton NS. 2010. Focused directed evolution of pentaerythritol tetranitrate reductase by using automated anaerobic kinetic screening of site-saturated libraries. Chembiochem 11(17):2433-47.

Hult K, Berglund P. 2007. Enzyme promiscuity: mechanism and applications. Trends Biotechnol 25(5):231-238.

International union of biochemistry and molecular biology. 1992. Enzyme nomenclature. San Diego: Academic press.

Iyer PV, Ananthanarayan L. 2008. Enzyme stability and stabilization—Aqueous and non-aqueous environment. Process Biochemistry 43(10):1019-1032.

Jenzsch M, Gnoth S, Beck M, Kleinschmidt M, Simutis R, Lübbert A. 2006. Open-loop control of the biomass concentration within the growth phase of recombinant protein production processes. J Biotechnol 127(1):84-94.

Julsing MK, Kuhn D, Schmid A, Bühler B. 2012. Resting cells of recombinant *E. coli* show high epoxidation yields on energy source and high sensitivity to product inhibition. Biotechnol Bioeng 109(5):1109-1119.

Kapust RB, Tözsér J, Fox JD, Anderson DE, Cherry S, Copeland TD, Waugh DS. 2001. Tobacco etch virus protease: mechanism of autolysis and rational design of stable mutants with wild-type catalytic proficiency. Protein Engineering 14(12):993-1000.

Katoh S, Yoshida F. 2011. Biochemical Engineering. Weinheim: Wiley-VCH.

Kaup B, Bringer-Meyer S, Sahm H. 2004. Metabolic engineering of *Escherichia coli*: construction of an efficient biocatalyst for D-mannitol formation in a whole-cell biotransformation. Appl Microbiol Biotechnol 64(3):333-339.

Kawai Y, Saitou K, Hida K, Dao DH, Ohno A. 1996. Stereochemical Control in Microbial Reduction. XXVIII. Asymmetric Reduction of α, β-Unsaturated Ketones with Bakers' Yeast. Bulletin of the Chemical Society of Japan 69(9):2633-2638.

Kergomard A, Renard MF, Veschambre H. 1982. Microbiological reduction of alpha,beta-unsaturated ketones by *Beauveria sulfurescens*. The Journal of Organic Chemistry 47(5):792-798.

Khan H, Harris RJ, Barna T, Craig DH, Bruce NC, Munro AW, Moody PCE, Scrutton NS. 2002. Kinetic and Structural Basis of Reactivity of Pentaerythritol Tetranitrate Reductase with NADPH, 2-Cyclohexenone, Nitroesters, and Nitroaromatic Explosives. Journal of Biological Chemistry 277(24):21906-21912.

Kitzing K, Fitzpatrick TB, Wilken C, Sawa J, Bourenkov GP, Macheroux P, Clausen T. 2005. The 1.3 A crystal structure of the flavoprotein YqjM reveals a novel class of old yellow enzymes. J Biol Chem 280(30):27904-13.

Knowles WS. 2002. Asymmetric hydrogenations (Nobel lecture). Angewandte Chemie-International Edition 41(12):1999-2007.

Kohli RM, Massey V. 1998. The oxidative half-reaction of old yellow enzyme - The role of tyrosine 196. J Biol Chem 273(49):32763-32770.

Kosmulski M, Gustafsson J, Rosenholm JB. 2004. Thermal stability of low temperature ionic liquids revisited. Thermochimica Acta 412(1):47-53.

Kratzer R, Pukl M, Egger S, Nidetzky B. 2008. Whole-cell bioreduction of aromatic alpha-keto esters using *Candida tenuis* xylose reductase and *Candida boidinii* formate dehydrogenase co-expressed in *Escherichia coli*. Microb Cell Fact 7:37.

Kratzer R, Pukl M, Egger S, Vogl M, Brecker L, Nidetzky B. 2011. Enzyme identification and development of a whole-cell biotransformation for asymmetric reduction of o-chloroacetophenone. Biotechnol Bioeng 108(4):797-803.

Kuhn D, Bühler B, Schmid A. 2012. Production host selection for asymmetric styrene epoxidation: *Escherichia coli* vs. solvent-tolerant *Pseudomonas*. Journal of Industrial Microbiology & Biotechnology 39(8):1125-1133.

Laane C, Boeren S, Vos K, Veeger C. 1987. Rules for optimization of biocatalysis in organic solvents. Biotechnol Bioeng 30(1):81-87.

Langemann T, Koller VJ, Muhammad A, Kudela P, Mayr UB, Lubitz W. 2010. The bacterial ghost platform system: production and applications. Bioengineered 1(5):326-336.

Lee WT, Levy HR. 1992. Lysine 21 of *Leuconostoc mesenteroides* glucose 6-phosphate dehydrogenase participates in substrate binding through charge–charge interaction. Protein Science 1(3):329-334.

Leng DE, Calabrese RV. 2004. Immiscible Liquid–Liquid Systems. Handbook of Industrial Mixing: John Wiley & Sons, Inc. p 639-753.

Leuenberger HGW, Boguth W, Widmer E, Zell R. 1976. Synthesis of optically-active natural carotenoids and structurally related compounds .1. synthesis of chiral key compound (4R,6R)-4-hydroxy-2,2,6-trimethylcyclohexanone. Helv Chim Acta 59(5):1832-1849.

Lewis J. 1954. The mechanism of mass transfer of solutes across liquid-liquid interfaces: Part I: the determination of individual transfer coefficients for binary systems. Chemical Engineering Science 3(6):248-259.

Lewis W, Whitman W. 1924. Principles of gas absorption. Industrial & Engineering Chemistry 16(12):1215-1220.

Lichty JJ, Malecki JL, Agnew HD, Michelson-Horowitz DJ, Tan S. 2005. Comparison of affinity tags for protein purification. Protein Expr Purif 41(1):98-105.

List B, Yang JW. 2006. The organic approach to asymmetric catalysis. Science 313(5793):1584-6.

Liu L, Braun M, Gebhardt G, Weuster-Botz D, Gross R, Schmid RD. 2013. One-step synthesis of 12-ketoursodeoxycholic acid from dehydrocholic acid using a multienzymatic system. Appl Microbiol Biotechnol 97(2):633-639.

Lopez-Gallego F, Schmidt-Dannert C. 2010. Multi-enzymatic synthesis. Curr Opin Chem Biol 14(2):174-83.

Lowe JR, Tolman WB, Hillmyer MA. 2009. Oxidized dihydrocarvone as a renewable multifunctional monomer for the synthesis of shape memory polyesters. Biomacromolecules 10(7):2003-2008.

Lü W, Du J, Wacker T, Gerbig-Smentek E, Andrade SLA, Einsle O. 2011. pH-Dependent Gating in a FocA Formate Channel. Science 332(6027):352-354.

Lye GJ, Woodley JM. 1999. Application of in situ product-removal techniques to biocatalytic processes. Trends Biotechnol 17(10):395-402.

Mansell DJ, Toogood HS, Waller J, Hughes JMX, Levy CW, Gardiner JM, Scrutton NS. 2013. Biocatalytic Asymmetric Alkene Reduction: Crystal Structure and Characterization of a Double Bond Reductase from *Nicotiana tabacum*. Acs Catalysis:370-379.

Matsuda T. 2013. Recent progress in biocatalysis using supercritical carbon dioxide. Journal of Bioscience and Bioengineering 115(3):233-241.

Matsumoto M, Mochiduki K, Kondo K. 2004. Toxicity of ionic liquids and organic solvents to lactic acid-producing bacteria. Journal of Bioscience and Bioengineering 98(5):344-347.

Mehta NB, Phillips AP, Lui FF, Brooks RE. 1960. Maleamic and Citraconamic Acids, Methyl Esters, and Imides. J Org Chem 25(6):1012-1015.

Messiha HL, Munro AW, Bruce NC, Barsukov I, Scrutton NS. 2005. Reaction of morphinone reductase with 2-cyclohexen-1-one and 1-nitrocyclohexene: proton donation, ligand binding, and the role of residues Histidine 186 and Asparagine 189. J Biol Chem 280(11):10695-709.

Meyer HP, Eichhorn E, Hanlon S, Lutz S, Schurmann M, Wohlgemuth R, Coppolecchia R. 2013. The use of enzymes in organic synthesis and the life sciences: perspectives from the Swiss Industrial Biocatalysis Consortium (SIBC). Catalysis Science & Technology 3(1):29-40.

Michaelis L, Menten ML. 1913. Die Kinetik der Invertinwirkung. Biochem. z 49(333-369):352.

Milner SE, Maguire AR. 2012. Recent trends in whole cell and isolated enzymes in enantioselective synthesis.

Monod J. 1942. Research on the Glowth of Bacterial Cultures. Research on the Glowth of Bacterial Cultures.

Montgomery DC. 2009. Design and analysis of experiments: Wiley New York.

Mueller NJ, Stueckler C, Hauer B, Baudendistel N, Housden H, Bruce NC, Faber K. 2010a. The Substrate Spectra of Pentaerythritol Tetranitrate Reductase, Morphinone

Reductase, N-Ethylmaleimide Reductase and Estrogen-Binding Protein in the Asymmetric Bioreduction of Activated Alkenes. Advanced Synthesis & Catalysis 352(2-3):387-394.

Mueller NJ, Stueckler C, Hauer B, Baudendistel N, Housden H, Bruce NC, Faber K. 2010b. The substrate spectra of pentaerythritol tetranitrate reductase, morphinone reductase, N-ethylmaleimide reductase and estrogen-binding protein in the asymmetric bioreduction of activated alkenes. Adv Synth Catal 352(2-3):387-394.

Muller A, Hauer B, Rosche B. 2007. Asymmetric alkene reduction by yeast old yellow enzymes and by a novel Zymomonas mobilis reductase. Biotechnol Bioeng 98(1):22-9.

Müller A, Hauer B, Rosche B. 2006. Enzymatic reduction of the α, β-unsaturated carbon bond in citral. Journal of Molecular Catalysis B: Enzymatic 38(3-6):126-130.

Müller A, Stürmer R, Hauer B, Rosche B. 2007. Stereospecific Alkyne Reduction: Novel Activity of Old Yellow Enzymes. Angewandte Chemie 119(18):3380-3382.

Noyori R. 2002. Asymmetric catalysis: Science and opportunities (Nobel lecture). Angewandte Chemie-International Edition 41(12):2008-2022.

O'Brien PJ, Herschlag D. 1999. Catalytic promiscuity and the evolution of new enzymatic activities. Chemistry & Biology 6(4):R91-R105.

Oberdorfer G, Steinkellner G, Stueckler C, Faber K, Gruber K. 2011. Stereopreferences of old yellow enzymes: structure correlations and sequence patterns in enoate reductases. ChemCatChem 3(10):1562-1566.

Ohta T, Miyake T, Seido N, Kumobayashi H, Takaya H. 1995. Asymmetric hydrogenation of olefins with aprotic oxygen functionalities catalyzed by BINAP-Ru (II) complexes. The Journal of Organic Chemistry 60(2):357-363.

Ouellet SG, Tuttle JB, MacMillan DWC. 2005. Enantioselective organocatalytic hydride reduction. Journal of the American Chemical Society 127(1):32-33.

Padhi SK, Bougioukou DJ, Stewart JD. 2009. Site-saturation mutagenesis of tryptophan 116 of *Saccharomyces pastorianus* old yellow enzyme uncovers stereocomplementary variants. J Am Chem Soc 131(9):3271-80.

Paul CE, Gargiulo S, Opperman DJ, Lavandera I, Gotor-Fernández V, Gotor V, Taglieber A, Arends IWCE, Hollmann F. 2012. Mimicking Nature: Synthetic Nicotinamide Cofactors for C═C Bioreduction Using Enoate Reductases. Organic Letters 15(1):180-183.

Paul EL, Atiemo-Obeng V, Kresta SM. 2004. Handbook of industrial mixing: science and practice: Wiley. com.

Pernak J, Sobaszkiewicz K, Mirska I. 2003. Anti-microbial activities of ionic liquids. Green Chemistry 5(1):52-56.

Perrin DD, Dempsey B. 1974. Buffers for pH and metal ion control: Chapman and Hall London.

Peters J. 1998. Dehydrogenases - characteristics, design of reaction conditions, and applications. In: Rehm HJ, Reed H, editors. Biotechnology. Weinheim: Wiley-VCH.

Pfruender H, Amidjojo M, Kragl U, Weuster-Botz D. 2004. Efficient Whole-Cell Biotransformation in a Biphasic Ionic Liquid/Water System. Angewandte Chemie International Edition 43(34):4529-4531.

Pfruender H, Jones R, Weuster-Botz D. 2006. Water immiscible ionic liquids as solvents for whole cell biocatalysis. J Biotechnol 124(1):182-190.

Pfründer H. 2005. Ganzzell-Biokatalyse in Gegenwart ionischer Flüssigkeiten: Dissertation.

Pham TPT, Cho C-W, Yun Y-S. 2010. Environmental fate and toxicity of ionic liquids: A review. Water Research 44(2):352-372.

Pollard DJ, Woodley JM. 2007. Biocatalysis for pharmaceutical intermediates: the future is now. Trends Biotechnol 25(2):66-73.

Puskeiler R, Kaufmann K, Weuster-Botz D. 2005. Development, parallelization, and automation of a gas-inducing milliliter-scale bioreactor for high-throughput bioprocess design (HTBD). Biotechnol Bioeng 89(5):512-523.

Reich S, Kress N, Nestl BM, Hauer B. 2013. Variations in the stability of NCR ene reductase by rational enzyme loop modulation. Journal of Structural Biology(0).

Richter N, Neumann M, Liese A, Wohlgemuth R, Weckbecker A, Eggert T, Hummel W. 2010. Characterization of a whole-cell catalyst co-expressing glycerol dehydrogenase and glucose dehydrogenase and its application in the synthesis of L-glyceraldehyde. Biotechnol Bioeng 106(4):541-52.

Ridings JE. 2013. The Thalidomide Disaster, Lessons from the Past. Teratogenicity Testing: Springer. p 575-586.

Riedlberger P. 2012. Miniaturisierte Rührreaktoren zur enzymatischen Hydrolyse von suspendierten Pflanzenmaterialien: München, Technische Universität München, Diss., 2012.

Riedlberger P, Brüning S, Weuster-Botz D. 2012. Characterization of stirrers for screening studies of enzymatic biomass hydrolyses on a milliliter scale. Bioprocess and Biosystems Engineering:1-9.

Riedlberger P, Weuster-Botz D. 2012. New miniature stirred-tank bioreactors for parallel study of enzymatic biomass hydrolysis. Bioresour Technol 106:138-46.

Rippka R, Deruelles J, Waterbury JB, Herdman M, Stanier RY. 1979. Generic assignments, strain histories and properties of pure cultures of cyanobacteria. J Gen Microbiol 111(Mar):1-61.

Rohdich F, Wiese A, Feicht R, Simon H, Bacher A. 2001. Enoate reductases of Clostridia. Cloning, sequencing, and expression. J Biol Chem 276(8):5779-87.

Sakai T, Matsumoto S, Hidaka S, Imajo N, Tsuboi S, Utaka M. 1992. Asymmetric Reduction of Carbon‐Carbon Double Bonds of Conjugated Enones with Fermenting Baker′s Yeast. ChemInform 23(8).

Sawers R. 2005. Formate and its role in hydrogen production in *Escherichia coli*. Biochemical Society Transactions 33(1):42-46.

Schaller F, Biesgen C, Müssig C, Altmann T, Weiler EW. 2000. 12-Oxophytodienoate reductase 3 (OPR3) is the isoenzyme involved in jasmonate biosynthesis. Planta 210(6):979-984.

Schittmayer M, Glieder A, Uhl MK, Winkler A, Zach S, Schrittwieser JH, Kroutil W, Macheroux P, Gruber K, Kambourakis S and others. 2011. Old Yellow Enzyme-Catalyzed Dehydrogenation of Saturated Ketones. Advanced Synthesis & Catalysis 353(2-3):268-274.

Schlyter F, Smitt O, Sjödin K, Högberg HE, Löfqvist J. 2004. Carvone and less volatile analogues as repellent and deterrent antifeedants against the pine weevil, Hylobius abietis. Journal of applied entomology 128(9‐10):610-619.

Schmolzer K, Madje K, Nidetzky B, Kratzer R. 2012. Bioprocess design guided by in situ substrate supply and product removal: process intensification for synthesis of (S)-1-(2-chlorophenyl)ethanol. Bioresour Technol 108:216-23.

Scordino M, Di Mauro A, Passerini A, Maccarone E. 2003. Adsorption of flavonoids on resins: Hesperidin. Journal of Agricultural and Food Chemistry 51(24):6998-7004.

Seddon KR. 1997. Ionic liquids for clean technology. Journal of Chemical Technology and Biotechnology 68(4):351-356.

Seddon KR, Stark A, Torres M-J. 2000. Influence of chloride, water, and organic solvents on the physical properties of ionic liquids. Pure and Applied Chemistry 72(12):2275-2287.

Shimoda K, Kubota N, Hamada H, Kaji M, Hirata T. 2004. Asymmetric reduction of enones with *Synechococcus* sp. PCC 7942. Tetrahedron Asymmetry 15(11):1677-1679.

Sikkema J, De Bont J, Poolman B. 1994a. Interactions of cyclic hydrocarbons with biological membranes. Journal of Biological Chemistry 269(11):8022-8028.

Sikkema J, Debont JAM, Poolman B. 1995. Mechanisms of Membrane Toxicity of Hydrocarbons. Microbiological Reviews 59(2):201-222.

Sikkema J, Weber FJ, Heipieper HJ, Bont JAMD. 1994b. Cellular Toxicity of Lipophilic Compounds: Mechanisms, Implications, and Adaptations. Biocatalysis and Biotransformation 10(1-4):113-122.

Silva VD, Stambuk BU, Nascimento MD. 2012. Asymmetric reduction of (4R)-(-)-carvone catalyzed by Baker's yeast in aqueous mono- and biphasic systems. Journal of Molecular Catalysis B-Enzymatic 77:98-104.

Simon A, Karl U. 2010. Expanding the scope of industrial biocatalysis. Speciality Chemicals Magazine(January):36-38.

Simon H. 1992. Properties and Mechanistic Aspects of Newly Found Redox Enzymes from Anaerobes Suitable for Bioconversions on Preparatory Scale. Pure and Applied Chemistry 64(8):1181-1186.

Singh RK, Tiwari MK, Singh R, Lee JK. 2013. From protein engineering to immobilization: promising strategies for the upgrade of industrial enzymes. International Journal of Molecular Sciences 14(1):1232-77.

Slonczewski JL, Rosen BP, Alger JR, Macnab RM. 1981. pH homeostasis in Escherichia coli: measurement by 31P nuclear magnetic resonance of methylphosphonate and phosphate. Proceedings of the National Academy of Sciences 78(10):6271-6275.

Snape JR, Walkley NA, Morby AP, Nicklin S, White GF. 1997. Purification, properties, and sequence of glycerol trinitrate reductase from *Agrobacterium radiobacter*. J Bacteriol 179(24):7796-7802.

Stampfer W, Kosjek B, Moitzi C, Kroutil W, Faber K. 2002. Biocatalytic asymmetric hydrogen transfer. Angewandte Chemie International Edition 41(6):1014-1017.

Strassner J, Furholz A, Macheroux P, Amrhein N, Schaller A. 1999. A homolog of old yellow enzyme in tomato. Spectral properties and substrate specificity of the recombinant protein. J Biol Chem 274(49):35067-73.

Stueckler C, Hall M, Ehammer H, Pointner E, Kroutil W, Macheroux P, Faber K. 2007. Stereocomplementary bioreduction of alpha,beta-unsaturated dicarboxylic acids and dimethyl esters using enoate reductases: Enzyme- and substrate-based stereocontrol. Org Lett 9(26):5409-5411.

Stueckler C, Reiter TC, Baudendistel N, Faber K. 2010. Nicotinamide-independent asymmetric bioreduction of C=C-bonds via disproportionation of enones catalyzed by enoate reductases. Tetrahedron 66(3):663-667.

Stuermer R, Hauer B, Hall M, Faber K. 2007. Asymmetric bioreduction of activated C=C bonds using enoate reductases from the old yellow enzyme family. Curr Opin Chem Biol 11(2):203-13.

Suller M, Lloyd D. 1999. Fluorescence monitoring of antibiotic ‐ induced bacterial damage using flow cytometry. Cytometry 35(3):235-241.

Sun B, Kantzow C, Bresch S, Castiglione K, Weuster-Botz D. 2013. Multi-enzymatic one-pot reduction of dehydrocholic acid to 12-keto-ursodeoxycholic acid with whole-cell biocatalysts. Biotechnol Bioeng 110(1):68-77.

Swiderska MA, Stewart JD. 2006. Stereoselective enone reductions by *Saccharomyces carlsbergensis* old yellow enzyme. Journal of Molecular Catalysis B: Enzymatic 42(1-2):52-54.

Tasnádi G, Winkler CK, Clay D, Sultana N, Fabian WMF, Hall M, Ditrich K, Faber K. 2012. A Substrate-Driven Approach to Determine Reactivities of α,β-Unsaturated Carboxylic Esters Towards Asymmetric Bioreduction. Chemistry – A European Journal 18(33):10362-10367.

Tauber K, Hall M, Kroutil W, Fabian WM, Faber K, Glueck SM. 2011. A highly efficient ADH-coupled NADH-recycling system for the asymmetric bioreduction of carbon-carbon double bonds using enoate reductases. Biotechnol Bioeng 108(6):1462-7.

Tishkov V, Popov V. 2004. Catalytic mechanism and application of formate dehydrogenase. Biochemistry (Moscow) 69(11):1252-1267.

Tishkov VI, Popov VO. 2006. Protein engineering of formate dehydrogenase. Biomol Eng 23(2-3):89-110.

Toogood HS, Fryszkowska A, Hare V, Fisher K, Roujeinikova A, Leys D, Gardiner JM, Stephens GM, Scrutton NS. 2008. Structure-Based Insight into the Asymmetric Bioreduction of the C=C Double Bond of alpha,beta-Unsaturated Nitroalkenes by Pentaerythritol Tetranitrate Reductase. Adv Synth Catal 350(17):2789-2803.

Toogood HS, Gardiner JM, Scrutton NS. 2010. Biocatalytic reductions and chemical versatility of the old yellow enzyme family of flavoprotein oxidoreductases. ChemCatChem 2(8):892-914.

Tufvesson Pr, Lima-Ramos J, Nordblad M, Woodley JM. 2010. Guidelines and cost analysis for catalyst production in biocatalytic processes. Organic Process Research & Development 15(1):266-274.

Uchiyama T, Miyazaki K. 2009. Functional metagenomics for enzyme discovery: challenges to efficient screening. Curr Opin Biotechnol 20(6):616-22.

Utaka M, Konishi S, Mizuoka A, Ohkubo T, Sakai T, Tsuboi S, Takeda A. 1989. Asymmetric reduction of the prochiral carbon-carbon double bond of methyl 2-chloro-2-alkenoates by use of fermenting bakers' yeast. The Journal of Organic Chemistry 54(21):4989-4992.

van der Donk WA, Zhao H. 2003. Recent developments in pyridine nucleotide regeneration. Curr Opin Biotechnol 14(4):421-426.

van Dyk MS, van Rensburg E, Rensburg IPB, Moleleki N. 1998. Biotransformation of monoterpenoid ketones by yeasts and yeast-like fungi. Journal of Molecular Catalysis B: Enzymatic 5(1–4):149-154.

Vaz AD, Chakraborty S, Massey V. 1995. Old Yellow Enzyme: aromatization of cyclic enones and the mechanism of a novel dismutation reaction. Biochemistry 34(13):4246-4256.

Vermuë M, Sikkema J, Verheul A, Bakker R, Tramper J. 1993. Toxicity of homologous series of organic solvents for the gram-positive bacteria *Arthrobacter* and *Nocardia* Sp. and the gram-negative bacteria *Acinetobacter* and *Pseudomonas* Sp. Biotechnol Bioeng 42(6):747-758.

Vermue M, Tramper J. 1995. Biocatalysis in non-conventional media: medium engineering aspects. Pure and Applied Chemistry 67:345-345.

Vicenzi JT, Zmijewski MJ, Reinhard MR, Landen BE, Muth WL, Marler PG. 1997. Large-scale stereoselective enzymatic ketone reduction with *in situ* product removal via polymeric adsorbent resins. Enzyme and Microbial Technology 20(7):494-499.

Warburg O, Christian W. 1933. Über das gelbe Ferment und seine Wirkung. Biochem Z 266:377-411.

Wenda S, Illner S, Mell A, Kragl U. 2011. Industrial biotechnology-the future of green chemistry? Green Chemistry 13(11):3007-3047.

Weuster-Botz D. 2005. Parallel reactor systems for bioprocess development. Technology Transfer in Biotechnology: Springer. p 125-143.

Weuster-Botz D. 2007. Process intensification of whole-cell biocatalysis with ionic liquids. Chem Rec 7(6):334-40.

Weuster-Botz D, Puskeiler R, Kusterer A, Kaufmann K, John GT, Arnold M. 2005. Methods and milliliter scale devices for high-throughput bioprocess design. Bioprocess and Biosystems Engineering 28(2):109-119.

Weuster-Botz D, Stevens S, Hawrylenko A. 2002. Parallel-operated stirred-columns for microbial process development. Biochemical Engineering Journal 11(1):69-72.

Wichmann R, Vasic-Racki D. 2005. Cofactor regeneration at the lab scale. Advances in Biochemical Engineering/ Biotechnology 92:225-260.

Wilks JC, Slonczewski JL. 2007. pH of the cytoplasm and periplasm of Escherichia coli: rapid measurement by green fluorescent protein fluorimetry. J Bacteriol 189(15):5601-5607.

Williams RE, Rathbone DA, Scrutton NS, Bruce NC. 2004. Biotransformation of explosives by the old yellow enzyme family of flavoproteins. Appl Environ Microbiol 70(6):3566-74.

Wilms B, Hauck A, Reuss M, Syldatk C, Mattes R, Siemann M, Altenbuchner J. 2001. High-cell-density fermentation for production of L-N-carbamoylase using an expression system based on the *Escherichia coli* rhaBAD promoter. Biotechnol Bioeng 73(2):95-103.

Winkler CK, Clay D, Davies S, O'Neill P, McDaid P, Debarge S, Steflik J, Karmilowicz M, Wong JW, Faber K. 2013. Chemoenzymatic Asymmetric Synthesis of Pregabalin Precursors via Asymmetric Bioreduction of β-Cyanoacrylate Esters Using Ene-Reductases. The Journal of Organic Chemistry 78(4):1525-1533.

Winkler CK, Stueckler C, Mueller NJ, Pressnitz D, Faber K. 2010. Asymmetric synthesis of O-protected acyloins using enoate reductases: stereochemical control through protecting group modification. Eur J Org Chem(33):6354-6358.

Winkler CK, Tasnádi G, Clay D, Hall M, Faber K. 2012. Asymmetric bioreduction of activated alkenes to industrially relevant optically active compounds. J Biotechnol 162(4):381-389.

Wolfenden R, Snider MJ. 2001. The depth of chemical time and the power of enzymes as catalysts. Accounts of Chemical Research 34(12):938-945.

Wu JT, Wu LH, Knight JA. 1986. Stability of Nadph - Effect of Various Factors on the Kinetics of Degradation. Clinical Chemistry 32(2):314-319.

Yang JW, Hechavarria Fonseca MT, Vignola N, List B. 2004. Metal-free, organocatalytic asymmetric transfer hydrogenation of alpha,beta-unsaturated aldehydes. Angew Chem Int Ed Engl 44(1):108-10.

Yanto Y, Winkler CK, Lohr S, Hall M, Faber K, Bommarius AS. 2011. Asymmetric bioreduction of alkenes using ene-reductases YersER and KYE1 and effects of organic solvents. Org Lett 13(10):2540-2543.

Yanto Y, Yu HH, Hall M, Bommarius AS. 2010. Characterization of xenobiotic reductase A (XenA): study of active site residues, substrate spectrum and stability. Chem Commun (Camb) 46(46):8809-8811.

Yazbeck DR, Martinez CA, Hu S, Tao J. 2004. Challenges in the development of an efficient enzymatic process in the pharmaceutical industry. Tetrahedron: Asymmetry 15(18):2757-2763.

Zajkoska P, Rebros M, Rosenberg M. 2013. Biocatalysis with immobilized *Escherichia coli*. Appl Microbiol Biotechnol.

Zhang R, Xu Y, Xiao R, Zhang B, Wang L. 2012. Efficient one-step production of (S)-1-phenyl-1, 2-ethanediol from (R)-enantiomer plus NAD+–NADPH in-situ regeneration using engineered *Escherichia coli*. Microb Cell Fact 11(1):167.

Zhao H. 2012. Ionic Liquids as (Co-)Solvents for Hydrolytic Enzymes. Ionic Liquids in Biotransformations and Organocatalysis: John Wiley & Sons, Inc. p 151-227.

Zhao H, van der Donk WA. 2003. Regeneration of cofactors for use in biocatalysis. Curr Opin Biotechnol 14(6):583-589.

Zhou Y, Minami T, Honda K, Omasa T, Ohtake H. 2010. Systematic screening of *Escherichia coli* single-gene knockout mutants for improving recombinant whole-cell biocatalysts. Appl Microbiol Biotechnol 87(2):647-655.

Abbreviations

Abbreviation	Signification
ADH	alcohol dehydrogenase
BCA	bicinchoninic acid
BLAST	Basic Local Alignment Search Tool
BSA	bovine serum albumin
bp	base pair
CDW	cell dry weight, g
CV	column volumn
ddH_2O	double distilled water
de	diastereomeric excess, %
DNA	deoxyribonucleic acid
dNTP	deoxyribonucleotide triphosphate
DMF	dimethylformamide
DO	dissolved oxygen, %
DTT	1,4-dithiothreitol
EC	Enzyme Commission
E. coli	*Escherichia coli*
EDTA	ethylenediaminetetraacetic acid
ee	enantiomeric excess, %
ER	ene-reductase
FAD	flavin adenine dinucleotide
FDH	formate dehydrogenase
FMN	flavin mononucleotide
FPLC	Fast Protein Liquid Chromatography
GC	gas chromatography
GDH	glucose dehydrogenase
G6PDH	glucose-6-phosphate dehydrogenase
His_6	hexahistidin
[HMIM]	1-hexyl-3-methylimidazolium
[HMPL]	1-hexyl-1-methylpyrrolidinium
[HPYR]	1-hexyl-3-methylpyridinium
IPTG	Isopropyl β-D-1-thiogalactopyranoside
IL	ionic liquid
kb	kilobase pair

Abbreviation	Signification
LB	Luria broth
$\log D_{IL/aq}$	decadic logarithm of the distribution coefficient of a substance between the ionic liquid and the aqueous phase, -
$\log D_{IL/hexane}$	log DIL/hexane decadic logarithm of the distribution coefficient of a substance between the ionic liquid and *n*-hexane, -
log*P*	decadic logarithm of the partition coefficient of a substance between octanol and water
MBP	maltose binding protein
MOPS	3-(N-morpholino)propanesulfonic acid
MTBE	methyl tert-butyl ether
MW	molecular weight
NAD^+	nicotinamide adenine dinucleotide (oxidized)
NADH	nicotinamide adenine dinucleotide (reduced)
$NADP^+$	nicotinamide adenine dinucleotide phosphate (oxidized)
NADPH	nicotinamide adenine dinucleotide phosphate (reduced)
NCBI	National Center for Biotechnology Information
[NTF]	bis(trifluoromethylsulfonyl)imide
$[PF_6]$	hexafluorophosphate
OD	optical density
rbs	ribosome binding site
PAGE	polyacrylamide gel electrophoresis
PBS	phosphate buffered saline
PCC	Pasteur Culture Collection of Cyanobacteria
PCR	polymerase chain reaction
PMSF	phenylmethylsulfonyl fluoride
RT	room temperature
SDR	short chain dehydrogenase/ reductase
SDS	sodium dodecyl sulfate
TB	Terrific broth
TEMED	tetramethylethylenediamine
TEV	tobacco etch virus
Tris	tris(hydroxymethyl)aminomethane
Tris-HCl	tris(hydroxymethyl)aminomethane hydrochloride
TTN	total turnover number
U	enzyme unit, 1 U = 1 µmol min^{-1}
% (v/v)	volume percent
% (w/w)	weight percent

A Appendix

A.1 Equipment and consumables

Table A.1 General equipment.

Equipment	Manufacturer
Analytic scale Explorer E1M213	Ohaus, Gießen, Germany
Analytic scale Extend ED124S	Satorius, Göttingen, Germany
Autoklav Varioklav 500 E H+P	E H+P Labortechnik, Oberschleißheim
Bench-top centrifuge Biofuge	Stratos Kendro-Heraeus, Langenselbold, Germany
Bench-top centrifuge Mikro 20	Hettich, Tuttlingen, Germany
Drying oven E28	Binder, Tuttlingen, Germany
Floor-standing centrifuge Rotixa 50 RS	Hettich, Tuttlingen, Germany
Flow cytometry CyFlow® SL	Partec, Münster, Germany
Flow cytometry software FlowMax	Quantum Analysis, Münster, Germany
Incubator	Binder, Tuttlingen, Germany
Incubator Multitron II	Infors, Einsbach, Germany
Magnetic stirring plate	Variomag H+P Labortechnik, Oberschleißheim
Microman M10, M100, M1000	Gilson, Middleton, USA
Micropipette Transferpipette® 300 µL -8/ -12	Brand, Wertheim, Germany
Micropipette 20 μL 200 µL, 1000 μL	Brand, Wertheim, Germany
Micropipette 20 μL 200 µL, 1000 μL	Eppendorf, Hamburg, Germany
Mixer mill MM200	Retsch, Haan, Germany
MTP-photometer EL 808IU	Bio-Tek Instruments, Bad Friedrichshall, Germany
MTP-photometer Software KC Junior v.1.10	Bio-Tek Instruments, Bad Friedrichshall, Germany
MTP-photometer infinite M200	Tecan, Crailsheim, Germany
MTP-photometer software Magellan v.6.1	Tecan, Crailsheim, Germany
Multistirrer plate Multipoint 15	H+P Labortechnik, Oberschleißheim, Germany
Multistirrer plate Variomag Poly 15	H+P Labortechnik, Oberschleißheim, Germany
pH-electrode BlueLine 24 pH	Schott, Mainz, Germany
pH-meter CG 843	Schott, Mainz, Germany

Equipment	Manufacturer
Photometer Genesys 20	Thermo Spectronic, Neuss, Germany
Thermomixer comfort	Eppendorf, Hamburg, Germany
Thermoshaker for microtiter plates	NeoLab, Heidelberg, Germany
Vortex REAX top	Heidolph, Schwabach, Germany
Water bath	Thermo Haake, Karlsruhe, Germany
WiseCube shaking inkubatorWIS-20	Witeg Labortechnik, Wertheim, Germany

Table A.2 Gas chromatography and applied columns.

Equipment	Manufacturer /Specification
Gas chromatograph CP-3800	Varian, Darmstadt, Germany
Injector 1079 PTV	temperature programmable
Split control	electronic flow control (EFC)
Chromatographic column Astec Chiraldex-B-TA	Sigma Aldrich, Schnelldorf, Germany, 40 m, 0.25 mm, 0.25 µm
Chromatographic column CP-Chirasil-Dex CB	Agilent Technologies, Boblingen, Germany, 25 m, 0.32 mm, 0.25 µm
Chromatographic column Lipodex E	Macherey Nagel, Düren, Germany, 25 m, 0.25 mm, 0.25 µm
Flame ionization detector	fuel gas: hydrogen and air, carrier gas/make-up-gas: helium
Software Star Version 5.51	Varian, Darmstadt, Germany
Autosampler CombiPal	CTC Analytics, Zwingen, Switzerland
Helium 99.999 % (v/v)	Air Liquide, Krefeld, Germany
Hydrogen 99.999 % (v/v)	Air Liquide, Krefeld, Germany
Synthetic air	house pipe

Table A.3 Stirred-tank bioreactors used for cell cultivation and biotransformations.

Equipment	Manufacturer /Specification
Labfors reactor, 7.5 L	Infors HAT, Bottmingen-Basel, Switzerland
Labfors reactor, 1.2 L	Infors HAT, Bottmingen-Basel, Switzerland
Stirrer	2 six-bladed Rushton impellors
Drive top	top, mechanical seal drive coupling
Aeration	mass flow valve sparger
Control station	Infors HAT, Bottmingen-Basel, Switzerland
Software Iris-NT Pro Version 4.11	Infors HAT, Bottmingen-Basel, Switzerland
pH electrode 405-DPAS-SC-K8S/325	Mettler-Toledo, Gießen, Germany
pH electrode HA405-DPA-SC-S8	Mettler-Toledo, Gießen, Germany
pO2-probe InPro 6000	Mettler-Toledo, Gießen, Germany
Exhaust gas analyser Easy Line	ABB-Frankfurt, Germany
Exhaust gas filter Sartobran 300 2 μm	Watson-Marlow, Rommerskirchen, Germany
Mass flow controller Advance SCC-F	ABB, Frankfurt, Germany

Equipment	Manufacturer /Specification
Pump ISM 444	Ismatec Glattbrugg, Schweiz
Profors bubble column 400 mL	Infors HAT, Bottmingen-Basel, Switzerland
Magnetic drive Microtec AK 120	Infors, Einsbach, Germany
Stirrer	six-bladed Rushton impellor
Drive	bottom, magnetic drive

Table A.4 Milliliter parallel stirred-tank bioreactor unit.

Equipment	Manufacturer /Specification
Parallel bioreactor unit	2mag, Munich, Germany
Milliliter single-use bioreactors	PreSens Precision, Regensburg, Germany
Control device	2mag, Munich, Germany
Thermostat ME-12	Julabo, Seelbach, Germany
Cooling unit DLK-402	G. Heinemann, Schwäbisch Hall, Germany

Table A.5 Rotary evaporator.

Equipment	Manufacturer /Specification
Rotary evaporator LABOROTA 4003	Heidolph, Schwabach, Germany
Vacuum pump ROTAVAC vario control	Heidolph, Schwabach, Germany

Table A.6 Fast protein liquid chromatography (FPLC)-system and applied columns.

Equipment	Manufacturer Specification
GradiFrac FPLC-unit	GE Healthcare, Uppsala, Schweden
HisTrap FF crude columns, 1 mL and 5 mL	GE Healthcare, Uppsala, Schweden
IV-7 valve	GE Healthcare, Uppsala, Schweden
Pump P50	GE Healthcare, Uppsala, Schweden
UV spectrophotometer LKB Uvicord S II, 280 nm	GE Healthcare, Uppsala, Schweden
LabVIEW 6.0	National Instruments, Munich, Germany

Table A.7 Special consumables.

Equipment	Manufacturer	Article number
Cuvettes, semi-micro	Ratiolab	27-12-120
Filters, Ø 0,22 μm	Roth	KH54
Minisart HF filters Ø 0.45 µm	Satorius	16533
Glas beads, Ø 0,25-0,50 mm	Roth	A553
Magnetic stirrers, Ø 10 mm	VWR	442-0075
Needles, single-use, Ø 0.9 mm	Braun	4665791
Needles, single-use, Ø 2.1 mm	Braun	4665473
Rotilabo® glas vials, Ø 15 mm	Roth	H306.1
Short thread vial (11,6×32 mm)	VRW	548-0907
Short thread cap PP blue	VRW	548-0907
Screw vials N9-1	Macherey-Nagel	702283
Screw caps N9 PP blue	Macherey-Nagel	702732
96 well optical bottom plates (96F, untreated straight w/o)	Thermo Scientific/ Nunc	260836
Vivaspin concentrators 20 mL (MWCO 5 kDa)	VWR	512-3784

Table A.8 Programs and softwares.

Program	Manufacturer /Specification
Basic Local Alignment Search Tool (BLAST)	Alignment of DNA- and protein sequences (http://blast.ncbi.nlm.nih.gov/Blast.cgi)
GENtle	DNA and amino acid editing, database management and alignment (http://gentle.magnusmanske.de/)
ImageJ 1.46r	Image processing and analysis of SDS-PAGES (http://rsbweb.nih.gov/ij/)
MATLAB R2010b; R2012b	Mathematical program used for the Response Surface Methodology (RSM)
Multalin	Multiple sequence alignment (http://multalin.toulouse.inra.fr/multalin/)
Sigma Plot 12.3	Program for the analysis of enzyme kinetics; Systat Software, Chicago, USA

A.2 Chemicals and enzymes

Table A.9 General chemicals.

Chemicals	Purity	Manufacturer	Article number
Acetic acid	≥ 99.8 %	Merck	100058
Agar-Agar	n.a.	Roth	5210
Ammonia, 25 %	puriss.	Roth	5460
Ammonium chloride	≥ 99.0 %	Roth	5470
Ammonium formate	≥ 99.0 %	Sigma Aldrich	17843
Ammonium persulfate (APS)	98.0 %	Merck	101217
Ampicillin sodium salt	≥ 99.0 %	Roth	K029
Boric acid	≥ 99.0 %	Merck	100165
Bromphenol blue	ACS	Merck	108122
Calcium chloride · $2H_2O$	≥ 99.0 %	Merck	102382
Cobalt(II) chloride · $6H_2O$	≥ 99.0 %	Merck	102539
Coomassi Blue R 250	n.a.	Roth	3862
Copper(II) chloride · $2H_2O$	≥ 99.0 %	Merck	102733
Diammonium hydrogen citrate	≥ 99 %	Merck	101154
Diethyl ether	≥ 99.5 %	Roth	8810
1,4-Dithiothreitol (DTT)	≥ 99.0 %	Merck	111474
EDTA-Na_2· $2H_2O$	≥ 99 %	Fluka	108418
Ethanol	≥ 99.5 %	Merck	100986
Ethidium bromide solution 1.0 %	n.a.	Roth	2218
Ethyl acetate	≥ 99.5 %	Roth	6784.4
Flavin mononucleotide	≥ 70 %	Sigma Aldrich	6750
D-Glucose · H_2O	≥ 98.5 %	Roth	6780
Glycerol	≥ 98.0 %	Roth	7530
n-Hexane	≥ 98.0 %	Roth	7339
Hydrochloride acid	32 %	Merck	100319
Imidazole	≥ 99 %	Roth	3899
Iron(III) chloride · $6H_2O$	≥ 99.0 %	Merck	103943
Isopropanol	≥ 99.8 %	Roth	6752
IPTG	≥ 99.0 %	Roth	CN08
Kanamycin sulfate	n.a.	Roth	T832
Magnesium sulfate · $7H_2O$	≥ 99.5 %	Merck	105886
Manganese(II) chloride · $4H_2O$	≥ 99.0 %	Merck	105927
MTBE	≥ 99.5 %	Roth	6746
NADH-Na2	≥ 98.0 %	Roth	AE12
NAD+	≥ 97.5 %	Roth	AE11
NADPH-Na_4	≥ 97.0 %	Roth	AE14
$NADP^+$	≥ 97.0 %	Roth	AE13
N,*N*-dimethylformamide	≥ 99.5 %	Roth	6251
Nickel(II) chloride · $6H_2O$	≥ 98.0 %	Merck	106717
Pepton from casein	n.a.	Roth	8986.1
Phenylmethylsulfonyl fluoride (PMSF)	≥ 99 %	Roth	6367

Chemicals	Purity	Manufacturer	Article number
Potassium carbonate	≥ 99.5 %	Merck	104924
Monopotassium phosphate	≥ 99.0 %	Roth	3907
Dipotassium phosphate	≥ 99.0 %	Roth	P749
Roti®Blue	n.a.	Roth	A152.1
Rotiphorese® Gel 40 (19:1)	n.a.	Roth	3030.1
Rotiphorese® 10x SDS-PAGE	n.a.	Roth	6367
Sodium chloride	≥ 99.5 %	Roth	3957
Sodium citrate	≥ 99.5 %	Fluka	71497
Sodium dodecylsulfat	≥ 85 %	Merck	817034
Sodium dihydrogenphosphate · H_2O	≥ 99.0 %	Merck	106346
Sodium formate	≥ 98.0 %	Fluka	71540
Sodium hydroxide	≥ 99.0 %	Roth	9356
Sodium molybdat-Dihydrat	≥ 99.5 %	Merck	106521
Sodium selenite	≥ 99.0 %	Sigma-Aldrich	214485
Sodium sulfate	≥ 99.0 %	Merck	822286
tert-Butyl methyl ether	≥ 99.5 %	Roth	6746
Tetramethylethylenediamine (TEMED)	≥ 99.0 %	Roth	2367
Toluene	≥ 99.5 %	Roth	9558
Yeast extract OHLY KAT	n.a.	Dt. Hefewerke	n.a.
Zinc sulfate heptahydrate	≥ 99.0 %	Merck	108883

Table A.10 Substrates and reference substances used for biocatalysis and analysis.

Chemical	Purity	Manufacturer	Article number
Maleimide	99 %	Sigma Aldrich	129585
2-Methylmaleimide	n.a.	Synthesis	-
2-Methyl-N-phenylmaleimide	98 %	Sigma Aldrich	337765
Citraconic anhydride	98 %	Sigma Aldrich	125318
2-Cyclopenten-1-one	98 %	Sigma Aldrich	C112909
2-Methyl-2-cyclopenten-1-one	98 %	Sigma Aldrich	304190
3-Methyl-2-cyclopenten-1-one	97 %	Sigma Aldrich	145777
2-Cyclohexen-1-one	≥ 98.0 %	Sigma Aldrich	92509
3-Methyl-2-cyclohexen-1-one	≥ 98 %	Sigma Aldrich	W336009
Ketoisophorone	≥ 98 %	Sigma Aldrich	W342106
(R)-Carvone	98 %	Sigma Aldrich	124931
(S)-Carvone	96 %	Sigma Aldrich	435759
Citral (*cis/trans*)	95 %	Sigma Aldrich	C83007
(R)-Pulegone	97 %	Sigma Aldrich	376388
(S)-Pulegone	98 %	Sigma Aldrich	328847
trans-2-Penten-1-al	≥ 95 %	Sigma Aldrich	W321818
trans-2-Hexen-1-al	98 %	Sigma Aldrich	132659
trans-2-Octen-1-al	≥ 94 %	Sigma Aldrich	W321508
3-Phenyl-2-methylpropenal	98 %	Sigma Aldrich	112275

Chemical	Purity	Manufacturer	Article number
1-Nitrocyclohexene	99 %	Sigma Aldrich	219533
Nitrobenzene	≥ 99.0 %	Sigma Aldrich	252379
1-Acetyl-1-cyclohexene	97 %	Sigma Aldrich	A14405
(S)-Perillaldehyde	≥ 92 %	Sigma Aldrich	W355704
Dimethyl maleate	96 %	Sigma Aldrich	238198
Itaconic acid	99 %	Sigma Aldrich	I29204
Mesaconic acid	99 %	Sigma Aldrich	131040
Citraconic acid	98 %	Sigma Aldrich	C82604
Succinimide	n.a.	Sigma Aldrich	S9381
2-Methylsuccinimide	n.a.	Synthesis	-
Cyclohexanone	≥ 99.5%	Sigma Aldrich	29140
3-Methylcyclohexanone	97 %	Sigma Aldrich	M38605
(R)-3-Methylcyclohexanone	98 %	Sigma Aldrich	M38583
2-Methylcyclopentanone	98 %	Sigma Aldrich	288438
Dihydrocarvone	77 % (2R,5R); 20 % (2S,5R)	Sigma Aldrich	37275
(R)-Limonene	≥ 99.0 %	Sigma Aldrich	62118

Table A.11 Ionic liquds and adsorbent resins

Ionic liquid	Manufacturer	Article number
[HMIM][NTF]	Merck	490031
[HMIM][PF_6]	Merck	490065
[HMPL][NTF]	Merck	490100
Amberlite™ XAD™ 4	Fisher Scientific	10721671
Amberlite™ XAD™ 7	Fisher Scientific	10606062
Amberlite™ XAD™ 1180	Fisher Scientific	10003400

Table A.12 Enzymes

Enzyme	Manufacturer	Article number
Antarctic Phosphatase	New England Biolabs	M0289
Phusion® High-Fidelity DNA-Polymerase	Finnzymes	F-530
Phusion® Hot Start High-Fidelity DNA-Polymerase	Finnzymes	F-540
Restriction enzyme BamHI-HF	New England Biolabs	R3136
Restriction enzyme BlpI	New England Biolabs	R0585
Restriction enzyme EcoRI-HF	New England Biolabs	R3101
Restriction enzyme HindIII-HF	New England Biolabs	R3104
Restriction enzyme KpnI-HF	New England Biolabs	R3142
Restriction enzyme NcoI-HF	New England Biolabs	R3193
Restriction enzyme NdeI	New England Biolabs	R0111
Restriction enzyme NheI HF	New England Biolabs	R3131
Restriction enzyme NotI-HF	New England Biolabs	R3189
Restriction enzyme SbfI	New England Biolabs	R3642
T4 DNA-Ligase	New England Biolabs	M0202
Taq DNA-Polymerase	New England Biolabs	M0321

Table A.13 Kits and standards

Kits and standards	Manufacturer	Article number
Bicinchoninic acid (BCA), Protein Assay Kit	Thermo Scientific	23227
dNTP)-Mix	New England Biolabs	N0447S
100 bp DNA-ladder extended	Roth	T835
GenElute™ HP Plasmid Miniprep Kit	Sigma Aldrich	PLN70
GenElute™ Gel Extraction Kit	Sigma Aldrich	NA1111
GenElute™ PCR Clean-Up Kit	Sigma Aldrich	NA1020
QuikChange® Lightning Site-Directed Mutagenesis Kit	Agilent Technologies	210518
Roti®-Mark Standard	Roth	T851
Perfect Protein^{TM} Markers, 10 – 225 kDa	Merck	69079

A.3 Oligonucleotids, vectors and strains

A.3.1 Oligonucleotids

Table A.14 Oligonucleotids used for cloning.

Primer	Sequence (5'→ 3')	Plas-mids
Cloning of ERs from cyanobacterial strains[a]		
Syn7942-ndeI-for	AGAGATCAT**ATG**TCCGAATCGCTCAAACTGCTGACG	1, 2
Syn7942-ncoI-for	AGAGAT CCATGG*AC***ATG**TCCGAATCGCTCAAACTG CTGA CG	3
Syn7942-notI-rev1	AGAGATGCGGCCGCGACAGATGCTGCTTCCAAACTGG GATAG	1
Syn7942-notI-rev2	AGAGATGCGGCCGC*TTA*GACAGATGCTGCTTCCAAACT GGGA	2, 3
Lyngbya1-ndeI-for	GGATATCCAT**ATG**AATACTACTCTAAATTTGTTAAAAC	1, 2
Lyngbya1-bamHI-rev	CGCGGATCC**TTA**AACTGTCGTCAATACTTTTG	1, 2
Lyngbya2-ndeI-for	GGAATTCCAT**ATG**TCAACTCAAACCTCCTC	1, 2
Lyngbya2-bamHI-rev	CGCGGATCC**TTA**ACTATTTGCTGTTGTTAAGTC	1, 2
Cyanoth1-ndeI-for	GGAATAGCAT**ATG**CAAAAAATGGAGACGAC	1, 2
Cyanoth1-bamHI-rev	CGCGGATCC**TTA**GCTGGCAACTTGTTCTAG	1, 2
Cyanoth2-ndeI-for	AGAGATCAT**ATG**AATACTCCCACTGCTTCC	1, 2
Cyanoth2-bamHI-rev	CGCGGATCC**CTA**ATAAGTGGGAAAATCAATATAACC	1, 2
Nospunc1-ndeI-for	GCTTATCCAT**ATG**ACTACTGAGATCAATTTATTC	1, 2
Nospunc1-bamHI-rev	CGCGGATCC**TTA**CGCCTTAGCTACCG	1, 2
Nospunc2-ndeI-for	GGATAAGCAT**ATG**GTCGAATACTACACCC	1, 2
Nospunc2-bamHI-rev	CGCGGATCC**TCA**ATGGAGTTGCGG	1, 2
Nospunc3-ndeI-for	GGAATTCCAT**ATG**GCACATCTGTTTGAACC	1, 2
Nospunc3-bamHI-rev	CGCGGATCC**TCA**TAGCCAAGCTCGATCG	1, 2
Nostoc1-ndeI-for	GGAATTCCAT**ATG**TCTGATGAAGCAGAGAGG	1, 2
Nostoc1-bamHI-rev	CGCGGATCC**TTA**CTTATTAGCAACTGCTAAAAA TGG	1, 2
Nostoc2-ndeI-for	GGAATTCCAT**ATG**ACTCATCTATTTGAACCAC	1, 2
Nostoc2-bamHI-rev	CGCGGATCC **TTA**CAACCAAGCTCGGTC	1, 2

Primer	Sequence (5'→ 3')	Plas-mids
Syn7002-ndeI-for	GGAATTCCAT**ATG**ACAACGACTTTTGCAAC	1, 2
Syn7002-bamHI-rev	CGCGGATCC **CTA**GGCGGCATAGGTCG	1, 2
Anabaena1-ndeI-for	GGAATTCCAT**ATG**TCTACCAACATCAACC	1, 2
Anabaena1-bamHI-rev	CGCGGATCC **CTA**TTTGCTAGCAACTTCT	1, 2
Anabaena2-ndeI-for	GGAATTCCAT**ATG**ACTCATCTATTTGAACCAC	1, 2
Anabaena2-bamHI-rev	CGCGGATCC **TTA**CAACCAAGCTCGGTC	1, 2
Anabaena3-ndeI-for	GGAATTCCAT**ATG**GATTTGTTTACTCCAC	1, 2
Anabaena3-bamHI-rev	CGCGGATCC **TCA**CCTTCTCTGTCGT	1, 2
Acaryo1-nheI-for	CTAGCTAGC**ATG**TCAATTTCATCCGTG	1, 2
Acaryo1-bamHI-rev	CGCGGATCC**CTA**TGCGGCAGTTATTAGTG	1, 2
Acaryo2-ndeI-for	GGAATAGCAT**ATG**ACAGCAACAGGAACATCC	1, 2
Acaryo2-bamHI-rev	CGCGGATCC**TTA**GGTGGTTTTGACTTGGG	1, 2
Acaryo3-ndeI-for	GGAATTCCAT**ATG**ACGGCAACAGGAGC	1, 2
Acaryo3-bamHI-rev	CGCGGATCC**TTA**GGCTTGGGATTCTGAATAG	1, 2
Acaryo4-ndeI-for	GGAATAGCAT**ATG**ACGGCAACAGGAAC	1, 2
Acaryo4-bamHI-rev	CGCGGATCC**TTA**GGCTTGAGATTCTGAATAGAC	1, 2
Acaryo5-ndeI-for	GGAATTCCAT**ATG**ACCTCAGACATTATCTTTCAGC	1, 2
Acaryo5-bamHI-rev	CGCGGATCC **TTA**TGCCGTTTGCTCGG	1, 2
Gloeo-ndeI-for	GGAATTCCAT**ATG**CACCTGTTTGCACC	1, 2
Gloeo-bamHI-rev	CGCGGATCC**TCA**CGGTTTGGCCC	1, 2
Cloning of whole-cell biocatalysts[b]		
rbsGDH-hindIII-for	CCCAAGCTT*AAGGAG*ATATAC**ATG**TATCCGGAT TTAAAAGGAAAAGTCGTC	4, 5
rbsGDH-notI-rev	AAGGAAAAAAGCGGCCGC**TTA**ACCGCGGCCTGCCTGG	4, 5
rbsFDH-hindIII-for	CCCAAGCTT*AAGGAG*ATATAC**ATG**GCAAAGGTCCTGTG CGT	4, 5
rbsFDH-notI-rev	AAGGAAAAAAGCGGCCGC**TCA**GACCGCCTTCTTGAAC TTGG	4, 5
Nostoc1-bamHI-for	CGCGGATCC **ATG**TCTGATGAAGCAGAGAGG	6
Nostoc1-sbfI-rev	GATACACCTGCAGG**TTA**CTTATTAGCAACTGCTAAAAA TGG	6
FDH-ndeI-for	AGGAATTCCAT**ATG**GCAAAGGTCCTGTGCGT	6, 7
FDH-kpnI-rev	CGGGGTACC**TCA**GACCGCCTTCTTGAACTTGG	6, 7

Primer	**Sequence (5'→ 3')**	**Plas-mids**
pCOLA-MCS1end-hindIII-for	CCCAAGCTTATAATGCTTAAGTCGAACAGAAAG	4
pCOLA-MCS1end-blpI-rev (=T7 term)	CTAGTTATTGCTCAGCGGT	4
rbsNostoc1-ecoRI-for	GCGAATTCG**TGA***AAGGAG*ATATAC**ATG**TCTGATGAAGC AGAGAGG	8
rbsNostoc1-hindIII-rev	CCCAAGCTT**TTA**CTTATTAGCAACTGCTAAAAATGG	8
Primers used for side-directed mutagenesis		
FDH D221Q	CACCTGCACTACACCCAGCGTCACCGCCTGCCG-	-
FDH C145S	GCGGAAGTCACCTACTCAAACTCGATCAGCGTCG-	-
FDH C225V	GGTGACGCTGAACGTTCCGCTGCACCCC-	-
Primers used for colony PCR and sequencing		
ACYCDuetUP1	GGATCTCGACGCTCTCCCT	-
pET reverse primer	CTAGTTATTGCTCAGCGG	
T7	TAATACGACTCACTATAGGG	-
T7 term	CTAGTTATTGCTCAGCGGT	-

[a] Primers were used for cloning of ER genes into the plasmids: (1) pET21a(+), (2) pET28a(+), (3) pETM41a(+). Genomic cyanobacterial DNA were used as template

[b]Primers were used for cloning of whole-cell biocatalysts. Respective genes were integrated into the plasmids: (4) pET28a(+)-Nostoc1, (5) pET28a(+)-Anabaena3, (6) pCOLADuet-1, (7) pCOLADuet-1-Nostoc1, (8) pET21a(+)-FDHD221G. Plasmids containing the respective genes for GDH, FDH D221G or NostocER1 were used as templates. In case of pCOLA-MCS1end forward and reverse primers, the pCOLADuet-1-FDH_{1M} vector was used as template.

A.3.2 Genomic DNA and vectors

Table A.15 Genomic DNA and vectors.

Vectors	Manufacturer / Specification
Commercially available vectors	
pET21a(+)	Novagen, San Diego, USA
pET28a(+)	Novagen, San Diego, USA
pETM41a(+)	EMPL, Heidelberg, Germany
pCOLA-Duet-1	Novagen, San Diego, USA
Genomic DNAs and vectors provided by the Institute of Biochemical Engineering (Technische Universität München)	
pET21a(+)-FDH D221G	This vector contains the FDH D221G gene (NdeI/EcoRI) with a base deletion at the position 1202 and a C-terminal His_6 tag (Gebhardt 2006; Liu et al. 2013).
pET21a(+)-FDH C145S/D221Q/ C255V	This vector contains the FDH C145S/D221Q/ C255V gene (NdeI/EcoRI) with a base deletion at the position 1202 and a C-terminal His_6 tag (Hoelsch et al. 2012) and was kindly provided by K. Castiglione (Institute of Biochemical Engineering).
pET21a(+)-FDHmutant	Vectors containing genes of various FDH mutants were provided by K. Castiglione (Institute of Biochemical Engineering) (Hoelsch et al. 2012).
Genomic DNAs of cyanobacterial strains	The genomic DNAs of cyanobacterial strains were kindly provided by K. Castiglione (Institute of Biochemical Engineering) (Hölsch and Weuster-Botz 2010).

A.3.3 Strains

Table A.16 *Escherichia coli* strains.

Strain	Genotype	Manufacturer
Escherichia coli DH5α	F^- endA1 glnV44 thi-1 recA1 relA1 gyrA96 deoR nupG Φ80d*lacZ*ΔM15 Δ(*lacZYA-argF*)U169, hsdR17(r_K^- m_K^+), λ–	Invitrogen Carlsbad, USA
Escherichia coli BL21(DE3)	$F^–$ ompT gal dcm lon $hsdS_B(r_B^-$ $m_B^-)$ λ(DE3 [lacI lacUV5-T7 gene 1 ind1 sam7 nin5])	Novagen, San Diego, USA
Escherichia coli XL-10 Gold	endA1 glnV44 recA1 thi-1 gyrA96 relA1 lac Hte Δ(mcrA)183 Δ(mcrCB-hsdSMR-mrr)173 tet^R F'[proAB $lacI^qZ$ΔM15 Tn10(Tet^R Amy Cm^R)]	Stratagene, La Jolla, USA

A.4 Cultivation media and buffers

A.4.1 Cultivation media

Table A.17 Luria broth (LB) medium.

Component	Concentration	
Peptone	10.0	g L^{-1}
Yeast extract	5.0	g L^{-1}
sodium chloride	5.0	g L^{-1}
Agar	12.0	g L^{-1}

Table A.18 Terrific broth (TB) medium.

Component	Concentration	
Peptone	12.0	g L^{-1}
Yeast extract	24.0	g L^{-1}
Glycerol	4.0	mL L^{-1}
Sodium chloride	5.0	g L^{-1}
Potassium dihydrogen phosphate	2.13	g L^{-1}
Dipotassium hydrogen phosphate	12.54	g L^{-1}

Table A.19 TfbI medium.

Component	Concentration	
Potassium acetate	2.95	g L^{-1}
Rubidium chloride	12.10	g L^{-1}
Sodium chloride	1.11	g L^{-1}
Manganese chloride	6.30	g L^{-1}
Glycerol	150	mL L^{-1}

Table A.20 TfbII medium.

Component	Concentration	
MOPS	1.05	g L^{-1}
Rubidium chloride	0.61	g L^{-1}
Sodium chloride	4.16	g L^{-1}
Glycerol	75	mL L^{-1}

Table A.21 Wilms minimal medium

Component	Concentration	
$(NH3)_2$H-citrate	1.00	g L^{-1}
Na_2SO_4	2.00	g L^{-1}
$(NH_3)_2SO_4$	2.68	g L^{-1}
NH_3Cl	0.50	g L^{-1}
K_2HPO_4	14.6	g L^{-1}
$NaH_2PO4 \cdot 2H_2O$	4.00	g L^{-1}

Table A.22 Trace element solution.

Component	Concentration
$CaCl_2$	0.50 g L^{-1}
$ZnSO_4 \cdot 7H_2O$	0.18 g L^{-1}
$MnSO4 \cdot H_2O$	0.10 g L^{-1}
Na_2-EDTA $\cdot 2H_2O$	11.13 g L^{-1}
$FeCl_3 \cdot 6H_2O$	13.90 g L^{-1}
$CuSO_4 \cdot 5H_2O$	0.16 g L^{-1}
$CoCl_2 \cdot 6H_2O$	0.18 g L^{-1}

A.4.2 Buffers

Table A.23 Buffers for protein purification of His_6-tagged proteins.

Component	HisTrap binding buffer	HisTrap elution buffer
Sodium phosphate	50 mM	50 mM
Imidazole	40 mM	500 mM
Sodium chloride	500 mM	500 mM
pH	7.4	7.4

Table A.24 Buffers for protein purification and application of TEV protease.

Component	TEV-binding buffer	TEV elution buffer
Sodium phosphate	50 mM	50 mM
Imidazole	25 mM	200 mM
Sodium chloride	100 mM	100 mM
Glycerol	10 % (v/v)	10 % (v/v)
pH	8.0	8.0

Component	TEV dialysis buffer
Sodium phosphate	25 mM
EDTA	2 mM
Sodium chloride	200 mM
DTT	1 mM
pH	8.0

Table A.25 Buffers for preparation of samples and gels for SDS-PAGE.

Component	Stacking gel buffer stock (2 x)	Separating gel buffer stock (4 x)
Tris-HCl	250 mM, pH 6.8	1.5 M, pH 8.8
SDS	0.4 % (w/v)	0.8 % (v/v)

Component	Laemmli buffer (5x)
Tris-HCl	300 mM, pH 6.8
Glycerol	50 % (v/v)
SDS	10 % (w/v)
β-mercaptoethanol	5 % (v/v)
bromophenol blue	0.05 % (w/v)

Component	Running buffer (10 x)
Tris	250 mM
Glycin	1.92 M
SDS	1 % (w/v)
Rotiphorese 10 x SDS-PAGE buffer (Roth, article number 3060)	

Table A.26 Buffers for staining of SDS gels.

Component	Fairbanks A	Fairbanks B	Fairbanks C
Isopropanol	25 % (v/v)	10 % (v/v)	10 % (v/v)
Acetic acid	10 % (v/v)	10 % (v/v)	-
Coomassie Brilliant Blue R250/ G250	0.05 % (w/v)	0.005 % (w/v)	-

A.5 Supplementary data

A.5.1 SDS-PAGE

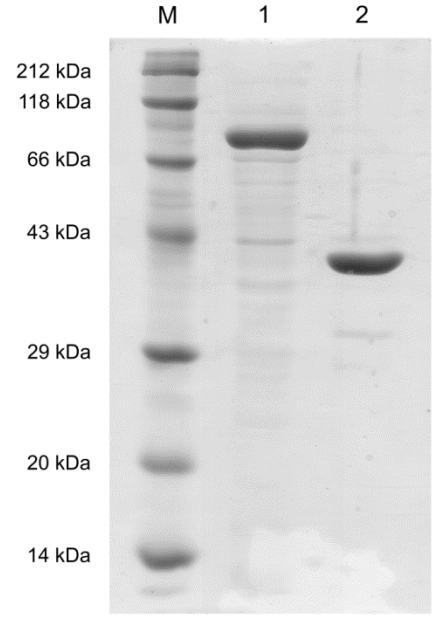

Figure A.1 SDS-PAGE analysis of purified Syn7942ER. Lane M: molecular weight marker, lane 1: crude extract, lane 2 purified Syn7942ER (after cleavage of the His_6-maltose-binding-protein tag).

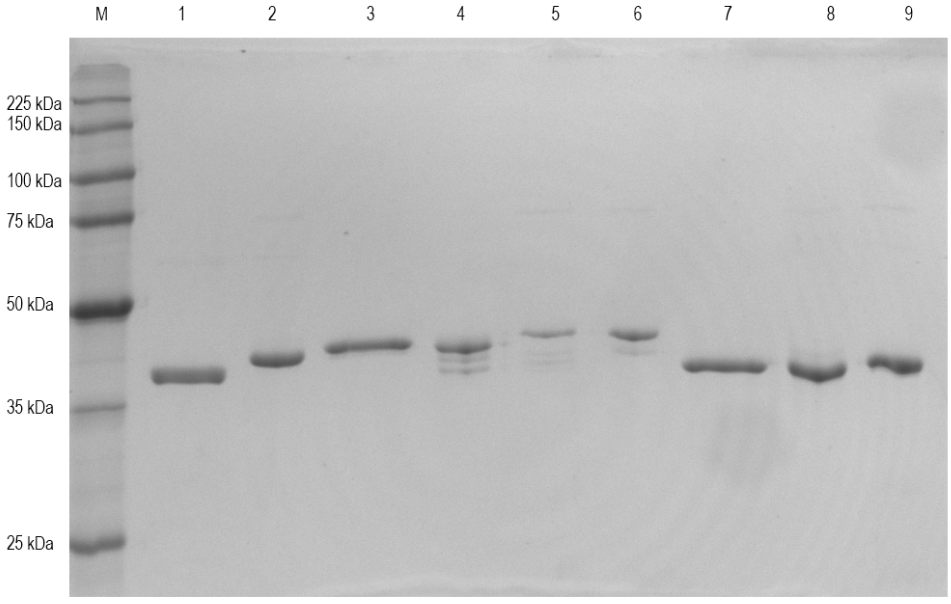

Figure A.2 SDS-PAGE of purified ERs from cyanobacteria. Lane M: molecular mass marker, lane 1: Cyanoth1 (YP_002370366.1), lane 2: CyanothER2 (YP_002371879.1), lane 3: LyngbyaER1 (ZP_01620253.1), lane 4: NospuncER1 (YP_001869478.1), lane 5: NostocER1 (NP_484870.1), lane 6: AcaryoER1 (YP_001519129.1), lane 7: AcaryoER3 (YP_001522070.1), lane 8: AnabaenaER3 (YP_320425.1) and lane 9: GloeoER (NP_926774.1). The calculated molecular masses were in the range of 38.4 kDa to 43.9 kDa.

A.5.2 Sequence alignment

```
           1                                                  #                                 100
     OYE1                              MSF VKDFKPQALG DTNLFKPIKI GNNELLHRAV IPPLTRMRAL HPGNIPNRDW AVEYYTQRAQ RPGTMIITEG
     OYE3                              MPF VKGFEPISLR DTNLFEPIKI GNTQLAHRAV MPPLTRMRAT HPGNIPNKEW AAVYYGQRAQ RPGTMIITEG
    PETNR                                    MS AEKLFTPLKV GAVTAPNRVF MAPLTRLRSI EPGDIPT-PL MGEYYRQRAS --AGLIISEA
 Syn7942ER                                  MSE SLKLLTPVQV GRYELRNRIV MAPLTRNRAT GPDNIPN-DL NVLYYQQRAS --AGLIITEA
LyngbyaER1                                  MNT TLNLLKPFKL GAYELPNRMV MAPLTRMRAK -PGNIPQ-EM NQVYYTQRAS --AGLIISEA
NospuncER1                                  MTT EINLFSSYQL GNLELPNRIV MAPLTRNRAS -KGNVPY-EL NATYYAQRAS --AGLIISEA   “classical“ ERs
 NostocER1  MSDEAERQRG NNLYKNSPLL PVSISQVSTS QLRETEIMST NINLFSSYQL GELELPNRIV MAPLTRQRAG -EGNVPH-QL NAIYYGQRAS --AGLIIAEA
 AcaryoER1                                  MS ISSVFEPIRL GAVDLRNRMV MAPLTRGRSG -PDRVPN-AL MAEYYQQRAS --AGLIITEA
CyanothER1                                MQKMETTQ SMDLLTPVKL GSHTLSNRMI MAPMTRLRAV --GSIPT-PL MATYYAQRAS --AGLIITEC
CyanothER2                                  MNTPTA SPSLLSPFEL GDISLKNRVA MAPMTRARAG -AEGLAN-PL MAQYYTQRAS --AGLLITEA
 AcaryoER3                                  MTATGA SPTLLSSFNL HDLPLANRIV MAPMTRSRAG -EEMLAN-AM MAEYYAQRAS --TGLIVTEG
-----------------------------------------------------------------------------------------------------------------------------
AnabaenER3                                    MDLFTPLII RDITLPSRVA MSPMCQYSA- -ENGFAN-DW HFVHLGSRAV GGTGLIMVEA
   GloeoER                                    MHLFAPLTL RDITLRNRIA VSPMCQYSS- -IDGLAN-DW HFVHLGSRAV GGAGLVIFEA   „thermophilic-like“ ERs
      XenA                                   MSALFEPYTL KDVTLRNRIA IPPMCQYMA- -EDGLIN-DW HQVHYASMAR GGAGLLVVEA
      Yqjm                                  M ARKLFTPITI KDMTLKNRIV MSPMCMYSSH EKDGKLT-PF HMAHYISRAI GQVGLIIVEA

           101                                          #                                 200
     OYE1  AFISPQAGGY DNAPGVWSEE QMVEWTKIFN AIHEKKSFVW VQLWVLGWAA FPDNLARDGL RYDSASDNVF MDAEQEAKAK KAN----NPQ HSLTKDEIKQ
     OYE3  TFISPQAGGY DNAPGIWSDE QVAEWKNIFL AIHDCQSFAW VQLWSLGWAS FPDVLARDGL RYDCASDRVY MNATLQEKAK DAN----NLE HSLTKDDIKQ
    PETNR  TQISAQAKGY AGAPGLHSPE QIAAWKKITA GVHAEDGRIA VQLWHTGRIS HSSIQPGGQA PVSASALNAN TRTSLRDENG NAIRVDTTTP RALELDEIPG
 Syn7942ER  SQISPQGQGY PLTPGIHSPE QVEGWKPIVQ AVHDRGGCIF LQLWHVGRIS HPSLQPDGAL PVAPSAIQPA GM-AATFQGE QPF----VTP RALETEEIAG
LyngbyaER1  TQISPQGLGY PNTPGIHSPE QIQGWKKVTQ AVHENNGRIF LQLWHVGRIS HPSLQPNGEL PVAPSAIAPE GM-ANTFSGE QPF----VTP RALETEEIPA
NospuncER1  TQVTPEGQGY PATPGIHSPE QVEGWKLITD AVHQQGGRIF LQLWHVGRIS HPDLQPNGAL PVAPSAIAPK GE-AATYEGP KPF----VTP RALETSEIPQ   “classical“ ERs
 NostocER1  TQVTPQGQGY PHTPGIHSPE QVAGWKLVTD TVHQQGGRIF LQLWHVGRIS HPDLQPDGGL PVAPSAIAPK GE-VLTYEGK KPY----VTP RALDTSEIPA
Acaryo_ER1  TQVSEQAAGW SETPGIYSEA QIQAWRQVTD AVHQQDGKIF LQIWHTGRAS HPDFQLNGAR PISASAIKPA GE-VHTPQGK KPF----VTP RAVSLDEIPS
CyanothER1  TMVSPLSNGY MNCPGIYSSE QISGWQGVTK AVHDQGGKIF LQLWHCGRVA HPSL-LNGEI PVAPSAIAPV GE-LHSPAGK VAI----EIP RALEKFEIAE
CyanothER2  TSISHQAKGW VHAPNIYTEE HAEAWKQVTE AVRNQGTPIF MQLWHCGRAS HSSFQENGQL PVSASAIKIN GDYIHTPIGK QPY----ETP RALETPEIPR
 AcaryoER3  TFISDQAIGW QHVPGIYTQE QTQAWQVVTK AVHEKGGKVF LQLWHCGRAS HSSFHQDHQL PVAPSAIKLE GDSIHTPQGK QPY----ETP RALSTDEIPL
-----------------------------------------------------------------------------------------------------------------------------
AnabaenER3  TAVTPQGRIT PGDLGLWDDK QIEPLTRIVR FLRQQGSVTG IQLAHAGRKA SCNVPWLGGT PLTPEQGGW- QPVAPSPIPF QENA--P-VP ISLDERGIQE
   GloeoER  AAVEARGRIS PQDLGIWSDA HIEPLRRIND FIHRQESVAG IQIAHAGRKA STARPWEGGG PLTEGEGGWA DSVAPSALPF DAGY--P-VP EALDEAGIAA   „thermophilic-like“ ERs
      XenA  TAVAPEGRIT PGCAGIWSDA HAQAFVPVVQ AIKAAGSVPG IQIAHAGRKA SANRPWEGDD HIGADDARGW ETIAPSAIAF GAHL--PNVP RAMTLDDIAR
      Yqjm  SAVNPQGRIT DQDLGIWSDE HIEGFAKLTE QVKEQGSKIG IQLAHAGRKA ELEG------ ---------- DIFAPSAIAF DEQS--A-TP VEMSAEKVKE
```

```
           201                    #  # #                                                                  300
      OYE1 YIKEYVQAAK NSIAAGADGV EIHSANGYLL NQFLDPHSNT RTDEYGGSIE NRARFTLEVV DALVEAIGHE KVGLRLSPYG VFNSMSGGAE TGIVAQYAYV
      OYE3 YIKDYIHAAK NSIAAGADGV EIHSANGYLL NQFLDPHSNK RTDEYGGTIE NRARFTLEVV DALIETIGPE RVGLRLSPYG TFNSMSGGAE PGIIAQYSYV
     PETNR IVNDFRQAVA NAREAGFDLV ELHSAHGYLL HQFLSPSSNQ RTDQYGGSVE NRARLVLEVV DAVCNEWSAD RIGIRVSPIG TFQNVDNGPN E--EADALYL
  Syn7942ER IVEDYRRAAE NALAAGFDGV EVHGANGYLI DQFLQDGTNQ RSDRYGGSFE NRSRFLREVL DAVISVWGSD RVGLRLSPWG QFNDMRD-SD P--VGLFSYV
 LyngbyaER1 IVEQYRQGAK NALEAGFDGV EIHSANGYLL DQFLHDGSNK RTDQYGGSIE NRARFLMEVL EAVTSVWDAD KVGVRLSPSS TFGTVFD-SD T--EALFNYV
 NospuncER1 IVEQYRQGAA NALAAGFDGV EIHSANGYLI DQFLRDRTNQ RTDKYGGSIE NRTRFLLEVT EAVTSVWDSN RVGVRLSPSG TFNDIGD-SN P--LETFGYA   “classical“ ERs
  NostocER1 IVEQYRQGAA NALAAGFDGV EIHAANGYLI DQFLRDGTNQ RTDEYGGAIE NRARLLLEVT EAITSVWDSQ RVGVRLSPSG TFNDIRD-SH P--LETFGYV
  AcaryoER1 IVQDFAQATG NARKAGFDGV EIHGANGYLI DQFLRDGTNE RQDAYGGTIE NRTRFLLEVV EAAVAVWSAD HVGVRLSPTN AFNDMRD-SN P--ISTFTHA
 CyanothER1 IIEQFRAAAE NAKTAGFDGV ELHGAFGYLI DQFLQDGSNQ RTDEYGGSIK NRARFLLEVV EAVSDVWGAQ RVGIKLSPSN TFYGMVD-SN P--QATFSYV
 CyanothER2 IVEDYRQAAL KAKMAGFDGV EIHAANGYLI NQFLETKTNH RTDKYGGSLE NRYRFLQEIV EAILTVFPAN RVAVRLSPNG IYNDMGS-PD Y--RETFLYV
  AcaryoER3 VVEDYRNAAI NAKTAGFDGV EIHSANGYLL DSFLQSKTNQ RQDRYGGTLE NRYRFLKEVV EAISQVWPTH RIGVRLSPNG VFNDMGS-PD Y--RETFLYV
AnabaenER3 TIFAFVAAAQ RALQVGFQMI EIHAAHGYLL HSFLSPLSNR RTDRYGGSLE NRMRLLLEVV RRVRDVLP-N GMPLFVRISA TDWV-EGGWD ---LQQSIIL
   GloeoER TVQAFAAAAR RSLAAGFRVL EIHAAHGYLL HSFLSPLSNR RTDRWGGLFE NRIRLLLAVV EAVRGVWP-E RLPLFVRISA TDWT-EGGWD ---LEQSVLL   „thermophilic-like“ ERs
      XenA VKQDFVDAAR RARDAGFEWI ELHFAHGYLG QSFFSEHSNK RTDAYGGSFD NRSRFLLETL AAVREVWP-E NLPLTARFGV LEYDGRDEQT ---LEESIEL
      Yqjm TVQEFKQAAA RAKEAGFDVI EIHAAHGYLI HEFLSPLSNH RTDEYGGSPE NRYRFLREII DEVKQVWD-G --PLFVRVSA SDYT-DKGLD ---IADHIGF

           301                                                                                         400
      OYE1 AGELEKRAKA GKRLAFVHLV EPRVTNPFLT EGEGEYEGGS NDFVYSIWKG PVIRAGNFAL HPEVVREEVK DKRTLIGYGR FFISNPDLVD RLEKGLPLNK
      OYE3 LGELEKRAKA GKRLAFVHLV EPRVTDPSLV EGEGEYSEGT NDFAYSIWKG PIIRAGNYAL HPEVVREQVK DPRTLIGYGR FFISNPDLVY RLEEGLPLNK
     PETNR IEELAKR--- --GIAYLHMS ET-----DLA GGKPYSEAFR QKVR-ERFHG VIIGAGAYT- AEKAEDLIGK GLIDAVAFGR DYIANPDLVA RLQKKAELNP
  Syn7942ER AQMLNPY--- --NLAYLHWI EPRWD-KAEE SPEFNQMA-T PVFR-SLYNG PVIAAGGYS- RSTAEAAIAS GAADLVAFGR LYISNPDLVE RFALDAPLNP
 LyngbyaER1 VSKLNPF--- --NLAYLHIV EPRIQGNVTV EDDGNGLG-A SYFR-SIYQG TIITAGGYT- RETGEAVLEQ DDADLVAYGR LFIANPDLPK RFALNAPLNE
 NospuncER1 AQALNQF--- --NLAYLHIY EAT---EADI RHGGIIVP-T SHIR-DRFTG TLIVNGGYT- REKGDAVLAN KAADLVAFGT LFISNPDLPR RLALNAPLNE   “classical“ ERs
  NostocER1 AQALNRF--- --NLSYLHIF EAI---DADI RHGGTVVP-T SHLR-DRFTG TLIVNGGYT- REKGDTVIAN KAADLVAFGT LFISNPDLPE RLEVNAPLNQ
  AcaryoER1 AQALNTY--- --NLAYLHVL EAL---QGHM LAVEGERV-T PYIR-QVFQG PLMINGGYD- AVSGAAAIAN QEADLVAYGV PFIANPDLPE RFAKQAPLNE
 CyanothER1 LEALNPM--- --NLAYVHLM EPN---EIDL RNRDVLSPVT PLFR-RIYRG TLITNGNYT- QQTANAAIAD GNAELVSFGR LFLANPDLPK RFKLNSPLNE
 CyanothER2 AQQLNTY--- --GLAYLHLV NGL----EFG FHGLGEPMTL AEFR-AVFDG PLMGNCGYT- QETAEAAIKE GNADLIAFGR PFISNPDLVE RFANGWSLNP
  AcaryoER3 AQQLNAF--- --DLAYLHIL DGL----AFG FHELGEPMQL SEFR-SVYNG TIIGNCGYS- QEDADDRISN GNADLIAFGR PFISNPDLVE RFTNGWPLNP
AnabaenER3 SRELKTL--- --GVDLIDVS TGGLVPHARI PVEKGYQVPF AAKIREEAGI MTGAVGLINE AEYADQIITR GCADLVLIGR ELLRNPYWSI YARCSLD-EE
   GloeoER AQVLARS--- --GVDLIDCS SGGVIPGVRI PAGPGYQTRF AERIRAEADM LTGAVGQITS AEQADHIVRT GQADLVLIGR QLLRDPYWPL KAAVELR-AP    „thermophilic-like“ ERs
      XenA ARRFKAG--- --GLDLLSVS VGFTIPETNI PWGPAFMGPI AERVRREAKL PVTSAWGFGT PQLAEAALQA NQLDLVSVGR AHLADPHWAY FAAKELGVEK
      Yqjm AKWMKEQ--- --GVDLIDCS SGALV-HADI NVFPGYQVSF AEKIREQADM ATGAVGMITD GSMAEEILQN GRADLIFIGR ELLRDPFFAR TAAKQLNTEI
```

```
            401                #             433
      OYE1  Y-DR-DTFYQ MSAHGYIDYP TYEEALKLGW DKK
      OYE3  Y-DR-STFYT MSAEGYTDYP TYEEAVDLGW NKN
     PETNR  Q-RP-ESFYG GGAEGYTDYP SL
  Syn7942ER  Y-DR-NTFYG GDEHGYTDYP SLEAASV
LyngbyaER1  Y-DR-STFYG GDQRGYTDYP FLDDSKVLTT V                                                    “classical“ ERs
NospuncER1  A-NQ-ATFYG GGEQGYTDYP FWSAANEAVA KA
 NostocER1  A-DP-TTFYG GGEKGYTDYP FLAVANK
 AcaryoER1  P-DP-STFYT RGAEGYTDYP FLDPLITAA
CyanothER1  P-NP-RTFYS STQEGYTDYP FLEQVAS
CyanothER2  PADM-KDWYS FEPEGYIDFP TY
 AcaryoER3  PAEQ-SIWYS FEREGYTDFP IYSESQA
AnabaenER3  PNW--PVPYG YAVKRQRR
   GloeoER  GPW--PEQYQ RAKP                                                          „thermophilic-like“ ERs
      XenA  ASWTLPAPYA HWLERYR
      Yqjm  PA---PVQYE RGW
```

Figure A.3 Sequence alignment of cyanobacterial ERs under study and known ERs from the literature using Multalin (Corpet 1988). The ERs under study and the corresponding NCBI accession numbers were: Syn7942ER (YP_399492), Cyanoth1 (YP_002370366.1), CyanothER2 (YP_002371879.1), LyngbyaER1 (ZP_01620253.1), NospuncER1 (YP_001869478.1), NostocER1 (NP_484870.1), AnabaenaER3 (YP_320425.1), GloeoER (NP_926774.1), AcaryoER1 (YP_001519129.1) and AcaryoER3 (YP_001522070.1). ERs of this study were aligned to PETNR from *Enterobacter cloacae* st. PB2 (AAB38683), OYE1 from *Saccharomyces carlsbergensis* (Q02899), OYE3 from *Saccharomyces cerevisiae* (CAA97878), XenA from *Pseudomonas putida* (AAF02538) and Yqjm from *Bacillus subtilis* (P54550). ERs were classified in “classical ERs” (Group 1) and “thermophilic-like ERs” (Group 2) according to Toogood et al. (2010). The conservation of active site residues was highlighted (#) and the sequence patterns indicating the quaternary structure (white letters) were shown according to Oberdorfer et al. (2011).

A.5.3 Substrate spectra

Table A.27 Substrate spectra of cyanobacterial ERs under study.

Substrate	Enzyme activity, U mg^{-1}								
	CyanothER1	**CyanothER2**	**AnabaenaER3**	**LyngbyaER1**	**GloeoER**	**NospuncER1**	**NostocER1**	**AcaryoER1**	**AcaryoER3**
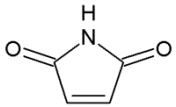	0.91 ± 0.14	24.25 ± 2.48	1.95 ± 0.20	2.05 ± 0.19	0.90 ± 0.07	3.13 ± 0.06	10.28 ± 0.28	14.80 ± 0.15	29.58 ± 1.84
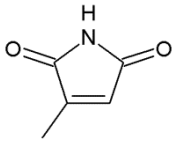	0.91 ± 0.05	1.79 ± 0.23	1.52 ± 0.23	12.00 ± 2.25	2.05 ± 0.22	3.77 ± 0.06	13.53 ± 2.63	9.90 ± 1.03	1.54 ± 0.32
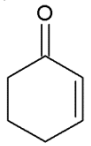	0.02 ± 0.04	0.68 ± 0.18	1.65 ± 0.43	0.77 ± 0.06	2.03 ± 0.11	0.30 ± 0.01	0.59 ± 0.03	2.03 ± 0.04	1.36 ± 0.56
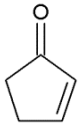	0.00 ± 0.01	0.00 ± 0.00	1.19 ± 0.05	0.29 ± 0.02	1.01 ± 0.06	0.09 ± 0.01	0.08 ± 0.05	0.51 ± 0.01	0.50 ± 0.30
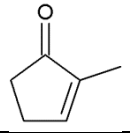	0.00 ± 0.00	0.00 ± 0.01	0.26 ± 0.03	0.01 ± 0.00	0.27 ± 0.01	0.03 ± 0.00	0.01 ± 0.01	0.04 ± 0.00	0.02 ± 0.01

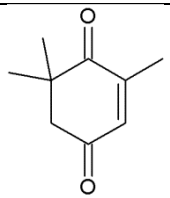	0.03 ± 0.01	1.00 ± 0.02	0.56 ± 0.15	0.34 ± 0.02	0.13 ± 0.07	0.68 ± 0.21	2.16 ± 0.09	2.00 ± 0.69	0.09 ± 0.15
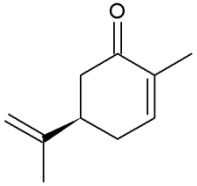	0.02 ± 0.01	0.11 ± 0.00	1.09 ± 0.10	0.07 ± 0.01	0.43 ± 0.25	0.21 ± 0.00	0.69 ± 0.02	0.56 ± 0.01	0.02 ± 0.00
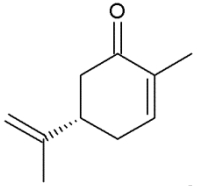	0.01 ± 0.01	0.10 ± 0.01	0.87 ± 0.14	0.02 ± 0.00	0.66 ± 0.44	0.27 ± 0.03	0.78 ± 0.12	0.27 ± 0.09	0.00 ± 0.00
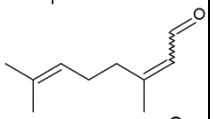	0.00 ± 0.05	0.03 ± 0.00	0.03 ± 0.01	0.00 ± 0.00	0.15 ± 0.01	0.04 ± 0.02	0.32 ± 0.19	0.07 ± 0.00	0.00 ± 0.30
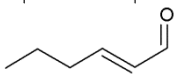	0.07 ± 0.04	1.33 ± 0.49	0.45 ± 0.21	1.63 ± 0.09	0.39 ± 0.16	0.27 ± 0.03	0.85 ± 0.22	1.71 ± 0.16	2.32 ± 0.28
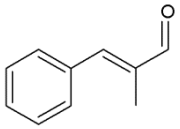	0.16 ± 0.08	0.13 ± 0.05	0.11 ± 0.03	0.10 ± 0.01	0.54 ± 0.53	0.22 ± 0.01	0.38 ± 0.09	0.02 ± 0.00	0.13 ± 0.20
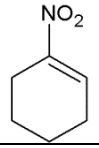	0.08 ± 0.01	0.48 ± 0.09	0.73 ± 0.23	1.59 ± 0.05	2.41 ± 0.28	0.24 ± 0.03	1.04 ± 0.01	0.81 ± 0.17	0.50 ± 0.30

A.5.4 Cell cultivation

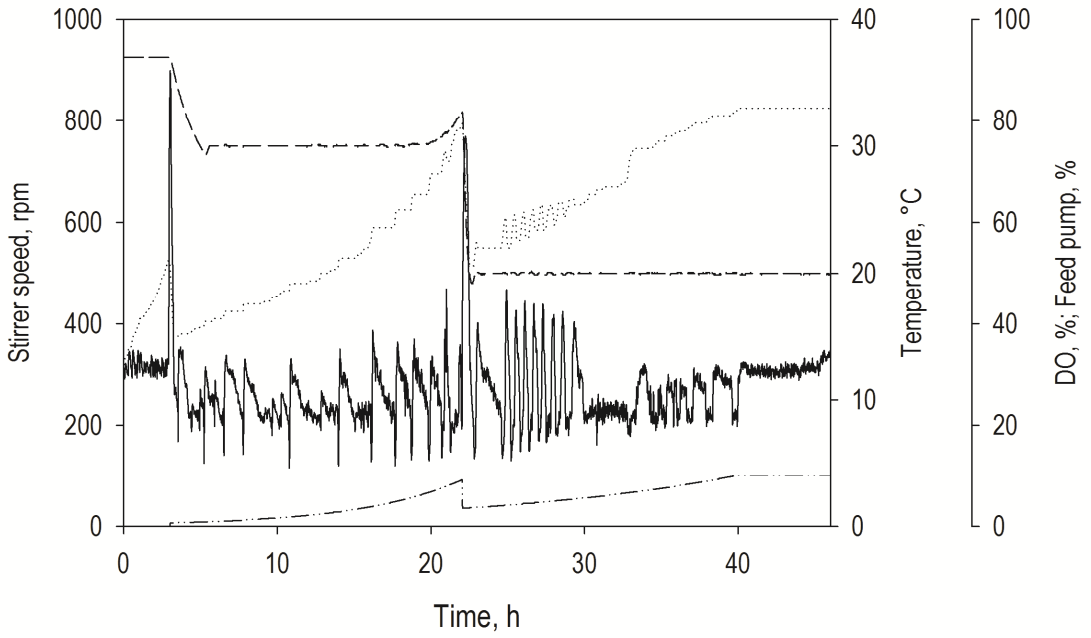

Figure A.4 Process data recorded during liter-scale cell cultivation of the whole-cell biocatalyst *E. coli* pET28NosT7FDH$_{3M}$. The stirrer speed (·····), the temperature (— —), the dissolved oxygen (——) and the feed pump signals (— ·· —) are given.

A.5.5 NMR

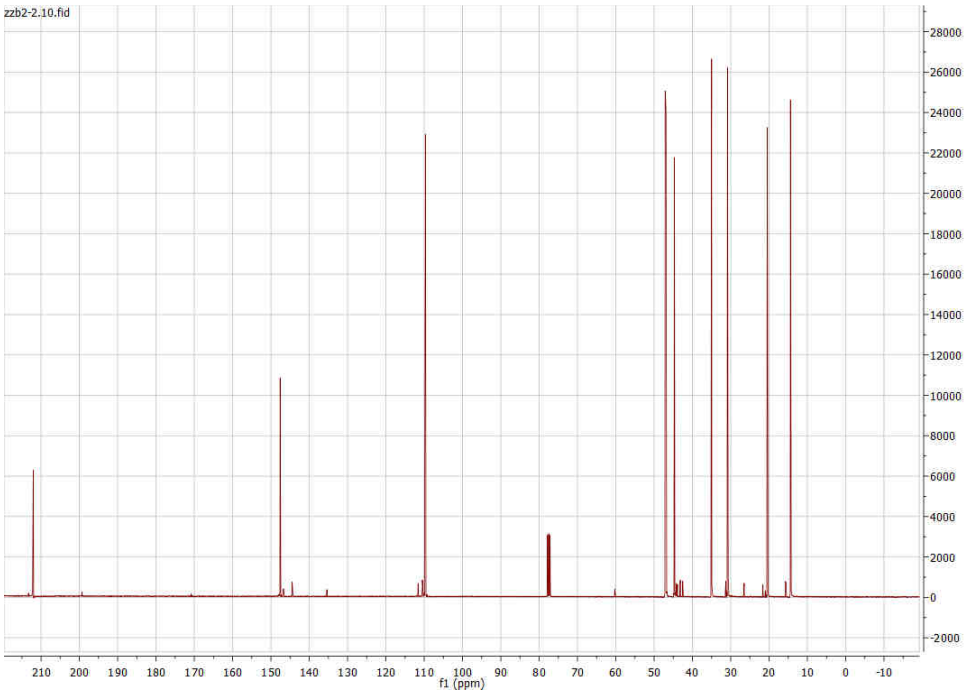

Figure A.5 ^{13}C-NMR spectrum of (2R,5R)-dihydrocarvone obtained after liter-scale whole-cell biotransformation with XAD4 and subsequent product purification by filtration and destillation.